Climate Change Impact Assessment on Hydropower Generation in Manitoba

By

Hamid Gozini

A thesis submitted to the Faculty of Graduate and Postdoctoral Studies of

The University of Manitoba

in partial fulfilment of the requirements of the degree of

DOCTOR OF PHILOSOPHY

Department of Civil Engineering

University of Manitoba

Winnipeg

Copyright © 2026 by Hamid Gozini

ABSTRACT

Assessing the future performance of Manitoba hydropower system is challenging due to its complex interconnected river-reservoir network and uncertainty in future water supply and electricity demand. This thesis develops and applies an integrated modelling framework to evaluate climate change impacts on the Manitoba hydropower system under deep inflow uncertainty and changing electricity demand. The first component of this thesis develops MB_HydroSim, an integrated water resources management model of the large-scale river-reservoir system in Manitoba. By incorporating both explicitly defined and implicitly derived operating rules, MB_HydroSim reproduces key system dynamics, including water levels, outflows, and hydropower generation, providing a reliable foundation for climate impact assessment and hydropower generation planning. The second component presents a target-based synthetic streamflow generator that enables the generation of a broad and controlled range of plausible inflow conditions beyond the historical record and the relatively limited range represented by GCM projections. The framework directly targets monthly streamflow magnitude, variability, and seasonality in real space, allowing statistically credible streamflow scenarios to be generated for multisite studies at low computational cost. The third component stress tests the Manitoba hydropower system under a wide range of plausible inflow conditions and historical and future electricity demand scenarios. Results show that dry conditions create greater performance losses than the benefits gained under comparable wet conditions. Higher inflows can improve hydropower generation outcomes, but also increase lake level excursions, indicating a benefit-stability trade-off in the system. Although annual assessments indicate lower expected system stress in the future, they mask important seasonal system behavior; increase in the number of seasons experiencing higher system stress in the future (summer and autumn). Overall, the findings demonstrate that adaptive operational strategies are needed beyond expanding hydropower generation capacity. The contributions of this thesis extend beyond Manitoba. MB_HydroSim provides a transferable example of operation-based simulation for complex, regulated, cold-regions river-reservoir systems. The target streamflow generation framework can be applied to multisite water systems where direct control of streamflow properties is needed for stress testing. The stress-testing framework can be adapted to other hydropower and regulated water systems by redefining system objectives, performance thresholds, and relevant stressors.

ACKNOWLEDGEMENTS

This study was conducted at the University of Manitoba, which is located on the traditional territories of the Anishinaabeg, Cree, Oji-Cree, Dakota, and Dene Peoples, and on the homeland of the Métis Nation. We recognize the Treaties made on these territories, acknowledge the harms and mistakes of the past, and affirm our commitment to working in partnership with Indigenous communities in the spirit of reconciliation and collaboration.

First and foremost, I would like to express my deepest gratitude to my family for their unconditional love, encouragement, and emotional support throughout this long academic journey. I am especially grateful to my parents, **Habib** and **Afsaneh**, and my siblings, **Meisam** and **Farnaz**, for supporting me along the way. I am also deeply thankful to my partner, **Shirin**, for her constant presence, encouragement, and support. Her ability to keep me moving forward during challenging times and to create a supportive environment has been invaluable throughout this journey.

I would like to express my sincere gratitude to my supervisor, **Dr. Masoud Asadzadeh**, first and foremost for giving me the opportunity to pursue my PhD and for his guidance throughout this journey. I am particularly grateful for the knowledge and experience he generously shared with me, which has contributed greatly to my academic and professional development. I am equally grateful to my co-advisor, **Dr. Tricia Stadnyk**, for her valuable guidance, support, and for generously sharing her time, knowledge, and experience.

I would also like to thank the members of my internal advisory committee, **Dr. Shawn Clark** and **Dr. Shaahin Filizadeh**, for their thoughtful comments and valuable feedback at different stages of this thesis.

Finally, I would like to acknowledge the professionals and collaborators who generously shared their time, expertise, and practical knowledge throughout this research. I am particularly grateful to the experts at **Manitoba Hydro**, especially **Jacob Snell** and **Phillip Slota**, and at **Hydrologic Forecasting Centre**, particularly **Dr. Habtamu Tolossa** and **Dr. Fisaha Unduche**, for their collaboration and valuable knowledge sharing. I would also like to sincerely thank **Dr. Saman Razavi**, **Pheobe Riddell**, and **Andrew Tefs** for their collaboration and contributions to this work.

TABLE OF CONTENTS

Chapter 1. Introduction 1

1.1 Problem Statement 1

1.2 Research Objectives 4

1.2.1 Developing a Hydropower System Simulation Tool 4

1.2.2 Developing a Streamflow Scenario Generator 5

1.2.3 Developing a Stress-testing Framework for Climate Change Impact Assessment 10

1.3 Thesis Content and Contributions 12

Chapter 2. Integrated Water Resources and Hydropower Generation Modelling in a Complex, Cold-Regions River-Reservoir System 15

2.1 Abstract 15

2.2 Introduction 15

2.3 Study Area 20

2.3.1 Hydropower Generation in Manitoba 21

2.3.2 Control Points 23

2.3.3 Existing In-House Operational and Forecasting Tools 25

2.4 Data 26

2.4.1 Inflow 28

2.4.2 Outflow 29

2.4.3 Water Level 30

2.4.4 Hydropower Generation 31

2.5 Methodology 32

2.5.1 MODSIM-DSS 35

2.5.2 Mass-balance Model 37

2.5.3 Operational Model 39

2.5.3.1 Operations Based on Established Guidelines 40

2.5.3.2 Operations by Daily Median Recorded Storage 41
2.5.3.3 Operations by Regression Equations 41
2.5.4 Model Performance Metric 45
2.6 Results and Discussion 46
2.6.1 MB_HydroSim Performance 47
2.6.2 MB_HydroSim Capabilities 49
2.6.2.1 Sensitivity Analysis 49
2.6.2.2 Climate Change Impact Assessment 51
2.6.2.3 Adaptation Policies 53
2.6.2.4 WE Nexus 54
2.6.2.5 Ice-cover Impact on Hydropower Generation 55
2.7 Conclusion, Limitations, and Future Work 55
2.8 Availability of Data and Materials 57
Chapter 3. Inflow Generation for Water System Planning in Multisite Studies using Target Synthetic Streamflow Generation 58
3.1 Abstract 58
3.2 Introduction 59
3.3 Methodology 65
3.3.1 Target Synthetic Streamflow Generation Framework 66
3.3.1.1 Input Data and Targets 67
3.3.1.2 Monthly Synthetic Streamflow Generator 68
3.3.1.3 Feasibility of Target Scenarios 70
3.3.1.4 Optimization Procedure 73
3.3.1.5 Local Inflow Location 74
3.3.1.6 Daily Disaggregation of Synthetic Flows 74
3.3.2 Illustrative Example 76
3.3.3 Case Study: Winnipeg River System 78
3.3.3.1 Historical Inflow Data 80

3.3.3.2 GCM-Driven Inflow Data 82
3.3.4 Framework Evaluation 83
3.3.5 Framework Application 86
3.4 Results and Discussion: 87
3.4.1 Historical Magnitude and Variability: Case RH-N vs. Case RH-O 87
3.4.2 Historical Statistical Structure: Case RH-O vs. Case RH-N and GCMs 88
3.4.3 Expanding beyond Historical Magnitude and Variability: Case EH-O vs. Case EH-N 92
3.4.4 Expansion Over Expected Future Magnitude and Variability: Case EG-O 94
3.4.5 Seasonality Change: Case EH-O vs. Case EG-O 96
3.4.6 Future Expected Statistical Structure: Case EH-O and EG-O 97
3.4.7 Computational Cost 99
3.4.8 Stress-Testing Application 101
3.4.8.1 Hydropower Generation 101
3.4.8.2 Flood Management 101
3.4.8.3 Water Demand Management 102
3.4.8.4 Matrix Year Uncertainty 104
3.5 Summary and Conclusion 104
3.6 Availability of Data and Materials 106
Chapter 4. Decision-Relevant Stress Testing of Hydropower Systems Under Deep Inflow Uncertainty and Electricity Supply-Demand Change 107
4.1 Abstract 107
4.2 Introduction 108
4.2.1 Manitoba Hydropower System 111
4.3 Methodology 114
4.3.1 Generating Target Inflow Scenarios 114
4.3.2 Defining Hydropower Target Scenario 116

4.3.3 Simulating Hydropower Generation 117
4.3.4 Evaluating System Response 117
4.4 Case Study 119
4.4.1 Data 122
4.4.1.1 Historical Inflow 122
4.4.1.2 GCMs-Driven Inflow 123
4.4.1.3 Recorded Hydropower Generation 125
4.4.1.4 Electricity Demand Projections 126
4.4.2 System Simulation Model 127
4.4.3 Construction of Target Scenarios 128
4.4.3.1 Inflow Scenarios 128
4.4.3.2 Hydropower Scenarios 129
4.4.3.3 Stress-Testing Scenarios 131
4.4.4 System Performance Metrics 133
4.4.5 Annual and Seasonal Heat Maps 135
4.5 Results and Discussion 136
4.5.1 Uncertainty Estimation, Case RH-R 136
4.5.2 Annual Evaluation, Case EH-R vs. EG-F 137
4.5.2.1 Hydropower Reliability 139
4.5.2.2 Hydropower Vulnerability 140
4.5.2.3 Hydropower Revenue 141
4.5.2.4 Lake Winnipeg Water Level Excursion 141
4.5.3 Seasonal Evaluation, Case EH-R vs. EG-F 142
4.5.3.1 Hydropower Reliability 143
4.5.3.2 Hydropower Vulnerability 144
4.5.3.3 Lake Winnipeg Water Level Excursion 145
4.5.4 Inflow Seasonality Change, Case RG-F vs. EG-F 147
4.5.4.1 System response to GCM-projected inflow seasonality 147

4.5.4.2 Consistency and divergence between EG-F and RG-F 148
4.5.5 The Dirty Thirties Stress Test 149
4.6 Conclusions, Limitations, and Future Work 149
4.7 Availability of Data and Materials 152

Chapter 5. Research Summary, Contribution, Significance, Limitations, and Recommendations for Future Work 153

5.1 Research Summary and Findings 153
5.2 Research Contribution and Significance 155
5.3 Limitations and Recommendations for Future Work 157

References 161

Supplementary Material 175

SM.1 Summarized Operational Rules 175
SM.2 Detailed Performance Results for Each Sub-system 178
SM.3 MB_HydroSim 188
SM.4 Stress-Testing Application: Hydropower Generation 188
SM.5 Stress-Testing Application: Flood and Water Demand Management 189
SM.6 Summary of seasonal inflow patterns 191
SM.7 Summary of Stress-Testing Findings for the Hydropower System in Manitoba 192
SM.8 Stress Testing Graphical Abstract 194

LIST OF FIGURES

Figure 1.1. Conceptual illustration of top-down and bottom-up approaches for climate change impact assessment of hydropower systems. 7

Figure 1.2. Illustration of forward and inverse approaches for using stochastic generators. 9

Figure 2.1. Location of NCRB (black solid border), study area (cream-colored area), hydropower stations (red-filled circles), lake, rivers, and important control points (green-filled circles) 22

Figure 2.2. Monthly average of (a) daily hydropower generation, energy demand, and air temperature in Manitoba, and (b) daily historical water level, inflow, and outflow for Lake Winnipeg. 32

Figure 2.3. Schematic of MB_HydroSim model development, illustrating the distinction and information flow between mass-balance, operational, and the integrated MB_HydroSim models. 33

Figure 2.4. Example of a simple model in MODSIM-DSS 37

Figure 2.5. Conditional statements to determine upper and lower bounds of Southern Indian Lake target storage. 43

Figure 2.6. Monthly average of the total daily recorded inflow into the entire system vs. monthly average of the daily inflow for the three most downstream hydropower stations: Kettle, Long Spruce, and Limestone. 48

Figure 2.7. Monthly timeseries of recorded vs. simulated for water level and hydropower generation at (a) Kettle and (b) Long Spruce hydropower stations, from 1980 to 2017. 49

Figure 2.8. Monthly average of daily inflow minus outflow at the Shellmouth Dam 52

Figure 2.9. Monthly average of daily water level at the Lake Winnipeg and Lake of the Woods. 52

Figure 3.1. The framework for generating target streamflow scenarios in multisite water systems. 66

Figure 3.2. The flowchart of the monthly synthetic streamflow generator developed by Kirsch et al. (2013). 69

Figure 3.3. Feasible (green region) and infeasible (red region) area of the exposure space, separated with a boundary line (red). 72

Figure 3.4. The flowchart of disaggregating monthly synthetic streamflow to daily, using the method of Nowak et al. (2010) 75

Figure 3.5. Monthly target mean (M_T) and SD (SD_T) changes in four target scenarios at (a) location 1 and (b) location 2. 77

Figure 3.6. Monthly mean and SD seasonality of the target scenarios (Figure 3.5) and the historical records at (a, b) location 1 and (c, d) location 2. 78

Figure 3.7. Location of the Winnipeg River Basin (cream-colored area), hydropower stations (red-filled circles), lake and control points (green-filled circles), and hydrometric stations (gray-filled circles). 79

Figure 3.8. (a) Monthly mean, (b) SD, and (c) CV of historical monthly inflow at fourteen inflow locations across the Winnipeg River Basin, from 1980 to 2017. 81

Figure 3.9. (a) Monthly mean change and (b) monthly SD change of total inflow into the water system in the Winnipeg River basin for the GCM-driven projections (2018-2055) compared to historical records (1980-2017). (c) Monthly mean and (d) CV of GCM-driven monthly inflow projections at fourteen inflow locations across the Winnipeg River Basin. 83

Figure 3.10. Boxplots of resultant monthly mean and SD deviations from the target for the non-optimized scenarios at locations B and N when reproducing historical records in case RH-N. 88

Figure 3.11. Average (solid line) and its 95% confidence intervals (dashed line) of the p-value for location and scale test against historical records from 1981 to 2017 at locations B and N. 89

Figure 3.12. (a) Autocorrelation and (b) cross-correlation functions of streamflow at locations B and N. 90

Figure 3.13. Resultant monthly mean and SD changes for optimized vs. non-optimized monthly synthetic scenarios at (a) location B and (b) location N. 92

Figure 3.14. (a) real-space and (b) logarithmic scale flow duration curves of the monthly synthetic scenarios in EH-O vs. historical records from 1980 to 2017. 93

Figure 3.15. Resultant monthly mean and SD changes for the optimized monthly synthetic scenarios in EG-O at (a) location B and (b) location N. 94

Figure 3.16. (a) real-space and (b) logarithmic flow duration curves of the monthly synthetic scenarios in EG-O, historical records from 1980 to 2017, and the monthly GCM-driven projections (2018 to 2055). 95

Figure 3.17. Resultant seasonality of monthly (a) mean and (b) SD for the optimized monthly synthetic scenarios in cases EH-O and EG-O. Case EH-O represents optimized scenarios expanding over historical records. 96

Figure 3.18. Average (solid line) and its 95% confidence intervals (dashed line) of the p-value for location and scale test in (a) EH-O and (b) EG-O against historical records from 1980 to 2017 and (c) EG-O against ensemble of monthly GCM-driven projections (2018 to 2055) at locations B and N. 97

Figure 3.19. A. (a) Autocorrelation and (b) cross-correlation functions of streamflow at locations B and N. 98

Figure 3.20. (a) Annual and (b) seasonal hydropower stress-testing assessment in the Winnipeg River Basin. (c) Flood frequency and (d) water-demand shortage frequency at Shellmouth Dam evaluated across the same stress-testing space. 103

Figure 4.1. Workflow of the proposed bottom-up framework for stress testing hydropower systems 113

Figure 4.2. An illustration of the smallest sample size R ($2<R<Y$) that yields a normalized interquartile range (IQR) greater than 0.9 for two performance metrics M_1 and M_2. 115

Figure 4.3. Location of the study area (cream-colored area), hydropower stations (red circles), hydrometric stations (black circles), and major lakes (yellow triangles). 120

Figure 4.4. (a) Monthly mean change and (b) monthly SD change of total inflow to the hydropower system for the GCM-driven projections (2018-2055) compared to hindcast (1981-2017). 125

Figure 4.5. Projections of (a) annual electricity demand and (b) monthly peak electrical demand in four scenarios. 127

Figure 4.6. Normalized interquartile range (IQR) of hydropower performance and system state metrics as a function of sample size in case RH-R..... 137

Figure 4.7. Annual-scale stress-testing heat maps for the hydropower (*Re*: Reliability, *Vu*: Vulnerability, *AR*: Average Annual Revenue) and system state (P_{LW}: Lake Winnipeg water level excursion) metrics under target case EH-R (a-d) and EG-F (e-h). 140

Figure 4.8. Seasonal-scale stress-testing heat maps for the hydropower reliability under target case EH-R (a-d) and EG-F (e-h). 143

Figure 4.9. Seasonal-scale stress-testing heat maps for hydropower vulnerability (GWh) under target case EH-R (a-d) and EG-F (e-h). 145

Figure 4.10. Seasonal-scale stress-testing heat maps for Lake Winnipeg water level excursion (P_{LW}, %) under target case EH-R (a-d) and EG-F (e-h). 146

LIST OF TABLES

Table 2.1. The summary of worldwide studies employed hydropower simulation models. ... 18

Table 2.2. Hydropower stations in Manitoba (Manitoba Hydro, 2025)..... 23

Table 2.3. Percentage and daily average of recorded and "local flow" in each sub-basin. 29

Table 2.4. Performance results of MB_HydroSim..... 47

Table 2.5. Model performance (monthly KGE) in water level simulation for sub-system 3 (MB_HydroSim vs. Beiraghdar (2019) model)..... 49

Table 2.6. Summary of the performance evaluations based on monthly KGE at different sub-systems of MB_HydroSim..... 50

Table 2.7. Potential objective functions and decision variables for developing adaptation policies using MB_HydroSim..... 53

Table 3.1. Inflow locations of the water system in the Winnipeg River Basin..... 80

Table 3.2. Description of five synthetic streamflow generation cases applied to the Winnipeg River Basin with fourteen locations (k) of inflow..... 85

Table 3.3. Computational cost of generating 100 synthetic scenarios across different frameworks. 100

Table 4.1. Summary of projected annual changes in temperature, precipitation, and total inflow across the 19 GCM scenarios. 124

Table 4.2. Summary of the four target sets of monthly inflow conditions used for stress testing of Manitoba hydropower system..... 129

Table 4.3. Monthly seasonality changes (%) in peak electricity demand for the four scenarios in 2042 relative to 2021-2022, extracted from Figure 4.5b. 131

Table 4.4. Annual hydropower performance metrics (median of 20 realizations), along with their likelihood bands and baseline values, for each GCM-driven inflow condition in RG-F compared against extracted values from EG-F..... 148

CHAPTER 1. INTRODUCTION

Hydropower is a renewable, operationally flexible, and relatively inexpensive source of electricity with a low lifecycle carbon footprint (Jamali et al., 2013). In 2024, hydropower contributed to 45% of total renewable energy production and more than 14% (4418 TWh) of total electricity production in the world (data from Ember (2025) processed by Ritchie et al. (2020)). Global hydroelectricity generation is projected to nearly double by 2050 (Dias et al., 2018). Despite the advantages, hydropower systems are highly sensitive to changes in the magnitude and timing of streamflow (Savelsberg et al., 2018), which are expected to change under future climate conditions (Haguma et al., 2014). Similarly, climate change is expected to alter energy demand patterns, with warmer temperatures expected to increase demand for cooling systems (Mutschler et al., 2021). In cold regions, warmer temperatures are expected to change peak electricity demand patterns by increasing summer peak demand while reducing winter peak demand (Manitoba Hydro, 2023b). Electricity demands are anticipated to further increase with urbanization, population growth, electrification of vehicles, and improvements in living standards (Berardi & Jafarpur, 2020). These supply- and demand-side pressures together necessitate comprehensive climate change impact assessments for hydropower systems to mitigate electricity supply deficits and maximize the benefits of potential opportunities within current system configurations.

1.1 Problem Statement

Canada relies heavily on hydropower generation, accounting for 60% of total electricity generation nationally (Canada Energy Regulator, 2024), although this is highly variable by region (province and territory). In 2024, Canada had the third-highest rate of contribution to global hydropower generation by 7.8% (347 TWh) (data from Ember (2025) processed by Ritchie et al. (2020)). Within the Province of Manitoba, hydropower generation plays a central role in the provincial energy system by supplying approximately 97% of the province's electricity, the highest proportion of hydroelectric generation among the provinces in Canada (Canada Energy Regulator, 2024). Other sources of electricity in Manitoba include wind, natural gas, biomass, solar, and petroleum-based generation.

The river-reservoir system in Manitoba is vast and complex, encompassing more than 100,000 lakes along with numerous rivers and tributaries, collectively covering about 16% of the province's

surface area (Government of Manitoba, 2025b). Streamflow is regulated through 28 major lakes and 43 control points, supporting the operation of 16 hydropower stations with a combined nominal capacity of 5,926 MW. This regulation is coordinated by Manitoba Hydro in collaboration with other departments and organizations within and beyond Manitoba. The system is further characterized by its nival (snowmelt-dominated) and cold-regions (subject to seasonal snow and ice cover) conditions and has a limited water storage capacity due to the flat terrain (Manitoba Hydro, 2014). Lake Winnipeg active storage corresponds to less than five months of water supply under median outflow conditions and less than four months under upper decile outflow conditions during the cold months, November to March, when electricity demand is typically highest. Another challenge for Manitoba Hydro is the temporal mismatch between the spring peak in water supply and the winter peak in electricity demand when fulfilling the provincial electricity needs. Despite these constraints, the system supports a robust energy economy, producing an average annual revenue of 2,743 million Canadian dollars over the past decade (Manitoba Hydro, 2024). This revenue forms a substantial portion of Manitoba's net income from government business enterprises, highlighting the strategic importance of hydropower to the province's fiscal sustainability (Government of Manitoba, 2025a).

Climate change has been more pronounced in Canada due to its relatively higher latitude, undergoing a 1.7 °C increase in annual mean temperature from 1984 to 2016, which is about twice the global average (Bush & Lemmen, 2019). An additional 0.2 °C warming was observed over the same period across the Canadian Prairies which include Manitoba (Bush & Lemmen, 2019). Rising temperatures are projected to increase drought risk in the southern Canadian Prairies due to smaller snowpacks and earlier snow and ice melt, thereby reducing the reliability of the dry-season water supply (Bush & Lemmen, 2019). However, future drought projection remains uncertain as changing snowpacks and snowmelt contributions are not the sole driver of change. In the Lower Nelson River Basin in Manitoba, Lilhare et al. (2022) projected an increase in summer streamflow by 2050, accompanied by substantial year-to-year variability and uncertainty arising from rapid snowmelt, more rainfall, reduced snowpacks, and warming soil temperatures. Warming is also expected to produce smaller snowmelt-driven events and more rainfall-generated flows, driving a transition from nival to mixed or even pluvial (rainfall-dominated) regimes, shifts that have already been observed in smaller prairie streams (Bush & Lemmen, 2019).

Climate change is of critical importance for hydropower in Manitoba, where generation depends primarily on streamflow rather than hydraulic head due to the limited storage capacity of hydropower stations relative to the volume of water passing through them. The extent of climate change impact on streamflow magnitude and seasonality is well examined in Manitoba. Although statistically significant increasing trend in annual streamflow have been detected, models' agreement remains low, leaving future projections highly uncertain (Kim et al., 2022; Lilhare et al., 2022; MacDonald et al., 2018; Stadnyk et al., 2021). Uncertainty in streamflow projections directly translates into uncertainty in reservoir inflow and water supply for hydropower generation. Kim et al. (2022) showed that this uncertainty is driven primarily by climate scenario selection, with limited agreement among simulations of reservoir inflow volume to the Lower Nelson River Basin. By contrast, there is a high confidence in projected shifts in streamflow seasonality (Bush & Lemmen, 2019), with higher and earlier peak flows (Stadnyk et al., 2021) driven by increased precipitation and warmer temperatures causing earlier snowmelt. Regulation further complicates these dynamics by damping climate-driven signals, as renaturalized simulations reveal stronger positive flow trends than regulated ones, underscoring the importance of human management in shaping seasonal hydrological patterns (Stadnyk et al., 2021).

Electricity demand in Manitoba is simultaneously increasing as the province undergoes an energy transition driven by five key factors: economic growth, decarbonization policy (reducing greenhouse gas emissions), electric vehicle adoption, the transition from natural gas to electricity for building heating, and customer self-generation of electricity (Manitoba Hydro, 2023b). Manitoba Hydro (2023a) notes that electrification of transportation and space heating is expected to be the largest contributor to the long-term electricity demand growth. However, the overall pace and scale of the increase remains uncertain as it is dependent on evolving policy, customer adoption, and the pace of technological advances. Emerging national priorities may further increase electricity demand uncertainty, including new electricity needs for sovereign AI compute and cloud infrastructure required to support data-intensive digital services, high-performance computing, and AI adoption across sectors (Prime Minister of Canada, 2026), as well as clean electricity infrastructure intended to replace imported diesel generation and support energy security, critical mineral supply chains, and defence-related applications in northern Canada (Prime Minister of Canada, 2025). The growing electricity demand, combined with the uncertain streamflow projections and limited storage capacity in Manitoba's complex, large-scale, nival-

dominated, and drought-prone river-reservoir system, poses a considerable challenge for future electricity planning in the province.

1.2 Research Objectives

This study aims to assess the impacts of climate change on hydropower generation in Manitoba by explicitly accounting for growing electricity demand while bypassing sole reliance on highly uncertain streamflow projections. This research is structured around three major objectives, outlined below, which focus on developing the required tools and analytical approaches necessary to facilitate comprehensive analysis of hydropower system behavior under changing climates, but also to address key research gaps identified in national and international studies with broad applicability to other systems.

1.2.1 Developing a Hydropower System Simulation Tool

A major limitation for climate change impact assessment of hydropower generation in Manitoba is the absence of an open-access yet comprehensive and integrated hydropower simulation tool. Although hydropower is the dominant source of electricity in the province of Manitoba, water resources are managed by multiple departments and organizations operating within and beyond Manitoba, each relying on independent and unique (often proprietary) water management and modeling tools. This reflects broader fragmentation of provincial and territorial water management practices in Canada (Arnal et al., 2023), a challenge that is also observed in multilevel water governance systems worldwide (OECD, 2011).

In addition, the only existing open-access hydropower simulation model developed for Manitoba is a MODSIM-DSS application focused on the Lake Winnipeg and Southern Indian Lake outlet systems (Beiraghdar, 2019). While this model successfully represented a large portion of the province's installed hydropower capacity (80%), reproducing historical hydropower generation and water levels, its reliance on median daily recorded lake levels to represent operations limits its ability to simulate realistic lake-level dynamics during non-median hydroclimatic conditions.

More broadly, the hydropower modeling literature indicates a lack of large-scale (i.e., multi-basin) hydropower simulation tools developed for Canadian systems. Existing large-scale hydropower generation models worldwide typically approximate water system operations using

simulation-optimization methods, such as linear programming (Caceres et al., 2021; Chowdhury et al., 2021; Graabak et al., 2017; Ng et al., 2017; Widén et al., 2024) or simplified operational rules (Dallison et al., 2021; Graham et al., 2007; Qin et al., 2020a, 2020b; Zhou et al., 2018), rather than explicitly representing real system operations. In cold-region countries, large-scale hydropower modeling has focused on simulation-optimization methods, as demonstrated by studies in Norway (Graabak et al., 2017) and Sweden (Widén et al., 2024). However, simulation-optimization methods are limited in the representation of observed system operations and coordinated decision-making across extensive river-reservoir networks, as they often assume optimized operation to maximize hydropower benefits rather than reflecting actual operating practices.

This research objective therefore seeks to develop an integrated, large-scale, operation-based hydropower simulation tool for Manitoba that extends existing modeling frameworks by representing the full river-reservoir system, incorporating all hydropower stations and key upstream inflow control points, and simulating coordinated system operations using operational rules derived explicitly from operational guidelines or implicitly from observed system behavior. Though the river-reservoir system model reflects the Manitoba Hydro system alone, the tools developed in this research are transferable to other water resource management system modelling frameworks.

1.2.2 Developing a Streamflow Scenario Generator

One major limitation in climate change impact assessment for hydropower systems is the absence of a tool for generating inflow scenarios with specific properties, including magnitude, variability, and seasonality of the changes in inflow (Bhattarai et al., 2024; Taner et al., 2017; Widén et al., 2024; Wild et al., 2019; Zhao et al., 2022). Generating inflow scenarios with specific distributional properties ensures that they reflect inflow conditions relevant to site-specific water system planning and operations, such as low-flow conditions with higher temporal variability. Inflow magnitude governs the available water volume, while inflow variability characterizes year-to-year fluctuations in water volume, and seasonality determines intra-annual fluctuations and when most of the water arrives. Collectively, these properties shape operational behavior and storage-release decisions within water systems (Culley et al., 2016; Herman et al., 2016; Quinn et al., 2018; Wild et al., 2019).

Two primary approaches are commonly used to develop climate change inflow scenarios to assess hydropower system response under future inflow uncertainty: the *top-do*wn and *bottom-up* approaches. These approaches differ in how climate information is generated, propagated, and linked to system performance in climate change impact assessments.

The *top-down* approach represents the conventional framework for evaluating climate change impacts on hydropower generation, which has been widely applied across major hydropower-producing regions worldwide (Zhao et al. (2022) in China; de Oliveira Serrão et al. (2023) in Brazil; Zhou et al. (2018) in the United States; Widén et al. (2024) in Sweden; and Chernet et al. (2013) in Norway). Within this framework (Figure 1.1a), outputs from global and regional climate models (GCMs and RCMs) are translated through hydrological model to produce ensembles of process-based streamflow projections, which are subsequently used as system inflows in water resources management model to estimate hydropower system performance. Satisfactory versus unsatisfactory (green versus red in Figure 1.1a) outcomes associated to each evaluated scenario provide insight into potential changes in system generation capacity. Streamflow projections from a top-down approach are useful for capturing a wide range of potential inflow conditions, and for attributing hydrological impacts to specific emissions scenarios. However, top-down streamflow projections are not designed to control the properties of the resulting inflow distribution, such as generation capacity under high or low flow conditions that are needed to support hydropower generation planning.

Rather than projecting the future, the *bottom-up* approach enables systematic exploration of a broad range of plausible inflow conditions (i.e., synthetic streamflow scenarios) and may extend beyond those projected by GCMs using the top-down approach (Brown et al., 2011). They can provide deeper insight into the risks and vulnerabilities of the hydropower system. As illustrated in Figure 1.1b, bottom-up assessments begin by defining an *exposure space* composed of possible climate or hydrologic conditions (black dots). When the exposure space is defined in terms of statistical properties of relevant climate variables (e.g., mean air temperature and precipitation), synthetic climate scenarios are generated using stochastic weather generators (Bhattarai et al., 2024; Ray et al., 2018; Taner et al., 2017), which are subsequently translated into streamflow via hydrological models. Alternatively, when the exposure space is defined in the hydrological space (i.e., streamflow statistical properties, such as mean and variability of system inflow), stochastic

streamflow generators are used to generate synthetic streamflow scenarios (Yuan Liu et al., 2023; Quinn et al., 2018, 2017; Wild et al., 2019). In both cases, each point in the exposure space corresponds to a synthetic streamflow scenario representing a plausible system inflow condition. System behavior is evaluated across these scenarios, with outcomes classified and mapped as resulting in satisfactory (green dots) versus unsatisfactory (red dots) system performance.

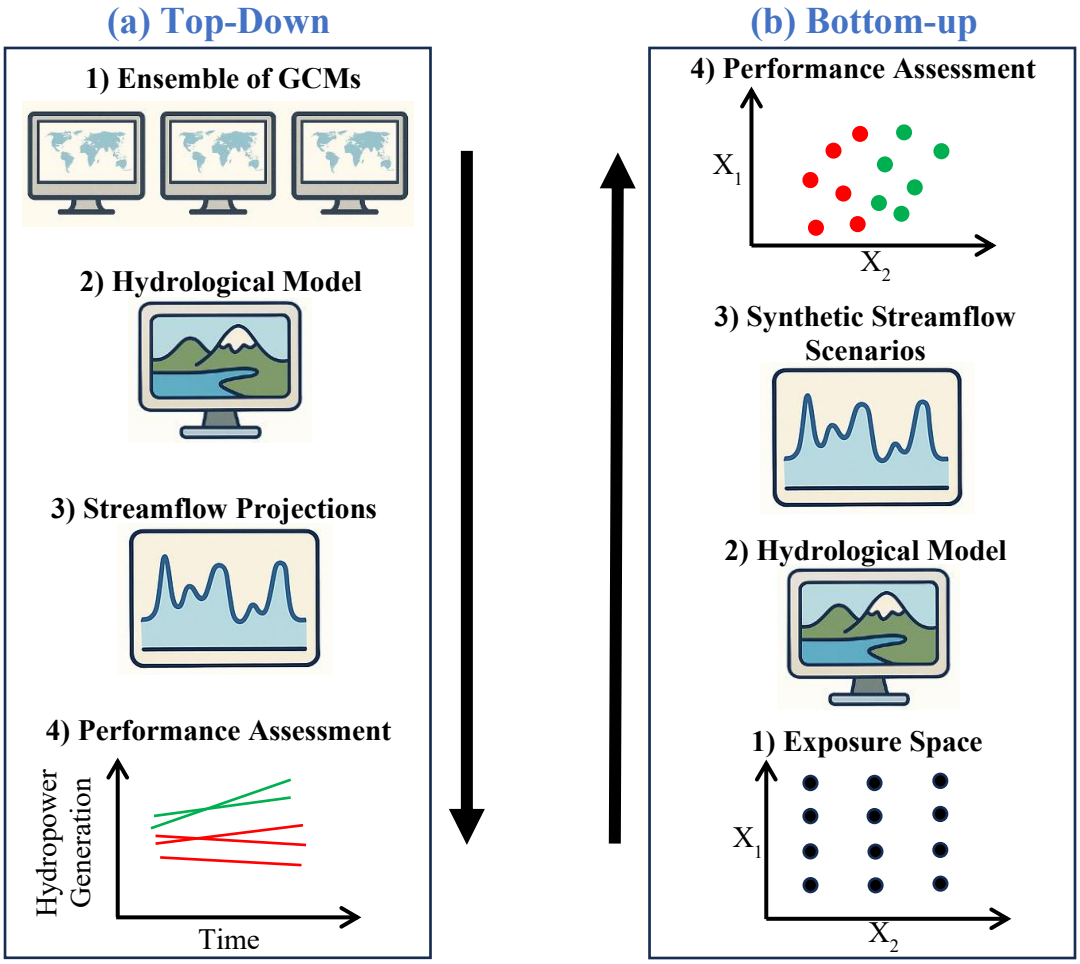


Figure 1.1. Conceptual illustration of top-down and bottom-up approaches for climate change impact assessment of hydropower systems. Axes X_1 and X_2 represent statistical properties (e.g., mean) of climate variables (e.g., air temperature) or hydrologic variables (e.g., streamflow). Therefore, dots denote possible climate or hydrologic conditions. Green indicates satisfactory hydropower performance, while red indicates unsatisfactory performance.

Both stochastic weather generators and stochastic streamflow generators generally lack the ability to ensure that generated (climate or streamflow) scenarios precisely achieve specified (target) statistical properties, due to the non-linear relationship between generator parameters and the resulting statistical properties (Guo et al., 2016). Consequently, the statistical properties

defined in the forcing exposure space differ from those computed in the resultant exposure space. This process is referred to as the forward approach (Figure 1.2). This lack of control over stochastic generators introduces three main challenges for bottom-up applications:

- Mismatch with physical and operational triggers: Undesired system outcomes may not be revealed if resulting scenarios fail to reproduce the hydrologic patterns that physically and operationally trigger unsatisfactory system performance. For example, low-flow conditions with the required magnitude and timing to induce hydropower underperformance may not be adequately represented.
- Insufficient extent of the exposure space: The exposure space may not span a sufficiently wide range of inflow conditions, resulting in scenarios that fail to generate a diverse range of desired and undesired system performance outcomes.
- Inefficient or uneven sampling of inflow conditions: The exposure space may not be uniformly sampled, leading to over-representation of some plausible inflow conditions and under-representation of others. Under-sampling increases the risk of missing critical system behavior, while over-sampling provides limited additional insight and increases computational cost.

To address these challenges, one commonly used approach is to rescale synthetic streamflow scenarios using multipliers to match target statistical properties. For example, Quinn et al. (2018) applied multipliers in log-space to perturb streamflow magnitude, variability, and seasonality for hydropower assessment under inflow uncertainty. However, interactions among these multipliers during transformation from log-space to real-space prevent real-space statistical targets from being directly achieved or uniformly sampled (Quinn et al., 2018). Targeting and uniformly sampling the exposure space in real space provides greater transparency and interpretability for decision-makers. For instance, a 20% increase in streamflow variability can be explicitly quantified (e.g., ±50 m^3/s to ±60 m^3/s), whereas an equivalent change in log-space variability lacks a clear physical interpretation due to the properties of the lognormal transformation. Direct rescaling approaches in real space remain limited, as existing multiplier-based methods can adjust streamflow magnitude and seasonal timing but do not allow simultaneous control of streamflow variability to achieve specified target values.

To address the challenges associated with rescaling approaches, an inverse approach (Figure 1.2) is introduced, in which the parameters of a stochastic generator are optimized to achieve desired real-space statistical targets in the resulting exposure space (Guo et al., 2016). Applying this approach on stochastic weather generators entails substantial computational expense (i.e., wall-clock runtime for scenario generation) because runoff and streamflow are influenced by multiple hydrometeorological variables, such as precipitation, temperature, humidity, and wind speed, each of which must be explicitly targeted during optimization. Subsequent studies reduced this burden by limiting the number of optimized variables (Guo et al., 2017) and by constraining parameter ranges or using penalty-based objective functions (Culley et al., 2019). Nevertheless, weather-generator-based inverse approaches still require repeated hydrological simulation. In contrast, applying the inverse approach to stochastic streamflow generators enables computationally efficient scenario generation, bypassing the need for hydrological model simulation, and affording direct manipulation of streamflow statistical properties.

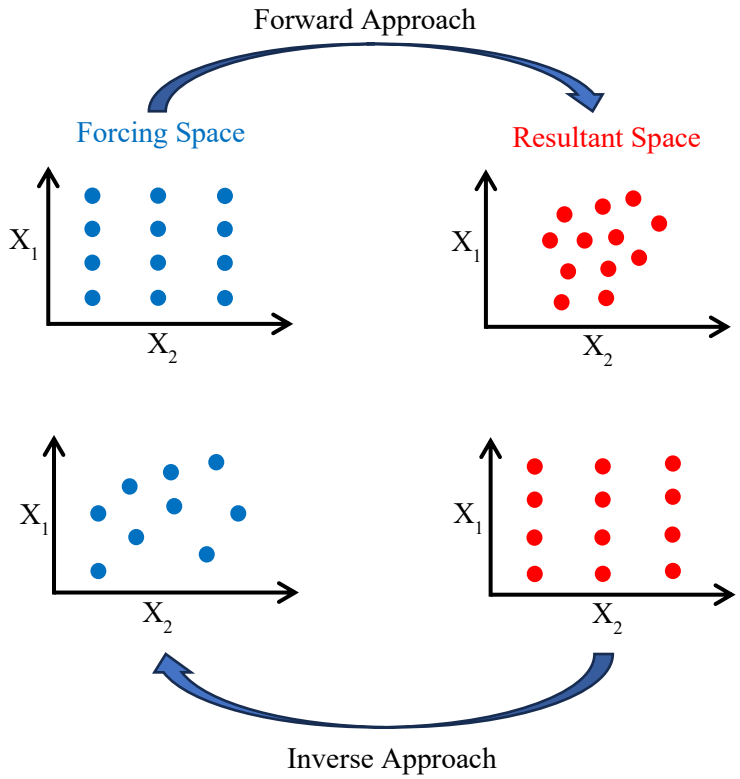


Figure 1.2. Illustration of forward and inverse approaches for using stochastic generators. Axes X_1 and X_2 represent selected statistical properties (e.g., mean) of climate variables (e.g., air temperature) or hydrologic variables (e.g., streamflow). Each dot denotes a plausible climate or hydrologic condition on the exposure space.

This research objective therefore seeks to develop a framework that applies the inverse approach to a stochastic streamflow generator, enabling direct control of streamflow properties (including magnitude, variability, and seasonality) in real space. This enables uniform and interpretable sampling of the exposure space and supports computationally efficient bottom-up hydropower impact assessment.

1.2.3 Developing a Stress-testing Framework for Climate Change Impact Assessment

In Canada, climate change impacts on hydropower generation and the development of adaptive operational policies have been assessed predominantly through the top-down approach (Arsenault et al., 2013; Haguma et al., 2017a, 2017b, 2015, 2014; Haguma and Leconte, 2018; Huaringa Alvarez et al., 2014; Kim et al., 2022; Minville et al., 2010b, 2010a, 2009; Sant'Anna et al., 2022; Sant'Anna and Tilmant, 2025). Applications in Quebec by Haguma et al. (2017b, 2015, 2014) and Minville et al. (2010b, 2009) projected increasing hydropower generation for the stations in Manicouagan and the Peribonka rivers in Quebec by applying adaptation policies to system operations. In contrast, Mandal et al. (2019) projected a decrease in future hydropower generation for the Campbell River basin in British Columbia, under current operating policies.

In Manitoba, two top-down studies have examined the impacts of climate change on hydropower generation in the Lower Nelson River Basin under existing reservoir regulation strategies. Kim et al. (2022) examined hydropower potential generation at seasonal and annual scales, projecting higher spring-summer but lower winter-fall generation with a slight upward annual trend. Lees (2022) focused exclusively on winter generation, projecting shorter and warmer ice-affected seasonality that increases cumulative winter outflow and provides the opportunity for hydropower generation increases. Notably, the differing winter results reflect the contrasting approach of Lees (2022), who focused on outlet hydraulics, versus Kim et al. (2022) who examined basin-scale water supply without accounting for shifts in ice impacts on operations and hydropower generation. Collectively, these findings indicate that seasonal changes are more robust than long-term annual trends, emphasizing the importance of adaptive management for Manitoba's hydropower system.

Employing the bottom-up approach provides the opportunity to bypass the exclusive reliance on uncertain streamflow projections derived from top-down approaches, and significant computational demand of hydrological simulation within the Manitoba Hydro system watershed

(~1.1 M km^2). Despite its growing international applications (Bhattarai et al., 2024; François et al., 2018; Yuan Liu et al., 2023; Quinn et al., 2018, 2017; Ray et al., 2018; Taner et al., 2017; Wasti et al., 2022; Wild et al., 2019), the bottom-up assessment of hydropower generation remains limited in Canada. Some Canadian studies have incorporated components related to bottom-up approaches, but these applications have generally been partial. For example, Côté et al. (2011) used synthetically generated hydroclimatic inputs to evaluate stochastic operating policies, while Jabbari & Nazemi (2019) used historical climate trends and statistical relationships to assess changes in Canadian hydropower generation potential. More recently, Sant'Anna et al. (2022) proposed a hydrologically driven adaptation assessment using clustered GCM-based hydrological projections and robustness evaluation of operating policies. However, these studies do not fully represent a bottom-up assessment, as they either focus on operating policy comparison, trend extrapolation, or projection-based hydrological scenarios rather than evaluating system response using projection-independent inflow scenarios.

The bottom-up approach can be extended to support stress-testing analyses for hydropower systems (François et al., 2018; Quinn et al., 2018; Ray et al., 2018; Taner et al., 2017). Stress testing provides additional insight into water system behavior by identifying inflow conditions under which system performance degrades or becomes unacceptable (Fowler et al., 2024). The boundary separating satisfactory and unsatisfactory outcomes (in step 4 of Figure 1.1b) defines the system's critical threshold conditions, beyond which undesirable system performance occurs.

Accounting for electricity demand extends the bottom-up assessment beyond hydropower generation potential, and facilitates evaluation of the system capability to meet electricity demand, or the severity of deficits when demand is not fully satisfied. This makes the assessment more directly relevant to operational and planning decisions across the time horizons considered. Although this dimension was not included in the Manitoba-focused studies by Lees (2022) and Kim et al. (2022), it is actively considered by Manitoba Hydro as part of its planning process (Manitoba Hydro, 2023b). Several top-down studies have incorporated electricity demand using regression-based models (Gaudard et al., 2013; Qin et al., 2020b), artificial neural networks (Hou et al., 2021), or machine learning methods (Obahoundje et al., 2022), with independent variables such as GDP, population, and climate indicators (e.g., air temperature) used to project future electricity demands. Other top-down studies assumed constant energy demand (Li et al., 2020;

Yuan Liu et al., 2023; Mandal et al., 2019) or relied on external agency projections (Chowdhury et al., 2021). Within the bottom-up literature, only François et al. (2018) explicitly incorporated electricity demand, estimating it using a piecewise linear function of air temperature. Air temperature alone is, however, insufficient to capture the drivers of future electricity demand, particularly in Manitoba, where the electrification of transportation and space heating is expected to be the primary contributor to the long-term demand growth (Manitoba Hydro, 2023b).

The third and final research objective therefore seeks to develop a transferable stress-testing framework for evaluating hydropower system performance. The framework is designed to support systematic assessment of how hydropower systems respond to a wide range of plausible inflow conditions, while generating clear and decision-relevant insights into hydropower planning and climate adaptation. This framework is demonstrated through application to the Manitoba hydropower system, representing the first bottom-up assessment of hydropower generation in Manitoba. The application expands the spatial scope of prior Manitoba-based studies (Kim et al., 2022; Lees, 2022) to include the entire provincial hydropower system. In addition, the assessment explicitly incorporates future electricity demand scenario, developed based on provincial demand projections reported by Manitoba Hydro (2023a), enabling a more comprehensive and decision-relevant assessment of hydropower system behavior under changing climatic and energy demand conditions.

1.3 Thesis Content and Contributions

The remainder of this thesis comprises four chapters. Chapters 2 to 4 closely mirror two peer-reviewed published research papers and one manuscript currently under peer review, each containing independent literature reviews, methodologies, results, and discussions. Although each chapter concludes with a brief summary, Chapter 5 provides comprehensive concluding remarks and outlines recommendations for future research.

Chapter 2 presents a published research article addressing Objective 1 (*Developing a Hydropower System Simulation Tool*). This publication introduces and evaluates a comprehensive hydropower simulation tool developed for Manitoba large-scale, cold-regions river-reservoir system. The initial model structure was developed by Beiraghdar (2019) and subsequently improved by Phoebe Riddell under the supervision of Masoud Asadzadeh and the author. Building

on this foundation, the author, Gozini, H., further developed, refined, and evaluated the simulation tool, including updating the model structure, improving the representation of system operations, extending spatial boundary of the model, conducting model simulations, analyzing results, and preparing the manuscript. Co-authors provided supervisory guidance, technical feedback, and critical review throughout the development of the study and manuscript. In this chapter, Table 2.4 has been modified from the version presented in the published paper. The modification applies to the weighted average Kling-Gupta Efficiency (KGE) for water level simulation in sub-system 1 and consequently the whole model (MB_HydroSim), which increased from 0.54 to 0.86, indicating improved model performance. This modification does not alter the interpretation, conclusions, or implications of the water level simulation presented in the manuscript. Therefore, the associated analyses and discussions in both the main text and Supplementary Material remain unchanged.

- **Gozini, H.**, Asadzadeh, M., Stadnyk, T.A., Riddell, P., Tolossa, H., (2026). Integrated Water Resources and Hydropower Generation Modelling in a Complex, Cold-Regions River-Reservoir System. *Sustainable Water Resources Management*. 12, 20. https://doi.org/10.1007/s40899-026-01335-7.

Chapter 3 presents a published research article addressing Objective 2 (*Developing a Streamflow Scenario Generator*Developing). This publication introduces a computationally efficient framework for generating synthetic streamflow scenarios that directly target key statistical properties of streamflow (magnitude, variability, and seasonality) at multiple locations, enabling systematic exploration of inflow uncertainty for water system planning. The author, Gozini, H. led the conceptual development of the framework, implementation of the scenario generation methodology, preparation and processing of streamflow data, design of the multisite scenario generation experiments, analysis and interpretation of results, and preparation of the manuscript. Co-authors provided supervisory guidance, technical feedback, and critical review throughout the development of the study and manuscript.

- **Gozini, H.**, Asadzadeh, M., Stadnyk, T., Slota, P., (2026). Inflow Generation for Water System Planning in Multisite Studies Using Target Synthetic Streamflow Generation. *Water Resources Research*. 62. https://doi.org/10.1029/2025WR042355.

Chapter 4 presents a submitted (under review) research article addressing Objective 3 (*Developing a Stress-testing Framework for Climate Change Impact Assessment*). This

publication introduces a transferable stress-testing framework for evaluating hydropower systems under deep inflow uncertainty and electricity demand change and demonstrates its application to the Manitoba hydropower system. The author, Gozini, H. led the conceptual development of the stress-testing framework, prepared and processed the inflow and electricity demand scenarios, conducted the hydropower system simulations, evaluated system performance across annual and seasonal scales, analyzed and interpreted the results, and prepared the manuscript. Co-authors provided supervisory guidance, technical feedback, support in interpreting the findings, and critical review throughout the development of the study.

- **Gozini, H**., Asadzadeh, M., Stadnyk, T.A., Razavi, S., (2026). Decision-Relevant Stress Testing of Hydropower Systems Under Deep Inflow Uncertainty and Electricity Supply-Demand Change. Manuscript submitted for publication to *Results in Engineering*.

CHAPTER 2. INTEGRATED WATER RESOURCES AND HYDROPOWER GENERATION MODELLING IN A COMPLEX, COLD-REGIONS RIVER-RESERVOIR SYSTEM

2.1 Abstract

The Province of Manitoba is highly dependent on hydropower, with 97% of its electricity generated from the extensive network of large rivers and lakes. A complex system of 28 major lakes and 43 major control points regulates the flow to and through 16 hydropower stations in Manitoba, having a combined nominal capacity of 5,926 MW. The expansive watershed (1.4 million km^2 drainage area) feeding this system extends across the drought-prone Canadian Prairie and westward to the Rocky Mountains of Canada. This study introduces MB_HydroSim, an advanced, transboundary, and comprehensive simulation tool developed for Integrated Water Resources Management in Manitoba, focusing on hydropower generation. MB_HydroSim addresses the lack of a single tool that integrates the hydrological and operational complexities of an expansive cold-regions river-reservoir system, incorporating operational rules and ice impacts. MODSIM-DSS is used to develop MB_HydroSim, simulating daily water level, outflow, and hydropower generation. MB_HydroSim is evaluated against observed data from 1980 to 2017 using a spatially weighted average monthly KGE, demonstrating high accuracy in simulating water level (KGE=0.86), outflow (KGE=0.85), and hydropower generation (KGE=0.94) across the system. Therefore, MB_HydroSim is a reliable tool that can be further utilized to analyze the future of hydropower generation in Manitoba, a region facing climate change and increasing electricity demands. Additionally, MB_HydroSim can be employed for sensitivity analysis, development of adaptation policies, and calculating the impact of ice-cover on hydropower generation. Collectively, these capabilities position MB_HydroSim as a fundamental tool for advancing Water-Energy Nexus assessments in the Province.

2.2 Introduction

In the Province of Manitoba, approximately 97% of electricity is sourced from 16 hydropower stations, which is the highest rate among Canadian provinces (Canada Energy Regulator, 2024). In comparison to the largest producers of hydroelectricity (China, Brazil, and the US), the river-

reservoir system of Manitoba has a unique set of characteristics. It is massive and complex due to the presence of over 100,000 lakes and numerous rivers and tributaries, approximately covering 16% of the Province (Government of Manitoba, 2025b). In addition, it is a cold-regions river-reservoir system, subject to seasonal snow and ice cover, impacting operations and hydropower generation (Lees et al., 2023). Compared with the cold-regions hydropower systems in Norway and Sweden, the river-reservoir system of Manitoba has limited water storage capacity, with less than four months supply due to the flat landscape of the Province. Water is supplied from an extensive river network stretching across three Prairie Provinces and originating in the Canadian Rocky Mountains and the Western part of the Canadian Shield.

Canada has experienced an increase in the annual mean temperature by 1.7 ºC from 1984 to 2016, which is twice the global average rate of warming for the same period (Bush & Lemmen, 2019). This increasing rate is 0.2 ºC higher for the Canadian Prairies over the same period (Bush & Lemmen, 2019). Consequently, the Canadian Prairies are drought-prone due to projected smaller snowpacks and earlier snow and ice melt associated with rising temperature (Bush & Lemmen, 2019). However, there is considerable uncertainty in the future drought projections due to the low model agreement on the projected trends and amounts of runoff and streamflow (Kim et al., 2022). The offset between the water supply peak in spring and the electricity demand peak in winter in such a drought-prone region, coupled with growing electricity demand (Canada Energy Regulator, 2024) and the limited water storage capacity, creates a considerable challenge in planning to meet future electricity needs of the Province.

Manitoba Hydro (MH) is the sole electricity provider in the Province, operating hydropower plants, fossil fuel generation, purchasing non-utility generation (including from wind and solar facilities) and the transmission network for distributing the electricity. The dominant energy supply is water, regulated by MH and other departments and organizations both within and outside of Manitoba. Each department currently uses its separate water management simulation tool. As a result of fragmented Provincial and Territorial water management practices in Canada (Arnal et al., 2023), there is no comprehensive, integrated (transboundary) simulation tool for MH's system. Such a tool would encompass major rivers, lakes, and reservoirs, and integrate operational decisions both within and outside the Province, impacting the water supply and net hydropower generation potential. Therefore, it is essential to have a reliable and efficient Decision Support

System (DSS) tool that closely reflects the interrelated complexities of changing water resource availability and seasonality with system operations and resulting hydropower generation. Such a DSS tool affords informed decisions and the assessment of trade-offs to best mitigate the negative impacts and maximize the benefits of potential opportunities.

Hydropower simulation models are extensively employed in the studies aimed at quantitatively assessing the impacts of climate change on future hydropower generation (see Table 2.1). While these studies reported spatially different trends in future hydropower generation, they all emphasized the importance of adaptation and highlighted opportunities to enhance hydropower generation. For such evaluation, inflow was forecasted by hydrological models or generated using stochastic scenario generators, which serve as the input to the hydropower simulation models. This approach was applied to the dam(s) or cascade(s) of reservoirs within a single river system or basin, as well as multi-basins or large-scale studies.

Recently, there has been a growing motivation to study the impacts of climate change on hydropower at large spatial scales (Turner and Voisin, 2022). Simulation-optimization was predominantly employed in hydropower simulation models (see Table 2.1), aiming to maximize hydropower generation or profit while considering other critical criteria within the system, such as water supply deficit. Dynamic, linear, and non-linear programming were used to derive optimal operational rules. This highlights the challenges of incorporating real system operations, specifically in large-scale studies, and the academic tendency to assume that the operators optimize the operation and profit of hydroelectricity generation. The remaining hydropower simulation models utilized software packages such as MODSIM-DSS, System Dynamics, and Machine Learning, or mass-balance equations, complemented by simple operational rules. The simplest hydropower simulation models estimated the changes in hydropower generation based on the variations in reservoir inflow, using the historical relationship between them (Graham et al., 2007). The literature indicates a lack of large-scale studies in Canada, despite such studies being conducted for other major contributors to global hydropower generation. To achieve this, the first necessary step is to develop a large-scale hydropower simulation tool. Moreover, in cold-regions countries like Sweden and Norway, hydropower simulation models are primarily based on simulation-optimization techniques.

Table 2.1. The summary of worldwide studies that employed hydropower simulation models. Blue color represents large-scale (i.e., multi-basins) studies. N is the number of hydropower stations included in the study.

Study: N, Country	Hydropower Simulation	Operation Rule	Study: N, Country	Hydropower Simulation	Operation Rule
Graham et al. (2007): 15, Sweden	Linear Regression	-	Qin et al. (2020a, 2020b): 5 and 21, China	Mass-balance	Water level rule curve
Minville et al. (2010b, 2009): 3, Canada	Simulation-Optimization	Dynamic programming	Caceres et al. (2021): 134, Brazil, Colombia, and Peru	Simulation-Optimization	Dynamic programming
Gaudard et al. (2013): 3, Switzerland	Simulation-Optimization	Non-linear programming	Chowdhury et al. (2021): 14, Southeast Asia	Simulation-Optimization	Linear programming
Jamali et al. (2013): 6, Iran	MODSIM-DSS	Outflow rule curve	Dallison et al. (2021): 25, the UK	Mass-balance	Water allocation licenses
Graabak et al. (2017): multiple, Norway	Simulation-Optimization	Stochastic dynamic programming	Hou et al. (2021): 1, Iran	Mass-balance	Not mentioned
Haguma et al. (2014, 2017): 5, Canada	Simulation-Optimization	Dynamic programming	Kim et al. (2022): 7, Canada	MODSIM-DSS	Median recorded water level
Ng et al. (2017): 1593, World	Simulation-Optimization	Stochastic dynamic programming	Sakki et al. (2022): 1, Greece	Simulation-Optimization	Non-linear programming
Quinn et al. (2017, 2018): 5, Vietnam	Simulation-Optimization	Non-linear programming	Obahoundje et al. (2022): 1, Togo	Machine Learning	-
Zhou et al. (2018): 149, the US	Mass-balance	Calibrated operational coefficients	Spanoudaki et al. (2022): 1, Greece	Mass-balance	Constant water level
Mandal et al. (2019): 2, Canada	System Dynamics	Operating zone for water level	Zhao et al. (2022): 5, China	Mass-balance	Outflow rule curve
Wild et al. (2019): 1, Cambodia	Simulation-Optimization	Non-linear programming	de Oliveira Serrão et al. (2023): 1, Brazil	Mass-balance	Not mentioned
Li et al. (2020): 5, China	Simulation-Optimization	Dynamic programming	Yuan Liu et al. (2023): 3, China	Simulation-Optimization	Dynamic programming
Liu et al. (2020): 12, China	Simulation-Optimization	Dynamic programming	Widén et al. (2024): 19, Sweden	Simulation-Optimization	Stochastic dynamic programming

Integrated Water Resources Management (IWRM) aims to balance social, economic, and environmental needs by involving all water sector users (like agriculture, industry, and municipal) and stakeholders (such as government, local communities, and private sectors). The objectives of the Water-Energy (WE) Nexus approach align with the aims of IWRM, but with a focus on the energy sector (Candido et al., 2022). The WE Nexus recognizes the interdependencies among water and energy sectors and assesses the impacts of decisions made in one sector on the other, thereby addressing the synergies and trade-offs among them (Gozini et al., 2021). Recent literature has increasingly focused on understanding the WE Nexus from a quantitative perspective (Fontenelle et al., 2022). To compare both approaches, a compelling example is the simulation of a multi-purpose reservoir. The IWRM approach focuses on balancing water allocation among various water sector users (including hydropower) and addressing the interests of multiple stakeholders. The WE Nexus approach suggests adding a model for the energy sector. This allows for a more comprehensive simulation that includes effective factors from the energy sector, such

as population, electricity price, electricity export, and transmission constraints and developments, and their dynamic impact on the operation of the dam.

MODSIM-DSS is an IWRM tool (Labadie, 2006). It is efficient and flexible making it well-suited for simulating complex river-reservoir systems, such as those in Manitoba. Although it is not an open-source tool, it offers custom coding in C#.NET or VB.NET for modelling any operational rules and hydraulics relationships. IWMSask, the integrated water management model of the Saskatchewan River Basin upstream of Manitoba, is an example of using MODSIM-DSS to develop a valuable tool for stakeholders and decision-makers to understand the interconnected complexities of the basin (Ali Shah, 2019). This model was further utilized for hydro-economic modelling (Eamen et al., 2021, 2022). Another example is the MODSIM-DSS model developed for Lake Winnipeg and Southern Indian Lake outlet systems, located in Manitoba (Beiraghdar, 2019). The case study covered roughly 80% of hydropower generation capacity in Manitoba. The model adequately simulated historical hydropower generation, outflow, and water level; however, inconsistencies arose because lake operations solely relied on daily median recorded water levels. Thus, the method failed to accurately simulate lake-level dynamics during periods when observed conditions deviated significantly from the median. This model was successfully coupled with hydrologic models to estimate water supply and hydropower generation changes under future climate scenarios in the Lower Nelson River Basin (Kim et al., 2022).

In this study, a hydropower simulation tool called MB_HydroSim is developed for Manitoba by extending and improving the MODSIM-DSS model developed by Beiraghdar (2019). The extension broadens the spatial scale to encompass all hydropower generation stations in Manitoba, as well as the major control points regulating inflows from upstream into the hydropower system. The improvements involve equipping the model with explicit and implicitly derived operational rules in place of daily median recorded water levels. This enhances the accuracy and realism of simulation outcomes by enabling the simulation of lake-level dynamics that differ from the median condition. Compared to the previous MODSIM-DSS models developed by Ali Shah (2019) and Jamali et al. (2013), which relied on standard configurations without custom coding, MB_HydroSim integrates complex operational rules implemented through custom coding. This provides a transferable example for developing and customizing MODSIM-DSS for other complex case studies. Serving as a DSS tool, MB_HydroSim plays a crucial role in simulating the decision-

making process on a single platform for the entire Province. Therefore, MB_HydroSim can extend the analysis of Kim et al. (2022), to address future hydropower generation challenges across the entire Province.

MB_HydroSim is in the context of IWRM because it integrates a diverse and complex river-reservoir system managed by different departments and organizations and extends the spatial boundary beyond Manitoba to include regulated inflow entering the provincial hydropower network. Developing MB_HydroSim offers the following novelties in the context of hydropower simulation models:

1. Unique Case Study: MB_HydroSim is developed for an expansive, complex, and drought-prone cold-regions river-reservoir system with limited water storage capacity. Although demonstrated for the Manitoba hydropower system, the custom coding of rule-based operations within MODSIM-DSS is readily transferable to other complex water-resource systems.
2. Large-Scale Example: MB_HydroSim provides an example of a large-scale hydropower simulation model in Canada, offering a tool for future climate impact assessment on a large spatial scale.
3. Operational-Based Approach: MB_HydroSim uses the existing explicit and implicitly derived operational rules instead of applying simulation-optimization methods which are dominant in large-scale models. It employs complex operations varying for different locations, seasons, and hydrological conditions. Moreover, operational equations were developed and used for locations lacking explicitly defined operations.

2.3 Study Area

Our study area (cream-colored area in Figure 2.1) is the river-reservoir and hydropower generation systems in Manitoba. It is the 30% most downstream portion of the 1.4 million km^2 Nelson-Churchill River Basin (NCRB). 11% of the NCRB catchment area is accounted for water bodies (Bajracharya et al., 2023). NCRB drains the Canadian Rockies, parts of the north-central United States, and parts of north-western Ontario into Manitoba and finally Hudson Bay located in the north-eastern part of the Province (Kim et al., 2022). Due to higher winter temperatures and other factors, such as better soil conditions for agriculture, most settlements are in the southern

part of the basin (Bajracharya et al., 2023). The major rivers that feed MH's system include the Saskatchewan, Assiniboine, Red, Winnipeg, and Churchill Rivers. The major lakes in our study area are Lakes Winnipeg, Manitoba, Winnipegosis, Cedar, St. Martin, Southern Indian, St. Joseph, Lac Seul, Rainy, and Lake of the Woods.

2.3.1 Hydropower Generation in Manitoba

MH generates 97% of its electricity from hydropower stations, which is the highest rate among provinces in Canada (Canada Energy Regulator, 2024). Hydropower generation capacity ranges between 10 MW to 1350 MW (Table 2.2). Six hydropower stations are located along the Nelson River and another station on the Burntwood River, with a combined hydropower generation capacity of 4857 MW (*V*, *W*, *X*, *Y*, *Z*, *AA*, and *AC* in Figure 2.1). They have the highest capacity, making up 81.96% of the hydropower generation capacity in Manitoba. The last three hydropower stations downstream of Nelson River, named Kettle, Long Spruce, and Limestone, have the highest generation capacity (1220, 980, and 1350 MW, respectively) in the Province. Limestone and Wuskwatim were added to the hydropower system in 1991 and 2012, respectively. In 2021, the Keeyask hydropower station added 695 MW to the lower Nelson River upstream of Kettle; however, this development falls outside of the temporal scope of this study. The cascade of six hydropower stations along the Winnipeg River, with a combined capacity of 580 MW (*M*, *N*, *O*, *P*, *Q*, and *R* in Figure 2.1), has the second-highest capacity, making up 9.79% of the hydropower generation capacity in Manitoba. Pointe Du Bois, the oldest hydropower station in the Province, started service in 1911. Located downstream of the Saskatchewan River sub-basin, the Grand Rapids hydropower station contributes to 8.08% (479 MW) of the hydropower generation capacity in Manitoba (*B* in Figure 2.1). Two relatively small hydropower stations situated within the Churchill River sub-basin contribute only 0.17%. Primarily used to support local electricity demand, these stations are located upstream of major reservoirs and do not significantly impact the simulation and management of the rest of the system. Therefore, they were excluded from MB_HydroSim. Generation capacity and transmission systems have been upgraded at several plants. One example is the increase in capacity of Grand Rapids between 1995 and 2000.

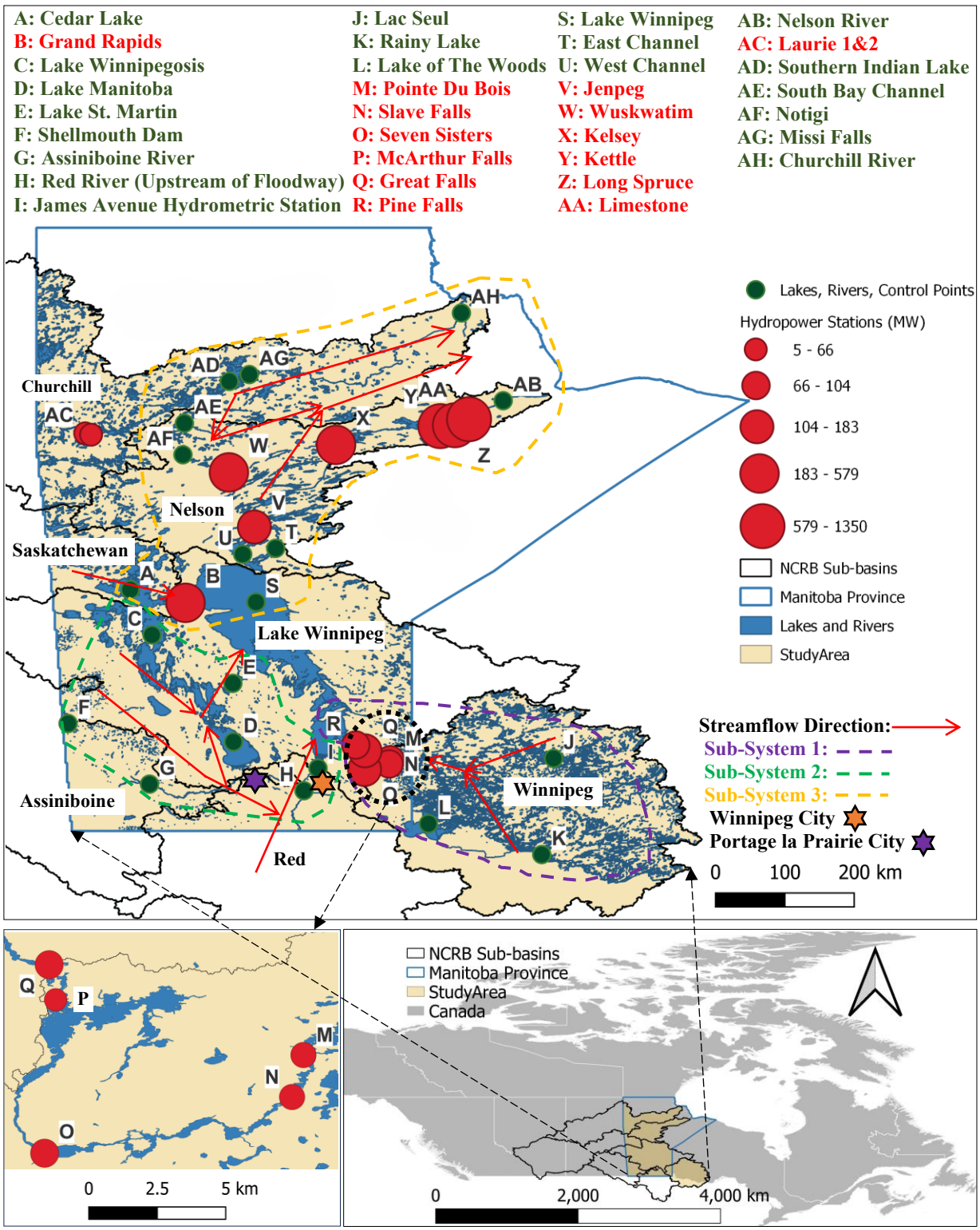


Figure 2.1. Location of NCRB (black solid border), study area (cream-colored area), hydropower stations (red-filled circles), lake, rivers, and important control points (green-filled circles) (NCRB and its sub-basins boundary shapefile is extracted from Ahmed et al. (2024), Manitoba boundary from https://geoportal.gov.mb.ca/, Canada boundary from https://www12.statcan.gc.ca/, and lakes and rivers from https://open.canada.ca/)

Table 2.2. Hydropower stations in Manitoba (Manitoba Hydro, 2025)

Basin	River	Hydropower Station Name	Capacity (MW)	Percentage (%)
Churchill River	Laurie	Laurie River 1&2	10	0.17
Nelson River	Nelson	Jenpeg	115	81.96
	Nelson	Kelsey	286	
	Nelson	Keeyask	695	
	Nelson	Kettle	1220	
	Nelson	Long Spruce	980	
	Nelson	Limestone	1350	
	Burntwood	Wuskwatim	211	
Saskatchewan River	Saskatchewan	Grand Rapids	479	8.08
Winnipeg River	Winnipeg	Pointe Du Bois	75	9.79
	Winnipeg	Slave Falls	68	
	Winnipeg	Seven Sisters	165	
	Winnipeg	McArthur Falls	56	
	Winnipeg	Great Falls	129	
Lake Winnipeg	Winnipeg	Pine Falls	87	

2.3.2 Control Points

As the largest lake in the system, Lake Winnipeg (*S* in Figure 2.1) serves as the most important control point for streamflow regulation in the Province. Roughly 40% of MH's available storage capacity is sourced from Lake Winnipeg (Gozini et al., 2023). The average daily inflow to Lake Winnipeg is recorded 2320 m^3/s. The main inflows to Lake Winnipeg are regulated along the Winnipeg, Red, Assiniboine, and Saskatchewan Rivers and the western part of Lake Winnipeg sub-basins.

Winnipeg River contributes 42% (980 m^3/s) to the average daily inflow to Lake Winnipeg. The inflow to the Winnipeg River and its hydropower stations (*M*, *N*, *O*, *P*, *Q*, and *R* in Figure 2.1) is regulated mainly on Lac Seul, Rainy Lake, and Lake of the Woods (*J*, *K*, and *L* in Figure 2.1) in the Ontario Province. The International Rainy-Lake of the Woods Watershed Board (IRLWWB) and Lake of the Woods Control Board (LWCB) are the organizations tasked with regulating these lakes in Ontario.

Cedar Lake (*A* in Figure 2.1) and its hydropower station, Grand Rapids (*B* in Figure 2.1), contribute 25% (590 m^3/s) to the average daily inflow to Lake Winnipeg. The inflow to Cedar Lake is regulated upstream in the provinces of Saskatchewan and Alberta. MH regulates the Grand Rapids station.

Assiniboine River (*G* in Figure 2.1) joins Red River (*H* in Figure 2.1) in Winnipeg City (Orange Start in Figure 2.1) and flows to Lake Winnipeg. These two rivers contribute 12% (282 m^3/s) to the average daily inflow to Lake Winnipeg. Lakes Winnipegosis, Manitoba, and St. Martin (*C*, *D*,

and *E* in Figure 2.1) form a river-reservoir system of three lakes. This system contributes 5% (109 m^3/s) to the average daily inflow to Lake Winnipeg. The Hydrologic Forecast Centre (HFC) is the regulatory agency responsible for operating river-reservoir systems in the Assiniboine River, Red River, and the western part of the Lake Winnipeg sub-basins. Their focus primarily involves flood management, with four key control points:

- Fairford control structure: constructed at the outlet of Lake Manitoba and controls the lake outflow.
- Shellmouth Dam (*F* in Figure 2.1): constructed at the outlet of Lake of the Prairies and used to manage streamflow along the Assiniboine River.
- Portage Diversion: located upstream of Portage la Prairie City (Purple Start in Figure 2.1) and diverts the Assiniboine River flow to Lake Manitoba. Russel, Miniota, Brandon, and Holland are the hydrometric stations located along the Assiniboine River and between Shellmouth and Portage Diversion. Southport and Headingly are the other important hydrometric stations located between Portage Diversion and Winnipeg City.
- Red River Floodway: situated upstream of Winnipeg City and provides a bypass for Red River flow (*H* in Figure 2.1). The Red River naturally joins the Assiniboine River in Winnipeg City. The water level at James Avenue hydrometric station (*I* in Figure 2.1) is the criterion to rule the Portage Diversion and Red River floodway.

Lake Winnipeg outflow passes through the East and West Channels (*T* and *U* in Figure 2.1). The West Channel links Lake Winnipeg with Jenpeg (*V* in Figure 2.1), the first control and hydropower station downstream of the lake. Jenpeg controls Lake Winnipeg outflow to a series of lakes and hydropower stations along the Nelson River (*X*, *Y*, *Z*, and *AA* in Figure 2.1). The West Channel conveys approximately 85% (1953 m^3/s on average) of the daily outflow from Lake Winnipeg. The flow from the East Channel converges with the Nelson River downstream of Jenpeg, ultimately flowing into Hudson Bay and the Arctic Ocean.

Southern Indian Lake (*AD* in Figure 2.1), located in the Churchill River sub-basin, is regulated by two control structures, Notigi and Missi Falls (*AF and AG* in Figure 2.1) (Manitoba Hydro, 2014). Water from Missi Falls flows down the Churchill River (*AH* in Figure 2.1) and ends up in Hudson Bay. Southern Indian Lake and Notigi are connected through the South Bay Channel (*AE* in Figure 2.1). Notigi diverts approximately 81% (776 cm on average) of Southern Indian Lake

daily outflow to the Nelson River. The West, East, and South Bay Channels are backwater-affected channels. For example, the outflow from Lake Winnipeg via the West Channel is dependent not only on the Lake Winnipeg water level but also on the water level at the forebay of Jenpeg. In other words, Jenpeg water level operations control both the outflow from Lake Winnipeg and Jenpeg itself. MH is the organization responsible for regulating the majority of the Manitoba river-reservoir systems in Saskatchewan, Churchill, and Nelson River sub-basins within the province of Manitoba.

2.3.3 Existing In-House Operational and Forecasting Tools

Currently, MH's models focus on the prediction of (water) supply, operations, and hydroelectricity generation using separate model interfaces, connected in a feed-forward modelling chain. MH runs hydrologic, e.g., WATFLOOD and HEC-HMS, and statistical models to predict system-wide water supply for the hydropower system. Reservoir operations for hydropower generation and control points use four simulation-optimization models for short-, mid-, and long-term system-wide analysis: MOST (Market Optimized Short-Term), an ST Vista model developed by Hatch; HERMES-EMMA (Hydro Electric Reservoir Management Evaluation System – Energy Management and Maintenance Optimization) developed by MH; and the SDDP (Stochastic Dual Dynamic Programming) and NCP models developed by PSR. Within these four models, the objective involves a weighted combination of various functions, including the revenue and costs from transactions with neighboring power systems (such as the Mid-Continent Independent System Operator (MISO)), the variable cost of hydroelectric and thermal generation sources, and the tradeoff between using storage in a given time step vs. saving the water for future use. Physical and operating limits on reservoir release, reservoir storage (water supply), electricity generation (including wind and solar) and transmission amounts, etc., are included as model constraints. Some of the constraints are defined with constraint violation penalties applied in the objective function. Models focused on longer-term horizons pass direction on reservoir management decisions to those with shorter-term horizons. In addition to the system-wide hydroelectric reservoir operation models, MH employs location-specific hydrological models to predict historical, current, near- and long-term water supply, as well as reservoir-specific models for release optimization. These models utilize rule sets that change in time and are specifically calibrated for the operation of the particular reservoir. Simplified energy models are also used to

estimate the sensitivity of energy generation potential under different inflow conditions. They use simplified assumptions that ignore system effects and reservoir operations impacts and are limited to estimates of annual energy production.

The HFC at Manitoba Transportation and Infrastructure (MTI) is another key department that regulates streamflow within the Province of Manitoba. HFC primarily focuses on providing accurate and timely forecasts of flows and water levels (referring to water surface elevation) for optimal operation of provincial water management infrastructure for flood and drought control. To achieve this, they have developed several hydrological models, such as WATFLOOD and HBV-IHMS, which simulate inflows into various parts of the system. HFC predicts inflows deterministically for a seven-day period using regional and global weather forecasts. For longer-term projections, historically recorded weather data from the last forty years is used to generate an ensemble of predictions. In locations lacking a hydrologic model setup, historic percentiles of observed inflows are instead used for forecasting. Streamflow and water levels at different control points are calculated based on the forecasted inflows and by utilizing stage-storage curves, stage-discharge rule curves, and regulatory guidelines. In addition, HEC-RAS is used for hydraulic routing and determination of the timing of peak flow and water level in urban or populated regions of the Province, or regions of water control, as part of their early warning and operational prediction systems.

2.4 Data

MH provided daily hydrometric and hydropower generation records (for MH's facilities) for the Nelson, Churchill, Saskatchewan, and Winnipeg River sub-basins. Hydrometric data provided by MH included records of daily water level (referring to water surface elevation), inflow (upstream and tributaries inflow), and outflow (through turbine and spill). Recorded data of water level at hydropower stations, separate turbine and spill outflow, and hydropower generation are not publicly available and are restricted for external researchers due to confidentiality policies enforced by MH. The remaining hydrometric data that was provided by MH can be found on the Environment and Climate Change Canada website (https://wateroffice.ec.gc.ca/index_e.html). Daily hydrometric recorded data for Assiniboine and Red River sub-basins, including water level, inflow, and outflow, was collected from the Environment and Climate Change Canada website. The 1980-2017 period was selected because it provides continuous data coverage for the entire

study area without any missing years or gaps. Inflow to the system is the most important input to the model. Other collected data including water level, outflow, and hydropower generation was used to evaluate the model performance.

The HFC provided the system configuration data, including operational rules, natural stage-discharge curves, and stage-storage curves, for control points, lakes, and reservoirs located in the Lake Winnipeg, Assiniboine, and Red River sub-basins. The operational rules included water level and outflow ranges and stage-discharge rule curves that vary for different seasons and inflow volumes. Natural stage-discharge curves were provided by HFC for uncontrolled outlets. Stage-storage curves were used to calculate the volume of water based on water level, and vice versa, in lakes and reservoirs. A summary of the general operational guidelines is available at https://www.gov.mb.ca/mti/wms/floodcontrol/index.html; however, access to detailed stage-discharge and stage-storage curves is restricted for external researchers due to confidentiality policies enforced by the HFC.

MH provided system configuration data, including natural stage-discharge curves, stage-storage curves, hydropower efficiency tables (for MH's facilities), and tailwater-discharge curves, in the Winnipeg, Saskatchewan, Churchill, and Nelson River sub-basins. These system configuration data are not publicly available to external researchers due to confidentiality restrictions. Natural stage-discharge curves were provided by MH for uncontrolled outlets. To enhance accuracy in estimating backwater-affected channel flow, MH provided 3D stage-discharge curves for the West, East, and South Bay channels. In these curves, channel flow can be estimated based on upstream and downstream water levels. Further details can be found in Gozini et al. (2023) ("*Backwater-affected (3D) stage-discharge curve*" section). Each hydropower station has its hydropower efficiency table. The efficiency and magnitude of hydropower generation vary for different values of flow and head. Determining the head involves the calculation of forebay using stage-storage curves, and tailwater derived from tailwater-discharge curves. MH does not have specific operational rules and instead uses its simulation and optimization models to inform reservoir release decisions. For the Winnipeg River sub-basin, operations were developed in this study based on historical data and the publicly available information at the IRLWWB (https://ijc.org/en/rlwwb) and LWCB websites (https://www.lwcb.ca/). Operational rules were primarily developed based on historical data for Saskatchewan, Churchill, and Nelson River sub-

basins. However, two published reports by Manitoba Hydro (2022, 2014) helped develop operational rules for two important lakes: Lake Winnipeg and Southern Indian Lake.

2.4.1 Inflow

The contribution of each sub-basin to the total amount of recorded inflow within the study area varies significantly. Churchill sub-basin has the highest contribution to the total recorded inflow, accounting for 30% with an average daily of 956 m^3/s. Winnipeg River sub-basin contributes 19% (618 m^3/s), Saskatchewan River sub-basin 18% (596 m^3/s), Lake Winnipeg sub-basin 16% (507 m^3/s), Nelson River sub-basin 8% (268 m^3/s), Red River sub-basin 7% (216 m^3/s), and Assiniboine River sub-basin 2% (79 m^3/s). Among the lakes, Southern Indian and Cedar have the highest rates of recorded inflow from outside of the study area, averaging 956 and 595 m^3/s, respectively. Across the study area, an average daily of 2320 m^3/s was recorded to be drained into Lake Winnipeg.

Alongside the recorded inflow, an additional category of flow data termed "local flow" was incorporated. It has been utilized by MH and HFC in their simulation, emphasizing its essential role in modeling the river-reservoir systems in Manitoba. The purpose of adding "local flow" is to encompass unmeasured inputs and losses. Unmeasured inputs include tributary inflows and precipitation over lakes, which are not accounted in the recorded inflow. Evaporation is the primary factor contributing to water loss from lakes. MODSIM-DSS cannot explicitly represent unrecorded tributary inflows and lake-surface precipitation and evaporation. Therefore, the "local flow" was calculated through the application of the mass-balance equation at the desired location using the recorded hydrometric data:

$$LF_t = S_{t+1} - S_t - I_t + O_t \tag{2.1}$$

Where LF is “local flow”, t is time (day from the start of the simulation), S is storage, I is inflow, and O is outflow. The calculated "local flow" in Equation (2.1) was considered "local inflow" when positive, or "local loss" when negative. Calculating the “local flow” with the mass-balance equation was done based on the assumption that the recorded hydrometric data and stage-storage curve, which converts water level to storage, are precise. However, measurement uncertainty is also inherent to the calculation of “local flow”, and can mislead water balance calculations in hydrological modelling (Moges et al., 2021). The "local flow" was calculated and assigned to the large lakes and reservoirs, as well as those for which MH and HFC reported a need for “local flow”

calculation in their simulation: St. Joseph, Lac Seul, Namakan, Rainy, Lake of the Woods, Whitedog, Shellmouth, Winnipeg, Winnipegosis, Manitoba, St. Martin, Southern Indian, Notigi, Jenpeg, Kelsey, and Kettle. In Table 2.3, the reported "local flow (%)" values are defined independently for each sub-basin, i.e., local inflow is divided by total inflow to that sub-basin and should not be interpreted as cumulative or system-wide percentages. In the Lake Winnipeg sub-basin, 88% of the flow is local due to the significant errors in the stage-storage curve of Lake Winnipegosis. A significant portion, 87%, of the total local flow in the Lake Winnipeg sub-basin is allocated to Lake Winnipegosis. According to HFC experts, the current stage-storage curve is the only existing curve to depict water level changes in Lake Winnipegosis. Local flows contribute to 44% of the total flow in the Winnipeg and Nelson River sub-basins, with 88% and 70% of that being local inflow, respectively. In the Winnipeg River, 56% of the local flow is allocated to the Lake of the Woods, the biggest lake in the sub-basin. Local flows have a minor contribution of 7.5% and 5% in the Assiniboine and Churchill River sub-basins. Recorded flow in the Saskatchewan and Red River sub-basins is sufficient to simulate the river-reservoir systems encompassed in the study area.

Table 2.3. Percentage and daily average of recorded and "local flow" in each sub-basin. The "local flow" was calculated through the application of mass-balance (Equation (2.1))

Sub-basins	Total flow in the system				Local Flow	
	Contribution (%)		Daily Average (m^3/s)		Contribution (%)	
	Local	Recorded	Local	Recorded	Inflow	Loss
Lake Winnipeg	88	12	3739	507	50	50
Winnipeg River	44	56	492	618	88	12
Nelson River	44	56	207	268	70	30
Assiniboine River	7.5	92.5	6.5	79	42	58
Churchill River	5	95	53	956	58	42
Saskatchewan River	0	100	0	596	-	-
Red River	0	100	0	216	-	-

2.4.2 Outflow

Upstream of Lake Winnipeg, the average daily flow passing through control points and hydropower stations varies from 17 to 980 m^3/s. In the Assiniboine River sub-basin, Shellmouth Dam releases an average daily flow of 17 m^3/s. The outflow from Shellmouth converges with other tributaries and the Red River, collectively contributing to an average daily discharge of 282 m^3/s. In the Lake Winnipeg sub-basin, Lake St. Martin maintains an average daily release of 109 m^3/s. In the Saskatchewan River sub-basin, the Grand Rapids hydropower station releases an average daily discharge of 590 m^3/s. In the Winnipeg River sub-basin, Lac Seul and Lake of the Woods

release an average daily of 296 and 457 m^3/s, respectively. These discharges unite with other tributaries downstream in the Winnipeg River and go through the final hydropower station, Pine Falls, with an average of 980 m^3/s.

Downstream of Lake Winnipeg, the average daily flow passing through control points and hydropower stations varies from 776 to 3604 m^3/s. In the Churchill River sub-basin, Southern Indian Lake contributes an average daily discharge of 776 m^3/s through the South Bay Channel, directed towards the Nelson River. In the Nelson River sub-basin, the Jenpeg hydropower station releases an average daily discharge of 1967 m^3/s. The outflow from the last hydropower station on the Nelson River, Limestone, averages 3604 m^3/s.

In Manitoba, total outflow from a reservoir with a hydropower station goes through two outlets: one through the turbine that generates hydroelectricity and the other through a side channel that works as a spill. The magnitude of generated hydropower determines the proportion of the total outflow that passes through turbines. The contribution of side channel flow to total outflows varies across hydropower stations. It ranges from a minimum of 1% at Grand Rapids to a maximum of 37% at Pointe Du Bois on average, with a weighted average of 10% across the whole system. Single hydropower station along a river, such as Grand Rapids and Wuskwatim, exhibit a minimal amount of side channel flow. However, in a series of hydropower stations, dams with lower hydropower generation capacity experience higher side channel flow to ensure an adequate flow for downstream hydropower stations with higher generation capacity. Seasonal variation of the side channel flow is notable, with the lowest during winter due to lower inflow. The highest values occur in spring because of higher inflow in this season, and limited storage and hydropower generation capacity in the Province.

2.4.3 Water Level

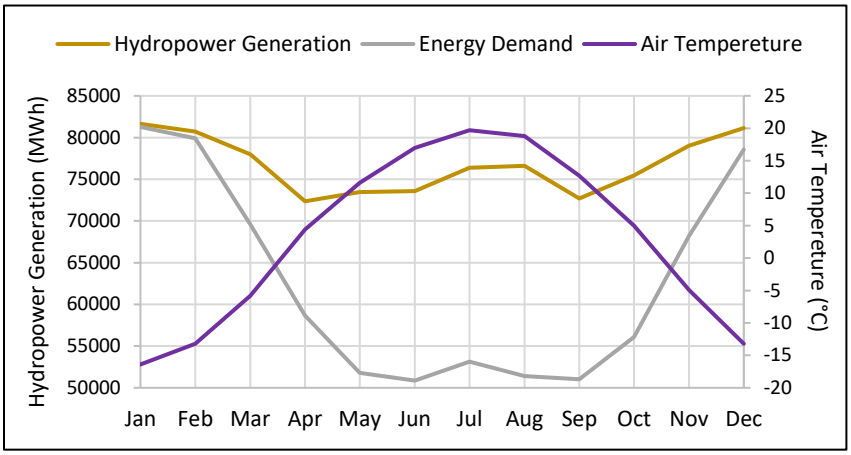
Water level (referring to water surface elevation; WSE) varies across the study area and in different lakes and reservoirs. The highest average is 426.85 meters above sea level (masl) at the forebay of Shellmouth Dam in the Assiniboine River sub-basin, with recorded minimum and maximum elevations of 421.54 and 431.62 masl, respectively. Among the top biggest lakes from other sub-basins, lower averages are as follows: Lake of the Woods in Winnipeg River sub-basin with 322 masl (321.99-323.78 masl), Southern Indian Lake in Churchill River sub-basin with 257 masl (256.9-258.55 masl), Cedar Lake in Saskatchewan River sub-basin with 255 masl (253.33-

256.6 masl), and Lakes Manitoba and Winnipeg in Lake Winnipeg sub-basin with 247 masl (246.93-249.05 masl) and 217 masl (216.82-218.51 masl), respectively. Water level variations in these lakes are on the order of 2 to 3 meters, highlighting their significant impact on streamflow and, consequently, hydropower generation, even with centimeter-level changes. The lowest average is 85 masl (79.79-85.26 masl) at the forebay of the Limestone hydropower station located in the Nelson River sub-basin.

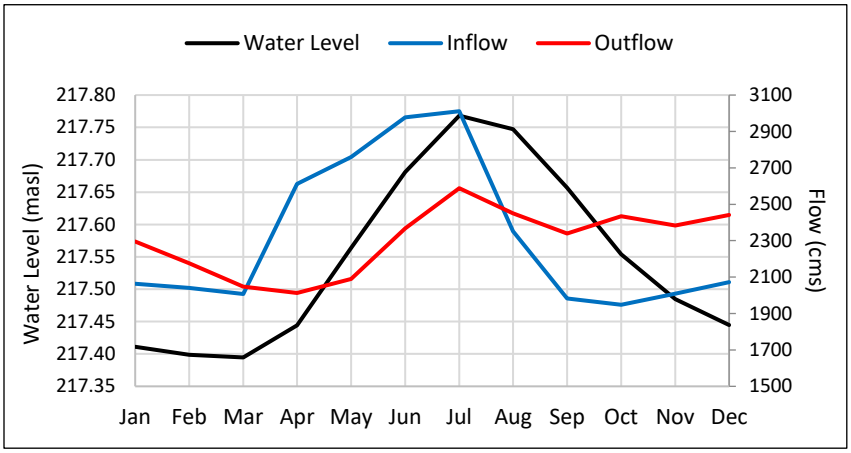
2.4.4 Hydropower Generation

Hydropower generation is relatively high from November to March, when the average daily air temperature is below 0 °C and there is increased energy demand for space heating (Figure 2.2a). Examining the operations of Lake Winnipeg reveals the response to the high electricity demand during this period. Due to the offset between water supply (high inflow from April to August in Figure 2.2b) and electricity generation need (high electricity generation and energy demand from November to March in Figure 2.2a), water is stored during the high-flow period; outflow is less than inflow and the lake water level is increasing from April to July (see Figure 2.2b). This allows increasing the Lake Winnipeg outflow to a target value with the start of the cold season in November to form a smooth ice and maximize the hydropower generation at downstream stations during the ice-on season. As winter progresses, outflow decreases by March due to the lake water level decline and growth in ice restrictions through winter. From April, the average daily air temperature is above 0 °C, enabling the Province to generate relatively lower hydroelectricity amounts in response to lower energy demand. Among warmer months, July and August have relatively higher electricity generation due to a combination of high inflows and full storage, and high energy demand in neighbouring power systems in the US.

In the Winnipeg River sub-basin, Seven Sisters has the highest average head of 17.9 m for generating hydroelectricity, while Slave Falls has the lowest with 8.7 m. In the Nelson River sub-basin, the average heads are 21.7, 15.8, and 8 m in Wuskwatim, Kelsey, and Jenpeg, respectively. The recorded head for the remaining hydropower stations in the Nelson River sub-basin was not available.



(a)



(b)

Figure 2.2. Monthly average of (a) daily hydropower generation, energy demand, and air temperature in Manitoba, and (b) daily historical water level, inflow, and outflow for Lake Winnipeg. Air temperature is based on the climate normal of Winnipeg Richardson International Airport, available at https://climate.weather.gc.ca/

2.5 Methodology

MODSIM-DSS, version 8.5.1, was employed to simulate the river-reservoir system within the study area from 1980 to 2017 with a daily time-step. It is a free integrated water resources management tool available at http://modsim.engr.colostate.edu/. Because the study area is expansive and encompasses numerous control points, rivers, lakes, and reservoirs, it was divided into 3 sub-systems. The first one covers the Winnipeg River and the southeastern part of the Lake Winnipeg sub-basin (dashed purple border in Figure 2.1). The second one covers the Assiniboine, Red River, and the western part of the Lake Winnipeg sub-basin (dashed green border in Figure 2.1). The third one covers the river-reservoir system of Saskatchewan, Churchill, and Nelson Rivers, and the rest of the Lake Winnipeg sub-basin (dashed yellow border in Figure 2.1). As

shown in Figure 2.3, two types of MODSIM-DSS models were developed independently for each sub-system: a mass-balance model and an operational model. The three operational models were integrated into one MODSIM-DSS model, referred to as MB_HydroSim.

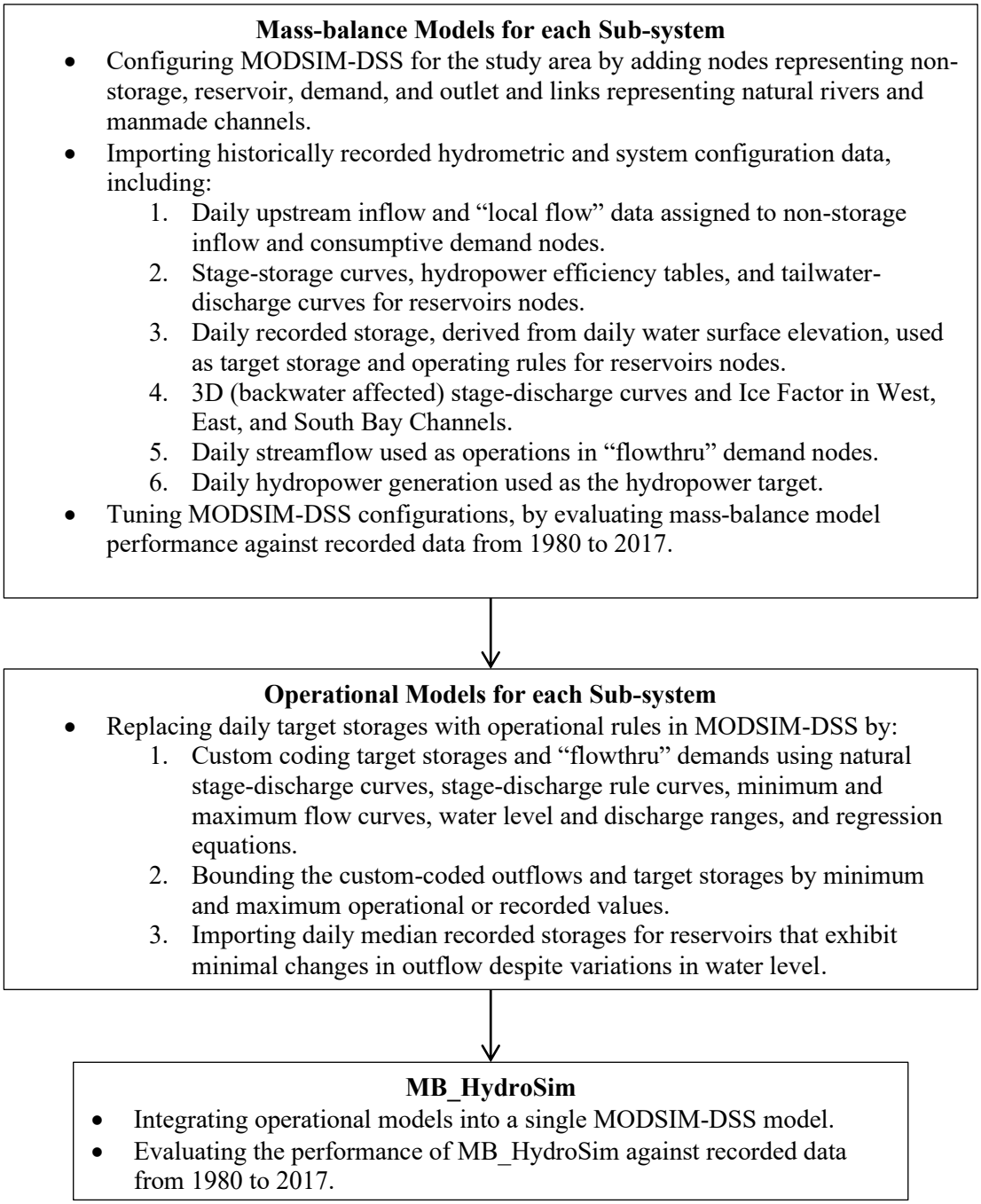


Figure 2.3. Schematic of MB_HydroSim model development, illustrating the distinction and information flow between mass-balance, operational, and the integrated MB_HydroSim models.

The mass-balance models were developed as a baseline to tune MODSIM-DSS for simulating the complex river-reservoir system in our study area. Nodes and links representing all system components were incorporated, followed by importing hydrometric and system configuration data into each mass-balance model. The tuning process involved configuring key MODSIM-DSS model features such as hydropower weights, the priority of reservoirs and demands, and link costs. Details of the MODSIM-DSS configuration are provided in the section "*2.5.1. MODSIM-DSS*". The mass-balance models are expected to simulate recorded data accurately because recorded storage was used as the operations for all lakes and reservoirs and recorded streamflow as the operations for non-reservoir control points. Consequently, they serve as reliable benchmarks for tuning MODSIM-DSS configuration, as its performance is not affected by operational uncertainties or calibration errors. Further details on the mass-balance models setup and tuning procedure are provided in the sections "*2.5.2. Mass-balance Model*". The tuning process was carried out by independently developing and evaluating the mass-balance model of each sub-system over 1980-2017 period.

The recorded storage and streamflow used in mass-balance models are replaced with operational rules, building the operational models for each sub-system. In the operational models, the inclusion of all collected formal operational rules (stage-discharge rule curves, minimum and maximum flow curves, and water level and discharge ranges) and natural stage-discharge curves enables simulating the real-world management practices. For locations without formal operational rules, regression equations were developed to represent operating behavior. The coefficients of these equations were calibrated using two-thirds of the historical period (1980-2005) and validated with the remaining one-third (2006-2017). Daily median recorded storage values were used to define operating rules for reservoirs exhibiting minimal outflow sensitivity to water-level variations. Subsequently, all three operational models were integrated into one MODSIM-DSS model, called MB_HydroSim, and evaluated against recorded data from 1980 to 2017. Further details on operational models are provided in section "*2.5.3. Operational Model*". The custom code of MB_HydroSim, which includes all coded operational rules in VB.NET, is publicly available on GitHub (https://github.com/Gozinih/MB_HydroSim_CustomCode), in which any sensitive data that requires authorization from MH or HFC has been replaced with placeholders 'Num'.

2.5.1 MODSIM-DSS

MODSIM-DSS is an integrated water resources management tool that can simulate complex river-reservoir systems using custom coding (Labadie, 2006). A river-reservoir system can be defined in MODSIM-DSS using non-storage, reservoir, demand, and sink nodes connected by links. Non-storage nodes are used to define upstream (e.g. "UpstreamInflow" in Figure 2.4) and tributary (e.g. "LocalInflow" in Figure 2.4) inflows to the system. Reservoir nodes (e.g. "LakeStJospeh" in Figure 2.4) represent dams, reservoirs, and lakes. Demand can be consumptive (e.g. "RatRapidDam" in Figure 2.4) or returns flow back to the system (e.g. "RootRiverDam" in Figure 2.4). In MODSIM-DSS, the demand node that returns flow back to the system is called a "flowthru" node. The Sink node ("Sink" in Figure 2.4) defines the outlet of the system. In addition to user-defined links and nodes, MODSIM-DSS automatically creates several artificial links and nodes, which are essential to maintain mass-balance throughout the network. By solving a Network Flow Optimization algorithm (Equation (2.2)) for each time step, MODSIM-DSS simulates the streamflow in each link.

$$
\begin{aligned}
&Minimize \sum_{k \in A} c_k q_k \\
&Subject\ to: \\
&\sum_{k \in O_i} q_k - \sum_{j \in I_i} q_j = b_i(q) \quad for\ all\ nodes\ i \in N \\
&l_k(q) \le q_k \le u_k(q) \qquad for\ all\ links\ k \in A
\end{aligned}
\tag{2.2}
$$

Where A is the set of all links (artificial and user-defined), N is the set of all nodes, O_i is the set of all outflow links from node i, I_i is the set of all inflow links to node i, b_i is the gain or loss at node i, q_k is the flow rate in link k, c_k is the cost in link k, and l_k and u_k are specified lower and upper bounds, respectively, on flow in link k. b_i , l_k , and u_k are functions of the flow vector q. The optimization relies on the defined link costs (c_k). Link costs can be defined (tuned) directly for user-defined links or indirectly for artificial links using priorities that users set for reservoir and demand nodes. Priority on reservoirs refers to storing water, while priority on demands refers to allocating water to demand. The desired value of storage in a reservoir is called "target storage".

Priorities are converted to "artificial carryover storage" link cost for reservoir nodes and "artificial demand" link cost for demand nodes based on Equation (2.3).

$$c_i = -\left(50000 - (10 \times PR_i)\right) \tag{2.3}$$

Where PR_i is the priority ranking that can be defined (tuned) from 1 to 5000 for reservoir or demand node *i*, and c is the artificial link cost. Lower PR_i indicates a higher ranking, resulting in more negative costs that maximize the flows to the higher-ranked nodes. More detailed information about priorities, costs, and the Network Flow Optimization algorithm is provided in the MODSIM-DSS manual.

MODSIM-DSS is not an open-source tool, but its custom-coding option in C#.NET or VB.NET allows users to define operational rules that cannot be specified by priorities and costs. These operations can be mathematical equations for defining target values of storage and demand. A simple example is to define an equation that calculates the value of a target storage based on the current inflow and water level. The custom code editor includes a built-in template and integrated help features that guide users on how to access and utilize node and link object methods. Through this interface, users can interact with the model at strategic points in the computational process, such as during data input, initialization of each time step, intermediate iterations, or output generation. Users have direct read and write access to most public variables, such as target storage for reservoirs, enabling implementation of knowledge-based operating rules. However, some internal variables, such as the tailwater elevation at reservoirs, are read-only within the custom code environment. Such parameters can still be modified indirectly by accessing and updating their values in the .xy files, which are stored as plain text and can be edited programmatically prior to model execution.

MODSIM-DSS users can define (tun) hydropower generation target and its weight. In the MODSIM-DSS manual, there is no mention of how this hydropower target and weight are incorporated during model simulation. According to the response from MODSIM-DSS support, an artificial diversion with the specified weight of cost temporarily takes water out of the network. The solver then iteratively solves Equation (2.4), and in the next iteration the withdrawn water is returned to the system.

$$Minimize \sum_{m \in B} |HG_m - HT_m| \tag{2.4}$$

Where B is the set of all hydropower stations, and HG_m and HT_m are hydropower generation and target at hydropower station m. Hydropower generation at time t and in each station is calculated as follows:

$$HG_t = Max(KQ_tH_te(Q_t, H_t), P_{max}).\Delta T_t \tag{2.5}$$

$$H_t = 0.5(FB_t + FB_{t+1}) - TW_t \tag{2.6}$$

Where K is a conversion constant, Q is turbine discharge, H is the average head, e is power plant efficiency, P_{max} is plant capacity, ΔT is generating hours, FB is forebay water level, and TW is tailwater level. Plant efficiency is interpolated from an efficiency table as a function of turbine discharge and head. The forebay water level is interpolated from the stage-storage table. The tailwater level can be a constant value, or variable which is interpolated from a tailwater-discharge table.

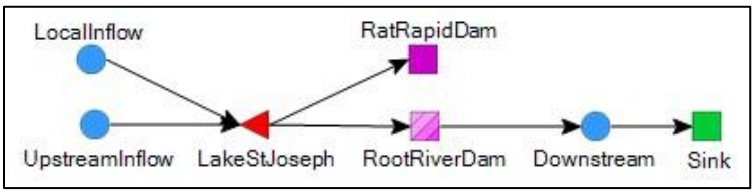


Figure 2.4. Example of a simple model in MODSIM-DSS

2.5.2 Mass-balance Model

For each sub-system, a mass-balance model was constructed by adding all required nodes, including non-storage, reservoir, demand (consumptive and "flowthru"), and sink, and linking them to represent the full system components. Hydrometric and system configuration data were then imported to parameterize model behavior, including recorded inflow and "local flow" data assigned to non-storage inflow and consumptive demand nodes, as well as stage-storage curves, hydropower efficiency tables, and tailwater-discharge curves for reservoir nodes. Variable tailwater elevation was integrated into MODSIM-DSS using tailwater-discharge curves, provided by MH. In cases where tailwater-discharge curves were unavailable, a constant tailwater elevation was identified through a trial-and-error process to minimize the bias of hydropower simulation.

Daily recorded storage across the system was used as the target storage for the corresponding reservoir in the model. Therefore, natural stage-discharge curves were not required in the mass-balance model. However, the 3D stage-discharge curves of the West, East, and South Bay Channels were still required to make the mass-balance model simulate backwater effects. Piecewise equations were fitted to the 3D curves, as represented in Equation (2.7), and custom coded in the mass-balance model.

$$Q_{3D} = a\left(WSE_{ups} - c\right)^{b} \quad \text{for} \quad x_1 < WSE_{dns} \leq x_2 \tag{2.7}$$

Where Q_{3D} is the channel flow, WSE_{ups} is the upstream water level, WSE_{dns} is the downstream water level, a, b, and c are the coefficients of the fitted equation, and x_1 and x_2 are thresholds of the piecewise equation. 3D curves estimate flow with high accuracy in open-water conditions, but overestimate flow during ice-on condition, requiring correction to account for the increased flow resistance caused by ice cover (Gozini et al., 2023). Beiraghdar (2019) showed that using daily median Ice Factor (IF) curves improves the simulation results of the West, East, and South Bay Channels. Therefore, the mass-balance model was equipped with daily median IF curves over the period of 1980 to 2017 to correct the 3D curves during ice-on condition. The median IF curve consists of the daily median value of historical IF over the desired period. Daily historical IF was calculated using Equation (2.8).

$$IF = \frac{Q_{3D}}{Q_m} \tag{2.8}$$

Where IF is Ice Factor, Q_{3D} is estimated channel flow by the 3D rating curve using historically measured water levels, and Q_m is historically measured discharge. Dividing 3D curves by the daily median IF corrects the curves for ice-on condition. Further details can be found in Gozini et al. (2023) ("*Ice impact on channel conveyance*" section).

"Local loss" was defined as a consumptive demand node and given the highest priority (1) to ensure the amount of water loss is subtracted from the system. For non-hydropower reservoirs with two outlets, "flowthru" demand nodes with a 100% coefficient of return flow were used. In these nodes, recorded streamflow was allocated as the demand value to specify the amount of water that should go through each outlet. Similarly, "flowthru" demand nodes with a 100% coefficient of

return flow were assigned for non-reservoir control points. "flowthru" nodes were given the highest priority (1) to ensure their demands were met as the operations of the system.

Priority number 99 was assigned for all reservoirs, control dams, and lakes. They were equally prioritized to meet the target storages across all of them. Number 99 was used to make sure the calculated artificial link cost (-49,010 based on Equation (2.3)) sufficiently differs from the ones for demand nodes with priority one (-49,990).

The default of a user-defined link cost is 0, meaning that the link will not be included in the objective function of the Network Flow Optimization algorithm (Equation (2.2)). Therefore, it will only be included in the constraints to ensure the mass-balance is satisfied. For hydropower stations, two outflow links ("multilink" option in MODSIM-DSS) were defined. One link was assigned for hydropower with a cost of -2, and one link was for the side channel with a cost of -1. The negative costs were defined to ensure the hydropower stations use the side channels, if needed, based on target storage. No water was passing the side channel link when using 0 or a positive cost for the multilink. The default cost of 0 was used for the remaining links in the system.

Recorded hydropower generation was included as the target, and the model was run with a weight of 1000 for hydropower. The chosen weight ensured the model simultaneously meets the reservoirs target storage, demands, and hydropower targets. Generating hours were set to 24 hours for all stations since they operate continuously.

2.5.3 Operational Model

In the operational model, target storages and "flowthru" demands were computed based on specified operations and natural stage-discharge curves. Depending on data availability, the operations were formulated as stage-discharge rule curves, minimum and maximum flow curves, water level and discharge ranges, daily median recorded storage, or regression equations. A summary of the methods used to calculate demands and target storages in each sub-system is provided in the Supplementary Material (Table S1). All methods were custom coded in the MODSIM-DSS model, except for the daily median recorded storage which was implemented as an input to the model. MATLAB was employed to determine the regression coefficients for each location using recorded data, with the process being carried out individually for each location. Two-thirds of the available data (1980-2005) was used for training, while the remaining one-third

(2006-2017) was used for evaluating the performance (KGE: Kling-Gupta Efficiency) of the curve. The custom-coded outflows and target storages were bounded by minimum and maximum operational or recorded values.

2.5.3.1 Operations Based on Established Guidelines

In sub-system 2, all target storages and flowthru demands were defined based on the reported operations. For Shellmouth Dam, the general guideline is to drawdown the water level in winter to prepare the dam for storing spring runoff. Subsequently, the water level is maintained within a specified range throughout the summer and autumn seasons. Therefore, Shellmouth was custom coded to look for a suitable outflow that meets the criteria for both water level and outflow of the Dam. Streamflow of the Assiniboine River at Russel, Miniota, Brandon, and Holland hydrometric stations was simulated by mass-balance of MODSIM-DSS using Shellmouth outflow and its downstream tributaries. The Portage Diversion, located downstream of Holland, diverts the Assiniboine River streamflow to Lake Manitoba during high-flow periods. Such diversion helps to keep the streamflow at Southport and the water level at James Avenue hydrometric stations below their maximum thresholds. The remaining non-diverted streamflow continues to the Southport and then Headingly hydrometric stations, downstream of Portage Diversion on the Assiniboine River. Southport streamflow was routed to Headingly, using the lag time method available in MODSIM-DSS. Finally, the Assiniboine River joins the Red River in Winnipeg City and flows to the James Avenue hydrometric station.

The Red River naturally passes through the Winnipeg City and James Avenue station, but the Floodway can divert water from the Red River during high-flow periods into the Red River downstream of the City of Winnipeg. Similar to Portage Diversion, the Floodway contributes to maintaining the water level at the James Avenue hydrometric station below its maximum threshold to control flooding within the city boundary. To find the best values for diverted flow, the model was custom coded to simultaneously look for suitable values for the Portage Diversion and Floodway "flowthru" demands that meet the defined maximum thresholds at Southport and James Avenue hydrometric stations. The maximum thresholds depend on the water level in Lake Manitoba. The James Avenue water level was calculated based on the stage-discharge curve at this station. Target storage of Lakes Winnipegosis and St. Martin was defined based on the natural stage-discharge curves. For Lake Manitoba, target storage was defined based on the stage-

discharge rule curves. Equations were fitted to these curves and custom coded to find the outflow based on the water level. Then the estimated outflow was used to calculate target storage (S_{t+1}) in Equation (2.9).

$$S_{t+1} = S_t + I_t - Q_{S-D}(WSE_t) \quad (2.9)$$

Where t is time (day from the start of the simulation), S is storage, I is inflow, and $Q_{S\text{-}D}(\ )$ is the fitted equation to stage-discharge curves (natural or rule curves). A similar approach was used for uncontrolled points in sub-system 3, including Footprint, Cross, Sipiwesk, and Split lakes.

2.5.3.2 Operations by Daily Median Recorded Storage

In the study area, certain locations exhibit minimal changes in outflow despite variations in water level. This is due to their low storage capacity relative to the volume of water passing through, which means outflow roughly equals inflow at these locations at the daily timescale. Daily median recorded storage was used for such locations where formal operational rules were not accessible, including:

- Sub-system 1: Pointe Du Bois, Slave Falls, Seven Sisters, McArthur Falls, Great Falls, and Pine Falls
- Sub-system 3: Wapisu, Opegano, Birchtree, Wuskwatim, Kelsey, Kettle, Long Spruce, and Limestone.

2.5.3.3 Operations by Regression Equations

Custom-coded regression equations were developed based on recorded data for locations that do not have a formal operational rule, and where the daily median recorded water level proved ineffective.

In sub-system 1, target storage was computed utilizing linear regression equations for non-hydropower stations. Equation (2.10) shows an example curve fitted by regression to the recorded data for calculating target storage:

$$S_{t+1} = S_t + I_t - (c_1 DOY_t + c_2 S_t + c_3 I_t + c_4 O_{t-1} + c_5) \quad (2.10)$$

Where *DOY* is the day of the year (January 1st = 1), *O* is outflow, and c_1 *to* c_5 are regression coefficients. St. Joseph, Lac Seul, Namakan, Rainy, and Lake of the Woods are the main control points for regulating flow throughout sub-system 1. For these lakes, a set of 12 regression equations was developed, each corresponding to one of the months in a year. St. Joseph outlets were defined as "flowthru" demand nodes. The demand value for each outlet was determined by the required volume of water release to meet the target storage. Operations of Whitedog Dam control the Minaki water level. Since data were not available to simulate Whitedog, Minaki hydrometric station was defined as a reservoir to be able to simulate this part of the system. For Minaki, the daily median recorded storage was used as the target storage when the outflow from Lake of the Woods was below 700 m^3/s. For outflows greater than 700 m^3/s, Minaki target storage was calculated based on a linear regression as follows:

$$S_{t+1} = c_6 O_{LOW_t} + c_7 \tag{2.11}$$

Where *LOW* refers to Lake of the Woods and c_6 and c_7 are regression coefficients.

In sub-system 3, turbine and side channel discharge of the Grand Rapids hydropower station were estimated using regression equations. Then, Grand Rapids target storage was custom coded as follows:

$$S_{t+1} = S_t + I_t - (c_8 HT_t + c_9) - (c_{10} S_t + c_{11}) \tag{2.12}$$

Where *HT* is the hydropower target, and c_8 to c_{11} are regression coefficients. Southern Indian Lake target storage was calculated using regression equations:

$$S_{t+1} = S_t + I_t - Q_{SIL}(I_t) \tag{2.13}$$

Where *SIL* refers to Southern Indian Lake, $Q_{SIL}()$ is the regression equation to find the outflow based on inflow. The regression equation has its own set of fitted coefficients for different months. It is linear for months September to February and second-degree polynomial for months March to August. Moreover, the calculated target storage was bounded to minimum and maximum amounts determined by inflow and median historical target storage (Figure 2.5).

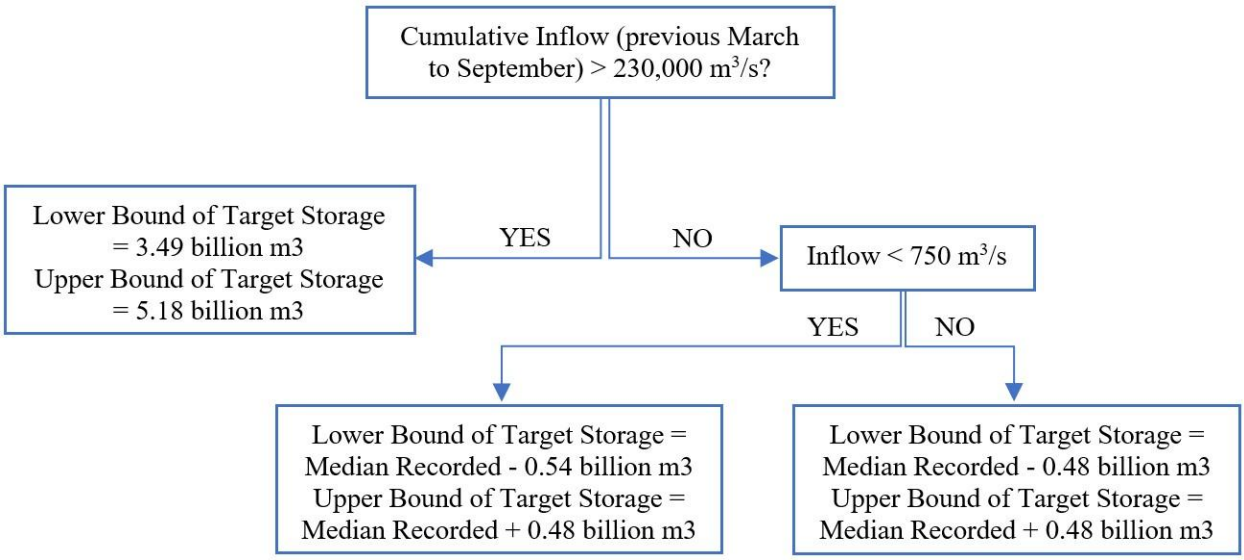


Figure 2.5. Conditional statements to determine upper and lower bounds of Southern Indian Lake target storage. All values are optimized in Excel using GRG (Generalized Reduced Gradient) solver, except 750 m^3/s which was chosen visually from the graph.

Missi Falls and South Bay Channel are two outlets of Southern Indian Lake. Outflow at Missi was determined as the sum of the minimum flow, which varies for different months (Manitoba Hydro, 2022), and regression equations dependent on the inflow and storage of Southern Indian Lake:

$$Q_{Missi_t} = \begin{cases} Q_{min}(curMonth) + \left(c_{12} I_{SIL_t}^2 + c_{13} I_{SIL_t} + c_{14}\right), & if\ S_{SIL_t} > 7074\ Mm^3\ \ AND\ \ I_{SIL_t} > 960\ m^3/s \\ Q_{min}(curMonth) + \left(c_{15} I_{SIL_t} + c_{16}\right), & otherwise \end{cases} \quad (2.14)$$

Where Q_{Missi} is the outflow at Missi, $Q_{min}(\ )$ is the minimum flow through Missi Falls, determined by the current month (*currMonth*), and c_{12} to c_{16} are regression coefficients. Outflow through the South Bay Channel was calculated using the 3D curve that involves the Notigi water level:

$$Q_{SBC_t} = \frac{Q_{3D}\left(WSE_{SIL_t}, WSE_{Notigi_t}\right)}{IF_{SBC_t}} \quad (2.15)$$

Where $Q_{3D}( )$ is the fitted equation to the 3D curve and IF_{SBC} is the median Ice Factor value in the South Bay Channel (*SBC*). The target storage at Notigi was calculated using a regression equation based on Southern Indian Lake target storage:

$$S_{Notigi_{t+1}} = f_{NT}\left(S_{SIL_{t+1}}\right) \tag{2.16}$$

Where $f_{NT}( )$ is the regression equation to find Notigi target storage based on Southern Indian Lake target storage. The regression equation has its own set of fitted coefficients for different months. It is linear for November to February and from May to July, and it is a second-degree polynomial for March to April and August to October. Furthermore, the resultant outflow was bounded to minimum and maximum amounts determined by regression equations. The maximum amount was calculated using a linear regression equation with Notigi Water Level as the independent variable. The water level at Notigi was the independent variable to find the minimum outflow but by using a third-order polynomial equation.

Lake Winnipeg has two outlet channels: the West and East Channels. The outflow from these channels is controlled by the Jenpeg forebay water level. The channel flows were calculated using 3D curves. This also determined the total outflow and subsequently the target storage in Lake Winnipeg as represented in Equation (2.17).

$$S_{t+1} = S_t + I_t - \left(\frac{Q_{3D}\left(WSE_{LW_t}, WSE_{Jenpeg_t}\right)}{IF_{NRWC_t}}\right) - \left(\frac{Q_{3D}\left(WSE_{LW_t}, WSE_{Jenpeg_t}\right)}{IF_{NREC_t}}\right) \tag{2.17}$$

Where *LW* refers to Lake Winnipeg, *NRWC* and *NREC* refer to Nelson River West and East Channels, respectively. Different types of methods were employed to simulate Jenpeg target storage. Month and Lake Winnipeg storage specified the method as follows:

$$S_{t+1} = \begin{cases} Winter\ Minimum\ Storage, & if\ S_{LW_t} > 46\ for\ Winter \\ Non-Winter\ Minimum\ Storage, & if\ S_{LW_t} > 46\ for\ Non-Winter \\ c_{17}S_t + c_{18}S_{LW_t} + c_{19}, & if\ 41 < S_{LW_t} \leq 46\ for\ Apr\ to\ Aug \\ \text{Daily median recorded storage}, & if\ 41 < S_{LW_t} \leq 46\ for\ Sep\ to\ Mar \\ \text{Daily Median recorded storage}, & if\ 28 < S_{LW_t} \leq 41 \\ c_{20}DOY_t + c_{21}S_{LW_t} + c_{22}DOW_t^2 + c_{23}DOW_tS_{LW_t} + c_{24}, & if\ S_{LW_t} \leq 28\ for\ Winter \\ \text{Daily median recorded storage}, & if\ S_{LW_t} \leq 28\ for\ Non-Winter \end{cases} \quad (2.18)$$

Where the unit for thresholds on Lake Winnipeg storage is billion cubic meters, *DOW* is the day of winter (1st of November = 1), and c_{17} to c_{24} are regression coefficients. c_{17} to c_{19} were determined separately for each month from April to August. The winter and non-winter minimum storage at Jenpeg corresponds to the minimum water levels given by Manitoba Hydro (2014). Analysis of the daily timeseries of historical Lake Winnipeg storage, historical Jenpeg storage, and median Jenpeg storage revealed that storage at Jenpeg deviates from its median when Lake Winnipeg storage is either very high or very low. Therefore, thresholds of Lake Winnipeg storage were chosen by visually comparing Lake Winnipeg and Jenpeg recorded storage. Whenever the daily median recorded storage was not suitable for Jenpeg (based on the calculated NSE), either regression equations or minimum storage values were used.

2.5.4 Model Performance Metric

Provincial river-reservoir operations are categorized on a monthly and seasonal basis. In addition, the shortest time span for hydropower supply and demand management is over the next few weeks. Therefore, the model performance was evaluated on a monthly basis with a focus on seasonal management. Performance refers to how well the simulation achieves historical outcomes. The Kling-Gupta Efficiency (*KGE*; Equation (2.22)) (Gupta et al., 2009) was selected as the model performance metric because it equally incorporates correlation (*r*; Equation (2.19)), variability (α; Equation (2.20)), and bias (β; Equation (2.21)) in one metric. Therefore, reporting *KGE* and its three components provides a complete evaluation of model accuracy and bias. *KGE* is unitless and can range from -∞ to 1, where 1 indicates the perfect simulation. *KGE* less than -0.41 suggests that the mean recorded value serves as a better indicator than the simulated value (Bajracharya et al., 2023). In this study, to more clearly present the model performance, *KGE* greater than 0.8 is categorized as "high performance", between 0.4 and 0.8 as "acceptable

performance", and less than 0.4 as "low performance". r, α, and β can range from -∞ to +∞ with the best value of 1. Alongside *KGE*, the deviations of r, α, and β from their ideal value of 1 are reported in this study to comprehensively assess model performance. Correlation is incorporated in *KGE* to achieve ideal values of variability and bias in optimization-calibration studies, and its perfect value of 1 is not attainable in practice (Gupta et al., 2009).

$$r = \frac{\sum_{i=1}^{n}(v_i^o - \overline{v^o})(v_i^s - \overline{v^s})}{\sqrt{\sum_{i=1}^{n}(v_i^o - \overline{v^o})^2}\sqrt{\sum_{i=1}^{n}(v_i^s - \overline{v^s})^2}} \tag{2.19}$$

$$\alpha = \frac{\sigma^s}{\sigma^o} \tag{2.20}$$

$$\beta = \frac{\overline{v^s}}{\overline{v^o}} \tag{2.21}$$

$$KGE = 1 - \sqrt{(r-1)^2 + (\alpha - 1)^2 + (\beta - 1)^2} \tag{2.22}$$

Where v refers to the variable, n is the number of time steps in the evaluation period, o refers to recorded values, s refers to simulated values, $\bar{v}$ is mean, and σ is standard deviation. *KGE* and its three components were calculated for simulated water level, outflow, and hydropower generation across the study area, in both mass-balance (individual sub-systems evaluated separately) and operational models (integrated within MB_HydroSim).

2.6 Results and Discussion

An overall assessment of the model performance is presented using the spatial weighted average monthly KGE of water level and outflow, as well as monthly KGE of total hydropower generation, for each sub-system and the entire MB_HydroSim model. The term "water level" refers to the forebay water surface elevation in lakes and reservoirs. The spatial weighted average of KGE is calculated for water level and outflow, with the weights being the mean recorded storage and the mean recorded outflow at each location, respectively. Detailed model performance is presented and discussed for each sub-system in the Supplementary Material (*SM.2 Detailed Performance Results for Each Sub-system*). However, some key findings from the detailed model performance assessment are summarized in this section. Additionally, this section discusses how MB_HydroSim can be employed for sensitivity analysis, climate change impact assessment,

adaptation policies development, and calculating the impact of ice-cover on hydropower generation.

2.6.1 MB_HydroSim Performance

Overall, the river-reservoir system is simulated with high and acceptable performance for each variable and across all sub-systems of MB_HydroSim (Table 2.4). The weighted average of monthly KGE for MB_HydroSim is 0.86 for water level and 0.85 for outflow. Hydropower generation is simulated with a high monthly KGE of 0.94 and a slight negative bias of 3% for the entire study area. This demonstrates that MB_HydroSim has successfully integrated all decision-making processes and operations, encompassing major rivers, lakes, and reservoirs within a single simulation tool, with the context of seasonal reservoir management. The high performance for water level simulation is primarily driven by the high KGE values achieved in simulating large lakes that function as major storage components, such as Lake Winnipeg. Overall, fewer discrepancies are observed for bias compared to variability and correlation. Variability in MB_HydroSim is underestimated for water level and outflow but overestimated for hydropower generation, with discrepancies in variability causing lower correlation in the simulation.

Table 2.4. Performance results of MB_HydroSim. The red color shows deviations from 1 for r, α, and β and KGE less than zero. The green color represents a monthly KGE of more than 0. The weighted average metric for water level is based on the mean recorded storage, and for outflow is based on the mean recorded outflow for each location.

Variable	Location	(r-1)	(β-1)	(α-1)	KGE
Water Level	*Sub-System 1*	-0.14	0.00	-0.07	0.83
	Sub-System 2	-0.05	0.00	0.18	0.81
	Sub-System 3	-0.08	0.00	-0.05	0.89
	MB_HydroSim	-0.08	0.00	0.00	0.86
Outflow	*Sub-System 1*	-0.06	-0.03	-0.08	0.88
	Sub-System 2	-0.07	-0.02	-0.07	0.87
	Sub-System 3	-0.10	0.00	0.01	0.84
	MB_HydroSim	-0.09	-0.01	-0.01	0.85
Hydropower	*Sub-System 1*	-0.02	-0.03	0.07	0.92
	Sub-System 3	-0.01	-0.02	0.05	0.95
	MB_HydroSim	-0.01	-0.03	0.05	0.94

As a visual evaluation of MB_HydroSim performance, the total recorded inflow into the system is compared to the inflow of the Kettle hydropower station (Figure 2.6). The inflow of Kettle is chosen to represent the entire upstream operations that prepare the inflow for the three most

downstream hydropower stations, Kettle, Long Spruce, and Limestone. These hydroelectric stations contribute 60% to the Provincial hydroelectricity capacity. The result demonstrates that MB_HydroSim successfully alters the temporal characteristics of the total water supply and simulates the operated inflow with a temporal pattern similar to the recorded one. This implies MB_HydroSim capability to address the offset between water supply and hydroelectricity demand by managing the streamflow throughout the river-reservoir system.

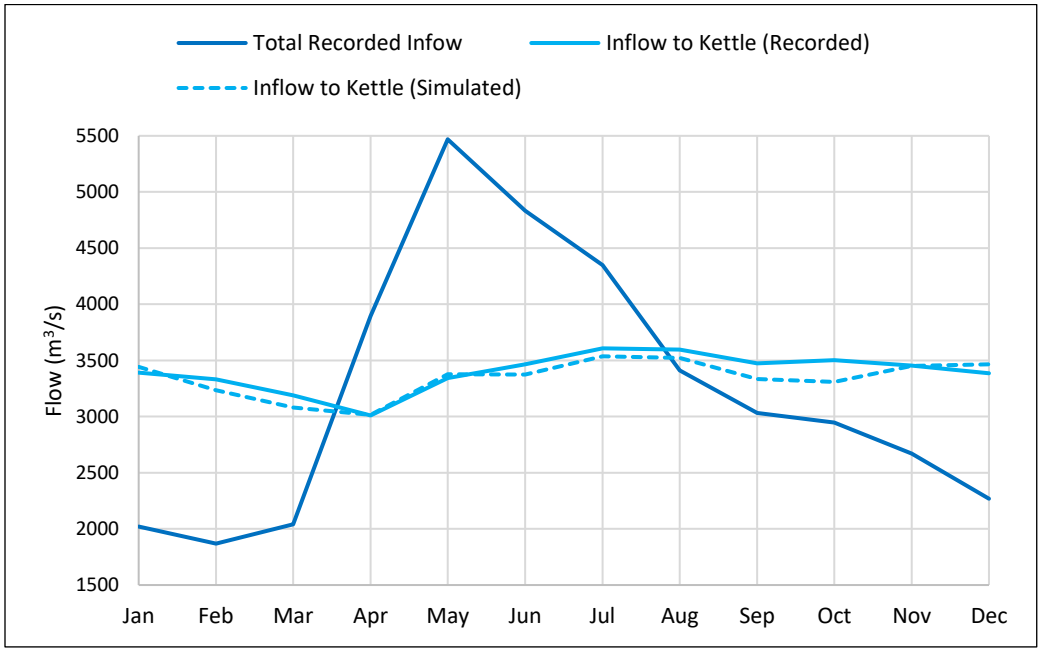


Figure 2.6. Monthly average of the total daily recorded inflow into the entire system vs. monthly average of the daily inflow for the three most downstream hydropower stations: Kettle, Long Spruce, and Limestone.

As a visual evaluation of MB_HydroSim performance for water level and hydropower generation, Figure 2.7 presents the results for Kettle and Long Spruce as representative stations. Simulated water levels at these two hydropower stations are based on the median recorded storage and therefore differ from the actual recorded water levels throughout the period. However, water level variations at these stations have a minimal influence on outflow because their storage capacity is small relative to the large volumes of water passing through. Consequently, outflow is approximately equal to inflow at a daily timescale, and the outflow simulation performance is primarily governed by the accuracy of inflow estimates. Thus, despite inconsistencies in simulated water levels, hydropower generation is reproduced with realistic magnitude and temporal behavior, indicating that outflows are also simulated appropriately.

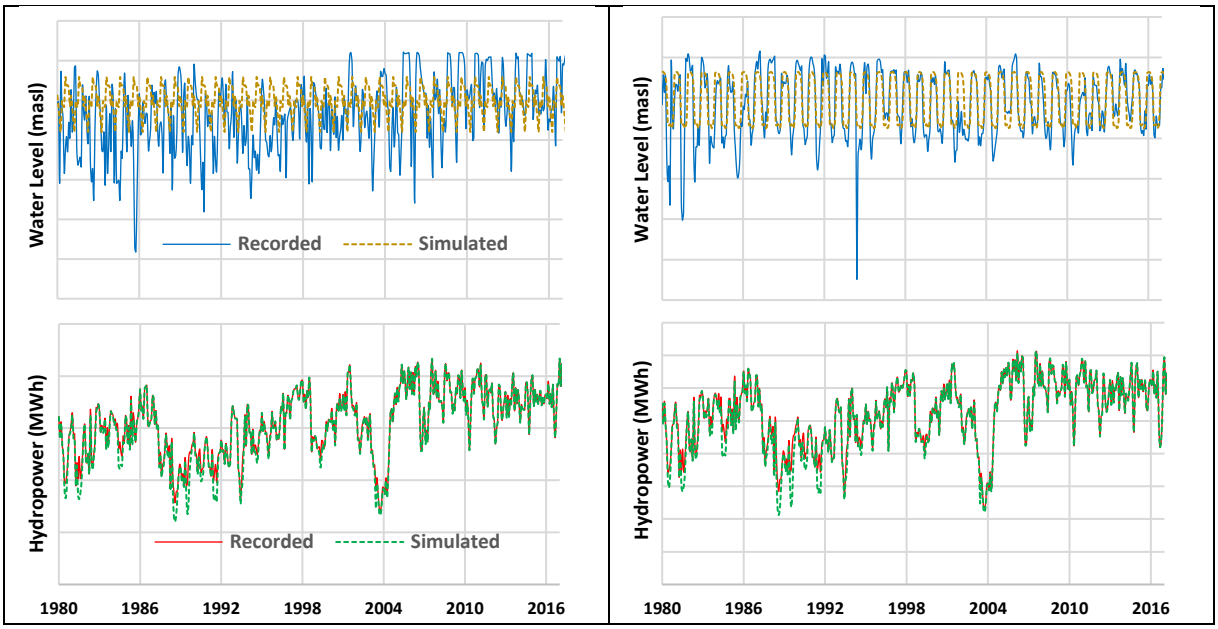


Figure 2.7. Monthly timeseries of recorded vs. simulated for water level and hydropower generation at (a) Kettle and (b) Long Spruce hydropower stations, from 1980 to 2017. Y-axis values are intentionally omitted to protect the confidentiality of recorded data; the figure is intended to illustrate relative agreement and temporal dynamics rather than absolute magnitudes.

Since there are no published studies on the simulation of sub-systems 1 and 2 for comparison, MB_HydroSim can serve as a benchmark for future model development in these sub-systems. MB_HydroSim outperforms Beiraghdar (2019) model, specifically in simulating four key control points of sub-system 3 (Table 2.5). At the Notigi control structure, Beiraghdar (2019) achieved a KGE of 1.0 by using historical recorded storage. However, MB_HydroSim employs an operational rule at this control point, representing an advancement in the simulation of Notigi.

Table 2.5. Model performance (monthly KGE) in water level simulation for sub-system 3 (MB_HydroSim vs. Beiraghdar (2019) model)

Location	MB_HydroSim	Beiraghdar (2019)
Lake Winnipeg	0.96	0.23
Jenpeg	0.9	0.63
Southern Indian Lake	0.82	0.63
Notigi	0.66	1

2.6.2 MB_HydroSim Capabilities

2.6.2.1 Sensitivity Analysis

MB_HydroSim integrates the operations of the complex river-reservoir system in Manitoba, enabling the capability of doing sensitivity analysis in the Province of Manitoba. This analysis can now be conducted for any major control point to assess its impact on the system performance at

any other key locations. For instance, changes in the operations of the HFC infrastructure for flood control (e.g., using the Portage and Floodway diversions) can be assessed for their impact on MH's hydroelectricity generation potential by examining the resultant inflow to Lake Winnipeg and the available water for downstream hydropower generation. Therefore, evaluating the performance of MB_HydroSim in each sub-system and major control point is crucial.

Table 2.6. Summary of the performance evaluations based on monthly KGE at different sub-systems of MB_HydroSim.

Location	Number of Evaluations			
	Total	High Performance (KGE>=0.8)	Acceptable Performance (0.4<=KGE<0.8)	Low Performance (KGE<0.4)
Sub-system 1	41	29	5	7
Sub-system 2	16	12	4	0
Sub-system 3	45	26	13	6
MB_HydroSim	102	67	22	13

In detail, 67 out of a total of 102 evaluations (water level, outflow, and hydropower generation at each node) for MB_HydroSim demonstrate high performance (Table 2.6). Of the remaining evaluations, 22 represent acceptable performance, and only 13 show low performance. All 13 low performances in sub-systems 1 and 3 are associated with water level simulation for small lakes and reservoirs. Water level variation at these locations has a minimal impact on outflow due to having low storage capacity compared to the volume of water passing through. Therefore, their inconsistencies in water level simulation do not affect outflow and hydropower generation performance in the study area. Notably, none of the evaluations at major streamflow control points (stated in the section "*2.3.2.Control Points*") show low performance. Out of 32 water level and outflow evaluations at major streamflow control points, 25 have high performance, and seven show acceptable performance. Moreover, hydropower generation is simulated at each station with monthly KGE values ranging from 0.81 to 0.97 (high performance). Comparing the operational models in MB_HydroSim with the mass-balance models shows that the operational models have relatively lower performance, mainly because the operational rules do not perfectly match daily recorded storage values. For further details about the model performance at each sub-system (mass-balance and operational) look at the Supplementary Material (*SM.2 Detailed Performance Results for Each Sub-system*).

2.6.2.2 Climate Change Impact Assessment

MB_HydroSim enables the capability of large-scale and transboundary climate change impact assessments, given that the study area is a drought-prone region with high uncertainty. Since daily inflow at different hydrometric stations has already been generated for the entire NCRB over a continuous 90-year record (1981-2070) (Braun et al., 2021; Stadnyk et al., 2021), conducting the climate impact assessment involves simply updating the inflow time-series in MB_HydroSim. MB_HydroSim daily inflow data can be updated using the GCM-driven inflow scenarios for both the hindcast (1981-2017) and future (2017-2055) periods, allowing the desired system performance metric to be calculated and compared between the two periods. Such a study has already been done by Kim et al. (2022) for potential hydropower generation changes in the Lower Nelson River basin. However, MB_HydroSim can perform similar assessments for the entire Province, addressing both future flood management and hydropower generation challenges. Synthetic streamflow scenarios provide another means of assessing climate change impacts. Similar to GCM-driven scenarios, synthetic streamflow series can be generated and incorporated into MB_HydroSim. The stochastic streamflow generator developed by Kirsch et al. (2013) is a notable example, widely applied in previous studies (e.g., Quinn et al. 2017, 2018) due to its simplicity and effectiveness in producing weekly or monthly streamflow scenarios for multisite water systems. To provide the daily resolution required by MB_HydroSim, the monthly or weekly synthetic streamflow scenarios can be disaggregated using the approach of Nowak et al. (2010).

To evaluate flood control operations, MB_HydroSim can quantify the daily amount of water stored at the Shellmouth Dam (Figure 2.8) and Lake Manitoba by subtracting outflow from inflow. It also simulates the flow diverted through the Portage and Floodway diversion structures, as well as streamflow at Southport and the water level at James Avenue hydrometric stations. The daily results can be aggregated into seasonal and annual timescales to assess system performance under each inflow scenario of interest.

For hydropower generation analysis, MB_HydroSim simulates the daily amount of hydroelectricity produced, enabling evaluation of the changes in generation volumes under different inflow scenarios. Since hydropower targets are integrated within MB_HydroSim, performance metrics such as reliability (i.e., the system's ability to meet energy demand) can also be calculated. MB_HydroSim can assess the ability of the upstream river-reservoir system to store

water for downstream hydroelectricity generation by monitoring the water level changes at the major control points (e.g., the Lake Winnipeg and Lake of the Woods in Figure 2.9). Results can be analyzed at annual or seasonal timescales, and across individual sub-basins or the entire study area.

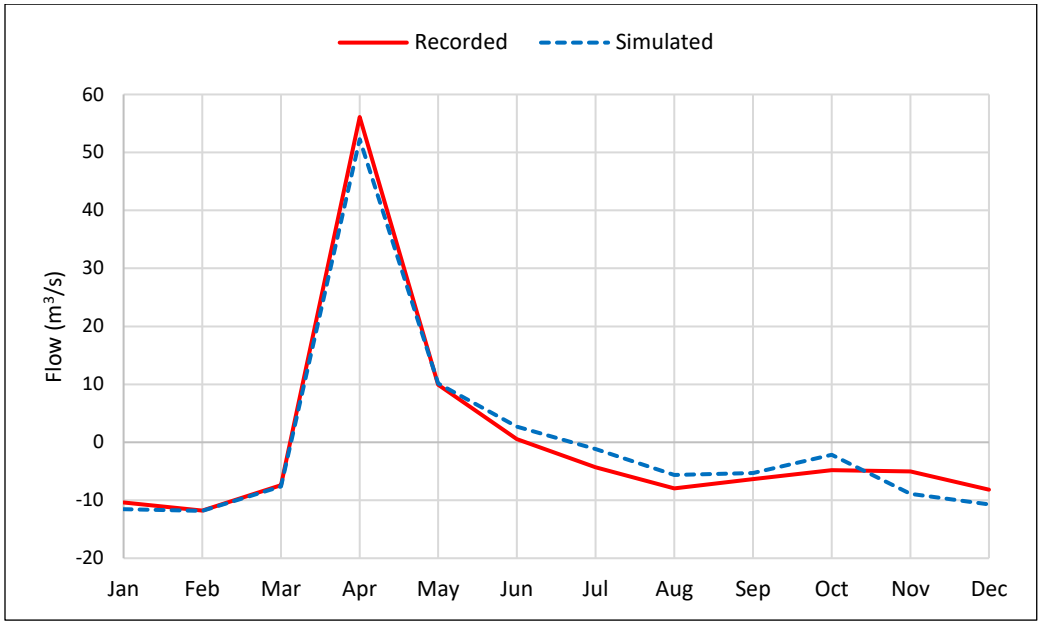


Figure 2.8. Monthly average of daily inflow minus outflow at the Shellmouth Dam

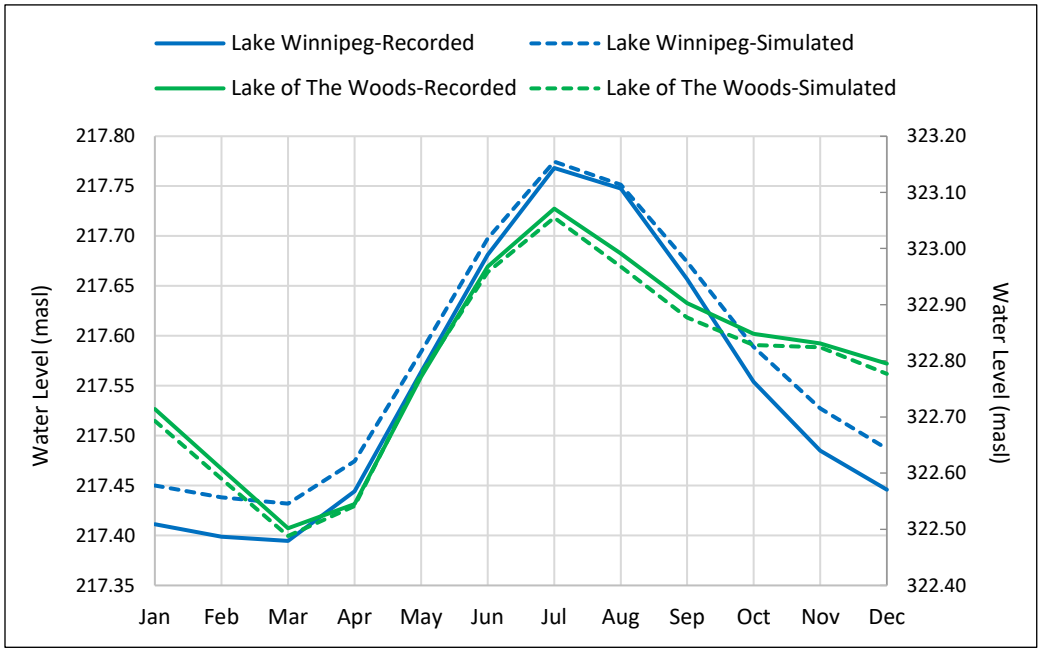


Figure 2.9. Monthly average of daily water level at the Lake Winnipeg and Lake of the Woods. The right-hand axis is for the Lake of The Woods water level.

2.6.2.3 Adaptation Policies

MB_HydroSim can develop adaptation policies for both purposes of flood control and hydropower generation planning (Table 2.7). Since MB_HydroSim operational rules are custom coded, they can be optimized using an external optimization algorithm. The custom-coding capability of MODSIM-DSS enables external coupling between MB_HydroSim and optimization algorithms.

Table 2.7. Potential objective functions and decision variables for developing adaptation policies using MB_HydroSim

Type of Operational Rule	Sub-System	Objective Function	Decision Variables
Established Guidelines	2	Minimizing Flood Risk	• Shellmouth dam: minimum and maximum water level for drawdown and peak, minimum and maximum thresholds of outflow in different seasons, water level bounds for operation during summer and autumn • Lake Manitoba: operational water level bound and its stage-discharge rule curve • Portage and Floodway diversions: thresholds on the James Avenue hydrometric station water level and the Southport hydrometric station flow
Daily Median Recorded Storage	1 & 3	Maximizing Hydropower Generation	-
Regression Equations	1 & 3		• Coefficients of regression equations (equations 10-18, except 15 and 17) • Thresholds on the regression equations, including the one stated for Southern Indian Lake in Figure 2.5.

The objective function can be designed to maximize the hydropower generation or minimize the flood risk. Alternatively, other metrics, such as reliability of hydropower generation, can replace total generation in the objective function. Constraints can be applied to water level variations at Lake Winnipeg and Lake of the Woods, allowing them to remain within seasonally

or annually defined limits. Flood risks can be quantified as the frequency of water level exceedance beyond a specified threshold at the James Avenue hydrometric station. Additional flood control considerations, such as daily storage at the Shellmouth Dam and Lake Manitoba, flows diverted through the Portage Diversion and Red River Floodway, and streamflow at the Southport hydrometric station, can also be constrained within the optimization process. Finally, multi-objective trade-off analyses can be performed to explore and balance hydropower and flood-management objectives, enabling more advanced and adaptive policy design.

In sub-system 2, the critical water level and outflow thresholds in the operational guidelines (listed in Table 2.7) serve as the potential decision variables. For the locations with daily median recorded storage as the operational rule, optimization is unnecessary, since their water level change does not significantly impact streamflow. For the control points with regression equations (sub-systems 1 and 3) as the operational rule, the coefficients can serve as the decision variables, as well as the thresholds in the piecewise equations. In addition, converting natural outlets to controlled ones can be examined by optimizing the coefficients of the fitted equations to the natural stage-discharge curves. However, this would be combined with an assessment of the feasibility of constructing an outlet with properties represented by the optimized coefficients.

2.6.2.4 WE Nexus

From the energy sector perspective, both climate change impact assessments and the development of adaptation policies can benefit from examining hydropower target scenarios that differ from the historically recorded one. Hydropower target scenarios could be derived from an external analysis method that evaluates the broader electricity sector. This method could incorporate socio-economic drivers such as population growth, GDP, interchange with the neighboring power systems, and the electrification of transportation and space heating (e.g., adoption of electric vehicles and substitution of natural gas with electricity for heating). Incorporating these variables enables the quantification of how developments in the energy sector may affect the water sector and hydropower generation. Moreover, coupling with an energy sector simulation tool that captures the dynamics of electricity demand allows hydropower generation to be evaluated in economic terms (e.g., revenue in dollars) and to identify when hydropower would be most valuable to the electricity system. This underscores that MB_HydroSim can serve as one of the fundamental tools for addressing the WE Nexus in the Province. MB_HydroSim can be

dynamically coupled with such an energy system model, allowing two-way feedback where hydropower targets within MB_HydroSim adjust in response to energy system conditions. Moreover, any potential or newly added hydropower station, such as Keeyask, can be incorporated into MB_HydroSim by simply adding the node and the relevant data.

2.6.2.5 Ice-cover Impact on Hydropower Generation

MB_HydroSim, as a cold-regions river-reservoir simulation tool, is capable of assessing the impact of ice-cover on hydropower generation. This can be achieved by running the model during the ice-on season with and without daily median IF curves. Instead of daily median IF values, MB_HydroSim can be equipped with an ice-impact module to simulate changes in channel conveyance under potential climate change scenarios. Such a tool has already been developed by Gozini et al. (2023) and Lees et al. (2023). The custom coding capability of MODSIM-DSS facilitates the coupling of such modules with MB_HydroSim.

2.7 Conclusion, Limitations, and Future Work

MB_HydroSim represents a significant advancement in hydropower simulation, offering a robust framework for simulating Manitoba's complex, drought-prone, and cold-regions river-reservoir system. The case study area includes water control structures and hydropower facilities for part of the Nelson Churchill River Basin in Manitoba and Ontario. MODSIM-DSS is used to simulate the river-reservoir systems with a daily time-step across the study area. Historically recorded data, including water level (referring to water surface elevation), outflow, and hydropower generation, are used to evaluate the model from 1980 to 2017. In addition, system configuration data, such as operational rules, natural stage-discharge curves, hydropower efficiency tables, tailwater-discharge curves, and stage-storage curves, are the essential inputs. Results demonstrate that MB_HydroSim simulated the historical timespan with high performance and can serve as a baseline for any future research. Water level and outflow are simulated with weighted average monthly KGE of 0.86 and 0.85, respectively. The model effectively responds to historical variations in streamflow and hydropower targets, as demonstrated by a high monthly KGE of 0.94 for total hydropower generation. Although demonstrated for the Manitoba hydropower system, custom coding of the sophisticated rule-based operations within MODSIM-

DSS provides a transferable example for developing and customizing MODSIM-DSS for other complex case studies.

MB_HydroSim is a promising tool for simulating future hydropower performance in Manitoba. It enables evaluation of how the water system responds to projected changes in inflows, assuming the current operational rules remain unchanged, thereby establishing a baseline for assessing climate impacts. Moreover, MB_HydroSim can be employed for developing climate-change adaptation policies by optimizing the current custom-coded operational rules. Other capabilities of MB_HydroSim include conducting sensitivity analysis and calculating the impact of ice-cover on hydropower generation. Collectively, these features position MB_HydroSim as a key decision-support tool for advancing WE Nexus assessments and adaptive water-resources management in in the Province.

One of the limitations of simulating future hydropower generation is the reliance of MB_HydroSim on the median recorded Ice Factor, which may not represent future conditions under a changing climate. Future work will focus on equipping MB_HydroSim with an ice-impact module to simulate changes in channel conveyance under potential climate change scenarios. Such a tool has already been developed by Gozini et al. (2023) and Lees et al. (2023). Fixed operational rules only reflect past operational practices; however, they can be adapted through application of optimization algorithms in future work. Implementing an external routing could significantly improve flow simulation at the hydrometric stations downstream of Shellmouth. In addition, MB_HydroSim has the capability to be expanded further by connecting it to the upstream MODSIM-DSS model named IWMSask (Ali Shah, 2019). This will involve the upstream operations and decisions made for any future simulations.

Another limitation of this study is the treatment of "local flow." Because MODSIM-DSS is an integrated water resources management model, unrecorded tributary inflows and lake-surface precipitation and evaporation cannot be explicitly represented. Accordingly, MB_HydroSim can be further coupled with hydrological models to better represent dynamics of "local flow" contributions. In this study, "local flow" is derived directly from recorded hydrometric data; therefore, its inclusion does not influence model performance but enables the model to be evaluated under observed inflow conditions. The inclusion of "local flow" is essential for

simulating the system, as its absence prevents the model from reproducing observed system behavior.

For climate-change impact assessment and the development of adaptation policies, coupling MB_HydroSim with hydrological models enables the representation of future changes in "local inflow". However, when hydrological models are not used, keeping "local flow" constant between historical and future simulations provides a consistent basis for comparison. This approach supports relative comparisons between past and future conditions rather than precise estimates of absolute changes in hydropower generation. Finally, updating the current stage-storage relationship for Lake Winnipegosis would reduce the uncertainty associated with "local flow" in the Lake Winnipeg sub-basin.

2.8 Availability of Data and Materials

While this study relies on proprietary data provided by MH and HFC, efforts were made to maximize transparency and reproducibility. The publicly available datasets used in this study are referenced in "*2.4. Data*" section. Certain datasets, including hydropower generation records, calibrated operational rules, and system configuration data, are confidential and not publicly accessible; however, they may be obtained directly from MH and HFC under formal data-sharing agreements. For transparency, all model structures, equations, and operational rule formulations are fully described in the main text (section "*2.5.3. Operational Model*"), the Supplementary Material (Table S1), and the custom code in VB.NET available at https://github.com/Gozinih/MB_HydroSim_CustomCode. In the shared custom code, any sensitive data that requires authorization from MH or HFC has been replaced with placeholders 'Num' to protect confidentiality while preserving reproducibility.

CHAPTER 3. INFLOW GENERATION FOR WATER SYSTEM PLANNING IN MULTISITE STUDIES USING TARGET SYNTHETIC STREAMFLOW GENERATION

3.1 Abstract

Robust water-system planning under deep inflow-condition uncertainty requires synthetic streamflow scenarios that capture a wide range of target changes in magnitude, variability, and seasonality; the primary drivers of water-system operations. Targeting these properties ensures that streamflow scenarios align with site-specific operational requirements and effectively capture water-system vulnerabilities. Climate-driven projections provide scenario diversity but do not offer control over streamflow properties. Stochastic generators cannot control streamflow properties, and optimization-based frameworks that do so are computationally expensive. This study introduces a computationally efficient optimization-based framework for generating statistically credible synthetic streamflow scenarios that match target monthly mean and standard deviation at multiple inflow locations. By optimizing the parameters of a widely used streamflow generator, the framework: (i) directly targets streamflow magnitude, variability, and seasonality, (ii) enforces physical and mathematical feasibility of targets scenarios, (iii) uniformly covers the exposure space, avoiding redundancy and ensuring no plausible condition is overlooked. Monthly sequences are disaggregated to daily using k-nearest neighbors method. The framework is demonstrated in the Winnipeg River Basin, Canada, generating synthetic inflows across fourteen locations under historical and future GCM-driven conditions. Results show that optimization improves matching of target statistics and enables uniform exposure space sampling, while preserving or modifying autocorrelation and cross-correlation structures depending on target seasonality. Beyond offering a computationally efficient alternative to prior optimization-based frameworks, the approach complements top-down method: while GCMs provide physically plausible futures, the proposed framework enables transparent, baseline-consistent, and broader exploration of uncertainty informed by top-down insights, supporting stress testing and risk-informed decision-making under deep inflow-condition uncertainty.

3.2 Introduction

Climate change is intensifying the pressure on water systems by altering streamflow regimes, increasing the frequency and severity of hydrologic extremes, and amplifying uncertainty in water supply reliability (Haguma et al., 2017b; Liu et al., 2020). These uncertain changes challenge existing planning paradigms, which have traditionally relied on historical records or a limited set of climate model projections to guide infrastructure design, operations, and policy. Consequently, water resources practitioners seek to assess the operational sensitivities and vulnerabilities of water systems across a broader range of inflow conditions under deep uncertainty; a context characterized by multiple future states with unknown relative probabilities (Beh et al., 2015; Walker et al., 2013). Water resources planning is not well equipped to address deep uncertainty associated with inflow conditions (Rezazadeh et al., 2025).

To support such assessments, it is necessary to generate streamflow scenarios (i.e., inflow conditions) with specific properties, including magnitude, variability, and seasonality, that expand beyond historical observations. Streamflow magnitude governs the available water volume, variability characterizes year-to-year fluctuations in water volume, and seasonality determines intra-annual fluctuations and when the majority of water arrives. Collectively, these properties shape operational behavior and storage-release decisions within water systems (Culley et al., 2016; Herman et al., 2016; Quinn et al., 2018; Wild et al., 2019). Producing specific properties ensures that streamflow scenarios align with site-specific operations and regulatory procedures for the water system planning. For instance, water supply vulnerability assessment under frequent low-flow conditions (Herman et al., 2016), hydropower generation planning and flood management under high-flow conditions with higher temporal variability and seasonal changes (Quinn et al., 2018; Wild et al., 2019), or irrigation and flood management under high-flow conditions with seasonal changes (Culley et al., 2019). Accordingly, streamflow scenarios representing high-flow, low-flow, increased variability, and seasonal change are defined through systematic increases or decreases in inflow magnitude and variability relative to site-specific historical baselines, rather than fixed discharge thresholds. This approach enables consistent application across water systems with differing hydrologic regimes. Expanding beyond historical observations facilitates a deeper understanding of water system sensitivities (Borgomeo et al., 2015). This is particularly important

because the most severe hydrologic events may not be represented in the historical record yet remain plausible in the future (Studnicka & Panu, 2025).

In the *top-down* paradigm, ensembles of global or regional climate model (GCMs and RCMs) outputs are propagated through hydrological models to produce process-based and physically plausible streamflow projections (Fowler et al., 2024). This prominent approach has been successfully applied to assess the impact of climate change on different aspects of water resources management, such as hydropower generation (Kim et al., 2022; Mandal et al., 2019; Minville et al., 2009; Zhao et al., 2022), flood management (Meresa et al., 2021; Yan et al., 2022), and agriculture (Heryani et al., 2022; Karan et al., 2022). These projections are useful for capturing a range of potential inflow conditions and for attributing impacts to specific emissions scenarios. However, top-down streamflow projections are not designed to provide control over the statistical properties of the resulting streamflow series, such as mean flows, low-flow frequencies, or seasonal timing which are critical for system operation and design evaluation.

An alternative is the *bottom-up*, or vulnerability-based framework, which focuses on the water system itself and evaluates its performance under a range of synthetically generated streamflow scenarios (Brown et al., 2011; Fowler et al., 2024). Rather than projecting the future, the bottom-up approach allows for a wider exploration of plausible inflow conditions than those projected by GCMs through the top-down approach; therefore, it can be more flexible for evaluating the operational sensitivities, risks, and vulnerabilities of water resources systems and identifying the viability of adaptive decisions (Alodah & Seidou, 2019; Whateley et al., 2014). By identifying the system's response, this approach facilitates robust decision-making without relying on specific climate models or emissions pathways, affording stress testing of a water system.

Stress testing is a bottom-up approach that enables water resources practitioners to identify critical thresholds in system performance, points at which the water system may fail or perform undesirably (Fowler et al., 2024). This process begins by generating a suite of plausible future streamflow scenarios (i.e., inflow conditions), each characterized by a specific combination of climate or hydrologic stressors within the system's *exposure space*, or the space to which the water system is exposed (Fowler et al., 2024). When climate stressors construct the exposure space dimensions, each stressor represents variations in the statistical properties of climate variables (e.g., annual average air temperature and precipitation; Figure 3 in Culley et al. (2016)). In contrast,

when hydrologic stressors are used to construct the exposure space, each dimension represents variations in the statistical properties of hydrologic variables (e.g., streamflow mean and standard deviation; see Figure 9 in Quinn et al. (2018)). These future streamflow scenarios may or may not be physically plausible, since the goal is not to predict the future; however, they are plausible and expose the water system to a broad range of inflow conditions to assess its adaptive capacity. Water system performance can then be evaluated against each scenario to determine whether it meets operational or regulatory objectives. The boundary separating acceptable from unacceptable performance in the exposure space defines the system's critical threshold states, i.e., the statistical properties at which the failure (undesired outcome) occurs. Stress testing has been widely used in different studies for balancing flood control and irrigation supply (Culley et al., 2016, 2021), flood risk assessment (O'Shea et al., 2024; Prudhomme et al., 2010), drought and flood risk reduction (Steinschneider et al., 2015), hydropower system design (Taner et al., 2017), reservoirs planning for hydropower production, agricultural water supply, and flood protection (Quinn et al., 2018), and water supply-demand management (Herman et al., 2015; Whateley et al., 2015).

Risk-informed decision-making has been applied in sectors like water and energy to support decision-making under uncertainty (Alipour, 2015). It builds on stress testing by quantifying the risks associated with undesired events and providing robust strategies to reduce those risks. Risk is defined as the product of the probability and consequence of an undesired event (Van Staveren, 2018), thereby capturing both likelihood and severity of system failures. In water resources, inflows are uncertain, and stress testing and subsequent risk-informed decision-making require the generation of plausible future streamflow scenarios that:

1. Are statistically credible in terms of distribution, auto-correlation, and cross-correlation.
2. Appropriately target key statistical properties of streamflow, magnitude, variability, and seasonality, so that undesired events emerge in ways consistent with the water system context (e.g., hydropower, water supply, agriculture).
3. Span a wide range of inflow conditions to adequately represent deep uncertainty.
4. Uniformly cover the exposure space, ensuring that no inflow condition is overrepresented or overlooked and that full spectrum of plausible conditions is explored.
5. Remain physically and mathematically feasible, where physical feasibility requires non-negative magnitude and variability, and mathematical feasibility requires that target

magnitude-variability combinations are attainable under the parameterization of the adopted streamflow generator.

6. Can be generated computationally efficiently (run time for streamflow scenario generation), making large-scale assessments within practical timeframes.

There are two alternative methods in the bottom-up framework for generating plausible future streamflow scenarios: (1) rescaling historical data or (2) using stochastic generators. In the rescaling approach, one option is to rescale observed hydrometeorological data and use it as input into a hydrological model to generate the streamflow scenario (Culley et al., 2016; Prudhomme et al., 2010). Alternatively, the observed streamflow data itself can be directly rescaled. Rescaling allows for producing the target magnitude and seasonality but lacks the capability to simultaneously rescale variability for a target value. The second method applies stochastic weather or streamflow generators to produce plausible future streamflow scenarios. One option is to generate synthetic hydrometeorological data using stochastic weather generators and use it as input into a hydrological model to generate plausible future streamflow scenarios (Culley et al., 2021; Whateley et al., 2015). Alternatively, synthetic streamflow scenarios can be directly generated using stochastic streamflow generators (Yuan Liu et al., 2023; Sakki et al., 2022). Direct stochastic streamflow generation avoids uncertainties associated with hydrological model selection and parameterization (Herman et al., 2016).

Stochastic streamflow generators can be broadly classified as non-parametric or parametric. Non-parametric approaches, such as k-nearest neighbors bootstrap resampling (Lall & Sharma, 1996; Sharma et al., 1997), rely only on the historical record and therefore have limited ability to extrapolate beyond observed streamflow properties (You et al., 2014). AI-based streamflow generators, such as application of artificial neural network (ANN; Raman & Sunilkumar (1995)) also fall within the non-parametric category. While effective at reproducing non-linear dynamics, the internal representations of AI-based models are opaque, offering limited interpretability and control over the mechanisms used to generate synthetic streamflow scenarios (Studnicka & Panu, 2025). Compared to non-parametric generators, parametric generators enable extrapolation beyond observed streamflow properties, clearer identification of the dominant drivers shaping synthetic scenarios, and direct and systematic control over streamflow statistical properties. These

capabilities are essential for generating target inflow scenarios and supporting subsequent stress-testing and risk-informed decision-making analysis.

Parametric stochastic streamflow generators include autoregressive models, such as autoregressive (AR; A. Thomas & B Fiering (1962)), autoregressive moving average (ARMA; Hipel et al. (1977)), and periodic autoregressive moving average (PARMA; Rasmussen et al. (1996)), as well as Markov-based models (Yakowitz, 1979). These models rely on linear dependence structures typically under stationarity assumptions, which limits their flexibility in representing non-linear changes in streamflow statistical properties (Studnicka & Panu, 2025). Another parametric approach involves distribution-based generators, which assume prescribed probability distributions for streamflow to represent the non-linear changes in streamflow statistical properties (e.g., Gaussian; Kirsch et al. (2013)). Distribution-based stochastic streamflow generators allow direct, systematic, and transparent extrapolation beyond observed streamflow properties. However, they cannot guarantee that generated streamflow scenarios automatically meet the target statistical properties. This limitation arises from the non-linear relationship between the generator parameters and the resultant statistical properties (Guo et al., 2016).

Guo et al. (2016) successfully applied the inverse approach for generating synthetic rainfall scenarios with target statistical properties by optimizing parameters of stochastic weather generators, but at high computational cost. Since runoff and streamflow are influenced by multiple hydrometeorological variables, such as rainfall, temperature, humidity, and wind speed, Guo et al. (2017) showed that restricting the inverse approach to the most influential variables is necessary to constrain the dimensionality of the exposure space and reduce computational burden. Culley et al. (2019) further reduced computational costs of the optimization process by adding bounds on the parameters of weather generators and the use of penalty-based objective functions. However, weather-generator-based inverse approaches still require repeated execution of hydrological models. In contrast, stochastic streamflow generators bypass hydrological modeling, reducing computational cost while allowing direct control over streamflow statistical properties. For this reason, Borgomeo et al. (2015) and Wheeler et al. (2025) applied optimization on a non-parametric synthetic streamflow generator in single-site and multisite case studies, respectively. Compared to parametric, application of inverse approach on a non-parametric stochastic streamflow generator

allows greater control over streamflow properties but at the expense of higher computational effort, since optimization must adjust the entire time series rather than a set of parameters. Therefore, a gap remains in applying the inverse approach to parametric stochastic streamflow generators that can generate computationally efficient scenarios by directly targeting key statistical properties of streamflow in multisite studies without relying on a hydrological model.

The parametric, distribution-based stochastic streamflow generator developed by Kirsch et al. (2013) has been widely applied in the literature due to its simplicity and effectiveness in generating weekly or monthly scenarios for multisite water systems (Giuliani et al., 2018; Gold et al., 2023; Lau et al., 2023; Yueyi Liu et al., 2023; Quinn et al., 2024, 2018, 2017; Trindade et al., 2017; Wild et al., 2019; Zeff et al., 2016). The stochastic streamflow generator by Kirsch et al. (2013) is often coupled with the disaggregation approach by Nowak et al. (2010) to convert monthly or weekly synthetic streamflow into daily values. This disaggregation is essential for operating water systems, which typically function daily (Giuliani et al., 2018; Gold et al., 2023; Lau et al., 2023; Yueyi Liu et al., 2023; Quinn et al., 2024, 2018, 2017; Trindade et al., 2017; Wild et al., 2019; Zeff et al., 2016). Accordingly, the present study also incorporates Nowak et al. (2010) method solely to provide the capability to disaggregate target monthly scenarios into daily. The monthly-to-daily disaggregation is not a factor impacting the purpose and evaluation of the developed framework in this study. This study focuses on generating target monthly streamflow scenarios. In addition, disaggregation to daily resolution is based on the k-nearest neighbors method, which resamples historical daily patterns that may not occur in the future under substantially different streamflow regimes.

This study addresses the aforementioned limitations by introducing a novel framework for generating synthetic streamflow scenarios with target (user-specified) statistical characteristics in multisite water resources systems. The framework applies the inverse approach (optimization) to the parametric stochastic streamflow generator introduced by Kirsch et al. (2013), enabling direct control over the key statistical properties of streamflow including monthly mean (i.e., magnitude or volume) and standard deviation (SD; i.e., variability) at multiple locations. By targeting streamflow magnitude and variability, the framework has the capability to generate scenarios that align with site-specific operational or regulatory objectives, and are statistically credible in terms of distribution, auto-correlation, and cross-correlation. By targeting a specific set of 12 monthly

means and SD, this framework can capture specific seasonality of streamflow magnitude and variability, a critical feature for the operational systems affected by seasonal peaks and low-flow. The framework uniformly covers the exposure space, avoiding redundancy while exploring all target plausible conditions. Furthermore, by characterizing and constraining the feasible region of the exposure space, the framework ensures that only physically and mathematically feasible scenarios are produced. Collectively, the framework enables a computationally efficient generation of scenarios, offering a powerful alternative to other optimization-based frameworks for synthetic streamflow generation, and thereby supporting effective stress testing and risk-informed decision-making in complex multisite water systems. The practical relevance of the framework is demonstrated through example stress-testing applications using the generated target scenarios.

The efficiency and impact of applying the inverse approach is evaluated by comparing its results with those obtained using Kirsch et al. (2013) methodology (non-optimized scenarios) in a multisite case study in the Winnipeg River Basin. The assessment focused on the ability to target and uniformly expand historical streamflow magnitude and variability while preserving seasonality. To explore seasonality change under future conditions, additional scenarios are also generated based on GCM-informed targets. The statistical credibility of the target scenarios is assessed through analysis of distribution, autocorrelation, and cross-correlation, examining both the preservation of historical structure and the effects of seasonal shifts in comparison to GCM-driven scenarios. The computational efficiency of the framework is evaluated by comparing its computation time (run time per 100 target scenarios generation) against the results reported by Guo et al. (2016), which presents application of inverse approach on stochastic weather generators, as well as Borgomeo et al. (2015) and Wheeler et al. (2025), which demonstrate inverse-approach application on non-parametric stochastic streamflow generators.

3.3 Methodology

This section presents the framework and its components (Section 3.3.1), provides an illustrative example of expected outcomes when targeting scenarios (Section 3.3.2), and describes a case study used to evaluate the framework capability to generate scenarios that meet targets while maintaining statistical credibility (Sections 3.3.3 and 3.3.4). In addition, three examples of stress-testing

applications are presented to demonstrate how the generated target scenarios can be used in practice (Section 3.3.5).

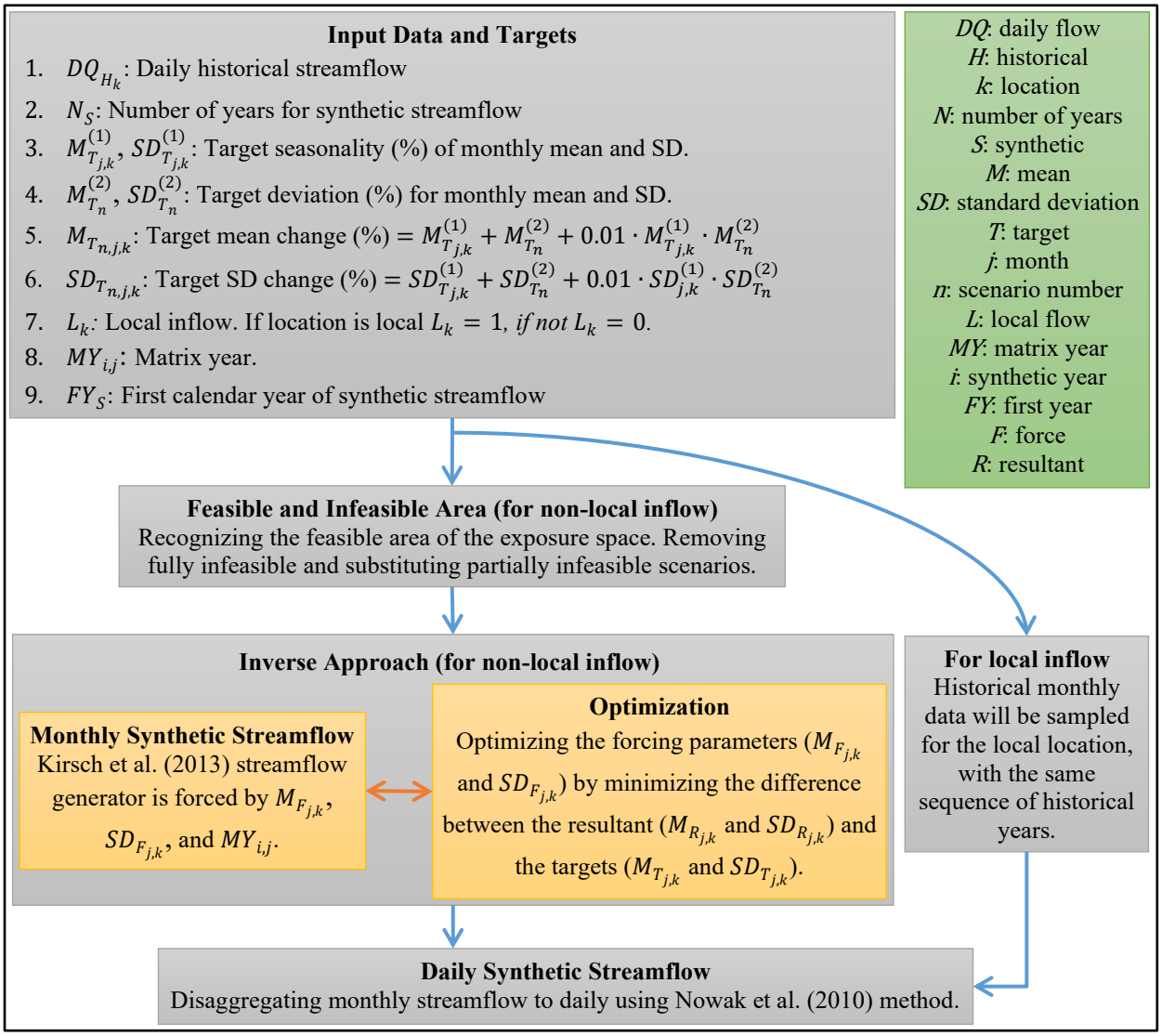


Figure 3.1. The framework for generating target streamflow scenarios in multisite water systems.

3.3.1 Target Synthetic Streamflow Generation Framework

This section outlines the inverse (optimization) framework developed to generate target synthetic streamflow scenarios. The framework builds on the generator developed by Kirsch et al. (2013) for monthly streamflow generation and applies the disaggregation method of Nowak et al. (2010) to obtain daily series. A high-level overview is shown in Figure 3.1. The framework consists of several modular components, described in the following subsections. The entire

framework is coded in Python and is publicly available on Gozini et al. (2025). Supplementary plotting scripts are also provided to visually display the resultant target streamflow scenarios.

3.3.1.1 Input Data and Targets

The key input data used across the various components of the framework include daily historical streamflow for each location, the target number of years for the synthetic streamflow, target seasonality and deviation for monthly mean and SD, locations with local flow, matrix year, and the first calendar year of synthetic streamflow.

The sum of daily flow (DQ) for each month provides the historical monthly streamflow (Q) timeseries. The historical monthly timeseries exhibits 12 monthly mean and SD values for the streamflow at each location. In this study, the seasonality of streamflow refers to the relative variations among the 12 monthly mean and SD values. To generate monthly synthetic streamflow for a target duration of N_S years, the historical monthly mean and SD of streamflow can be altered by changing the seasonality ($M_T^{(1)}$and $SD_T^{(1)}$) and applying deviation ($M_T^{(2)}$and $SD_T^{(2)}$) from that seasonality. Seasonality can be altered by applying a target percentage change ($M_{T_{j,k}}^{(1)}$and $SD_{T_{j,k}}^{(1)}$) for each month (j) and location (k). Since the percentage change can vary by month, it will alter the monthly mean and SD seasonality. Users also have the option to adjust the seasonality differently at each location. Another target alteration over monthly mean and SD involves applying a uniform percentage change (deviation or delta change) for all months and locations ($M_{T_n}^{(2)}$and $SD_{T_n}^{(2)}$). Different percentage deviations can be targeted in different scenarios (n). Since it is a uniform change, it does not change the seasonality of monthly mean and SD. The combination of the two target changes gives the scenarios of the target mean and SD changes on the exposure space for each location and month ($M_{T_{n,j,k}}$ and $SD_{T_{n,j,k}}$). The combined impact of the two percentage changes is not simply additive, and it incorporates an interaction term (Equation 3.1). Term "$M_{T_n}^{(2)} + 0.01 \cdot M_{T_{j,k}}^{(1)} \cdot M_{T_n}^{(2)}$" in Equation (3.1) represents the final deviation percentage from the target seasonality, $M_{T_{j,k}}^{(1)}$. The same logic applies to the target SD change.

$$M_{T_{n,j,k}} = \left(\left(1 + \frac{M_{T_{j,k}}^{(1)}}{100}\right) \cdot \left(1 + \frac{M_{T_n}^{(2)}}{100}\right) - 1\right) \cdot 100 = M_{T_{j,k}}^{(1)} + M_{T_n}^{(2)} + 0.01 \cdot M_{T_{j,k}}^{(1)} \cdot M_{T_n}^{(2)} \quad (3.1)$$

Each target scenario is generated by following the steps outlined below.

3.3.1.2 Monthly Synthetic Streamflow Generator

The synthetic streamflow generator developed by Kirsch et al. (2013) is suitable for multisite studies since it applies Cholesky decomposition to preserve autocorrelation and bootstrap resampling to maintain cross-correlation. The historical (H) monthly streamflow data, derived from daily timeseries and spanning N_H years, are utilized to generate the monthly synthetic (S) streamflow for a target duration of N_S years. The following steps are followed at each location (k) separately to generate a monthly synthetic streamflow scenario (Figure 3.2):

1. Log-transform ($Y_{H_{i',j,k}}$, where i' and j are the historical year and month) monthly streamflow records.
2. Standardize ($Z_{H_{i',j,k}}$) the log-transformed monthly streamflow records.
3. Generate matrix year ($MY_{i,j}$) which is an array with a size of N_S×12 and is randomly sampled with replacement from historical years (1 to N_H) for each year and month of the monthly synthetic streamflow. The matrix year is held constant for all locations in a single scenario to preserve cross-correlation.
4. Generate the uncorrelated synthetic data ($C_{i,j,k}$, where i is the synthetic year) by bootstrap sampling with replacement from the standardized data ($Z_{H_{(MY_{i,j}),j,k}}$) based on the matrix year.
5. Calculate monthly historical autocorrelation (P_{H_k}).
6. Calculate Cholesky decomposition of monthly historical autocorrelation.
7. Generate monthly synthetic correlated data (Z_{S_k}) by multiplying the upper triangle (U_k), resulted from the Cholesky decomposition, with the uncorrelated data ($C_{i,j,k}$).
8. Generate monthly synthetic correlated data (Z'_{S_k}) by applying steps 4-6 to the observed data excluding the first and last 6 months (Z'_H). This preserves the year-to-year autocorrelation.

9. Concatenate Z_{S_k} and Z'_{S_k} to produce the final normalized, log-transformed, and correlated monthly synthetic data (Z_{S_k}).
10. Transform the monthly synthetic data to real space ($Y_{S_{i,j,k}}$).

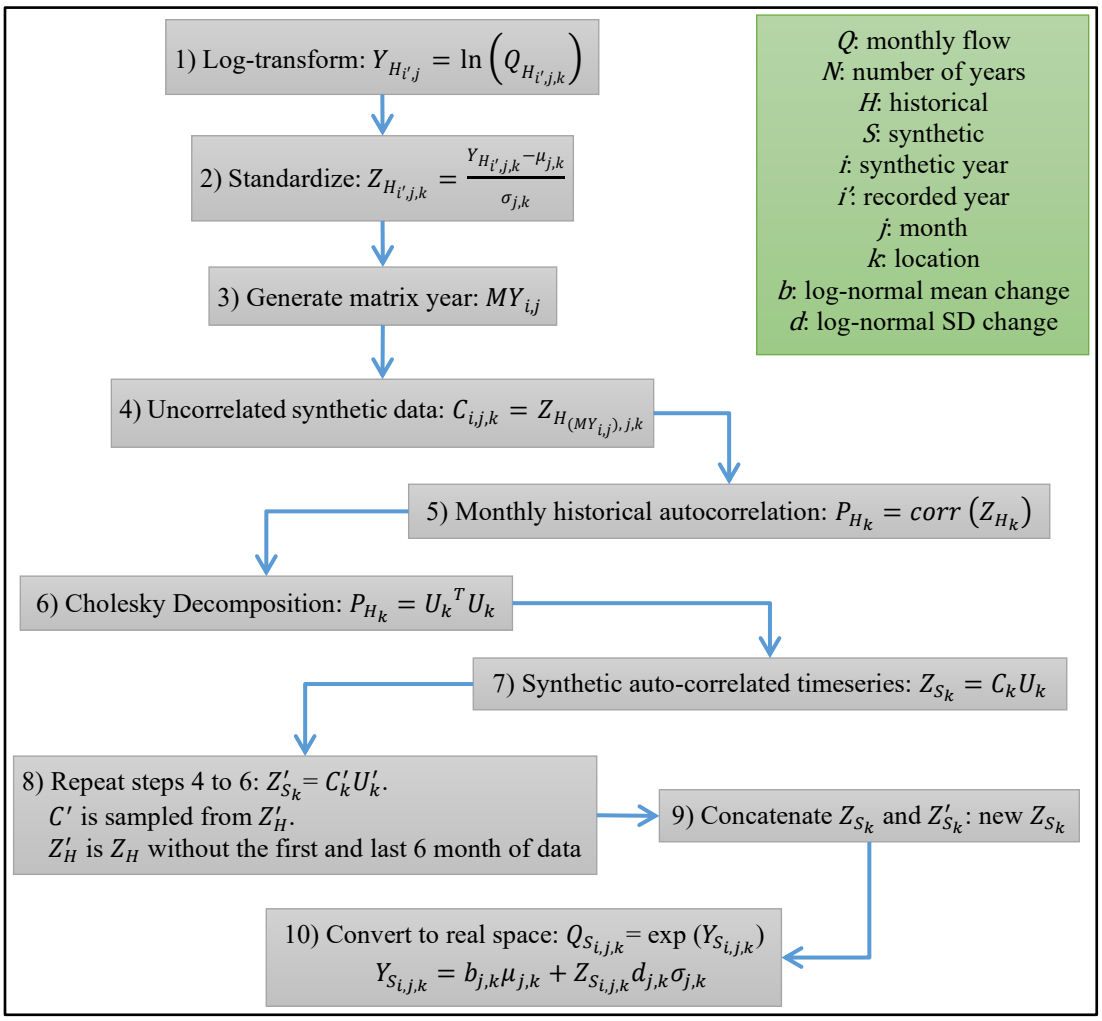


Figure 3.2. The flowchart of the monthly synthetic streamflow generator developed by Kirsch et al. (2013).

When reverting the log-transformed normalized data back to real space, the real-space mean and SD can be adjusted. The unknown change coefficients in the log-normal space (b and d) can be calculated based on the known changes in the real space (a and c):

$$a_{j,k} = 1 + \frac{M_{F_{j,k}}}{100} \tag{3.2}$$

$$c_{j,k} = 1 + \frac{SD_{F_{j,k}}}{100} \tag{3.3}$$

$$b_{j,k} = \frac{\ln(a_{j,k}) + \mu_{j,k} + \frac{\sigma_{j,k}^2}{2} - \frac{1}{2}\ln\left[\left(\frac{c_{j,k}}{a_{j,k}}\right)^2 . \left(e^{\sigma_{j,k}^2} - 1\right) + 1\right]}{\mu_{j,k}} \tag{3.4}$$

$$d_{j,k} = \sqrt{\ln\left[\left(\frac{c_{j,k}}{a_{j,k}}\right)^2 . \left(e^{\sigma_{j,k}^2} - 1\right) + 1\right]} \tag{3.5}$$

Where $M_{F_{j,k}}$ and $SD_{F_{j,k}}$ are forcing mean and SD changes in real space, μ is the log-normal mean, and σ is the log-normal SD of historical records. The retransformation is non-linear causing the resultant real-space mean and SD change ($M_{R_{j,k}}$ and $SD_{R_{j,k}}$) to differ from the forced ones ($M_{F_{j,k}}$ and $SD_{F_{j,k}}$).

In addition to the real-space mean and SD forcing changes, matrix year (MY) is the other variable in the monthly synthetic streamflow generator. One single set of forcing mean and SD changes can produce different monthly synthetic streamflow timeseries by randomly resampling a different matrix year.

3.3.1.3 Feasibility of Target Scenarios

Feasible target scenarios are those that the framework is capable of generating and are located within the feasible area of the exposure space (green-shaded in Figure 3.3). Due to the presence of the term $\ln(a)$ in Equation (3.4), a must be greater than zero, implying forcing mean change in real space (M_F) must be greater than -100%. Forcing SD change in real space (SD_F) can be any value since there is no boundary on c in Equations (3.4) and (3.5). However, when forcing, the resultant monthly mean (M_R) and SD (SD_R) changes of the synthetic streamflow cannot reach a specific area of the exposure space. This area is called infeasible (red-shaded area in Figure 3.3) since the stochastic streamflow generator cannot produce any scenarios for that region. This infeasibility reflects mathematical constraints imposed by the adopted log-normal retransformation and forcing formulation in Equations (3.2)-(3.5). If an alternative distribution (e.g., Gamma) or a non-parametric generator were adopted, the shape and extent of the mathematically infeasible region would differ and may be reduced or eliminated.

Obviously, resultant mean and SD changes cannot exceed -100%, as this would result in negative mean and SD values which are physically infeasible. A lower bound of -95% is used instead of -100% to ensure streamflow values remain near zero without becoming exactly zero.

Beyond this bound, the parameterization of the adopted stochastic streamflow generator defines an infeasible area. Specifically, it is infeasible to significantly decrease the mean while decreasing the SD of streamflow (1 in red-shaded area) since significant reduction in the mean causes monthly streamflow to approach low values, making it infeasible to modify SD except in cases with a high rate of decrease. Similarly, increasing SD while adjusting the mean (2 in red-shaded area) is also infeasible in some cases when the minimum flow value would need to drop below zero (physically impossible for streamflow). Consequently, locations with a low mean and high SD exhibit higher coefficient of variation ($CV = \frac{SD}{Mean}$) and a larger infeasible area, as relatively smaller adjustments bring the values closer to zero, limiting SD and mean adjustment. Therefore, the size and shape of the infeasible area vary across locations and months, as their mean and SD influence the retransformation in Equations (3.4) and (3.5).

In principle, the feasible area is not bounded in the positive direction, as large increases in mean can be combined by substantial SD increase. In practice, the effective upper bounds, denoted as M_R^{max} and SD_R^{max} in Figure 3.3, are imposed to enable numerical construction of feasible and infeasible area in the exposure space. To distinguish between the feasible and infeasible areas, their boundary on the exposure space (red line in Figure 3.3) is identified explicitly. This boundary is generated for each location and month by running the monthly synthetic streamflow generator under extreme forcing scenarios; combinations of M_F = -99 to 2000% and SD_F = -2000%. The resultant mean and SD changes of these extreme scenarios are archived. The resultant changes corresponding to M_F = 2000% and SD_F = -2000% define M_R^{max} and SD_R^{max}. The archived values along with the lower bounds of -95% for both mean and SD changes define the polygon of the feasible area for each location and month. Increasing M_F beyond +2000% would further expand the upper-right boundary of the feasible region and can be implemented depending on user objectives. To provide context for the magnitude of these extreme conditions, the case study evaluated in this work yields a minimum M_R^{max} of 1595% across all locations and months.

Target mean and SD changes that fall outside the feasible area (red, orange, and blue dots on Figure 3.3) are considered infeasible. The framework eliminates fully infeasible scenarios (i.e., those with infeasible targets across all locations and months). Moreover, the framework replaces infeasible targets in partially infeasible scenarios (i.e., those with infeasible targets in some locations and months) with the nearest feasible target within the exposure space of the

corresponding location and month. To replace infeasible targets in partially infeasible scenarios, the framework first identifies infeasible targets with mean or SD change lower than -95% (red dots on Figure 3.3) and replaces them with -95% (orange and yellow dots). Next, if the target remains infeasible (orange dot) or if the infeasible target has a mean and SD changes higher than -95% (blue dot), the SD change target is replaced with the nearest feasible SD change (green dots), while keeping the target mean change unchanged. Identifying and modifying partially infeasible scenarios ensures computational efficiency and broader coverage of the exposure space while maintaining feasibility, specifically when applying seasonality changes. For example, a scenario at one location might specify an infeasible target mean and SD change of -98% for January and a feasible target mean and SD change of -50% for February, while another location has a feasible target mean and SD change of -40% for both months. Replacing the infeasible -98% target with the feasible -95% ensures that the flow in January at the first location remains low and near zero while still allowing the feasible -40% and -50% targets at the other location and month to be achieved.

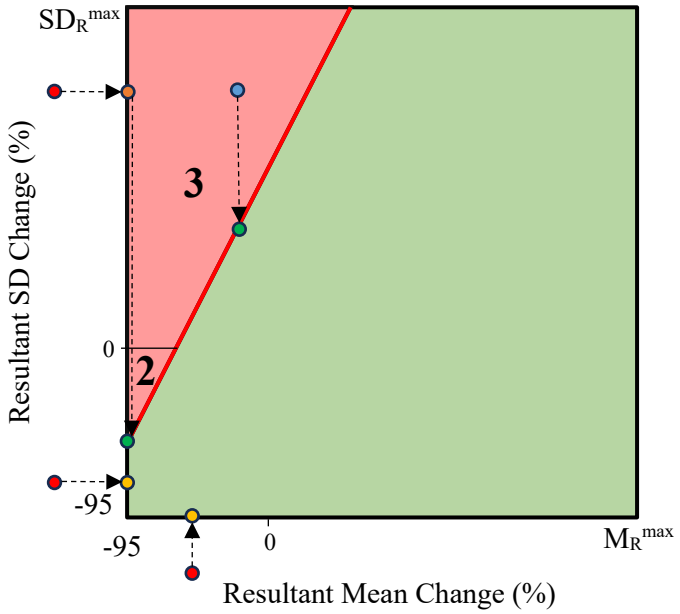


Figure 3.3. Feasible (green region) and infeasible (red region) area of the exposure space, separated with a boundary line (red). The boundary is a curve due to the non-linear retransformation in Equations (3.4) and (3.5); however, it is shown as a straight line for visual clarity. Infeasible area is divided into two sections, when decreasing (1) or increasing (2) the SD. Red, orange and blue dots represent infeasible targets, replaced by feasible targets shown as green and yellow dots.

3.3.1.4 Optimization Procedure

Optimization is performed separately for each month (j) and location (k); optimized parameters of the monthly synthetic streamflow generator at each location do not impact optimized values at the other locations. Similarly, the mean and SD forcing changes for each month only affect that specific month. The forcing parameters of the monthly synthetic streamflow generator ($M_{F_{j,k}}$ and $SD_{F_{j,k}}$) are optimized by minimizing the difference ($D_{j,k}$) between the resultant change of monthly mean and SD ($M_{R_{j,k}}$ and $SD_{R_{j,k}}$) and the target one ($M_{T_{j,k}}$ and $SD_{T_{j,k}}$):

$$\begin{aligned} &\min D_{j,k} = \left|M_{R_{j,k}} - M_{T_{j,k}}\right| + \left|SD_{R_{j,k}} - SD_{T_{j,k}}\right| \\ &\textit{Where}: \\ &\quad M_{R_{j,k}} = f\left(M_{F_{j,k}}, SD_{F_{j,k}}\right) \\ &\quad SD_{R_{j,k}} = f\left(M_{F_{j,k}}, SD_{F_{j,k}}\right) \\ &\textit{Constraints}: \\ &\quad -99 \le M_{F_{j,k}} \le 2000 \\ &\quad -2000 \le SD_{F_{j,k}} \le 2000 \end{aligned} \tag{3.6}$$

Terms $M_{R_{j,k}} = f\left(M_{F_{j,k}}, SD_{F_{j,k}}\right)$ and $SD_{R_{j,k}} = f\left(M_{F_{j,k}}, SD_{F_{j,k}}\right)$ show that monthly mean and SD change of the generated synthetic streamflow are functions of forcing mean and SD change. Since the monthly synthetic streamflow generator is non-linear, these functions are also non-linear. The "*differential evolution*" algorithm from "*SciPy*" library in Python is used to minimize the objective function in Equation (3.6). Constraints are set to 2000 to provide a sufficient range for identifying the optimized parameters, while also limiting the search space to reduce computational costs. If larger resultant monthly mean or SD changes are required, this upper bound can be increased accordingly, provided that the feasible area is re-delineated under the expanded forcing range. The only strict constraint is on the lower bound of the forced mean change, which must remain greater than -100%. The mean and SD are equally weighted in the objective function because the purpose of this study is to assess whether both properties can be simultaneously optimized toward their target values without imposing subjective priorities. In practice, users may introduce weights on the absolute differences to emphasize specific properties; for example, a higher weight may be assigned to the mean than to the SD. Because the mean represents inflow magnitude, it often exerts a stronger influence on decision-making by governing both the overall and seasonal volume of streamflow.

When generating multiple scenarios with different target mean and SD change, a single matrix year is generated and used for all scenarios to force the synthetic streamflow generator. This will ensure all scenarios are consistent regarding the matrix year. Conversely, to generate multiple scenarios for a single target mean and SD changes, a different matrix year must be generated and used for each scenario.

3.3.1.5 Local Inflow Location

The framework provides the ability to flag inflow locations as local or non-local. For local locations, historical monthly data is resampled while preserving the original temporal sequencing. In contrast, optimization to match target magnitudes and variability is applied to non-local inflows. In cases where "local flow" contributions are computed from the application of a mass-balance to determine unmeasured inputs and losses into a water system (Gozini et al., 2026a), these inputs can be treated as local inflow locations. Since these computed "local inflows" are not a natural time series, it is not possible to optimize them to meet specific statistical targets.

3.3.1.6 Daily Disaggregation of Synthetic Flows

The k-nearest neighbors method, as described by Nowak et al. (2010) is used to disaggregate monthly synthetic streamflow into daily timeseries' (Figure 3.4). The selected year (y_i'), which is one of the historical years (i', from 1 to N_H), is identified separately for each synthetic year (i, from 1 to N_S) to apply the disaggregation. The selected year represents the nearest historical year to the synthetic year, where nearness is measured using the Euclidean distance (ED) between monthly synthetic and observed streamflow. To compute *ED*, only non-local inflow locations (k) are considered, since local inflows are directly resampled from observations and should not influence *ED* calculation. Once the selected year is identified, its proportional daily historical streamflow (*PD*; daily divided by total monthly) is applied for disaggregation across all locations (k'), including both local and non-local. Disaggregation steps are as follows:

1. Calculate the Euclidean distance ($ED_{i,i'}$), which defines the nearness between each year (i) of synthetic monthly streamflow and each year (i') of observed monthly streamflow and is the sum of the distance (difference between monthly synthetic and observed streamflow) for all non-local locations and months.
2. Sort the recorded years based on Euclidean Distance from the lowest to highest.

3. Calculate K ($= \lfloor {N_H}^{0.5} \rfloor$).
4. Identify the first K nearest years (y_i) for each synthetic year from the sorted recorded years in step 2.
5. Calculate the probability (p) of the K nearest years based on their ranks (r: from 1 to K) using the Kernel estimator ($p_{y_i} = \frac{1/r_i}{\sum_{r=1}^{K} 1/r_i}$).
6. Calculate cumulative probability (P_{y_i}) of the K nearest years.
7. Randomly select a year (y_i') from the K nearest years based on their cumulative probability.
8. Calculate the proportional daily historical streamflow of the selected year ($PD_{y_i',k'}$) by dividing the daily observed streamflow ($DQ_{H_{y_i',k'}}$) by the total monthly observed streamflow ($Q_{H_{y_i',k'}}$) at each location.
9. Generate the daily synthetic streamflow ($DQ_{S_{i,k'}}$) is by multiplying the monthly synthetic streamflow ($Q_{S_{i,k'}}$) by the proportional daily historical streamflow of the selected year.

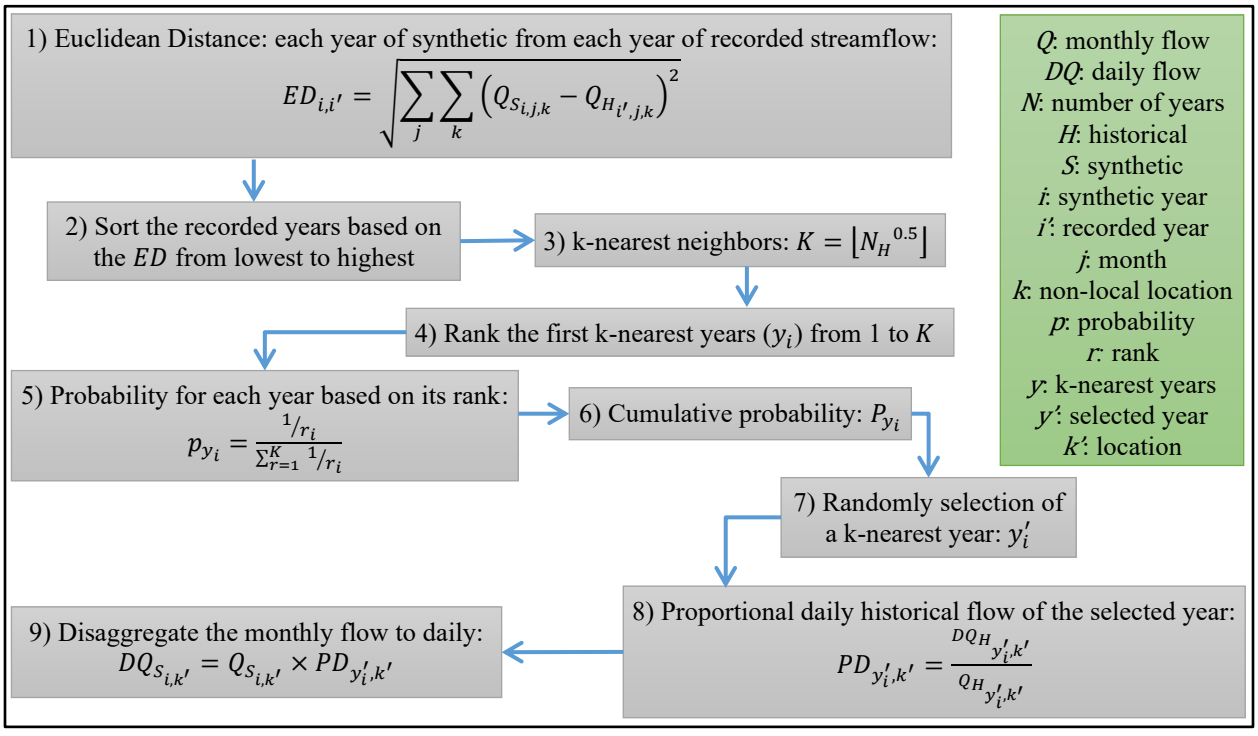


Figure 3.4. The flowchart of disaggregating monthly synthetic streamflow to daily, using the method of Nowak et al. (2010)

Once disaggregation is completed, the full daily timeseries must be adjusted for leap and non-leap years. The selected year might be a historical leap (non-leap) year and is used for the monthly-to-daily disaggregation of a synthetic non-leap (leap) year. Therefore, each synthetic year in the daily timeseries is numbered sequentially, starting from FY_S (the first calendar year of synthetic streamflow). The code then identifies the leap and non-leap years and adjusts the daily streamflow where necessary by either adding or removing the absent or extra day.

3.3.2 Illustrative Example

As an illustrative example, the framework is applied through four feasible scenarios for an imaginary and simple two-location case study (k) with a three-month streamflow (j). While this example is intentionally simple, the framework is applicable to multisite case studies and is not limited to two locations. It is assumed that none of the locations are local, and the same matrix year is used across all scenarios. In the first scenario, no changes are introduced in an effort to reproduce the historical record of monthly mean and SD (i.e., mean and SD changes for both locations and all three months are set to 0 in the exposure space; red circles and squares on Figure 3.5, representing locations 1 and 2, respectively). Consequently, monthly streamflow generated at both locations (i.e., red circles and squares on Figure 3.6) has the same monthly mean and SD as the historical record (i.e., black-outlined circles and squares on Figure 3.6).

The second scenario targets monthly streamflow with a set percent deviation from the historical mean (a%) and SD (b%) for both locations and all months (i.e., blue circles and squares on Figure 3.5). Due to the application of percentage deviations (i.e., delta change), resultant streamflow (i.e., blue circles and squares on Figure 3.6) follows the same historical monthly mean and SD seasonality at both locations.

The third scenario aims to change the mean ($a_{k,j}$%) and SD ($b_{k,j}$%) seasonality at both locations while preserving a deviation change of 0%. At the first location (i.e., green circles on Figure 3.5a), the mean for the first and third months is targeted to increase ($a_{1,1}$ and $a_{1,3}$), while decreasing in the second month ($-a_{1,2}$), with no change to the seasonality of monthly SD. Figure 3.6a, shows that the seasonality of the mean has changed at location one (i.e., green circles), with low-flow occurring in month two, where historically the peak flow occurred (i.e., black-outlined circles). At the second location (i.e., green squares on Figure 3.5b), mean streamflow seasonality is targeted to increase the peak flow in month one ($a_{2,1}$) and decrease the relatively lower flow in months two

and three ($-a_{2,2}$ and $-a_{2,3}$), and the SD for all three months is targeted to increase ($b_{2,1}$,$b_{2,2}$, and $b_{2,3}$). The low flow in months two and three (i.e., green squares Figure 3.6c) have higher rates of SD change increase (i.e., green squares on Figure 3.6d).

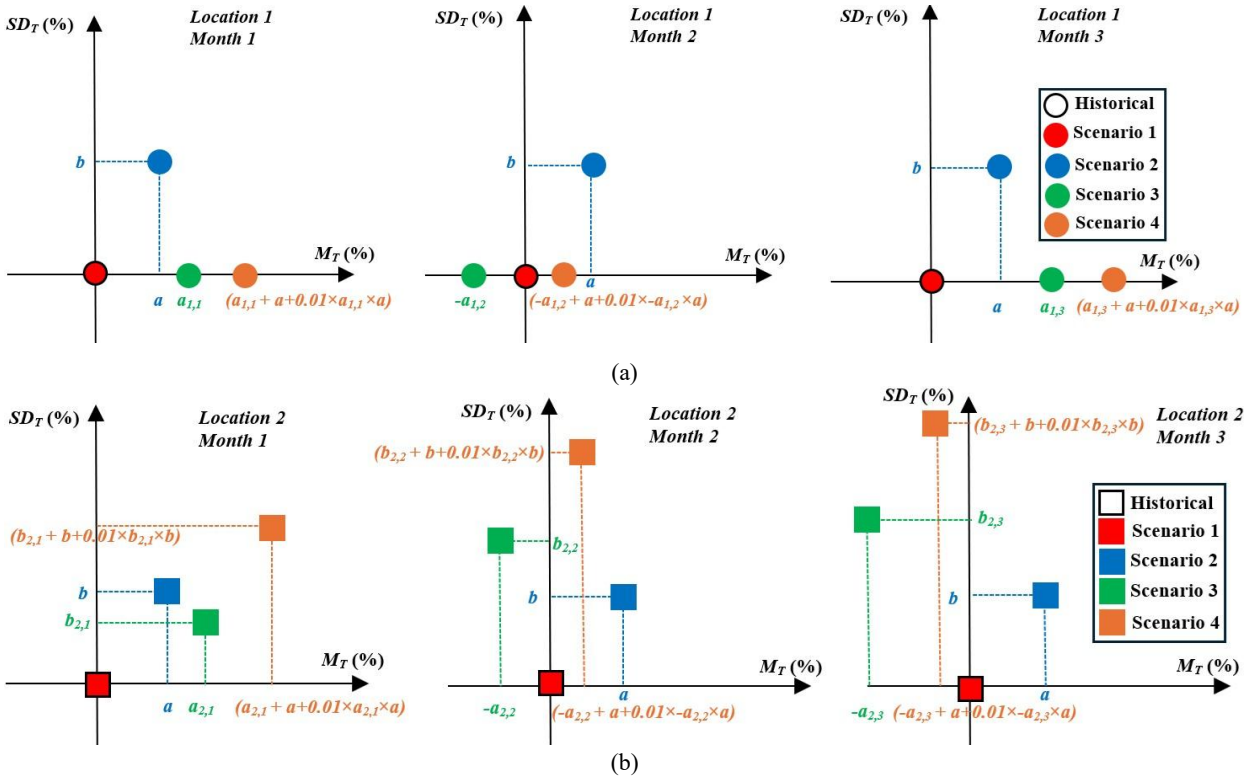


Figure 3.5. Monthly target mean (M_T) and SD (SD_T) changes in four target scenarios at (a) location 1 and (b) location 2. Circles represent location 1, while squares represent location 2.

The fourth scenario (i.e., orange circles and squares on Figure 3.5) targets both the deviation of the mean and SD from scenario two and seasonality change from scenario three. The combined impact of these two percentage changes is based on Equation (3.1). As shown on Figure 3.6 (orange circles and squares), scenario four deviations are from the target seasonality of scenario three, and the magnitude of deviation is based on the interactive term mentioned for Equation (3.1).

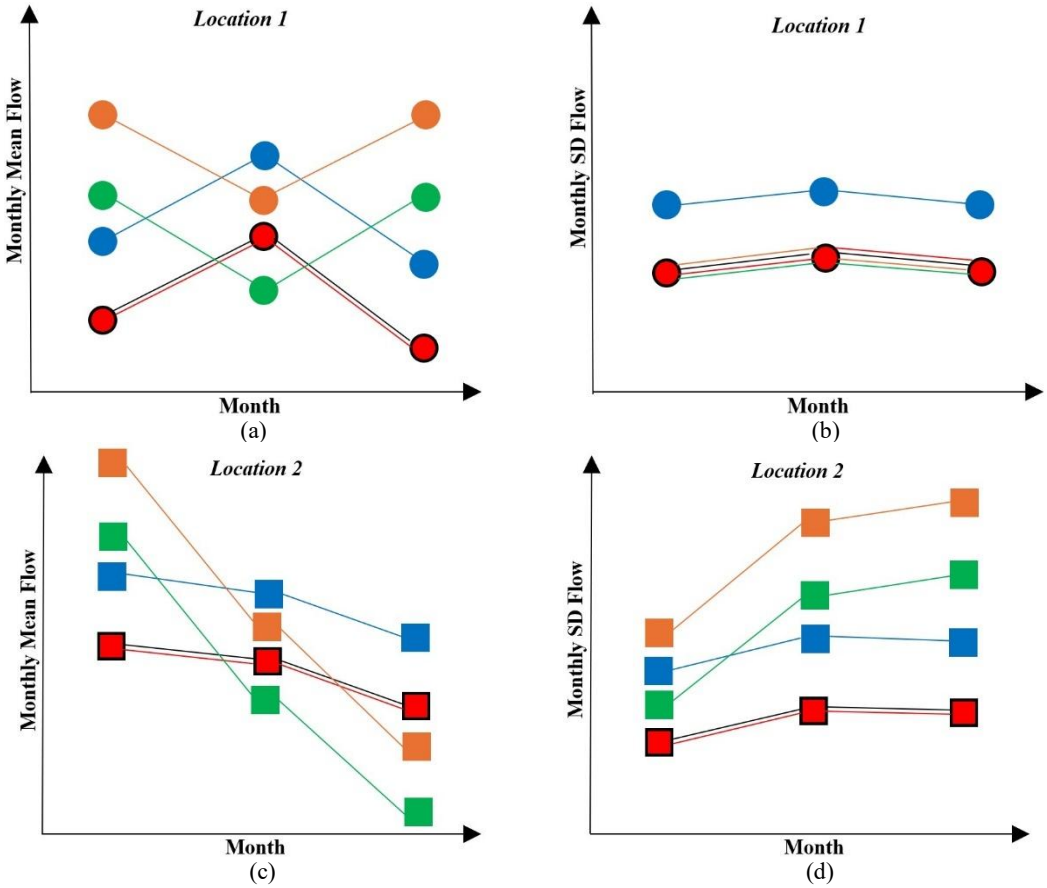


Figure 3.6. Monthly mean and SD seasonality of the target scenarios (Figure 3.5) and the historical records at (a, b) location 1 and (c, d) location 2. Circles represent location 1, while squares represent location 2.

3.3.3 Case Study: Winnipeg River System

The Winnipeg River Basin in central Canada is used as a case study to apply the framework and assess its capacity to generate target streamflow scenarios as inflow to a multisite water system (Figure 3.7). The Winnipeg River Basin covers 136,840 km^2, with 8% located in the Province of Manitoba and 71% in the Province of Ontario, Canada. The remaining 21% is situated in the U.S., the state of Minnesota. The water system of the Winnipeg River Basin consists of eleven major lakes and control points in the Province of Ontario (A to K in Figure 3.7), controlling the inflow to a cascade of six hydropower generation stations, with a combined capacity of 580 MW, along the downstream reach of the Winnipeg River in the Province of Manitoba (L to Q in Figure 3.7). Upstream, eleven major lakes and control points are distributed along two branches of the water system, with flow generally from east to west and south to north in the basin. In the northern branch (A to F), Lac Seul (B) primarily regulates the inflow to the downstream. Although Lake St. Joseph (A) is located outside the Winnipeg River Basin, its outflow is diverted into Lac Seul. In the

southern branch (G to K), Rainy Lake (I) and Lake of the Woods (J) play a key role in controlling the downstream streamflow. The two branches converge into the Winnipeg River, which then flows and contributes 42% (980 m^3/s) to the average daily inflow to Lake Winnipeg.

Data required to evaluate the framework for the case study includes observed and GCM-driven daily streamflow. Observed streamflow are directly used within the framework to generate synthetic scenarios with different magnitude, variability and seasonality. GCM-driven streamflow is used as a basis to define seasonality changes for generating plausible future scenarios. GCM-driven streamflow provides process-based projections that offer valuable guidance for the projected magnitude of seasonal shifts.

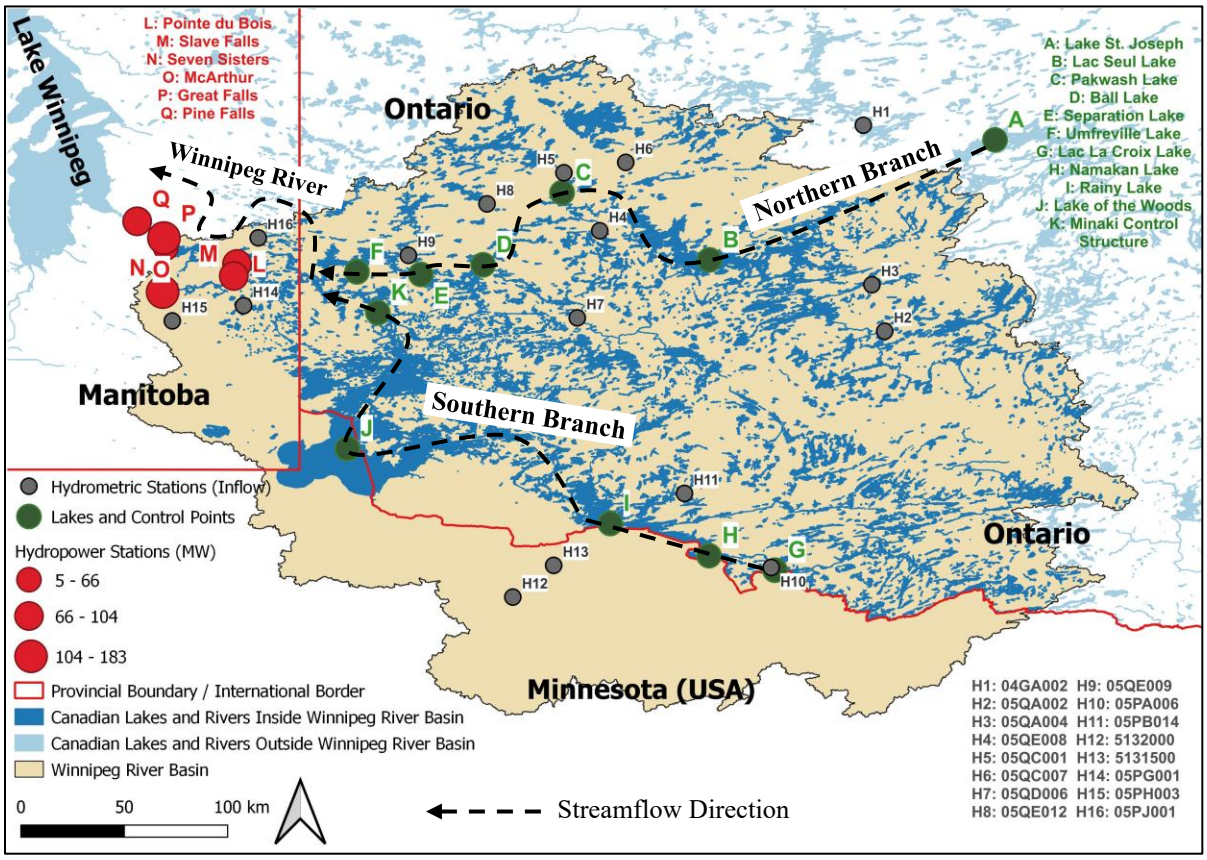


Figure 3.7. Location of the Winnipeg River Basin (cream-colored area), hydropower stations (red-filled circles), lake and control points (green-filled circles), and hydrometric stations (gray-filled circles). The boundary shapefile of the Winnipeg River Basin is extracted from Ahmed et al. (2024), Manitoba boundary form Data MB, Ontario boundary from Ontario GeoHub, and lakes and rivers from Government of Canada.

3.3.3.1 Historical Inflow Data

Sixteen hydrometric stations (H_1 to H_{16}; Figure 3.7) are used to calculate the total inflow to the water system in the Winnipeg River Basin. Manitoba Hydro, the sole electricity provider in the Province of Manitoba, provided daily flow data for these hydrometric stations from 1980 to 2017, which are publicly available on the Environment and Climate Change Canada website (https://wateroffice.ec.gc.ca/index_e.html). Monthly inflow is calculated as the sum of daily flows for each month. Monthly inflows to each lake, control point, and hydropower station (A to Q; Figure 3.7) are estimated using the monthly hydrometric station data (H_1 to H_{16}; Figure 3.7), as presented in Table 3.1. Of seventeen lakes, control points, and hydropower stations, fourteen have gauged inflow and are considered as 'inflow' locations for modelling.

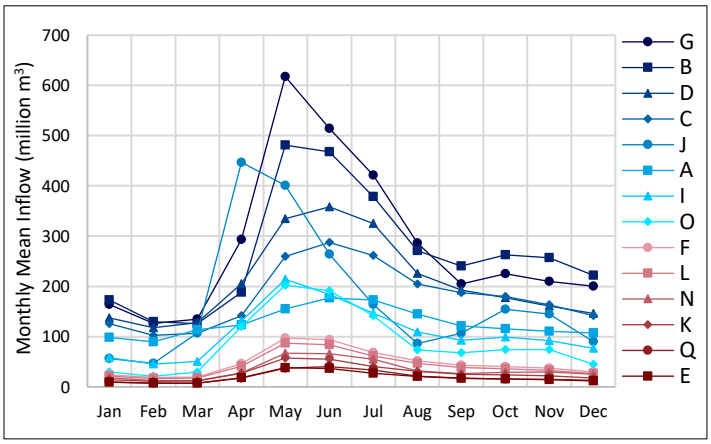
Table 3.1. Inflow locations of the water system in the Winnipeg River Basin. Multiplication factors associated with selected inflow IDs are provided by Manitoba Hydro and represent calibrated scaling factors used to calculate inflow at each location.

Name	ID on Figure 3.7	Location	Location Type	Inflow ID(s) on Figure 3.7	Share of Location Inflow in the Total Inflow (%)	Mean of Monthly Inflow (Mm^3)
St. Joseph	A	Northern Branch	Controlled Lake	H_1	8	128
Lac Seul	B		Controlled Lake	H_2+H_3	16	266
Pakwash	C		Controlled Lake	$H_4\times1.77+H_5+H_6$	11	180
Ball	D		Uncontrolled Lake	$H_4\times2.62+H_7+H_8$	13	209
Separation	E		Uncontrolled Lake	$H_9\times0.64$	1	19
Umfreville	F		Controlled Lake	$H_9\times1.63$	3	48
Lac La Croix	G	Southern Branch	Uncontrolled Lake	H_{10}	17	283
Namakan	H		Controlled Lake	no inflow	0	0
Rainy	I		Controlled Lake	H_{11}	7	108
Lake of the Woods	J		Controlled Lake	$H_{12}\times1.399+H_{13}\times1.095$	11	172
Minaki	K		Control Structure	$H_9\times0.96$	2	28
Pointe du Bois	L	Winnipeg River	Hydropower Station	$H_9\times1.46$	3	43
Slave Falls	M			no inflow	0	0
Seven Sisters	N			$H_{14}\times2.69$	2	33
McArthur	O			$H_{14}\times2.43+H_{15}+H_{16}$	5	89
Great Falls	P			no inflow	0	0
Pine Falls	Q			$H_{16}\times1.14$	1	29
Sum	-	-	-	-	100	1626

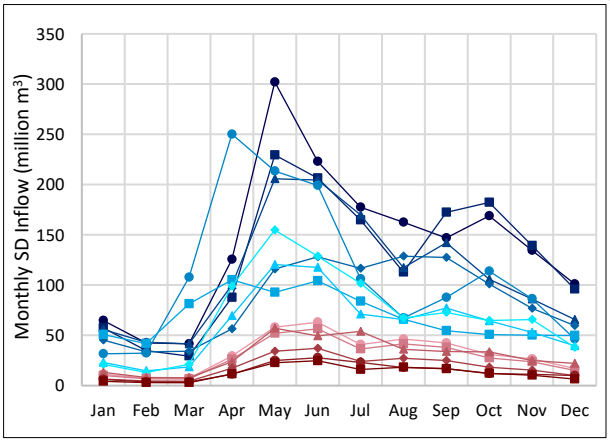
The mean total monthly inflow to all locations is 1,626 million m^3, equivalent to an average daily value of 627 m^3/s. On average, the northern branch receives 52% of the observed monthly inflow to the water system, the southern branch 36%, and the Winnipeg River 11%. The mean of monthly inflow at each location ranges from a minimum of 19 million m^3 (6.7 m^3/s daily mean) at Separation Lake (E), to a maximum of 283 million m^3 (109 m^3/s mean daily) at Lac La Croix Lake

(G). This variation demonstrates the suitability of the Winnipeg River Basin for testing the framework, as it encompasses a broad range of inflow conditions.

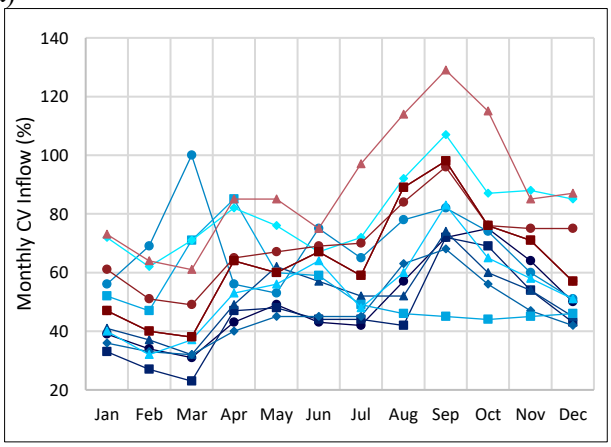
Each of the fourteen inflow locations exhibits a unique set of monthly mean values (Figure 3.8a); however, all inflows generally follow a similar seasonal pattern; except Lake of the Woods (J). The inflow to Lake of the Woods comes from the Big Fork and Little Fork Rivers (H_{12} and H_{13}, respectively), originating in the State of Minnesota, USA. The peak inflow month varies across locations, with nine peaks occurring in May, five in June, and one in April. The difference in the structure of monthly SD seasonality across inflow locations varies more relative to monthly mean seasonality (Figure 3.8b). Notably, Figure 3.8c demonstrates that locations with relatively lower inflow magnitude exhibit higher coefficient of variation (CV), indicating greater variability compared to locations with higher inflow magnitude.



(a)



(b)



(c)

Figure 3.8. (a) Monthly mean, (b) SD, and (c) CV of historical monthly inflow at fourteen inflow locations across the Winnipeg River Basin, from 1980 to 2017. Locations are color-coded from dark blue to dark red, representing their relative contribution to the total inflow of the water system from 1980 to 2017 (indicated in Table 3.1), with dark blue indicating the highest contribution and dark red the lowest.

3.3.3.2 GCM-Driven Inflow Data

An ensemble of nineteen GCM scenarios, developed as part of the BaySys project, provided the basis for defining future seasonality patterns in this study (Braun et al., 2021). This ensemble was previously used by Kim et al. (2022) to assess hydropower generation changes under future climate scenarios in the Lower Nelson River Basin, and by Gozini et al. (2023) to evaluate the impact of ice cover on flow conveyance in the Nelson River West Channel under future climate conditions. The ensemble is comprised of fourteen GCMs and two Representative Concentration Pathways (RCPs), with further details provided in Table 1 of Braun et al. (2021). Braun et al. (2021) selected nineteen members from 54 simulations of the CMIP5 ensemble, capturing roughly 90% of the variability in future climate projections, including annual mean temperature and precipitation over the Hudson Bay Drainage Basin, which encompasses the Winnipeg River Basin. Stadnyk et al. (2021) developed GCM-driven daily streamflow scenarios from this nineteen-member ensemble and provided results for the sixteen hydrometric stations within the Winnipeg River Basin; however, GCM-driven streamflow scenarios were not available for location A. Therefore, the projected changes in magnitude and variability at location B are applied to A when targeting the future seasonality pattern. The GCM-driven scenarios cover the period 1981-2070, of which 1981-2017 is used as the hindcast period and 2018-2055 as the projection period. The projection period is defined to match the length of the historical period (38 years), as GCM-driven streamflow is used to characterize seasonality changes for generating plausible future scenarios of equal duration.

Projections indicate a shift in the peak streamflow caused by earlier and larger spring snowmelt which in turn leads to reduced summer streamflow (Stadnyk et al., 2021). As shown in Figure 3.9a, the ensemble projects an overall increase in the magnitude of total monthly inflow into the water system for all months, except June and July in summer. The highest rate of magnitude increase is expected in March and April. This variation results in the projection of an earlier peak compared to historical records (Figure 3.9c), where the peak monthly mean inflow is expected in April at all locations except one, which remains in May. Moreover, Figure 3.9c highlights the projected spatial variation in inflow magnitude, where Lake of the Woods (J) is expected to surpass Lac La Croix (G) as the largest contributor to total inflow of the water system. Figure 3.9b illustrates that, on average, the variability of total monthly inflow into the water system is expected to increase, except

for May and June, with nearly zero changes. Locations with relatively lower inflow magnitude are projected to have higher CV (Figure 3.9d) compared to historical values (Figure 3.8c).

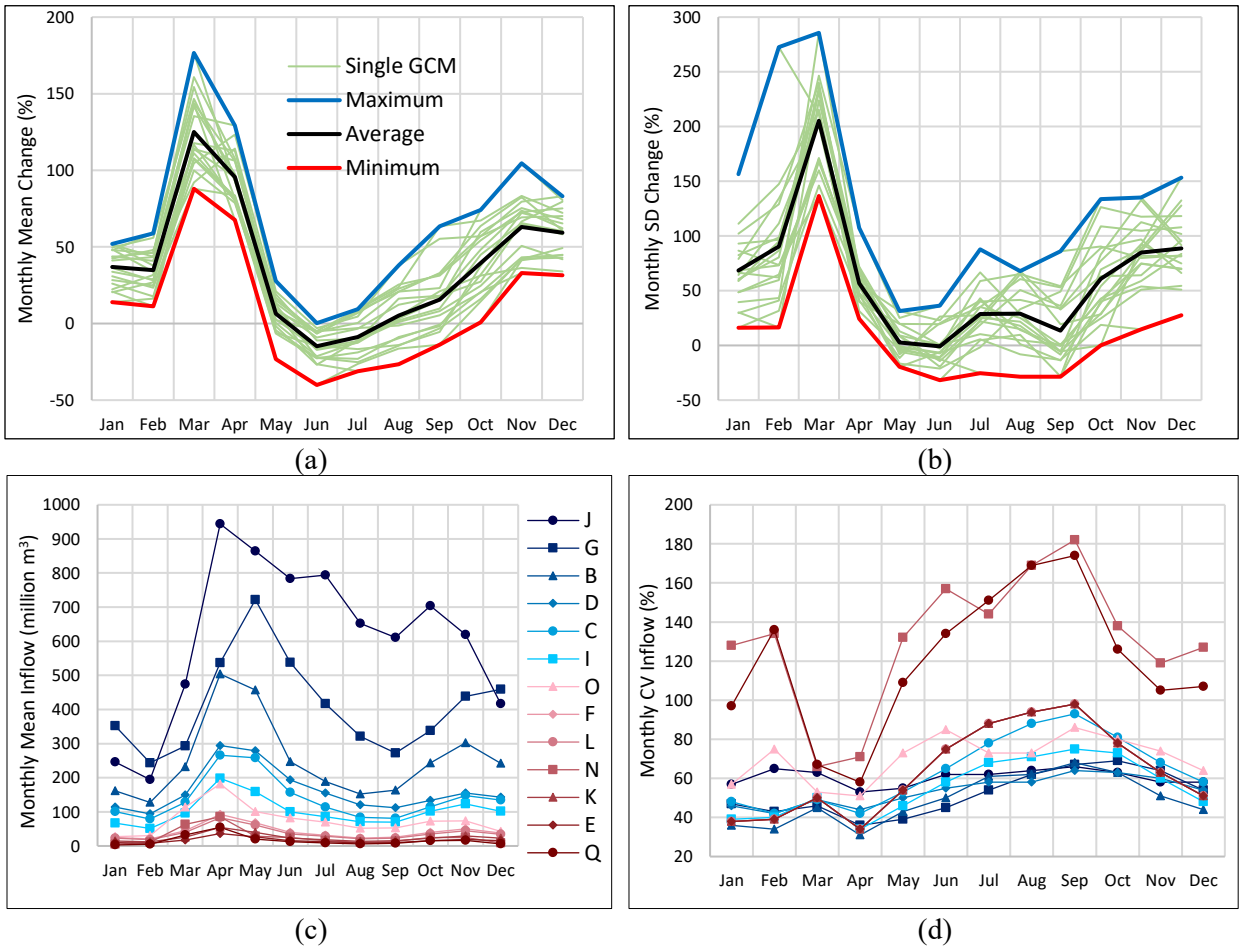


Figure 3.9. (a) Monthly mean change and (b) monthly SD change of total inflow into the water system in the Winnipeg River basin for the GCM-driven projections (2018-2055) compared to historical records (1980-2017). (c) Monthly mean and (d) CV of GCM-driven monthly inflow projections at fourteen inflow locations across the Winnipeg River Basin. Locations are color-coded from dark blue to dark red, representing their relative contribution to the total inflow of the water system from 2018 to 2055, with dark blue indicating the highest contribution and dark red the lowest.

3.3.4 Framework Evaluation

To evaluate the framework developed in this study, five distinct cases of synthetic streamflow generation are considered for the Winnipeg River Basin (Table 3.2) across fourteen inflow locations. All locations are flagged as "*non-local*". Evaluation of the framework begins by comparing generated monthly synthetic streamflow (optimized scenarios) with those produced using the Kirsch et al. (2013) methodology (non-optimized scenarios). This comparison assesses the monthly magnitude and variability change of the generated synthetic streamflow, aiming to

reproduce historical with non-optimized and optimized approaches (RH-N and RH-O) and expanded (EH-N and EH-O) over historical magnitude and variability, while preserving seasonality. To evaluate the applicability of seasonality changes, plausible future scenarios in EG-O are targeted based on the median magnitude and variability projected by the nineteen-member ensemble of GCM-driven (G) streamflow scenarios across the same fourteen inflow locations from 2018 to 2055. All cases include 38 years of synthetic streamflow to ensure comparability with historical records from 1980 to 2017.

For RH-N and RH-O (Table 3.2), 100 scenarios are generated to reproduce historical records. RH-N represents the non-optimized scenarios, where the monthly synthetic streamflow generator is forced with zero monthly mean and SD change. RH-O corresponds to the optimized scenarios, targeting zero changes in seasonality and deviation of monthly mean and SD. Both RH-N and RH-O employ 100 matrix years to generate different timeseries for the same forcing and target scenarios. Comparison of these scenarios demonstrates the effectiveness of the inverse approach in reducing discrepancies between the targeted and achieved streamflow characteristics.

In EH-N and EH-O (Table 3.2), 289 scenarios are forced and targeted to expand beyond monthly magnitude and variability observations while preserving historical monthly seasonality. EH-N represents the non-optimized scenarios, where the monthly synthetic streamflow generator is forced with monthly mean and SD changes ranging from -80% to +80% in increments of 10%. EH-O represents optimized scenarios, targeting deviations ranging from -80% to +80% in increments of 10% and 0% change in monthly mean and SD seasonality. To ensure comparability, a constant random matrix year is used for all scenarios in EH-N and EH-O. Performance is evaluated visually by assessing the number of generated timeseries that fall within the target exposure space for EH-N and EH-O. The uniformity of the generated timeseries in covering the target exposure space is examined visually for EH-N and EH-O. Flow duration curves of monthly synthetic streamflow scenarios in EH-O are plotted to evaluate deviations of quantiles of flow relative to the historical record. Spaghetti plots of monthly mean and SD provide an evaluation of optimized scenarios in EH-O, and whether they preserve the historical seasonality in monthly magnitude and variability of streamflow.

EG-O (Table 3.2) targets the median monthly magnitude and variability of the nineteen-member ensemble of GCM-driven projections, while also expanding beyond it. This expansion

ensures that a broader range of uncertainty is represented, which is essential for stress testing of the system. Seasonality changes are targeted for each location based on the median monthly mean and SD changes projected by the GCM ensemble from 2018 to 2055. The deviation ranges from -80% to +80% in increments of 10%, resulting in 289 scenarios. The same matrix year used in EH-N and EH-O is applied to EG-O. Plotting the resultant monthly mean and SD assesses the uniformity of the generated timeseries in covering the target exposure space across all locations and months for EG-O. Flow duration curves and spaghetti plots are generated as well to assess changes in the distribution of flows and seasonality of flows compared to historical records and GCM-driven projections (2018 to 2025).

Table 3.2. Description of five synthetic streamflow generation cases applied to the Winnipeg River Basin with fourteen locations (k) of inflow

Case	Type		ID	# of scenarios (n)	Percentage of Monthly (j) Mean (Mc) and SD Change (SDc): Forcing (F) or Target (T)		# of matrix year
1	Reproducing Historical records	Non-optimized	RH-N	100	$Mc_{F_{j,k}} = 0$ $SDc_{F_{j,k}} = 0$		100
2		Optimized	RH-O	100	seasonality $Mc^{(1)}_{T_{j,k}} = 0$ $SDc^{(1)}_{T_{j,k}} = 0$	deviation $Mc^{(2)}_{T_n} = 0$ $SDc^{(2)}_{T_n} = 0$	100
3	Expanding over Historical records or GCMs	Non-optimized	EH-N	289	$Mc_{F_{j,k}}: -80\%\ to + 80\%$ $SDc_{F_{j,k}}: -80\%\ to + 80\%$		1
4		Optimized	EH-O	289	seasonality $Mc^{(1)}_{T_{j,k}} = 0$ $SDc^{(1)}_{T_{j,k}} = 0$	deviation $Mc^{(2)}_{T_n}: -80\%\ to + 80\%$ $SDc^{(2)}_{T_n}: -80\%\ to + 80\%$	1
5		Optimized	EG-O	289	seasonality $Mc^{(1)}_{T_{j,k}}: GCMs^*$ $SDc^{(1)}_{T_{j,k}}: GCMs^*$	deviation $Mc^{(2)}_{T_n}: -80\%\ to + 80\%$ $SDc^{(2)}_{T_n}: -80\%\ to + 80\%$	1

* Median of monthly mean and SD change projected by the nineteen-member ensemble of GCM-driven projections (2018 to 2055).

The distribution, autocorrelation, and cross-correlation of generated streamflow timeseries in RH-N have already been tested in the literature, demonstrating the synthetic non-optimized scenarios preserve the historical structure of these properties (Herman et al., 2016; Quinn et al., 2017). In this study, the distribution, autocorrelation, and cross-correlation of the optimized generated streamflow timeseries for RH-O are similarly evaluated for their ability to preserve the historical statistical structure (stationary test) from 1981 to 2017. The same evaluation is applied to the GCM-driven hindcasts (1981 to 2017) and RH-N, enabling direct comparison with RH-O. Since there are nineteen GCM-driven hindcasts, nineteen members of monthly synthetic

streamflow scenarios in RH-O and RH-N are randomly selected for this assessment. Additionally, distribution, autocorrelation and cross-correlation of synthetic streamflow timeseries (full ensemble) in EH-O and EG-O are evaluated to identify significant differences in their structure compared to historical records from 1980 to 2017 (non-stationary test) and GCM-driven projections (2018 to 2055).

Distribution testing of monthly streamflow is conducted using the Wilcoxon rank-sum and Levene's tests. The rank-sum test assesses the null hypothesis that the two independent sample distributions (synthetic and observed in the same month) come from populations with equal medians. Levene's test evaluates the null hypothesis that the variances of the two distributions are equal. For both tests, a low p-value (typically <0.05) provides significant statistical evidence against the null hypothesis, indicating differences in either location (median) or scale (variance) of distributions. Monthly autocorrelation function up to 50 months lag and the cross-correlation function between pairs of locations are calculated. Deviation from historical record is evaluated both visually, by plotting monthly autocorrelation cross-correlation functions, and quantitatively using the Root Mean Square Error (RMSE), computed by comparing the ensemble-averaged autocorrelation and cross-correlation structures against the historical record.

3.3.5 Framework Application

Two sub-systems of MB_HydroSim (Gozini et al., 2026a), as an integrated water resources management tool, are used to demonstrate the stress-testing applications across different performance objectives. A description of MB_HydroSim and its sub-systems configuration is provided in *SM.3SM.4 MB_HydroSim*. The first example application focuses on the hydropower system in the Winnipeg River Basin, where hydropower reliability is used as the primary performance metric (details in *S.4 Stress-Testing Application: Hydropower Generation*). The second example examines the Shellmouth Dam in Manitoba, where flood frequency and water-demand shortage are used as the performance metrics (details in *SM.5 Stress-Testing Application: Flood and Water Demand Management*).

To conduct stress testing for each application, system performance metrics are evaluated across an ensemble of 25 daily synthetic streamflow scenarios, each spanning a 38-year period. Target deviations in monthly mean and SD range from -20% to +20% in 10% increments, while the observed historical seasonal inflow pattern (1980-2017) is preserved by imposing no changes (0%)

to monthly mean and SD seasonality. Performance metrics computed for each synthetic scenario are subsequently interpolated onto a 2% grid of inflow conditions and visualized by classifying system response at each inflow condition as either "*success*" or "*failure*". Success indicates acceptable or improved system performance, whereas failure denotes undesirable system performance relative to a baseline. The baseline is defined as the reproduced historical inflow scenario corresponding to 0% deviation in both monthly mean and SD. Inflow conditions yielding performance equal or superior to the baseline are classified as success; otherwise, they are considered as failure. By connecting the success scenarios closest to the failure ones, a critical threshold is delineated, beyond which changes in inflow distribution moments lead to undesirable (i.e., degraded) system performance. Additional decision-relevant insights derived from this stress-testing analysis are discussed in Section 3.4.8.

3.4 Results and Discussion:

To visualize the results in an informative yet concise manner, the framework evaluation plots are presented for locations B and N, representing the lowest and highest monthly historical CV of inflow, respectively among the fourteen inflow locations (Figure 3.8c). Results (Sections 3.4.1 to 3.4.6) are representative of the general behavior observed across all locations. Computational cost of the proposed framework for generating 100 synthetic scenarios is reported, highlighting efficiency gains relative to previously developed frameworks (Section 3.4.7). An example application is provided to illustrate how target scenarios can be applied in a stress-testing context (Section 3.4.8).

3.4.1 Historical Magnitude and Variability: Case RH-N vs. Case RH-O

Synthetic monthly non-optimized scenarios in RH-N deviate from the target value, namely observed monthly magnitude and variability (Figure 3.10). The deviation from the target is more pronounced for SD compared to the mean because SD squares the differences between each data point and the mean. Location N exhibits a higher range of deviation from the target due to its highest monthly streamflow CV (Figure 3.8c) relative to other locations. The greatest mean and SD deviations from the target are +123% and +438%, respectively, occurring at location N, indicating the monthly synthetic scenarios generated for RH-N do not accurately reproduce the observed monthly magnitude and variability. Instead, they can be used as stochastic scenarios that

expand historical observations, representing a broader but random range of potential streamflow conditions. The boxplots in Figure 3.10 cross 0% at all locations and months, but this does not imply that a non-optimized synthetic scenario exists with simultaneous 0% deviation from target for both mean and SD of all months. Instead, it indicates that if optimization is applied, 0% deviation from target can be achieved simultaneously across all months for both mean and SD. This is precisely what is accomplished in RH-O, the optimized monthly synthetic scenarios reproducing historical magnitude and variability from observed records. The boxplots of deviation from target for both mean and SD in RH-O, for all locations and months, align exactly at 0% and are not represented in Figure 3.10 for visual clarity. The framework successfully generated 100 synthetic monthly scenarios for RH-O with the same historical monthly magnitude and variability, showing its advantage over non-optimized scenarios in RH-N when targeting a specific monthly magnitude and variability.

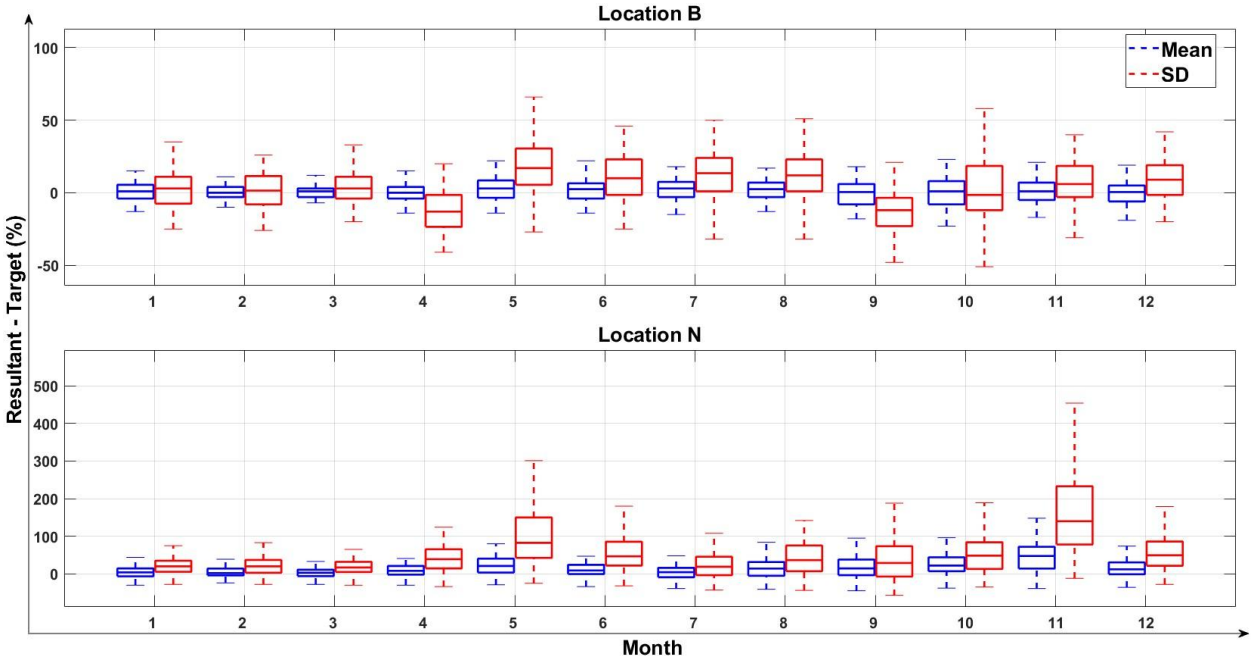


Figure 3.10. Boxplots of resultant monthly mean and SD deviations from the target for the non-optimized scenarios at locations B and N when reproducing historical records in case RH-N.

3.4.2 Historical Statistical Structure: Case RH-O vs. Case RH-N and GCMs

The proposed inverse scenario generation framework successfully preserves the median and variance of the historical monthly streamflow distribution when reproducing historical observations in RH-O (Figure 3.11). The average (solid lines) and 95% confidence intervals (dashed lines) of the p-values from the rank-sum (dark blue) and Levene's (light blue) tests for

nineteen randomly selected synthetic scenarios in RH-O consistently remain above the 0.05 threshold, indicating insufficient evidence to reject the null hypothesis that the monthly distribution of synthetic scenarios and historical records have the same median and variance. This same null hypothesis is rejected for the GCM-driven hindcasts (dark and light red) in some months, with p-values below 0.05 indicating statistically significant differences from median and variance of historically monthly streamflow distribution. Compared to synthetic scenarios in RH-N (dark and light green), RH-O scenarios exhibit higher p-values for both statistical tests. This indicates that applying optimization and constraining the streamflow generator to reproduce the historical monthly mean and SD of streamflow does not distort the reproduction of historical streamflow distribution structure; instead, statistical consistency with the historical record is improved.

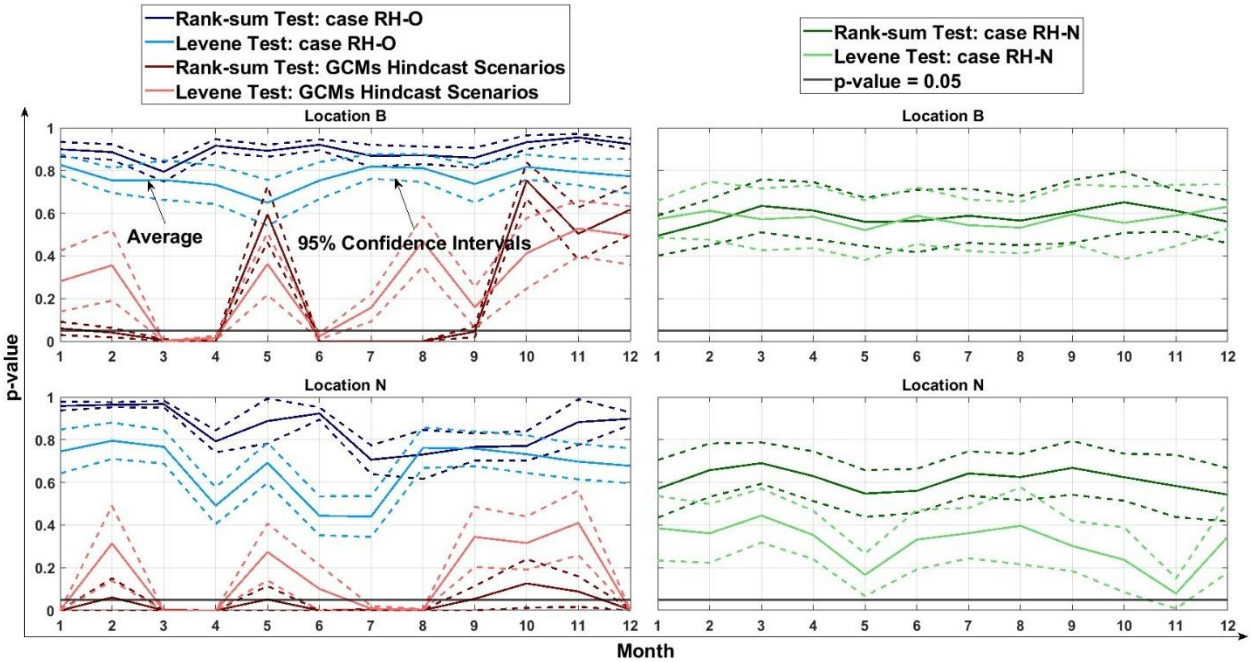
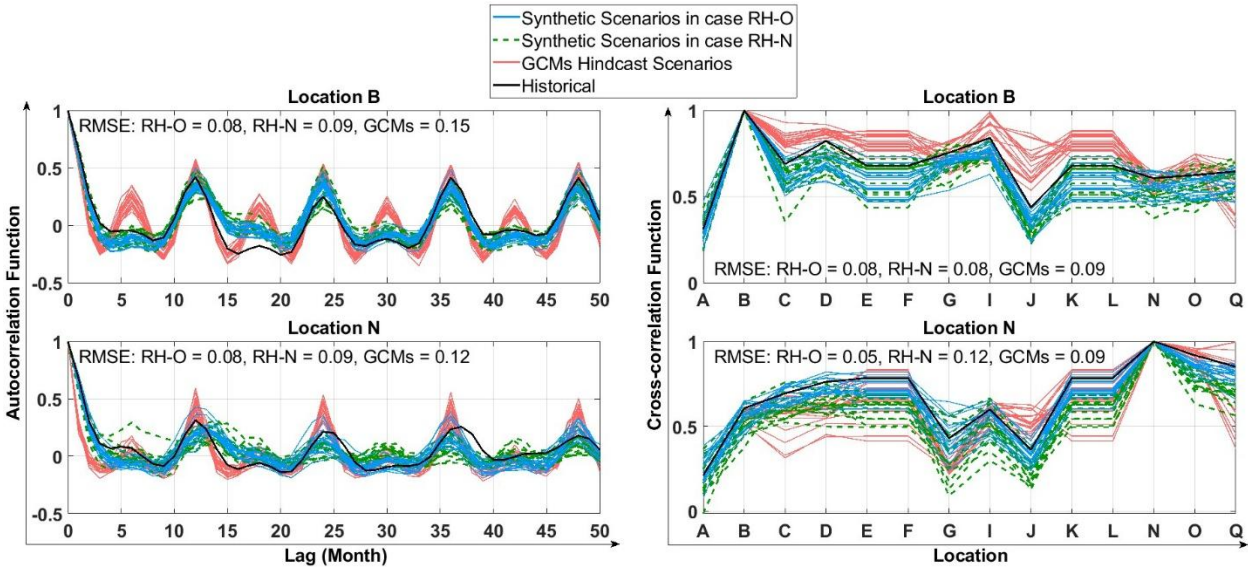


Figure 3.11. Average (solid line) and its 95% confidence intervals (dashed line) of the p-value for location and scale test against historical records from 1981 to 2017 at locations B and N. The tests are conducted for the ensemble of optimized and non-optimized monthly synthetic streamflow when reproducing historical records (RH-O and RH-N), and the ensemble of monthly GCM-driven hindcasts (1981 to 2017).

The autocorrelation functions for nineteen randomly selected synthetic scenarios in RH-O and RH-N (blue and green lines; Figure 3.12a) follow the historically observed autocorrelation structure (black line; Figure 3.12a). The discrepancies (as measured by RMSE values) between synthetic and historical autocorrelation functions in RH-O and RH-N are attributed to retransformation bias (Herman et al., 2016). Both RH-O and RH-N underestimate autocorrelation

at short monthly lags (up to 12 months). Importantly, optimization reduced the autocorrelation bias at both locations from 0.09 in RH-N to 0.08 in RH-O. This indicates that applying optimization to reproduce historical monthly mean and SD of streamflow does not distort the reproduction of historical autocorrelation structure, but instead improves it. GCM-driven hindcasts (red lines; Figure 3.12a) exhibit autocorrelation structures that differ from observations, with larger biases (RMSE = 0.15 and 0.12 at locations B and N) than those obtained under the RH-O (RMSE = 0.08 at both locations).



(a) (b)

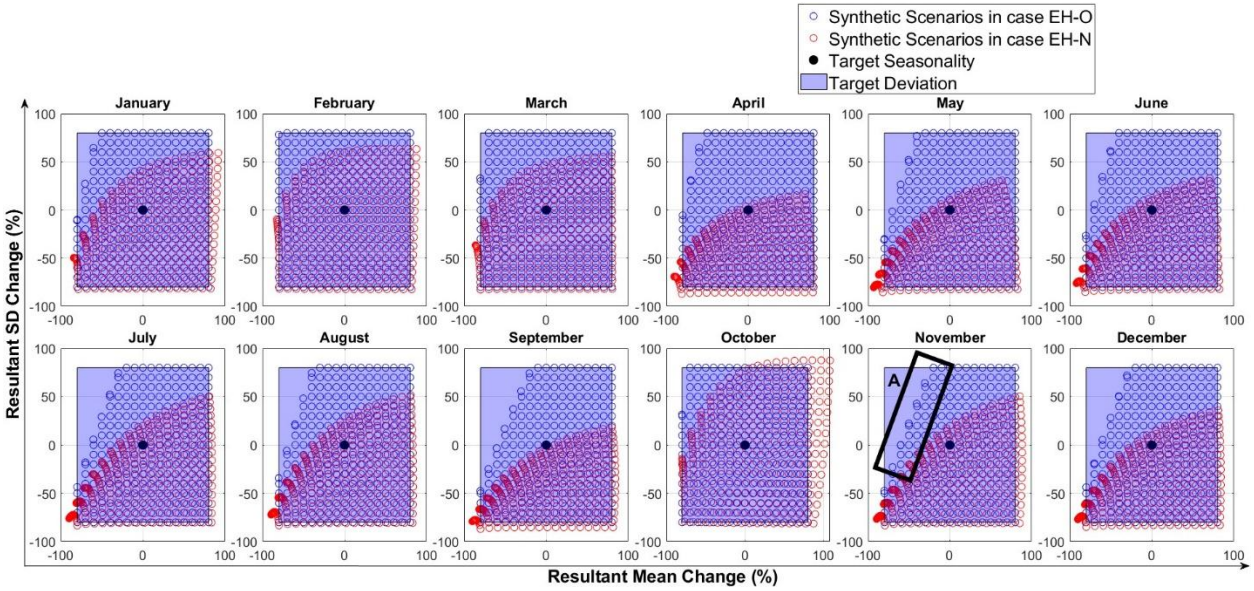
Figure 3.12. (a) Autocorrelation and (b) cross-correlation functions of streamflow at locations B and N. Autocorrelation up to 50 months lag and cross-correlation between pairs of locations are plotted for historical records from 1981 to 2017, the ensemble of optimized and non-optimized monthly synthetic streamflow when reproducing historical records (RH-O and RH-N), the ensemble of monthly GCM-driven hindcasts (1981 to 2017). The GCM-driven streamflow scenarios were not available at location A. Root Mean Square Error (RMSE) is computed by comparing ensemble-averaged autocorrelation and cross-correlation structures against the historical record.

The cross-correlation function between pairs of inflow locations in the RH-O and RH-N synthetic scenarios (blue and green lines; Figure 3.12b) reproduce the observed structure (black line; Figure 3.12b). RH-O and RH-N underestimate the cross-correlation, a bias caused by applying Cholesky Decomposition (Herman et al., 2016). Similar to autocorrelation, optimization reduced the bias of cross-correlation in location N from 0.12 in RH-N to 0.05 in RH-O, verifying the historical distribution of cross-correlation structure was not distorted. GCM-driven hindcasts (red lines; Figure 3.12b) follow the observed cross-correlation structure but tend to overestimate

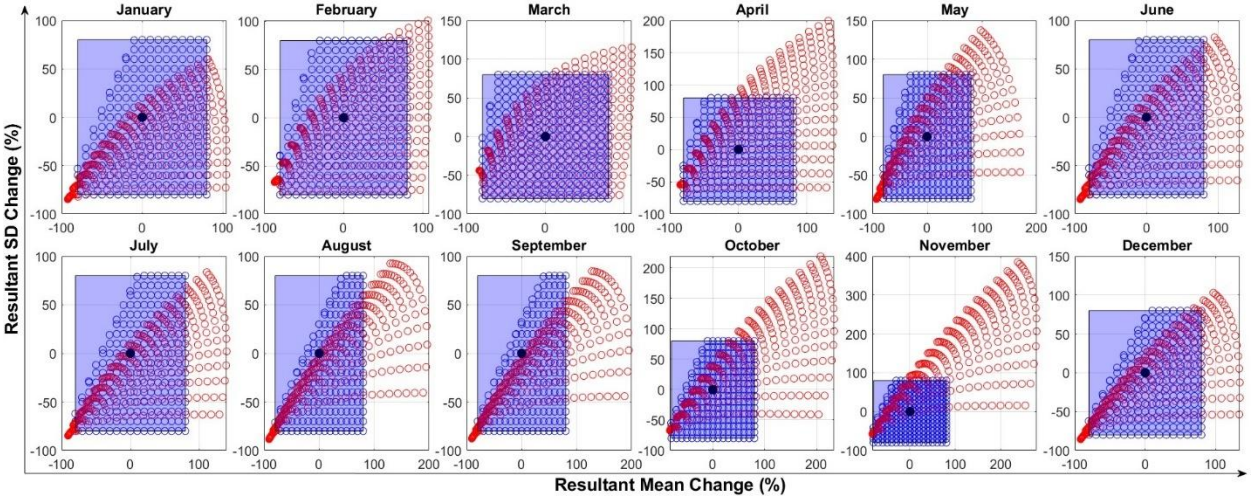
it, exhibiting greater bias (RMSE = 0.09 at both locations) compared to the synthetic optimized scenarios in RH-O (RMSE = 0.08 and 0.05).

Compared with the GCM-driven hindcast scenarios, the RH-O synthetic streamflow scenarios more effectively replicate the historical streamflow distribution structure, as well as the autocorrelation and cross-correlation of streamflow. This enables direct and internally consistent comparison of system performance under future synthetic scenarios (EH-O and EG-O) against a synthetic baseline (RH-O) that explicitly maintains statistical stationarity. GCM-driven scenarios (top-down) are not designed to maintain statistical stationarity when hindcasting the historical period; instead, they aim to capture future process-based and non-stationary inflow dynamics, leading to non-stationary statistical properties in hindcast simulations. Process-based GCM-driven scenarios from the top-down approach retain the advantage of physical plausibility, whereas synthetic scenarios represent statistically-credible plausible inflow conditions independent of the likelihood of occurrence.

Compared with the historical record, the underestimation of autocorrelation (within the first 12 monthly lags) and cross-correlation in RH-O leads to the underestimation of system performance. Observed water-system performance is finely tuned not only to historical monthly inflow magnitude and variability, but also to their temporal and spatial dependence structures; as a result, system performance under RH-O will be underestimated relative to observations. Such underestimation does not have uniform meaning across performance metrics; for flood-related performance measures, reduced temporal and spatial dependence of high-flow events leads to optimistic risk estimates, whereas for metrics of hydropower reliability, underestimation of dependence tends to yield conservative performance estimates. Importantly, this underestimation does not affect the interpretation of system response under future synthetic scenarios (EH-O and EG-O), because all future responses will be evaluated relative to RH-O, which serves as a consistent baseline (as discussed in Section 3.3.5). To further reduce discrepancies in RH-O autocorrelation and cross-correlation and more precisely target stationary dependence structures, future work could incorporate target autocorrelation and cross-correlation functions directly into the optimization objective and include additional decision variables, such as the matrix year. This would provide greater control over dependence structures, albeit at the expense of increased computational cost.



(a)



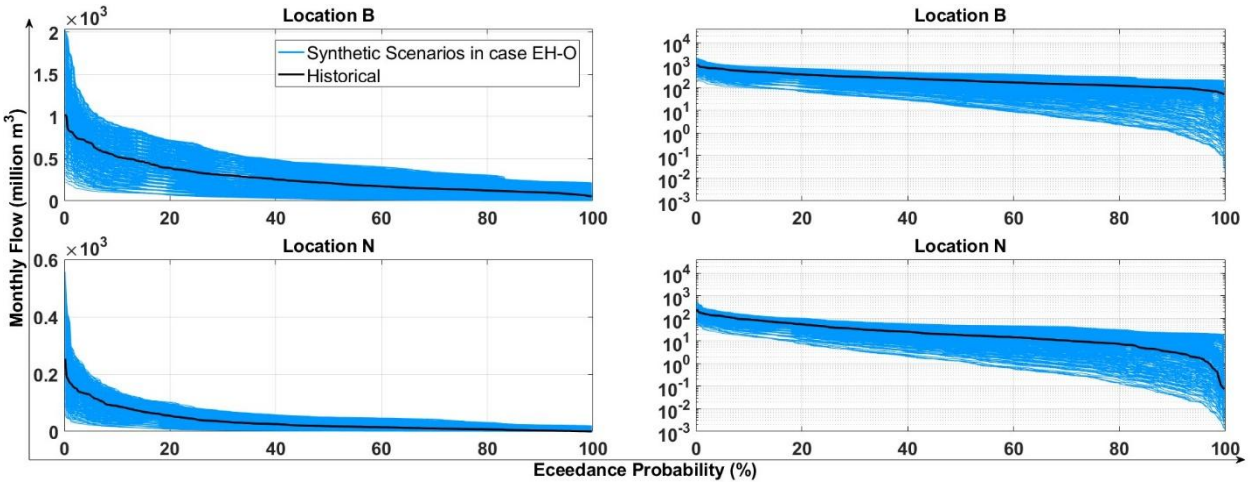
(b)

Figure 3.13. Resultant monthly mean and SD changes for optimized vs. non-optimized monthly synthetic scenarios at (a) location B and (b) location N. Case EH-O represents the optimized scenarios expanding over historical records. Case EH-N represents the non-optimized scenarios expanding over historical records. Black rectangle A is an example of successfully replacing partially infeasible scenarios with feasible ones.

3.4.3 Expanding beyond Historical Magnitude and Variability: Case EH-O vs. Case EH-N

Figure 3.13 demonstrates the advantage of optimized monthly synthetic scenarios in EH-O (blue circles) generated by the proposed framework, over non-optimized scenarios in EH-N (red circles). The optimized scenarios in EH-O reside within the target deviation (blue-shaded rectangle) and are uniformly sampling the exposure space; deviation in EH-O is from the observed monthly mean and SD seasonality, represented as a black dot on Figure 3.13 with 0% change. Like

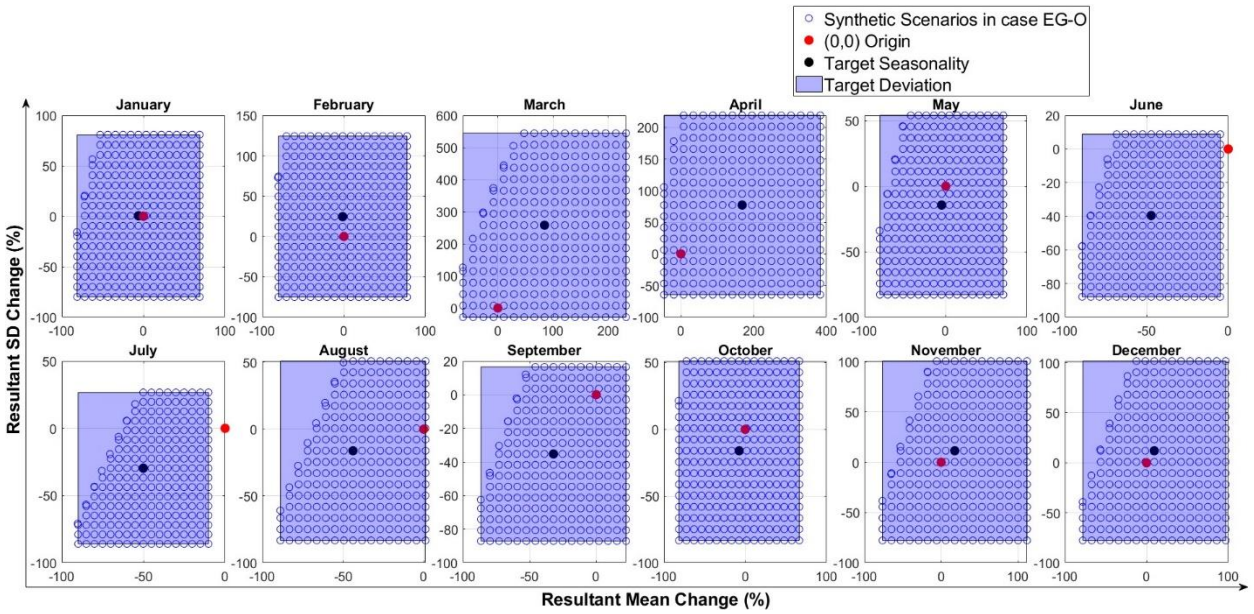
RH-N, EH-N scenarios are stochastic in nature and expand beyond the observed record, representing a broader but random range of potential (likely or not) streamflow. A larger number of EH-N scenarios fall outside the target deviation for location N compared to location B due to higher monthly streamflow CV, resulting in a greater deviation from the target (see Section 3.4.1). This also results in longer computational time when optimizing scenarios for location N in EH-O.



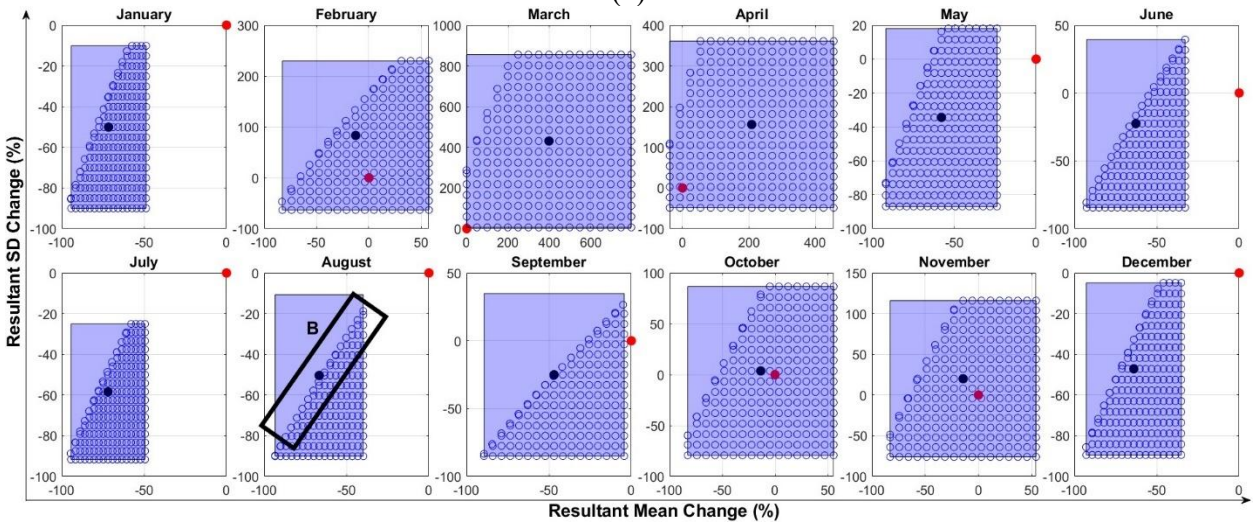
(a) (b)

Figure 3.14. (a) real-space and (b) logarithmic scale flow duration curves of the monthly synthetic scenarios in EH-O vs. historical records from 1980 to 2017. Case EH-O represents optimized scenarios expanding over historical records.

The infeasible area of the exposure space, or the portion blue-shaded rectangle not covered by the blue circles on Figure 3.13, is larger for location N compared to location B due to its higher CV. Several blue circles lie along the boundary between feasible and infeasible areas (black rectangle A; Figure 3.13), indicating that partially infeasible scenarios have been successfully replaced with feasible ones. To further validate this and demonstrate the expansion of the optimized scenario from EH-O over historical observations, monthly flow duration curves are assessed (Figure 3.14). Figure 3.14a confirms the framework effectively expands the distribution of flow for both high and low flows without introducing any unexpected results (i.e., physically infeasible or impossible flows). Figure 3.14b, in logarithmic scale, highlights the extension of low flows more clearly, notably, the framework extends monthly low flows up to 10^{-3} million m^3, equivalent to an average daily value of 0.0003 m^3/s.



(a)



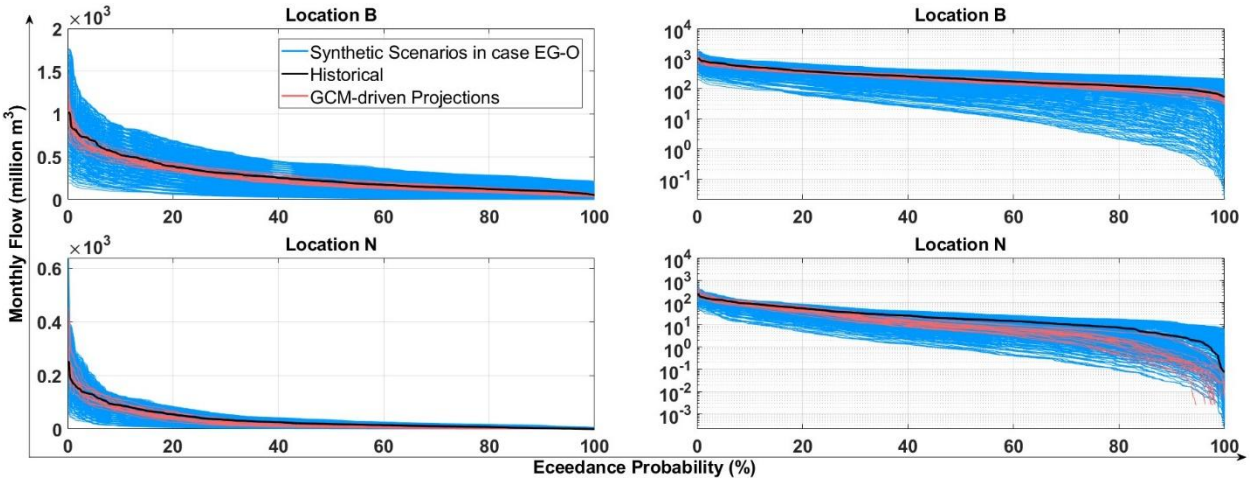
(b)

Figure 3.15. Resultant monthly mean and SD changes for the optimized monthly synthetic scenarios in EG-O at (a) location B and (b) location N. Case EG-O represents optimized scenarios expanding over the median of GCM-driven projections (2018 to 2055). Black rectangle B is an example of target seasonality that lies on the boundary of the feasible and infeasible area. Scale differences in target deviations (blue rectangle) occur because percentage change (Equation (3.1)) depends on target seasonality, which varies by location and month.

3.4.4 Expansion Over Expected Future Magnitude and Variability: Case EG-O

The proposed framework successfully targets scenarios in EG-O (blue circles), uniformly sampling the exposure space with the target deviation (blue-shaded rectangle; Figure 3.15). In EG-O, the deviation is defined relative to the median monthly mean and SD seasonality projected by the nineteen-member ensemble of GCM-driven projections (black dot), which differs from the

historical record (red dot). The final percentage deviation from the target seasonality of monthly mean and SD is determined using Equation (3.1) and depends on the target seasonality itself (note the scale differences in Figure 3.15). Consequently, the target deviation (blue rectangle) appears smaller for months with negative target seasonality percent change (e.g., January in Location N) compared to months with positive target seasonality percentage (e.g., April in Location N). However, if the resulting percentage changes are plotted with the origin shifted to the target seasonality value (i.e., treating the target seasonality as [0,0]), the target deviation would uniformly span -80% to +80% across all locations and months, consistent with the representation in Figure 3.13.



(a) (b)

Figure 3.16. (a) real-space and (b) logarithmic flow duration curves of the monthly synthetic scenarios in EG-O, historical records from 1980 to 2017, and the monthly GCM-driven projections (2018 to 2055). Case EG-O represents optimized scenarios expanding over the median of GCM-driven projections (2018 to 2055).

Target seasonality in EG-O is diverse, ranging from wetter conditions (e.g., March) where the monthly mean seasonality increases by roughly 90% and 400% for locations B and N, respectively (Figure 3.15); to drier conditions (e.g., July) where the monthly mean seasonality decreases by roughly 50% and 75% at locations B and N, respectively. This demonstrates the flexibility of the framework in targeting any seasonality or change to seasonality. Notably, in some months (for example, January, June, July, August, September, and December for location N), target seasonality lies on the boundary of the feasible and infeasible area (black rectangle B). Replacing partially infeasible scenarios with feasible scenarios addresses a common limitation of stochastic generators, faulted for generating targets that are unattainable, and highlighting the efficiency of

handling infeasible scenarios to ensure that all target scenarios remain feasible. Figure 3.16 demonstrates that the framework effectively extends the flow duration curve, or distribution of flows, beyond both observed and the GCM-driven projections for both low and high flows, without introducing unrealistic values. This also highlights how process-based projections from a top-down approach can be effectively combined with the flexibility of the framework to capture and validate a broader spectrum of plausible future streamflow conditions a system may be exposed to.

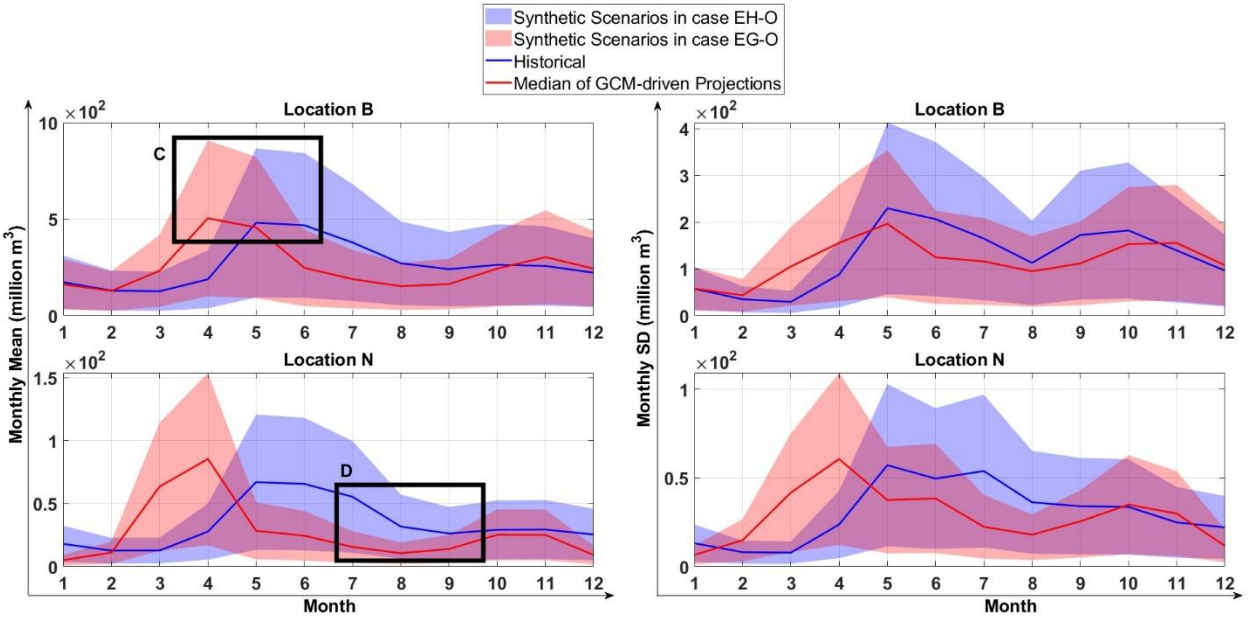
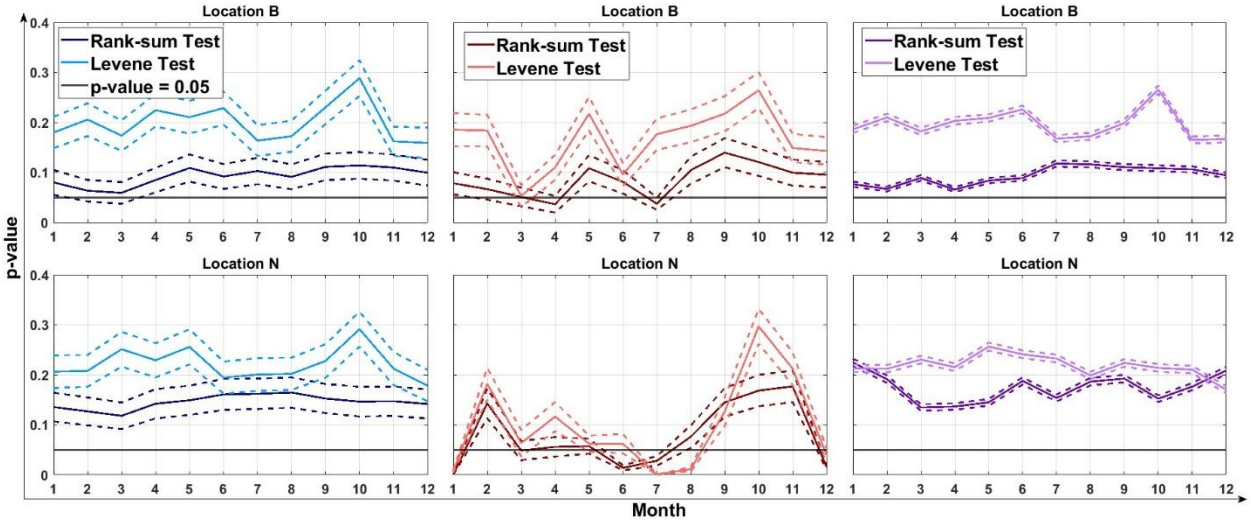


Figure 3.17. Resultant seasonality of monthly (a) mean and (b) SD for the optimized monthly synthetic scenarios in cases EH-O and EG-O. Case EH-O represents optimized scenarios expanding over historical records. Case EG-O represents optimized scenarios expanding over the median of GCM-driven projections (2018 to 2055). Black rectangle C is an example of one-month earlier peak flow. Black rectangle D is an example of a drastic decrease in a low monthly mean flow.

3.4.5 Seasonality Change: Case EH-O vs. Case EG-O

Figure 3.17 illustrates that the framework successfully preserves historical monthly mean, SD, and seasonality in EH-O, while effectively modifying the seasonality in EG-O. In EH-O, the patterns of monthly mean and SD (blue-shaded) follow those of the observed values (blue line), confirming the framework's ability to maintain historical seasonality. In contrast, in EG-O, the patterns of monthly mean and SD (red-shaded) align with the ensemble median of GCM-driven projections (red line), demonstrating the framework's capability to replicate target seasonal characteristics. Notably the framework successfully shifts peak flow from May to April (black

rectangle C). A substantial decrease in a low monthly mean flow (black rectangle D) produces near-zero flows. Since negative flows are not physically possible, more reduction for low-flow values is not allowed and they are retained near zero. For example, a scenario with -80% change in a high-flow month but -120% in a low-flow month can be adjusted to a scenario with -95% change in the low-flow month. This still yields a realistic low-flow while preserving the -80% change in high-flow month. This again highlights the importance and effectiveness of the framework in replacing infeasible near-zero scenarios with feasible alternatives, thereby preserving realistic hydrological behavior.



(a) EH-O vs. Historical (b) EG-O vs. Historical (c) EG-O vs. GCM Projections

Figure 3.18. Average (solid line) and its 95% confidence intervals (dashed line) of the p-value for location and scale test in (a) EH-O and (b) EG-O against historical records from 1980 to 2017 and (c) EG-O against ensemble of monthly GCM-driven projections (2018 to 2055) at locations B and N. Case EH-O represents optimized scenarios expanding over historical records. Case EG-O represents optimized scenarios expanding over the median of GCM-driven projections (2018 to 2055).

3.4.6 Future Expected Statistical Structure: Case EH-O and EG-O

Figure 3.18a indicates insufficient evidence (p-values above 0.05) to reject the null hypothesis that the monthly distribution of synthetic scenarios and historical records have the same median and variance for EH-O. Although expansion over historical records in EH-O does not produce statistically significant differences in the median and variance of monthly streamflow distributions, the associated p-values are lower than those obtained for RH-O (Figure 3.11). As expected, introducing changes in seasonality in the EG-O scenarios leads to statistically significant differences in the median and variance of monthly streamflow distributions relative to the historical records in some months (Figure 3.18b; p-values below 0.05). Figure 3.18c shows

insufficient evidence (p-values above 0.05) to reject the null hypothesis that the monthly distributions of EG-O synthetic scenarios and GCM-driven projections have the same median and variance. Because GCM-driven scenarios exhibit statistically significant differences from historical streamflow distributions (Figure 3.11), this demonstrates that the seasonal changes imposed in EG-O produce non-stationary streamflow distributional behavior.

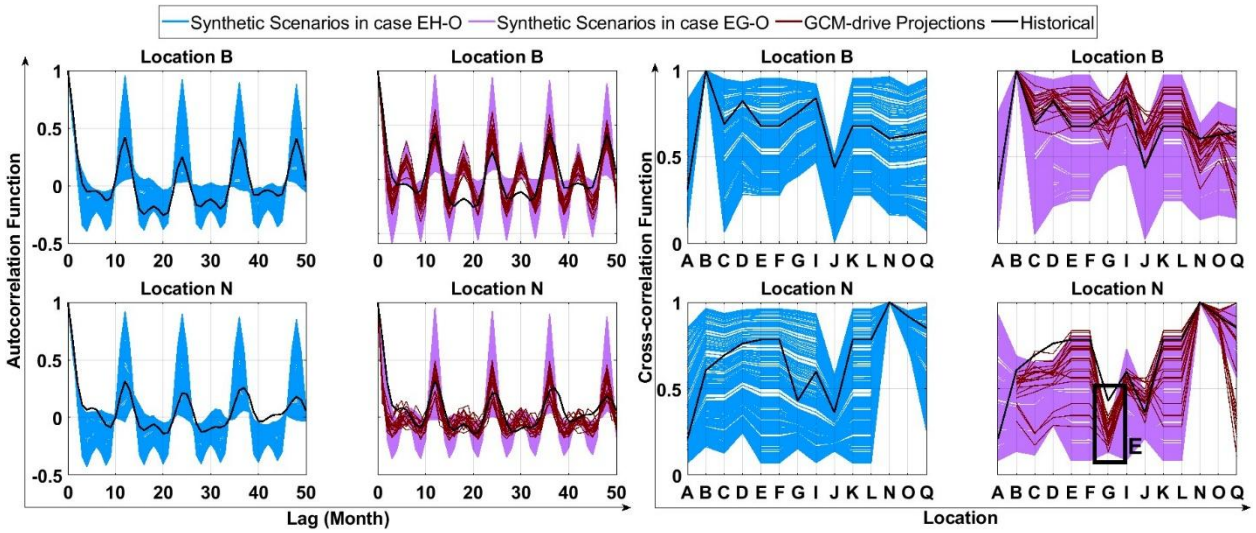


Figure 3.19. A. (a) Autocorrelation and (b) cross-correlation functions of streamflow at locations B and N. Autocorrelation up to 50 months lag and cross-correlation between pairs of locations are plotted for historical records from 1981 to 2017, the ensemble of optimized and non-optimized monthly synthetic streamflow in EH-O (expanding over historical records) and EG-O (expanding over the median of GCM-driven projections), and the ensemble of monthly GCM-driven projections (2018 to 2055). The GCM-driven streamflow scenarios were not available at location A. Black rectangle E is an example of similarity between the synthetic and GCMs scenarios in the cross-correlation structure.

Figure 3.19 demonstrates that autocorrelation and cross-correlation of synthetic scenarios in EH-O (blue lines) follow the historical autocorrelation and cross-correlation patterns (black line). In contrast, autocorrelation and cross-correlation patterns of the EG-O synthetic scenarios (purple lines) follow those of the GCM-driven projections (red lines) rather than historical (observed) data. Black rectangle "E" highlights the situation where all GCM-driven projections diverge from the historical cross-correlation structure, however, the synthetic scenarios in EG-O follow this same divergence, reinforcing their structural consistently with the GCM-driven projections rather than the observed data. This indicates that modifying seasonality causes the generated scenarios to exhibit non-stationary autocorrelation and cross-correlation structures that depart from historical behavior and instead reflect the dependence structure induced by the target seasonality.

Targeting -80% to +80% deviations in EH-O and EG-O contributes to the variation in auto- and cross-correlation values among the synthetic scenarios. The largest variations occur for the extreme target scenarios with +80% mean and -80% SD change, and -80% mean and +80% SD change. The [+80, -80] scenario exhibits the highest autocorrelation and cross-correlation values, which is physically consistent with a wetter and less variable regime that promotes enhanced temporal persistence and spatial coherence. In contrast, the [-80, +80] scenario exhibits the lowest autocorrelation and cross-correlation, consistent with a drier and more variable regime in which inflows are less temporally persistent and less spatially correlated. These variations are advantageous for stress-testing analysis, as they intentionally explore system response under contrasting dependence regimes.

3.4.7 Computational Cost

The comparison of computational cost across existing frameworks highlights the efficiency of the proposed framework (Table 3.3). Guo et al. (2016) employed a parametric stochastic weather generator for a single location, which required approximately 8 hours per 100 scenarios of 15-year rainfall. This approach also necessitates inclusion of additional variables such as air temperature and a subsequent hydrological model run to generate streamflow, which further increases computational demand. Borgomeo et al. (2015) applied a non-parametric streamflow generator for a single location, which had a runtime of 4 hours per 100 scenarios of 130-year length; however, the single-site design limits its applicability to multisite water systems. Wheeler et al. (2025) extended the non-parametric generator to 18 locations, but the computational cost escalated to 169 hours per 100 scenarios of 50-year length, with approximately 80% of the runtime (135 hours) attributed to optimizing cross-correlation structure. The proposed framework in this study generates 100 scenarios over 38 year-period at fourteen locations in 3.22 hours, on a comparatively less powerful hardware. This efficiency stems from directly targeting key streamflow statistics of interest (mean and variability) and within a parametric stochastic streamflow generator, which appropriately preserves and modify the autocorrelation and cross-correlation structures. Therefore, the framework achieves a favorable balance between computational efficiency and scenario relevance, making it well suited for multisite stress-testing applications. This efficiency, however, comes at the expense of reduced ability to capture non-Gaussian features and complex tail dependencies that may be preserved by non-parametric methods, reflecting the trade-off between

computational speed versus statistical flexibility. As further computational context, generating 38-year synthetic scenarios across fourteen locations requires, on average, approximately 150,736 objective-function evaluations in 115 seconds. This total corresponds to an average of 10,766 evaluations per location and 898 evaluations per monthly optimization.

Table 3.3. Computational cost of generating 100 synthetic scenarios across different frameworks.

Study	Generator Type	Number of Locations	Hardware	Timeseries Length (years)	Run Time per 100 Scenarios (hr)
Guo et al. (2016)	Parametric Stochastic Weather Generator	1	Intel Xeon E3, 2.6 GHz, 8 cores, 32 GB RAM	15	8
Borgomeo et al. (2015)	Non-Parametric Stochastic Streamflow Generator	1	3.4 GHz Processor	130	4
Wheeler et al. (2025)	Non-Parametric Stochastic Streamflow Generator	18	Dual Haswell CPU nodes 7 nodes × 16 cores), 2.6-3.4 GHz, 64 GB RAM	50	169
This Study	Parametric Stochastic Streamflow Generator	14	Intel Core Ultra 7 155U, 1.7 GHz, 12 cores, 16 GB RAM	38	3.22

The proposed framework is capable of incorporating additional targets into the optimization process, such as imposing a multi-year hydrologic condition within the generated time series (e.g., a consecutive multi-year drought). This can be achieved by specifying lower and upper bounds for the target variable (i.e., streamflow) in specific years of an *n*-year synthetic scenario. The same approach can be applied to represent other types of hydrologic or operational conditions of interest, depending on the intended application or desired stress test. This flexibility preserves the computational efficiency of the proposed framework, because only selected stress-relevant targets are explicitly enforced, while the parametric stochastic generator implicitly modifies the remaining statistical structure to capture non-stationary behavior without additional optimization.

Guo et al. (2016) produce streamflow scenarios conditioned on hydrometeorological variables, enabling direct interpretation of streamflow outcomes in terms of climate forcing. This approach is well suited for operational applications, such as flood forecasting, where anticipating streamflow extremes relies on evolving meteorological conditions. Borgomeo et al. (2015) and Wheeler et al. (2025) apply inverse approaches to non-parametric stochastic streamflow generators, enabling direct targeting of other streamflow properties, including autocorrelation, cross-correlation. In addition, because these generators do not rely on parametric retransformation, they do not impose a mathematically infeasible region in the exposure space, unlike parametric formulations.

3.4.8 Stress-Testing Application

3.4.8.1 Hydropower Generation

Figure 3.20a shows that annual-scale hydropower reliability is primarily controlled by changes in monthly inflow magnitude (horizontal axis), while changes in monthly inflow variability (vertical axis) exert only a minor influence on annual-scale hydropower reliability. This behavior is reflected in the near-vertical orientation of the critical threshold (solid black line), which spans inflow magnitude changes from approximately -2% to +6% as inflow variability (SD) varies from -20% to +20%. Reductions in inflow magnitude of about -4% or greater result in system failure (red dots) across the full ±20% range of inflow variability, whereas increases of approximately +6% or more lead to system-wide success (green dots) regardless of inflow variability within ±20%.

Seasonal stress testing in Figure 3.20b indicates that monthly inflow magnitude remains the dominant driver of hydropower reliability across all seasons. The overall level of stress is comparable among winter, spring, summer, and autumn, as reflected by a roughly similar number of failures in each season. This consistency suggests that the system has historically been well tuned (robust) to the observed inflow regime to maximize hydropower production. Historically, summer and spring contribute the largest fraction of total annual inflow, whereas autumn and winter receive substantially lower inflow. In contrast, peak electricity demand occurs from November to March, corresponding to late-autumn and winter, requiring the system to store summer inflows for subsequent energy production in later seasons. As a result, summer and autumn require inflow magnitude increases of approximately +6% or greater to achieve success across the full ±20% range of inflow variability, compared with approximately +4% or greater for winter and spring. Because reservoir levels are typically higher during summer and autumn, inflow variability becomes more influential in these seasons, as fluctuations in inflow more directly affect storage dynamics and, consequently, hydropower reliability.

3.4.8.2 Flood Management

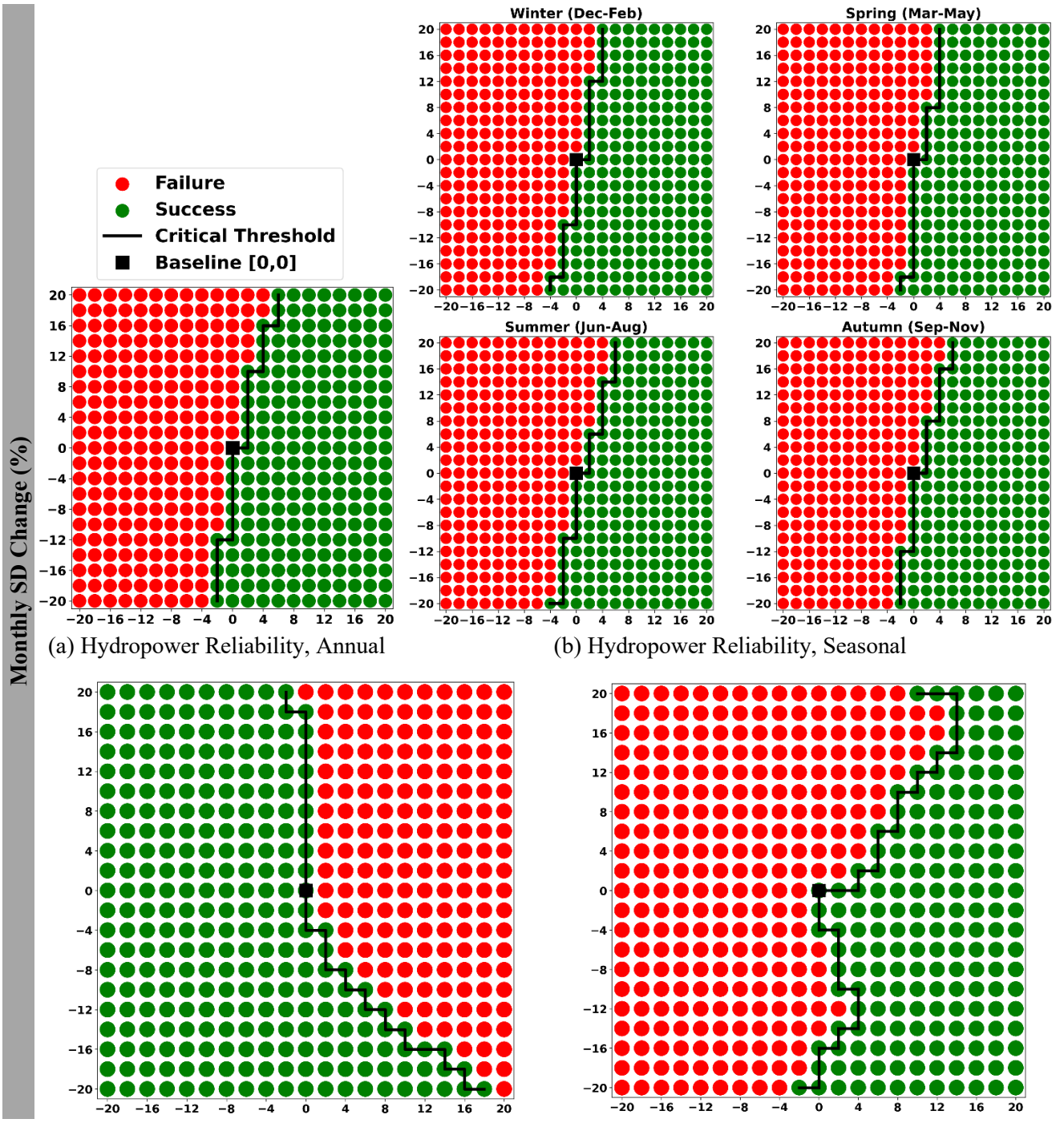
Figure 3.20c indicates that, relative to historical conditions at [0,0], Shellmouth Dam faces an increased risk of higher flood frequency during spring (April-June) as monthly inflow variability increases. When inflow variability increases by approximately 20%, maintaining historical inflow

magnitude or reductions in inflow magnitude are required for the system to remain within the success region of flood frequency performance. In contrast, when inflow variability decreases, flood frequency remains within the success region even for increases in inflow magnitude up to approximately +18%. Under reduced or near-historical inflow magnitude, even large increases in inflow variability do not result in more frequent flooding, as sufficient storage capacity remains available. This behavior indicates that current dam operations are well tuned to the historical inflow magnitude regime but are less robust to sustained increases in monthly inflow variability over the 38-year evaluation period.

3.4.8.3 Water Demand Management

Figure 3.20d shows that water-demand shortage frequency at Shellmouth Dam is primarily driven by changes in monthly inflow magnitude, with reductions in inflow magnitude rapidly pushing the system into the failure region. This behavior demonstrates that the lower operating guideline of 1400 ft has been well calibrated to historical inflow magnitude. Higher monthly inflow variability increases water-demand shortage frequency. To remain within the success region across the full ±20% range of inflow variability, inflow magnitude increases of approximately +14% or greater are required. This highlights the system-limited robustness to enhanced inflow variability under current operating rules and infrastructure design.

The stress-testing results for water-demand shortage frequency also reveal localized uncertainty near the critical threshold. For example, at +2% inflow magnitude, scenarios with -10% and -14% inflow variability fall within the success region, whereas a -12% variability scenario results in system failure. This behavior indicates that interpolating performance metrics at a finer resolution (2%) from inflow scenarios generated at coarser (10%) increments does not adequately capture system response near the critical threshold. As another example, at 0% change in inflow magnitude, reductions in inflow variability from -6% to -14% lead to failure, whereas further reductions from -16% to -20% result in success. Because it is unclear whether decreasing inflow variability under zero change in inflow magnitude consistently leads to failure or success, additional sets of scenarios should be generated for the same inflow conditions. This behavior reflects realization-level uncertainty, as discussed in the following section.



(a) Hydropower Reliability, Annual

(b) Hydropower Reliability, Seasonal

(c) Flood Frequency, April-Jun

(d) Water-Demand Shortage Frequency, July-Oct

Figure 3.20. (a) Annual and (b) seasonal hydropower stress-testing assessment in the Winnipeg River Basin. (c) Flood frequency and (d) water-demand shortage frequency at Shellmouth Dam evaluated across the same stress-testing space. Each scenario is classified as a success or failure, depending on whether its performance outperforms the baseline scenario at [0,0].

3.4.8.4 Matrix Year Uncertainty

The proposed framework allows multiple realizations to be generated for a given target inflow scenario through alternative matrix year selections. Different matrix year selections produce distinct monthly streamflow time series and corresponding autocorrelation and cross-correlation structures, as illustrated for the RH-O scenarios in Figure 3.12. Each set of monthly time series also defines a unique daily disaggregation through the k-nearest neighbors approach, resulting in distinct daily streamflow realizations. This realization-level uncertainty must be explicitly addressed within the stress-testing analysis. It can be accounted for by generating ensembles of realizations for each target inflow scenario and propagating them through all stages of simulation and performance evaluation. Ensemble-based evaluation supports estimation of the system likelihood, by comparing the performance for all realizations relative to a baseline, and identification of success versus failure, using statistics such as the median of realizations. It also enhances the robustness of risk-informed decision-making application by jointly quantifying event likelihood and consequence.

The same ensemble-based stress-testing approach is transferable to other water systems and a wide range of performance objectives. Beyond water resources, the framework is also applicable to other sectors in which system performance depends on the statistical properties of natural time series. Alternative seasonal patterns, such as those derived from GCMs projection, can be readily incorporated to assess future system stress and directly compare it with historical conditions. This capability enables systematic evaluation of evolving risks and supports climate-adaptive planning, resilient system design, and risk-informed decision-making under deep inflow-condition uncertainty.

3.5 Summary and Conclusion

This study introduces a flexible and computationally efficient framework for generating operationally relevant and statistically credible target synthetic streamflow scenarios to support multisite water system performance evaluations under deep inflow-condition uncertainty. Building upon Kirsch et al. (2013) streamflow generator, the framework employs an inverse approach to optimize generator parameters, enabling the user to directly target monthly streamflow magnitude (mean), variability (standard deviation, SD), and seasonality. In addition, the framework explicitly

checks feasibility, ensuring that only physically and mathematically feasible scenarios are produced. This targeted and feasibility-constrained approach allows for structured and uniform exploration of a wide range of inflow conditions, including those not represented in the historical record and climate-driven projections, without the need for computationally intensive optimization-based frameworks previously introduced for generating synthetic streamflow scenarios.

The framework is tested by applying it to the Winnipeg River Basin at fourteen inflow locations under five streamflow generation cases designed to reproduce and expand on historical conditions and GCMs-driven projections. Compared to non-optimized scenarios, optimization significantly improved the ability of the generator to match target monthly magnitude and variability while achieving uniform coverage of the exposure space across all locations. Uniform coverage prevents redundancy and guarantees that all plausible future inflow conditions are represented in stress testing. Moreover, replacing partially infeasible scenarios with feasible ones ensures broader coverage of the exposure space while maintaining plausibility, particularly when applying significant seasonality shifts or handling variables such as streamflow that have physical limits (i.e., streamflow cannot be negative). Statistical analyses and visual comparison confirm that the framework successfully retains historical correlation and distribution structures (i.e., statistically stationary behavior), without introducing unrealistic streamflow values when replicating historical seasonality, and appropriately modifies these structure when targeting altered seasonal patterns (i.e., statistically non-stationary behavior).

A key advantage over the traditional top-down approach lies in the framework's ability to generate synthetic scenarios that are directly comparable to a preserved historical baseline. This supports direct comparison to current operational conditions when evaluating altered system performance under different inflow conditions. Moreover, the framework provides a transparent and controlled exploration of system risk and vulnerability by allowing users to define specific streamflow properties, such as changes in magnitude, variability, or seasonality. In contrast, top-down methods typically represent a narrower range of uncertainty that may or may not diagnose critical system performance thresholds.

While top-down, GCM-driven scenarios offer the advantage of process-based physical plausibility, the proposed framework offers a wider range of scenarios that lack physical

plausibility, meaning they are plausible but may or may not occur. By combining the framework with the top-down approach, however, it is possible to leverage the strength of process-based GCM projections while expanding beyond GCM-implied futures to assess critical system thresholds. This hybrid approach maintains consistency with the statistical and operational characteristics of the water system, but facilitates broader exploration of uncertainty for more robust, risk-informed system planning.

In conclusion, the proposed framework provides a robust and practical tool for water system analysts and planners, offering direct control over key statistical properties of streamflow to generate operationally relevant and statistically credible scenarios. While the framework does not inherently ensure the physical plausibility of climate forcing, it enables transparent and comprehensive stress testing by systematically exploring a wide range of plausible inflow conditions. This capability meaningfully advances scenario-based water resources planning by complementing process-based, top-down approaches and addressing the growing need for risk-informed decision-making under climate and hydrologic uncertainty.

Future work will focus on enhancing the framework by incorporating autocorrelation and cross-correlation structures directly into the optimization objective. In addition, explicit persistence properties will be enabled, such as limiting maximum drought duration or enforcing multi-year drought conditions through constraint-based modifications within the framework. These additions will further improve the realism and application range of the framework for long-term planning, though at the cost of increasing the computational effort to meet the targets.

3.6 Availability of Data and Materials

The daily flow data for the hydrometric stations (H_1 to H_{16} in Figure 3.7) are publicly available from the Environment and Climate Change Canada website (https://wateroffice.ec.gc.ca/index_e.html). Processed inflow data derived from these stations, covering fourteen inflow locations, along with the Python code for the modeling framework and plotting scripts, are preserved in Zenodo by Gozini et al. (2025): https://doi.org/10.5281/zenodo.17195525. GCM-driven streamflow scenarios were generated by Stadnyk et al. (2021): https://doi.org/10.1525/elementa.2020.00098, and details on access and availability are provided in that publication.

CHAPTER 4. DECISION-RELEVANT STRESS TESTING OF HYDROPOWER SYSTEMS UNDER DEEP INFLOW UNCERTAINTY AND ELECTRICITY SUPPLY-DEMAND CHANGE

4.1 Abstract

Under conditions of deep uncertainty, stress-testing offers a robust pathway to inform planning and decision-making in hydropower systems. This study presents a stress-testing framework designed to assess hydropower systems under deep uncertainty for monthly inflow magnitude and variation, with changes in inflow seasonality and electricity demand. The framework identifies critical decision-relevant outcomes: dominant performance drivers, critical inflow thresholds, stress level, likelihood, and severity of hydropower systems. Its functionality is demonstrated for the hydropower system in Manitoba, Canada, evaluating hydropower generation reliability, vulnerability, revenue, and lake water-level excursion at annual and seasonal scales. Results show that inflow reductions cause severe system performance degradation, whereas equivalent increases in inflow yield limited benefits, indicating greater system sensitivity to dry conditions and limited system capacity to exploit wetter conditions. Moreover, improvements in hydropower performance under wetter conditions *likely* (≥66%) coincide with increasing lake level excursion frequency, revealing a benefit-stability trade-off within the system. Expanding generation capacity is expected to improve system reliability and revenue, but does not reduce dry-conditions vulnerability, or resolve the benefit-stability trade-off. Summer is expected to experience the greatest system stress, while spring is expected to exhibit potential surplus generation; however, the benefit-stability trade-off in spring is *very likely* (≥90%) to intensify. Collectively, these results highlight the need for adaptive management strategies beyond infrastructure expansion for the hydropower system. Overall, the framework captures system response under deeply uncertain inflow conditions, providing valuable insights for hydropower planning, and is transferable to other water resource systems, supporting risk-informed planning and climate adaptation decision-making.

Graphical Abstract: *SM.8 Stress Testing Graphical Abstract*

4.2 Introduction

Hydropower systems are highly sensitive to the magnitude and timing of streamflow (Savelsberg et al., 2018), which are expected to change under future climate conditions (Haguma et al., 2014). Similarly, climate change is expected to reshape electricity demand patterns, with rising temperatures increasing the need for cooling systems (Mutschler et al., 2021). Electricity demand is also projected to grow with urbanization, population growth, vehicles electrification, and higher living standards (Berardi & Jafarpur, 2020). Collectively, these supply- and demand-side pressures highlight the need for comprehensive climate impact assessments of hydropower systems to reduce electricity supply deficits and capitalize on potential opportunities within existing system configurations.

The *top-down* approach is the traditional framework for assessing climate change impacts on hydropower generation (Chernet et al., 2013; de Oliveira Serrão et al., 2023; Widén et al., 2024; Zhao et al., 2022; Zhou et al., 2018). In this paradigm, outputs from global and regional climate models (GCMs and RCMs) drive hydrological models to generate streamflow projections, which are then used to estimate hydropower generation. The strength of the top-down approach lies in its physically-based representation of climate-hydrology-hydropower linkages; however, it is constrained by the limited number of futures represented in GCM ensembles and typically provides only directional insights (i.e., increasing or decreasing in hydroelectricity generation) and adaptation policies tailored to this restricted set of scenarios.

The *bottom-up* approach has gained prominence for assessing climate change impacts on hydropower generation (Wasti et al., 2022), because it enables systematic exploration of a wide range of possible climate (e.g., air temperature and precipitation) and hydrologic (e.g., streamflow) conditions beyond those projected by GCMs (Brown et al., 2011). In doing so, it provides a practical means to address "deep uncertainty", a context characterized by multiple future states with unknown relative probabilities (Beh et al., 2015; Walker et al., 2013; Wu et al., 2025), by assessing system performance across a broad ensemble of plausible futures. Possible climate/hydrologic conditions build an *exposure space*, where each point on this space corresponds to a plausible future streamflow scenario (i.e., inflow condition). When climate conditions build the exposure space, they can be synthetically generated by scaling observed climate data (François et al., 2018) or by using stochastic weather generators (Bhattarai et al., 2024; Ray et al., 2018;

Taner et al., 2017), which are then translated into plausible future streamflow scenarios using hydrological models. Alternatively, when hydrological conditions are used to define the exposure space, plausible scenarios can be generated synthetically by stochastic streamflow generators (Yuan Liu et al., 2023; Quinn et al., 2018, 2017; Wild et al., 2019). Because streamflow scenarios are synthetically generated, they represent a wide spectrum of possible conditions independent of their probability of occurrence, whereas process-based, GCM-driven scenarios from the top-down approach retain the advantage of physical plausibility. That is why, when selecting the range of climate conditions in bottom-up approach, the process can be guided by GCM projections (François et al., 2018; Ray et al., 2018; Taner et al., 2017).

The bottom-up approach for climate change impact assessment on hydropower provides the opportunity to stress test systems (François et al., 2018; Quinn et al., 2018; Ray et al., 2018; Taner et al., 2017). Stress testing offers an additional insight by identifying the critical thresholds of the stressors at which the system may fail or operate undesirably (Fowler et al., 2024). Stressors are the statistical properties of hydrological or climate variables, for example, the mean and standard deviation of streamflow (Quinn et al., 2018) or of precipitation and temperature (François et al., 2018; Ray et al., 2018; Taner et al., 2017). Gozini et al. (2026b) demonstrated that generating streamflow scenarios with explicit targets of magnitude, variation, and seasonality provides some key benefits for stress testing: (i) it produces streamflow sequences that are directly relevant for site-specific operational analyses; (ii) it achieves uniform coverage of the exposure space, avoiding redundancy and ensuring that no plausible condition is overlooked; and (iii) it strengthens the connection with climate model outputs by enabling a clear, consistent, and systematic way to translate top-down information into a bottom-up framework for exploring uncertainty.

Quinn et al. (2018) presented a rigorous stress-testing framework for hydropower systems by perturbing inflow scenarios using multipliers in log-space to target streamflow magnitude, variation, and seasonality. This approach has since been adopted in subsequent studies, including Quinn et al. (2020) and Hadjimichael et al. (2020). However, the multipliers used in these studies interact during transformation from log-space to real-space, meaning real-space targets cannot be directly achieved or uniformly sampled (Quinn et al., 2018). Real-space inflow targeting offers clearer interpretability of exposure space for decision-makers; for example, a 20% increase in inflow variation can be directly quantified (e.g., ±50 m^3/s → ±60 m^3/s), whereas a 20% change in

log-space variation cannot be easily interpreted due to lognormal distribution properties (see Equations (2) to (5) in Gozini et al. (2026b)).

Direct application of multipliers in real space also faces restrictions, as scaling methods cannot independently control streamflow variation. To overcome this, Guo et al. (2017, 2016) introduced an optimization-based approach to adjust stochastic weather generator parameters to achieve prescribed climate targets, later extended by Culley et al. (2021, 2019) for multisite studies and stress testing. While effective, these frameworks are computationally expensive because targeting climate variables and translating them into streamflow scenarios requires high computational cost (Gozini et al., 2026b). Furthermore, for hydropower applications, stress testing based on streamflow targets remains more intuitive and transparent than targeting climate variables, since operational decisions depend directly on streamflow properties. To address this gap, Gozini et al. (2026b) developed a computationally efficient optimization-based framework for generating statistically credible synthetic streamflow scenarios that match real-space target of magnitude, variation, and seasonality across multiple inflow locations. The framework enables comprehensive water system assessment under deep inflow uncertainty.

Incorporating electricity demand into hydropower assessment extends the analysis beyond generation potential to include performance metrics such as reliability (i.e., system's ability to meet electricity demand) and vulnerability (i.e., the severity of deficits when electricity demand is not met), thereby offering additional decision-relevant insights. Future electricity demand scenarios can be developed using regression equations (Gaudard et al., 2013; Qin et al., 2020b), piecewise linear equations (François et al., 2018), artificial neural networks (Hou et al., 2021), or machine learning methods (Obahoundje et al., 2022), all by employing predictors such as GDP, population, and climate variables. Alternative approaches include assuming constant electricity demand (Li et al., 2020; Yuan Liu et al., 2023), relying on projections from governmental agency (Chowdhury et al., 2021), or using observed historical electricity demand (Mandal et al., 2019).

This study proposes a bottom-up stress-testing framework designed to evaluate hydropower system performance under deep inflow uncertainty and electricity demand change in multisite systems. The framework builds on the target inflow scenario generator introduced by Gozini et al. (2026b) and develops a structured, system-scale implementation capable of generating clear, decision-relevant insights for hydropower planning and climate adaptation. Real-space

perturbations of inflow magnitude, variation, and seasonality define the exposure space, enabling systematic construction of inflow uncertainty. System performance is evaluated using hydropower metrics under differing inflow conditions and electricity demand scenarios to address the following decision-relevant research questions, questions not previously examined in a comprehensive bottom-up study:

- Which inflow property serves as the dominant driver of system stress across performance metrics?
- What are the critical thresholds of inflow properties at which undesired performance occurs?
- What are the likelihoods associated with desired and undesired performance outcomes across the stress-testing space?
- How severe are the performance changes for desired and undesired outcomes, and what does this severity imply for system operation?
- How does the overall level of system stress projected for the future compared with the past, and which seasons become more or less stressed?
- How do alternative inflow seasonality patterns alter system performance and stress-testing results?

4.2.1 Manitoba Hydropower System

Supplying about 97% of the provincial electricity demand (Canada Energy Regulator, 2024), Manitoba hydropower generating system is the backbone of the provincial energy system and a central pillar of fiscal sustainability (Manitoba Hydro, 2024). The system spans a vast, complex river-reservoir network across a flat terrain, which limits water storage capacity to less than four months of supply (Gozini et al., 2026a). It is further characterized as a nival (snowmelt-dominated) and cold-regions (subject to seasonal snow and ice cover) water system with a persistent mismatch between the spring peak in water availability and the winter peak in electricity demand (Gozini et al., 2026a).

In Manitoba, climate change impacts on hydropower have been assessed exclusively through the top-down approach. Kim et al. (2022) examined hydropower potential generation at seasonal and annual scales in the Lower Nelson River Basin, projecting higher spring-summer but lower winter-autumn generation, with a slight upward annual trend under the current policy for reservoir operations. Lees (2022) focused exclusively on winter generation, projecting shorter and warmer ice-affected seasonality that increases cumulative winter outflow and provides the opportunity for hydropower generation increases. Notably, the differing winter results reflect the contrasting approach of Lees (2022), who focused on outlet hydraulics, versus Kim et al. (2022) who examined basin-scale water supply without accounting for shifts in ice impacts on operations and hydropower generation.

The framework is applied to the Manitoba hydropower system, which includes 16 hydropower stations and 49 hydrometric stations representing inflow locations. Manitoba hydropower system is evaluated under historical (1980-2017) and future (2018-2055) inflow and electricity demand conditions. Three hydropower performance metrics (reliability, vulnerability, and revenue) and one system state performance metric (water level excursions beyond the preferred operational range) are used to evaluate system behavior under each inflow condition at both seasonal and annual scales. This application makes several important contributions to both local (relative to Kim et al., (2022); Lees, (2022)) and global research (relative to Hadjimichael et al., (2020); Quinn et al., (2020, 2018)). Locally, in Manitoba, it (i) provides the first bottom-up assessment of the hydropower system; (ii) extends the spatial scope beyond the Lower Nelson River Basin to evaluate the entire hydropower system; and (iii) incorporates both stress testing and future electricity demand scenario, thereby providing a more comprehensive assessment of the hydropower system performance under changing climatic conditions. Globally, it (iv) introduces the first use of real-space targeting of streamflow scenarios for hydropower stress testing, enhancing transparency and interpretability of the exposure space for decision makers within a bottom-up framework.

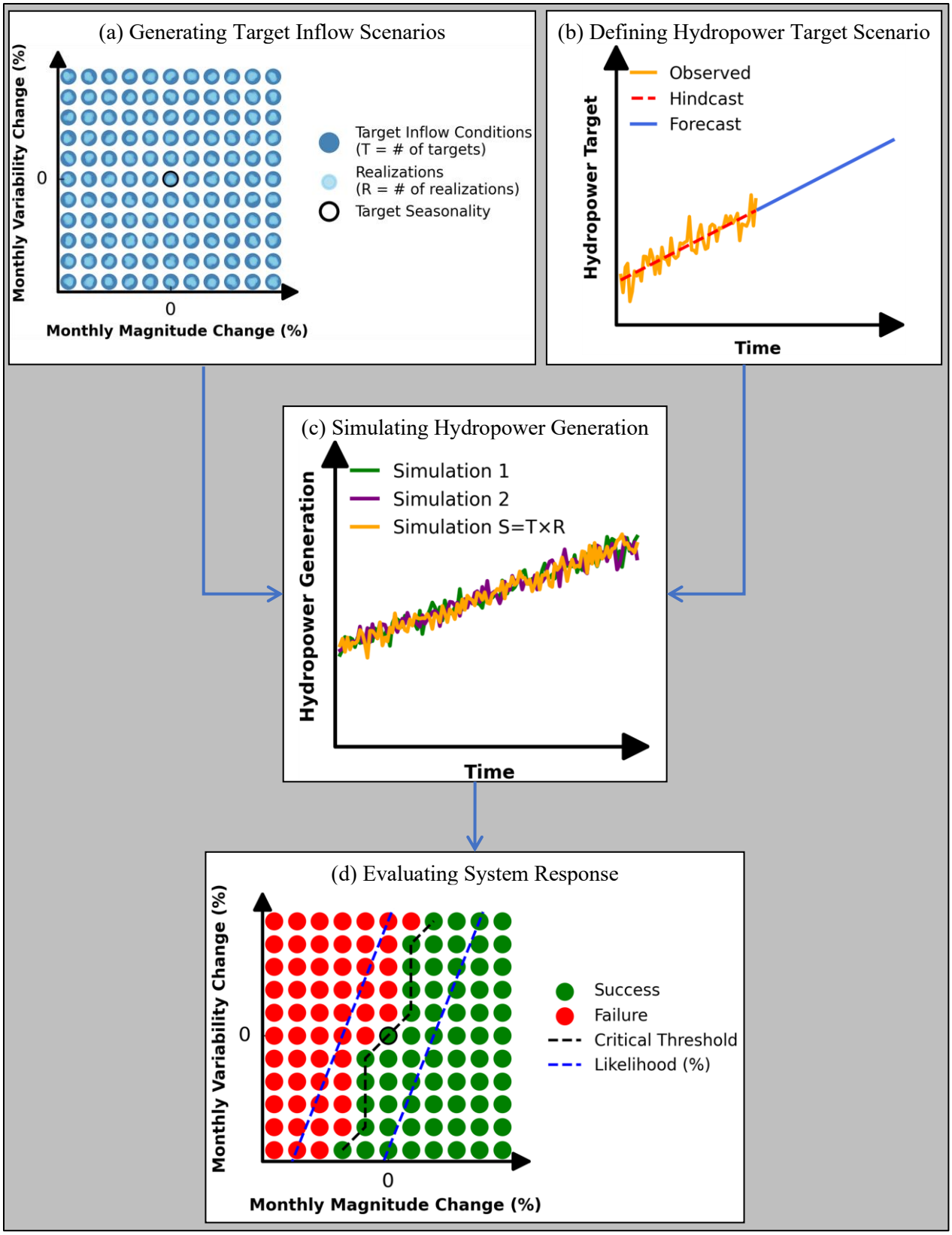


Figure 4.1. Workflow of the proposed bottom-up framework for stress testing hydropower systems

4.3 Methodology

The developed framework consists of four steps designed to conduct stress testing of hydropower systems (Figure 4.1). Each step is described in-depth in this section, outlining the corresponding tools, datasets, and implementation procedures, to demonstrate how the framework can be applied to any hydropower system.

4.3.1 Generating Target Inflow Scenarios

The first step involves generating R realizations (light-blue circles, Figure 4.1a) of T target inflow conditions (or hydrologic conditions; dark-blue circles in Figure 4.1a), each representing a specific combination of changes in monthly magnitude, variation, and seasonality. While the magnitude directly determines the volume of water available for hydropower generation, the variation captures inter-annual (year-to-year) fluctuations in inflow, and seasonality indicates intra-annual (within-year) fluctuations and when the majority of inflow arrives; information that collectively affects storage and release operations and consequently hydropower generation. Each realization of a target inflow condition represents a target inflow scenario. The center point (i.e., (0,0) coordinates, Figure 4.1a) on the exposure space corresponds to the target seasonality (black-border circle, Figure 4.1a) of the inflow scenarios. Seasonality is defined by the monthly variation in inflow magnitude and variation. When the historically observed seasonality is targeted, the center point represents the historical inflow condition. Alternatively, the seasonality derived from GCM-driven inflow scenarios can be used, in which case the center point represents the GCM-based inflow condition.

The monthly magnitude and variation of inflow conditions can be targeted for a specified range of deviation, desirable for stress testing system performance. An initial range of -20% to +20% with 10% increments provides a reasonable starting point. This range can later be refined, expanded or adjusted to smaller increments, based on the needs identified during system analysis (section "*4.3.4 Evaluating System Response*"). When historical seasonality is targeted, the range of changes in magnitude and variation are defined relative to the historical inflow condition. Similarly, when the GCM-driven seasonality is targeted, the associated ranges are defined relative to the GCM-based inflow condition.

Because inflow scenarios are generated synthetically, multiple realizations can be produced for each of the target inflow conditions. The uncertainty associated with selecting among these realizations must be considered in the stress-testing framework. To account for this uncertainty, multiple realizations are generated for each inflow condition and carried forward to subsequent steps. Generating multiple realizations for each target inflow condition also enables estimation of the likelihood of outcome when stress testing the hydropower system. To determine an adequate number of realizations, the normalized interquartile range (*IQR*) of the i^{th} system performance metric (M_i) is calculated for each sample size (y), as expressed in Equation (4.1). A large pool of X inflow scenarios is first generated targeting the historical inflow condition, and the system performance metrics are computed for all X inflow scenarios ($M_{i,X}$) in response to the recorded hydropower generation. For each sample size ($y = 2, 3, \ldots, Y$; where $Y < X$), Z random subsets are drawn from the X-scenario pool of performance results, and the *IQR* of each subset ($M_{i,y,z}$) is computed. The median of these Z values of *IQR* is then normalized by dividing it by the *IQR* derived from the full X-scenario pool. As illustrated in Figure 4.2, the smallest sample size R that yields a normalized *IQR* greater than 0.9 across all performance metrics (M_1 and M_2, Figure 4.2) is selected as the sufficient number of realizations for each target inflow condition.

$$Normalized\ IQR\left(M_{i,y}\right) = \frac{median_{z=1,\ldots,Z}\left(IQR\left(M_{i,y,z}\right)\right)}{IQR\ (M_{i,X})} \tag{4.1}$$

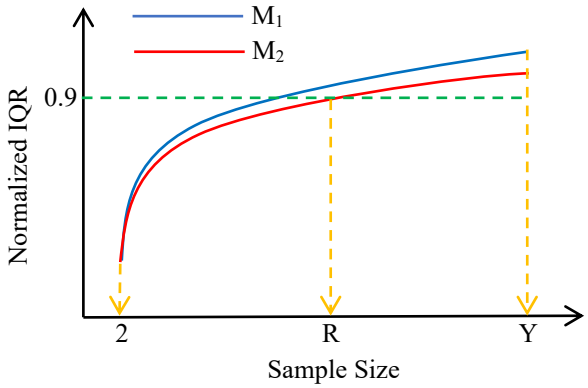


Figure 4.2. An illustration of the smallest sample size R (2<R<Y) that yields a normalized interquartile range (IQR) greater than 0.9 for two performance metrics M_1 and M_2. The smallest sample size R would be used as the number of realizations in Figure 4.1a.

The computationally efficient framework developed by Gozini et al. (2026b) is employed to generate target inflow scenarios with a specified temporal length (number of years); Python code

is publicly available in Zenodo (Gozini et al., 2025). This produces operationally relevant and statistically credible inflow scenarios (in terms of monthly distribution, autocorrelation, and cross-correlation) for multisite water system stress testing. A built-in feasibility check ensures that all generated scenarios are physically and mathematically feasible, enabling structured and uniform exploration of a wide range of possible inflow conditions beyond the historical record and for GCM-driven projections. This framework directly targets monthly magnitude, variation, and seasonality of streamflow in real space. It begins by defining seasonal monthly means and standard deviations (SD) of streamflow, then determines the required deviations from these baseline statistics to construct the exposure space. Once the targeted monthly statistics are achieved, the framework employs monthly-to-daily disaggregation to generate daily streamflow sequences suitable for water system simulation and stress testing. The only required input is the historical daily inflow data for the system. If the target seasonality is derived from GCM projections, the corresponding GCM-driven inflow scenario is also required to estimate the target seasonality.

4.3.2 Defining Hydropower Target Scenario

Defining a hydropower target scenario (Figure 4.1b) enables stress testing of the hydropower system for specific performance metrics, such as system reliability and vulnerability. The hydropower target represents the amount of electricity that hydropower stations are expected, or required, to produce. The first option is to use a recorded hydropower generation (orange line, Figure 4.1b) as the hydropower target scenario, which facilitates stress testing under historical hydropower demand conditions to provide insights into system performance within a historical context. Alternatively, a forecasted hydropower target (blue line, Figure 4.1b) can be used to assess system response under future hydropower demand conditions. Regression equations or projections of future electricity demand developed by government agencies can be deployed to establish projected hydropower targets. A simple trend line (extrapolation) derived from the recorded hydropower generation may also serve as a forecast. However, when using a forecasted hydropower target scenario, a corresponding hindcast (dashed red line, Figure 4.1b) is also required. This is necessary to quantify projected changes relative to historical performance, ensuring the stress-testing analysis has a consistent and meaningful baseline.

4.3.3 Simulating Hydropower Generation

In this step, hydropower generation is simulated under each target inflow condition (Figure 4.1c). Inflow scenarios are generated stochastically, keeping statistical characteristics of the distribution (mean and/or variance) at the target inflow condition. Therefore, the total number of system simulations (S) equals the number of inflow scenarios, calculated as the product of the number of target inflow conditions (T) and the number of realizations (R) per target. A suitable hydropower simulation tool (model) is required to translate each generated inflow scenario into simulated hydropower generation (e.g., water resource management model, WRMM). The choice of tool depends on the specific case study and how hydropower generation is projected.

System performance is computed under target combination of inflow and hydropower scenarios. These combinations form the basis of the system stress-testing framework. The target inflow conditions vary depending on inflow seasonality, either historical or GCM-derived future seasonality. Hydropower targets may reflect either recorded or forecasted electricity demand. For example, system performance can be evaluated under a case that uses historical inflow seasonality together with a recorded hydropower target, or under another case that uses GCM-derived inflow seasonality combined with a forecasted hydropower scenario. These combinations allow for a structured assessment of hydropower system response across a wide range of plausible hydrologic condition and electricity demand.

For each target case, the selected system performance metric(s) are calculated by comparing the simulated hydropower generation against the corresponding target values. This process yields a set of S system performance values for each performance metric.

4.3.4 Evaluating System Response

In the final stage, the system response is evaluated by classifying into one of two states: *success* and *failure* (green and red circles on Figure 4.1d, respectively). *Failure* refers to undesirable system performance that is inferior to the performance already observed under historical conditions, whereas success denotes acceptable or improved performance. As defined in Equation (4.2), for each inflow condition (t = 1, …, T), the median performance value of i^{th} metric across all realizations ($\bar{M}_{t,i}$) is used to be compared against a baseline (B): if the median performance outperforms ($\succcurlyeq$) the baseline value, that inflow condition is classified (C) as a success; otherwise,

it is considered a failure. The baseline is defined as the median system performance among all realizations in response to the recorded hydropower target under historical inflow condition. When the system response is against a forecasted hydropower target scenario, the corresponding hindcast hydropower target should be used for generating the baseline system performance, ensuring consistency.

$$C_{t,i} = \begin{cases} success, & if\ \bar{M}_{t,i} \succcurlyeq B_i \\ failure, & otherwisew \end{cases} \tag{4.2}$$

Heat maps are used to visualize the classified states associated with each inflow condition. The baseline contour delineating the success and failure regions in each heat map represents a system's critical threshold (dashed black line, Figure 4.1d). The slope of this baseline contour indicates whether monthly inflow magnitude or inflow variation is the dominant driver of system performance. A nearly vertical baseline contour implies that performance changes are governed primarily by inflow magnitude shifts, whereas a more horizontal contour indicates stronger sensitivity to changes in inflow variation.

To estimate the likelihood (%) of success or failure, all realizations of each target inflow condition are compared to all realizations from a baseline condition. The proportion of these comparisons is then used to construct likelihood contours (dashed blue lines, Figure 4.1d) across the heat map. The heat maps may be generated for various performance metrics of choice, as well as for annual and seasonal hydropower system responses, with a separate heat map produced for each metric and each season.

Each stress-test heat map corresponds to a specific case, defined by a unique combination of target inflow seasonality and hydropower scenario. Analyses involving different inflow seasonality patterns or different hydropower targets requires repeating the full workflow (except for determining the sufficient number of realizations in section "*4.3.1 Generating Target Inflow Scenarios*") and a comparison of resulting heat maps across cases. Comparisons should focus on two key aspects. First, the relative size of the failure and success regions showing stress level; a larger failure region indicates a higher-stressed system, whereas a larger success region indicates a less-stressed system. Second, the severity of performance change within the failure and success regions; heat maps with smaller failure area may exhibit relatively larger performance degradation

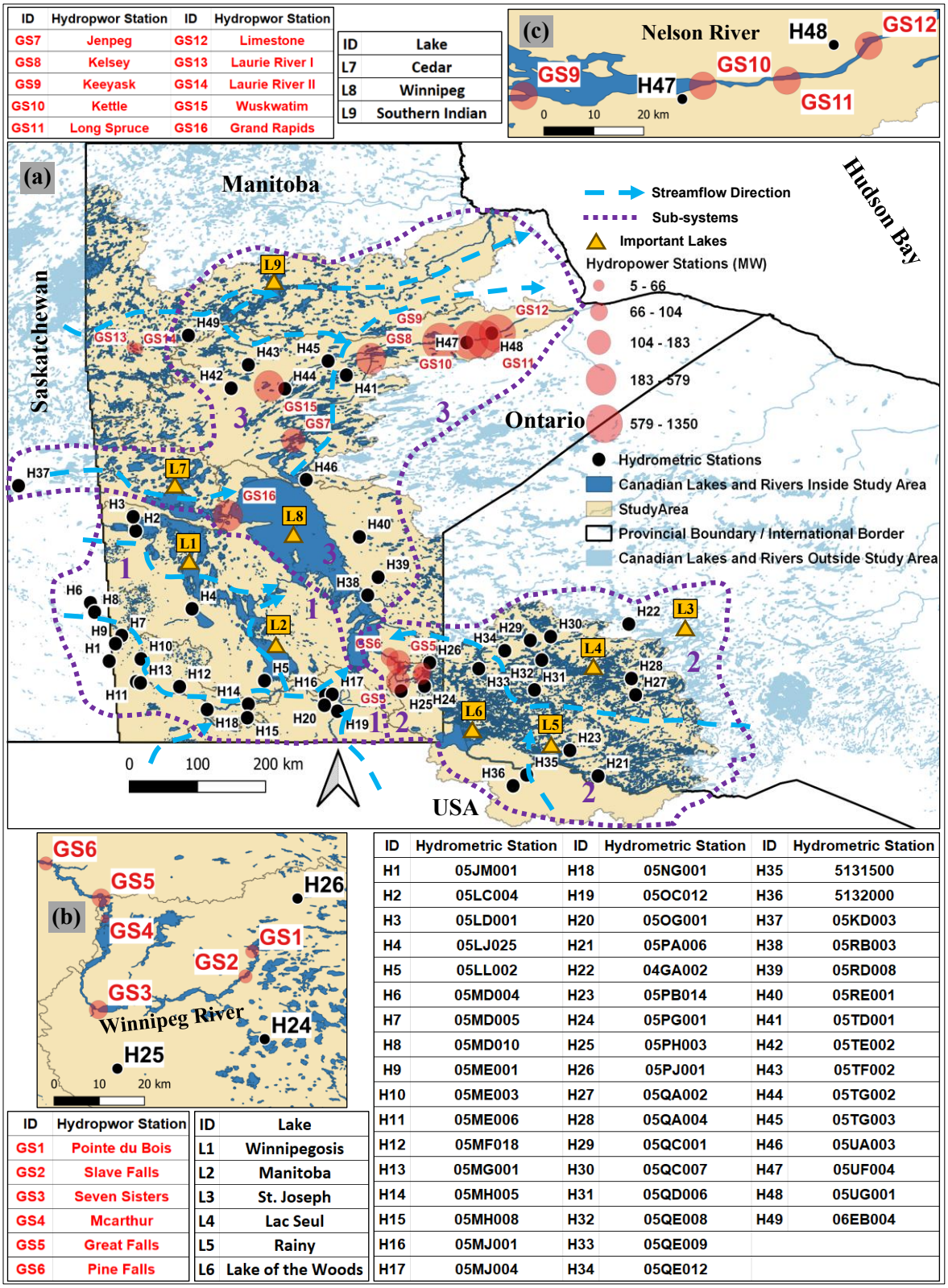
compared with another case that appears more stressed based solely on success-failure region proportioning. Both the spatial extent and severity of failure are necessary to fully interpret system stress across each target case.

The range of targets in monthly inflow magnitude and variation can be expanded or refined with smaller increments when necessary. For example, if a heat map shows no system failures, the user may expand the (in)decrease in inflow magnitude to capture inflow conditions under which failure occurs. Alternatively, system performance outcomes can be interpolated or extrapolated to estimate system behavior for untested inflow conditions. Although such estimates provide only approximation, they can offer useful insight without requiring additional inflow scenario generation.

4.4 Case Study

To demonstrate the implementation of the proposed stress-testing framework, it is applied to the hydropower system in Manitoba. The study area encompasses the interconnected river-reservoir and hydropower systems of Manitoba and part of Ontario (cream-colored area, Figure 4.3a). The study area represents roughly the lower 30% of the 1.4 million km² Nelson-Churchill River Basin, draining (dashed-cyan lines, Figure 4.3a) the Canadian Rockies in the west, portions of the north-central United States, and north-western Ontario, channeling it through Manitoba before ultimately discharging into Hudson Bay in the province northeast. To better describe the study area and its key components, it is divided into three Sub-systems, as shown in Figure 4.3a (dashed-purple lines).

Sub-system 1 includes 20 inflow locations (station ID H1 to H20, Figure 4.3a) within the southern and south-western portions of the basin. Based on the observed daily data from 1980 to 2017, these inflows contribute approximately 19% of the total inflow to the study area, with an average daily flow of 524 m³/s. Lake Winnipegosis and Lake Manitoba (L1 and L2, Figure 4.3a, respectively) are the major lakes included in this Sub-system. The Hydrologic Forecast Centre (HFC) regulates key components of this system, including the Shellmouth Dam, Portage Diversion, Fairford Control Structure, and the Red River Floodway. These infrastructures collectively manage flows along the Assiniboine, Red, and Dauphin Rivers, primarily for flood control and water level regulation.



ID	Hydropwor Station	ID	Hydropwor Station
GS7	Jenpeg	GS12	Limestone
GS8	Kelsey	GS13	Laurie River I
GS9	Keeyask	GS14	Laurie River II
GS10	Kettle	GS15	Wuskwatim
GS11	Long Spruce	GS16	Grand Rapids

ID	Lake
L7	Cedar
L8	Winnipeg
L9	Southern Indian

ID	Hydropwor Station
GS1	Pointe du Bois
GS2	Slave Falls
GS3	Seven Sisters
GS4	Mcarthur
GS5	Great Falls
GS6	Pine Falls

ID	Lake
L1	Winnipegosis
L2	Manitoba
L3	St. Joseph
L4	Lac Seul
L5	Rainy
L6	Lake of the Woods

ID	Hydrometric Station	ID	Hydrometric Station	ID	Hydrometric Station
H1	05JM001	H18	05NG001	H35	5131500
H2	05LC004	H19	05OC012	H36	5132000
H3	05LD001	H20	05OG001	H37	05KD003
H4	05LJ025	H21	05PA006	H38	05RB003
H5	05LL002	H22	04GA002	H39	05RD008
H6	05MD004	H23	05PB014	H40	05RE001
H7	05MD005	H24	05PG001	H41	05TD001
H8	05MD010	H25	05PH003	H42	05TE002
H9	05ME001	H26	05PJ001	H43	05TF002
H10	05ME003	H27	05QA002	H44	05TG002
H11	05ME006	H28	05QA004	H45	05TG003
H12	05MF018	H29	05QC001	H46	05UA003
H13	05MG001	H30	05QC007	H47	05UF004
H14	05MH005	H31	05QD006	H48	05UG001
H15	05MH008	H32	05QE008	H49	06EB004
H16	05MJ001	H33	05QE009		
H17	05MJ004	H34	05QE012		

Figure 4.3. Location of the study area (cream-colored area), hydropower stations (red circles), hydrometric stations (black circles), and major lakes (yellow triangles). The boundary shapefile of the sub-basins is extracted from Ahmed et al. (2024), Manitoba boundary form Data MB, Ontario boundary from Ontario GeoHub, and lakes and rivers from Government of Canada.

Sub-system 2 includes 16 inflow locations (station ID H21 to H36, Figure 4.3a) within the south-eastern portion of the study area. These inflows contribute approximately 18% of the total inflow to the study area, with an average daily flow of 498 m^3/s. This sub-system contains a cascade of six hydropower generating stations along the Winnipeg River (GS1-GS6, Figure 4.3b), with a combined installed capacity of 580 MW, representing 9.79% of Manitoba's total hydropower capacity. The inflow to this cascade of hydropower stations is primarily regulated by Lake St. Joseph, Lac Seul, Rainy Lake, and Lake of the Woods (L3-L6, Figure 4.3a, respectively), all located in Ontario. The International Rainy-Lake of the Woods Watershed Board (IRLWWB) and the Lake of the Woods Control Board (LWCB) are responsible for regulating these upstream lakes and controlling the outflows that influence the Winnipeg River hydropower system.

Sub-system 3 includes 13 inflow locations (station ID H37 to H49, Figure 4.3a) covering the central and northern portions of the study area. These inflows contribute approximately 63% of the total inflow to the system, with an average daily flow of 1,739 m^3/s. The Saskatchewan river inflow, recorded at hydrometric station H37, contributes about 15% of the total inflow, with an average daily flow of 413 m^3/s, and discharges into Cedar Lake (L7). The Grand Rapids generating station (GS16), located at the outlet of Cedar Lake, has an installed capacity of 479 MW, representing 8.08% of Manitoba total hydropower generation capacity. Outflow from Grand Rapids, together with outflows from sub-systems 1 and 2, drains into Lake Winnipeg (L8), the largest lake in the system and the most critical control point for streamflow regulation in Manitoba. Lake Winnipeg outflow passes through the East and West Channels, controlled by the Jenpeg generating station (GS7), the first control and hydropower facility downstream of the lake. Jenpeg regulates Lake Winnipeg outflow to a series of hydropower stations along the Nelson River (GS8-GS12). Together, Jenpeg and the downstream stations have a combined installed capacity of 4,646 MW, accounting for 81.96% of Manitoba total hydropower capacity. The Churchill River inflow, recorded at station H49, provides the largest single inflow contribution, accounting for 35% of the total inflow, with an average daily flow of 957 m^3/s. It flows to Southern Indian Lake (L9), from which approximately 81% of the outflow is diverted through the South Bay Channel toward the Nelson River. This diverted flow first passes through the Wuskwatim generating station (GS15) on the Burntwood River, with an installed capacity of 211 MW (3.56% of Manitoba hydropower capacity), before joining the Nelson River and its major hydropower stations cascade consisting of Keeyask (695 MW), Kettle (1,220 MW), Long Spruce (980 MW), and Limestone (1,350 MW)

(GS9-GS12, Figure 4.3c, respectively). Laurie River I and II (GS13 and GS14, Figure 4.3a), two small generating stations contribute only 0.17% of Manitoba total hydropower capacity, primarily are used to support local electricity demand.

4.4.1 Data

Data for this study were collected for the historical period 1980-2017, as this period provides complete and continuous coverage across the entire study area without missing years or data gaps. Data required to implement the stress-test framework include observed and GCM-driven daily streamflow at each hydrometric station; daily recorded hydropower generation; and projected annual and monthly electricity demand. Daily observed streamflow are used to generate target inflow scenarios and to represent historical inflow conditions (1980-2017). Daily GCM-driven streamflow are used to represent future inflow conditions (2018-2055). Daily recorded hydropower generation are used to assess hydropower system performance under historical conditions, and to establish the baseline performance metrics (i.e., benchmark) for stress testing. Future electricity demand projections are used to define forecasted hydropower target scenarios for stress testing the hydropower system in future contexts.

4.4.1.1 Historical Inflow

Manitoba Hydro quality controlled and provided daily observed inflow for hydrometric stations H21 to H49 on Figure 4.3a. The remaining station inflows (H1 to H20) were extracted from the Environment and Climate Change Canada website (https://wateroffice.ec.gc.ca/index_e.html). All daily inflow data at the 49 hydrometric stations can be retrieved from the Environment and Climate Change Canada website.

Average daily inflow across the hydrometric stations ranges from 0.37 m^3/s (H8) to 957 m^3/s (H49), demonstrating the wide range of flow magnitude within the system. The coefficient of variation (CV), expressing variation (SD) relative to magnitude (mean), varies from 0.37 to 5.03 across these stations. CV values suggest that stations with relatively low mean inflow exhibit higher variation, whereas stations with higher mean inflow tend to show lower variation.

In this study, seasons are defined as follows: winter (December-February), spring (March-May), summer (June-August), and autumn (September-November), consistent with the dominant hydroclimatic processes of the basin. Historically, summer and spring contribute the largest

fractions of annual total inflow to the system (32% and 30%, respectively), whereas autumn and winter receive substantially less (22% and 16%, respectively). The total inflow to the study area shows that peak monthly inflow occurs in May; however, the timing of peak inflow varies across individual locations. Among the 49 hydrometric stations, 26 stations exhibit peak monthly inflow in May, with these stations contributing approximately 61% of total basin inflow and include H49, the station with the highest individual contribution to total inflow. Eleven stations indicate peak inflow occurring in April, contributing about 11% of the total inflow; six stations (6% of total inflow) peak in June; while five stations (22% of total inflow) peak in July. The peak at station H37, the second-highest contribution to total inflow, occurs in July.

4.4.1.2 GCMs-Driven Inflow

An ensemble of nineteen GCM scenarios from the BaySys project (Braun et al., 2021) is used to define the future streamflow seasonality. The ensemble incorporates fourteen GCMs and two Representative Concentration Pathways (RCPs), with their IDs listed in Table 4.1. The nineteen scenarios were selected by Braun et al. (2021) from a larger set of 54 CMIP5 simulations. These nineteen selected GCM scenarios represent approximately 90% of the projected variation in annual mean temperature and precipitation across the Hudson Bay Drainage Basin. As shown in Table 4.1, all GCMs project future warming, with annual mean temperature changes ranging between +1.3 ºC and +5.7 ºC. Similarly, all GCMs projects a wetter future, with the projected increase in the annual mean precipitation between 2.6% and 18%. The highest precipitation increases (>13%) correspond to scenarios with projected warming greater than 3.5 ºC.

Stadnyk et al. (2021) generated daily GCM-driven streamflow for the nineteen-member ensemble over 1981-2070, providing regulated inflow simulations for the 49 hydrometric stations used in this study. From this dataset, the period 1981-2017 is used as the hindcast to ensure consistency with observed inflows, while 2018-2055 is adopted as the projection period. Using two periods of equal length (38 years) ensures a consistent and comparable stress-testing assessment between historical and future conditions. The projected annual changes, summarized in Table 4.1, reveal substantial future uncertainty in both the magnitude and variation of total inflow to the study area, as the values and direction of annual mean and SD change differ across the GCMs. This is consistent with previous findings, which similarly report low model agreement and highly uncertain streamflow projections (Kim et al., 2022; Lilhare et al., 2022; MacDonald et

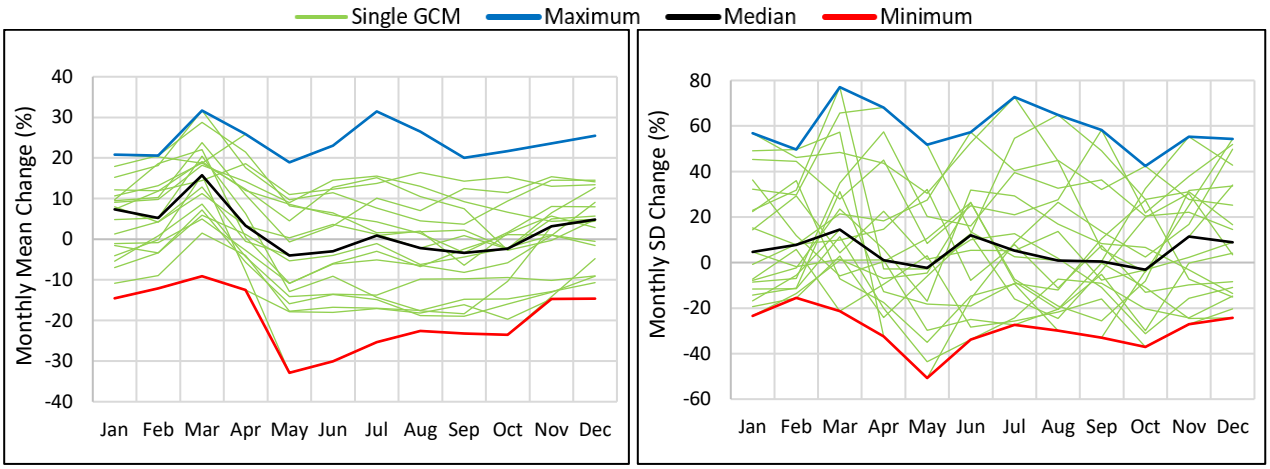
al., 2018; Stadnyk et al., 2021). Although all GCMs project temperature and precipitation changes in the same direction on an annual basis, the intra-annual (monthly) patterns of these changes play a critical role in shaping the regulated inflow response in such a cold-regions basin. The median response suggests an increase in annual inflow magnitude, while the annual inflow variation decreases.

Table 4.1. Summary of projected annual changes in temperature, precipitation, and total inflow across the 19 GCM scenarios. Temperature and precipitation changes correspond to the Hudson Bay Drainage Basin for 2041-2070 relative to 1981-2010, extracted from Figure 2 of Braun et al. (2021). Red shading indicates higher temperature change while blue shading indicates higher precipitation change. Inflow changes reflect total system inflow aggregated across all 49 hydrometric stations for 2018-2055 relative to 1981-2017. The horizontal bars illustrate increases (blue) or decreases (red) in mean and SD of inflow.

GCM ID	Annual Mean Temperature Change (°C)	Annual Mean Precipitation Change (%)	Annual Mean Inflow Change (%)	Annual SD Inflow Change (%)
A10-R41	3.3	5.6	2.74	-6.76
A10-R81	4.7	10	9.35	40.26
A13-R41	2.7	7.3	10.88	27
A13-R81	4	10.3	12.4	-26.38
CE2-R41	2.6	8.2	-0.57	-20.42
CMM-R41	3.5	14.6	-8.71	-32.5
CMS-R81	2.65	7.9	6.84	34.93
CN5-R41	3.8	13.2	-3.09	-12.11
GF3-R41	5	17.8	8.71	-10
IAL-R41	1.3	2.6	-15.77	-36.68
IAL-R81	2.7	5.7	-1.98	-13.93
INM-R41	3.95	8.1	0.77	44.71
MI5-R41	5.6	13.7	-12.73	-23.65
MI5-R81	5.7	17.7	9.67	15.26
MIC-R81	3.2	7.3	-4.99	-8.07
MIE-R81	4.8	10.6	-17.22	8.42
MR3-R41	1.7	9	13.92	6.78
MR3-R81	2.65	12.6	23.34	53.54
NOE-R41	3.1	7.2	-11.57	11.1
Median	3.30	9.00	0.77	-6.76

As shown in Table S5, the GCMs and their ensemble median produce fifteen distinct seasonal patterns of change in total inflow magnitude and variability. Four GCMs exhibit a pattern of concurrent increases, while three project concurrent decreases in both seasonal inflow magnitude and variability. Seasonal inflow variation decreases for winter and spring and increases for summer and autumn associated with the ensemble median. Climate change amplifies inter-annual inflow fluctuations at the seasonal level in summer and autumn, while reservoir regulation and compensating seasonal effects moderate year-to-year variation in the annual inflow.

Monthly inflow seasonality is an important component of this study because target inflow conditions are specified at the monthly scale. The ensemble median projects higher winter inflow magnitude from December to February and significantly higher spring inflow magnitude in March and April driven by earlier and more pronounced spring snowmelt events (Figure 4.4a). Earlier snowmelt reduces inflow in May and June, which results in decreasing summer inflow magnitude. In autumn, a projected increase in November inflow combined with decreasing inflow in September and October results in a net increase in autumn inflow magnitude. Although March and April inflow increases, the basin-wide peak inflow still occurs in May; however, its spatial distribution changes. Among the 49 hydrometric stations, there is a decrease in the number of stations with May-peaks from 26 to 19, while the number of stations peaking in April increases from 11 to 14, suggesting a shift toward earlier peak flow timing at three locations. Figure 4.4b shows that, based on the ensemble median, variability of monthly inflow increases in nearly all months except May and October, which exhibit close to net zero change. This confirms an overall increase in inter-annual variation of monthly inflow anticipated across the study domain.



(a) (b)

Figure 4.4. (a) Monthly mean change and (b) monthly SD change of total inflow to the hydropower system for the GCM-driven projections (2018-2055) compared to hindcast (1981-2017).

4.4.1.3 Recorded Hydropower Generation

Manitoba Hydro provided daily recorded hydropower generation for the period 1980-2017. Over this period, Manitoba produced an average of 28,034 GWh of hydroelectricity annually, with an annual variation of 6,378 GWh. This variation is primarily driven by year-to-year fluctuations in available water supply (i.e., inflow), and by changes in system capacity resulting from new infrastructure development. In particular, the addition of the Limestone (1991) and Wuskwatim

(2012) generating stations boosted system capacity to produce electricity. Seasonally, hydropower generation is relatively high from November to March when average daily air temperatures fall below 0 °C and energy demand for space heating increases (Gozini et al., 2026a).

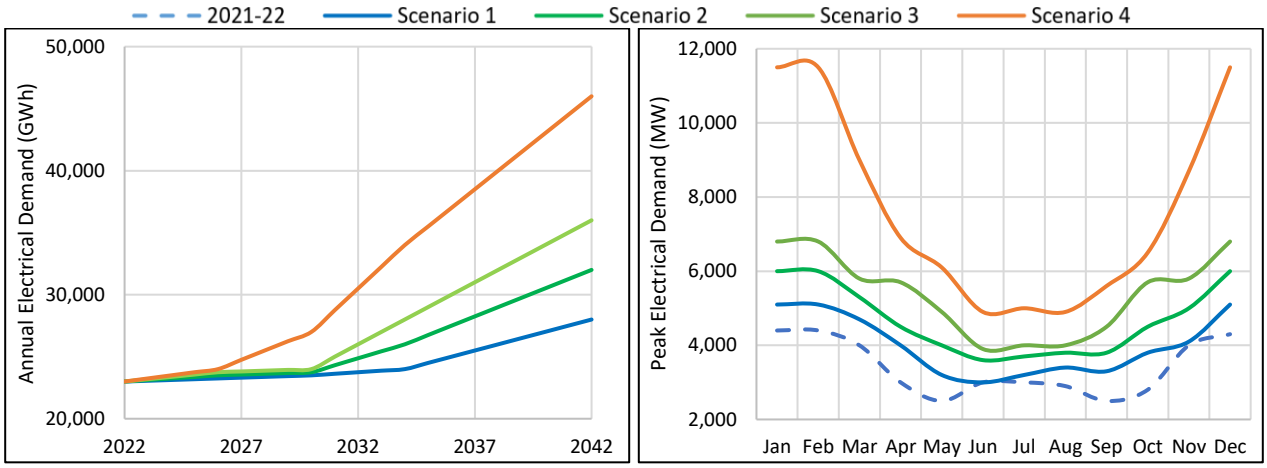
Not all hydroelectricity generated in Manitoba is used domestically, as Manitoba Hydro actively trades electricity with neighbouring power systems in Canada (Saskatchewan and Ontario) and the United States. When generation exceeds provincial electricity demand, surplus energy is exported, providing significant revenue and helping to keep electricity rates low for Manitobans. Conversely, electricity is imported when domestic supply is insufficient. The firm export and import capabilities in the transmission interconnections, as of 2022, show that export capacity is approximately 2.25 times greater than import capacity (Manitoba Hydro, 2023b).

4.4.1.4 Electricity Demand Projections

Manitoba Hydro (2023a) estimates that provincial electricity demand will rise by 2042, at different rates according to four distinct scenarios (Figure 4.5a). These scenarios are driven by five key factors: economic growth, decarbonization policy (reducing greenhouse gas emissions), electric vehicle adoption, the transition from natural gas to electricity for building heating, and customer self-generation of electricity. The intensity of change in these drivers increases progressively from Scenario 1 to Scenario 4. Greater adoption of electric vehicles and the transition from natural gas to electricity for building heating are expected to be the main contributors to the long-term electricity demand growth. Scenario 4 produces the greatest increase in provincial electricity demand. Due to increasing provincial electricity demand, Manitoba Hydro (2023a) plans not to renew existing export contracts once they expire; however, exports may still occur during periods of excess generation.

Manitoba Hydro (2023a) plans to maintain the current amount of electricity supplied by hydropower, rather than increasing hydropower capacity. This implies that no additional hydropower generation capacity will be added, even as provincial demand grows. The Keeyask generating station (2021) is anticipated to be the final hydropower facility added to the system before 2042. Manitoba Hydro (2023a) expects that the existing hydropower fleet produces an average of approximately 37,000 GWh annually. The utility plans to meet rising demand through improved energy efficiency, expanded electricity production from other sources (e.g., wind and natural gas turbines), and increased electricity imports. While actual hydropower generation may

be higher or lower than 37,000 GWh depending on inflow conditions, any deviation from this expected level directly affects the contribution required from other energy sources.



(a) (b)

Figure 4.5. Projections of (a) annual electricity demand and (b) monthly peak electrical demand in four scenarios. The electricity demand excludes export contracts, transmission and distribution losses, and planning reserve margin. The figure is reproduced using the data visually extracted from Figure 6.9 and 6.11 of the publicly available Manitoba Hydro (2023a) report.

Manitoba Hydro (2023a) projects that peak electricity demand will increase across all months by 2042 compared to 2021-22 (Figure 4.5b). Relative monthly increases are broadly similar under Scenarios 1–3, reflecting gradual electrification, moderate economic growth, and incremental adoption of electric vehicles. In Scenario 4, however, months with the historically highest electricity demand (November to March) show a much larger increase, reflecting the most aggressive decarbonization pathway, extensive fuel switching from natural gas to electric space heating, and the highest levels of electric vehicle adoption, factors that substantially intensify electricity demand during the coldest months of the year.

4.4.2 System Simulation Model

MB_HydroSim (Gozini et al., 2026a) is the hydropower simulation tool used in this study to simulate hydropower generation under a wide range of inflow and hydropower target scenarios, assuming current operational rules at the water control points remain unchanged. Developed specifically for the Manitoba hydropower system, MB_HydroSim captures the operational complexities of this large, cold-regions river-reservoir network. Built using MODSIM-DSS, MB_HydroSim simulates daily water levels, outflows, and hydropower generation while incorporating key system features such as operational rules, reservoir characteristics, hydropower

efficiency relationships, and ice-related impacts on channel conveyance (East, West, and South Bay Channels). MB_HydroSim has been evaluated against observations from 1980 to 2017 and has successfully reproduced water levels (KGE=0.86), outflows (KGE=0.85), and hydropower generation (KGE=0.94). The model slightly underestimates hydropower generation (Gozini et al., 2026a), making it a conservative tool for planning and stress-testing applications.

4.4.3 Construction of Target Scenarios

4.4.3.1 Inflow Scenarios

Four distinct target sets of monthly inflow are developed across the 49 hydrometric stations to support stress testing of Manitoba hydropower system (Table 4.2). These inflow conditions vary in monthly inflow magnitude, variation, and seasonality to explore a wide range of plausible hydrologic futures.

1. Reproducing Historical records (RH): Replicates historical inflow conditions (1980-2017), including the observed monthly magnitude, variability, and seasonality; serving as the baseline inflow condition for stress testing, with 20 realizations selected from an initial set of 100 (justification is provided in "*4.5.1. Uncertainty Estimation, Case RH-R*").

2. Expanding over Historical records (EH): Preserves historical inflow seasonality while varying monthly inflow magnitude and variability by ±20% in 10% increments. This creates an exposure space centered on the historical inflow condition (RH), facilitating stress testing of inflow regimes wetter/drier and more/less variable than historically observed.

3. Expanding over GCMs projections (EG): Preserves the median GCM-projected (2018-2055) inflow seasonality while varying monthly inflow magnitude and variability by ±20% in 10% increments. This constructs an exposure space centered on the median GCM-driven inflow condition, affording stress testing of wetter/drier inflow regimes that are more/less variable than the current median GCM projections. Since the median GCM projection show higher monthly inflow variation (Figure 4.4b), the EG inflow conditions represent greater monthly variation compared to the EH inflow conditions.

4. Reproducing GCMs projections (RG): Replicates the full ensemble of 19 GCM-driven inflow conditions, which evaluates the system response under different inflow seasonality

patterning. RG helps verify whether annual stress-tests results from EG remain feasible when inflow seasonality diverges from the ensemble median.

The validity of the generated target inflow scenarios, to ensure they meet the target condition and are statistically credible, has been previously evaluated by Gozini et al. (2026b) at stations H21 to H36 in Sub-system 2 (Figure 4.3a), with the same validation principles applying to all other stations in this study. Using monthly-to-daily disaggregation, daily inflow scenarios are generated and applied in stress testing.

Table 4.2. Summary of the four target sets of monthly inflow conditions used for stress testing of Manitoba hydropower system. "Historical" refers to the period 1980-2017, and "projections" refer to the period 2018-2055.

Sets of Target Inflow Condition	**Target Seasonality**	**Deviations from Seasonality (%)**			**# of Inflow Conditions**	**# of Realizations**
		Magnitude	**Variation**	**Increments**		
Reproducing Historical records (RH)	Historical observations	0	0	NA	1	100 and 20
Expanding over Historical records (EH)	Historical observation	-20 to +20	-20 to +20	10	25	20
Expanding over GCMs projections (EG)	Median of GCM-driven projections	-20 to +20	-20 to +20	10	25	20
Reproducing GCMs projections (RG)	GCM-driven projections	0	0	NA	19	20

4.4.3.2 Hydropower Scenarios

Three hydropower target scenarios are used to support stress testing of Manitoba hydropower system:

1. Recorded (R) hydropower targets (1980-2017): representing daily historical hydropower generation at each station; targets are used to evaluate system performance under historical electricity demand.

2. Forecasted (F) hydropower targets (2018-2055): representing expected future hydropower demand; used to assess system response under projected future electricity demand.

3. Hindcasted (H) hydropower targets (1980-2017): providing a consistent baseline aligned with the forecasted targets, enabling meaningful comparison and quantification of projected changes.

Forecasted (F) and hindcasted (H) annual hydropower targets reflect system changes in installed system capacity over the period 1980-2055. An annual hydropower target of 37,000 GWh is applied for the period 2021-2055, representing total expected hydropower generation from all

stations following the commissioning of Keeyask in 2021. For the earlier periods, targets are proportionally scaled down from 37,000 GWh based on installed generation capacity to reflect historical system configurations associated with major capacity expansions; Wuskwatim in 2012 and Limestone in 1991. Target values are defined stepwise as follows:

- 2021-2055: 37,000 GWh, 100% of the existing hydropower generation capacity.
- 2012-2020: 32,700 GWh, 88.38% of the existing hydropower generation capacity (exclusion of Keeyask).
- 1991-2011: 33,394 GWh, 84.85% of the existing hydropower generation capacity (exclusion of Keeyask and Wuskwatim).
- 1980-1990: 23,043 GWh, 62.28% of the existing hydropower generation capacity (exclusion of Keeyask, Wuskwatim, and Limestone).

During the hindcast period, generation capacity and transmission systems were upgraded at several plants, including capacity increases at Grand Rapids between 1995 and 2000 (Gozini et al., 2026a). To account for these expansions, annual hydropower targets are increased by 10% over the 2005-2020 period to align with recorded generation. This approach provides a more realistic representation of past system performance while establishing a conservative baseline, as the upward scaling increases the required system performance level.

Monthly share, defined as the proportion of annual hydropower target contributed by each month, is used to disaggregate the annual hydropower targets into monthly values. For the hindcast period, the monthly shares from 2017 hydropower generation are applied. For the forecast period, monthly adjustments from Table 4.3 are applied to 2017 monthly shares, assuming the seasonality of peak electricity demand projected for 2042 (Figure 4.5b) applies to the hydropower target for 2055. Among the four scenarios, Scenario 1 is selected to define monthly share adjustment. The adjustments in peak electricity demand are broadly similar across Scenarios 1 to 3, with the magnitude of change in each month increasing from Scenario 1 to Scenario 3 (Table 4.3). Therefore, seasonal stress-testing results based on Scenario 1 can be interpreted as conservative system outcomes, which may intensify under Scenarios 2 or 3. Scenario 4 is not used, as it represents an aggressively transformed energy system that primarily introduces non-hydropower electricity sources, resulting in seasonal electricity demand patterns that are not broadly relatable

to the other scenarios. Using 2017 monthly shares as the baseline, Scenario 1 monthly delta change factors (from Table 4.3) are applied with a linear transition from 2018 to 2055 to derive forecast monthly shares and disaggregate annual hydropower targets.

Table 4.3. Monthly seasonality changes (%) in peak electricity demand for the four scenarios in 2042 relative to 2021-2022, extracted from Figure 4.5b.

Month	Scenario 1	Scenario 2	Scenario 3	Scenario 4
Jan	-0.16	-0.11	-0.27	1.70
Feb	-0.16	-0.11	-0.27	1.70
Mar	-0.01	-0.37	-0.84	-0.03
Apr	0.98	0.65	1.46	0.14
May	0.54	0.99	1.45	0.50
Jun	-1.10	-0.95	-1.33	-2.03
Jul	-0.69	-0.77	-1.17	-1.92
Aug	-0.02	-0.35	-0.93	-1.79
Sep	0.75	0.63	0.83	-0.05
Oct	1.05	1.14	1.95	0.19
Nov	-1.26	-0.91	-0.84	-0.36
Dec	0.09	0.14	-0.03	1.95
Sum	0.00	0.00	0.00	0.00

Monthly hydropower targets are disaggregated into daily values using daily proportions recorded in 2017, which is selected as the baseline for the disaggregation process because it represents the most recent year for which complete daily hydropower generation data are available. Each day retains the same share of its month, as it was in 2017, with no future changes applied since the stress-testing analysis is performed at annual and seasonal time scales. Daily totals are allocated to individual stations based on their 2017 contributions, and adjusted for station availability (e.g., Wuskwatim, Limestone, and Keeyask have zero share before their commissioning). Using 2017 as the baseline ensures consistent operations for both hindcast and forecast scenarios.

4.4.3.3 Stress-Testing Scenarios

MB_HydroSim simulates the hydropower generation system under five cases (RH-R, EH-R, EG-F, RG-F, and RH-H) which are target combinations of inflow conditions (RH, EH, EG, and RG) and hydropower scenarios (R, H, and F).

Case RH-R determines the sufficient number of realizations required for each target inflow condition. Following the procedure described in "*4.3.1. Generating Target Inflow Scenarios*", 100

target inflow scenarios (1 inflow condition × 100 realizations) are generated to reproduce the historical inflow condition (RH) and evaluate the hydropower system response to the recorded hydropower target (R). For each candidate sample size, 500 random subsets are drawn from the pool of 100 scenarios.

Case EH-R stress tests the hydropower system in the historical context (1980-2017). Inflow conditions are designed to expand over historical inflow conditions (EH) in both monthly magnitude and variability. MB_HydroSim simulates the hydropower generation for 500 target inflow scenarios (25 inflow conditions × 20 realizations) in response to the recorded hydropower target. System performance for the center point of EH inflow conditions serves as the baseline for stress testing in this case and are identical to those in RH.

Case EG-F stress tests the hydropower system under future contexts (2018-2055). Inflow conditions are designed to expand over the median GCM-driven inflow condition (EG) in both monthly magnitude and variability. MB_HydroSim simulates hydropower generation for 500 target inflow scenarios (25 inflow conditions × 20 realizations) in response to the forecasted (F) hydropower target.

Case RG-F assesses the system response under future conditions with inflow seasonality differing from EG-F. Moreover, RG-F assesses whether the stress testing under EG-F remains applicable when inflow seasonality differs from the median GCM-projected pattern. Inflow conditions are designed to reproduce GCM-driven inflow conditions (RG). MB_HydroSim simulates the hydropower generation for 380 target inflow scenarios (19 inflow conditions × 20 realizations) in response to the forecasted hydropower target.

Case RH-H is a baseline for stress-test evaluations in EG-F and determines hydropower system performance change in RG-F. MB_HydroSim simulates the hydropower generation for 20 target inflow scenarios (1 inflow condition × 20 realizations) in response to the hindcasted (H) hydropower target.

Automated parallel execution (20 runs in parallel) is used to run MB_HydroSim. Hydropower targets are first updated manually by opening the "*.xy*" file in the MODSIM-DSS graphical interface; three versions of MB_HydroSim are prepared corresponding to the R, H, and F hydropower target scenarios for each station. The "*.xy*" file is the main configuration file of a

MODSIM-DSS model and can also be viewed and edited as a standard text file. For each simulation, inflows at all nodes are updated automatically using a Python script that reads and modifies the "*.xy*" file directly. MODSIM-DSS can be executed externally through its accompanying "*.exe*" file, enabling automated model runs. In Python, MODSIM-DSS is executed with a single system call: *subprocess.run([exe-path, xy-path])*. The python code is publicly available in Zenodo by Gozini (2026) and can serve as a useful reference for automating parallel execution of MODSIM-DSS models. Using an AMD Ryzen Threadripper PRO 3975WX (32-core, 3.5 GHz) processor and 512 GB RAM, 500 MB_HydroSim runs for target case EG-F were completed in 8.91 hours.

4.4.4 System Performance Metrics

After simulating hydropower generation for the target cases, system performance is evaluated using three hydropower performance metrics (reliability, vulnerability, and revenue), along with a key system state metric (the frequency of Lake Winnipeg water level excursions outside the preferred operating band).

Reliability is used to evaluate the capability of the hydropower system to meet the hydropower targets. Reliability (*Re*) is unitless, ranges from 0 to 1, and represents the fraction of days on which the system generates at least 95% of the daily hydropower target:

$$Re = \frac{1}{D}\sum_{d=1}^{D} I_d, \qquad I_d = \begin{cases} 1, E_d^{gen} \geq 0.95E_d^{tar} \\ 0, E_d^{gen} < 0.95E_d^{tar} \end{cases} \tag{4.3}$$

Where d (= 1, …., D) indexes days, I is the daily reliability indicator, E^{gen} is the total daily hydropower generation, and E^{tar} is the total daily hydropower target. Reliability is computed at both annual and seasonal scales. For annual reliability, D represents the total number of days in the full period; for seasonal reliability, D represents the total number of days in that season aggregated across all years. Because MB_HydroSim slightly underestimates hydropower generation, the simulated annual reliability for the historical period (1980-2017) is 0.88, reflecting model bias rather than actual system performance.

Vulnerability quantifies the average cumulative hydroelectricity shortfall per failure event. A failure event is defined as a continuous sequence of days during which the hydropower system

does not meet the target ($I_d = 0$). Vulnerability (Vu) is expressed in GWh, with an ideal value of zero, and is defined as:

$$Vu = \frac{1}{K}\sum_{k=1}^{K}\sum_{d=s_k}^{e_k}\left(E_d^{tar} - E_d^{gen}\right) \tag{4.4}$$

where k (= 1, …., K) indexes the failure events, s_k and e_k denote the start and end days of failure event k. Vulnerability is computed at both annual and seasonal scales. For annual vulnerability, all failure events and their associated cumulative energy deficits are aggregated over the full period. For seasonal vulnerability, only the portions of failure events occurring within a given season are considered. Because MB_HydroSim slightly underestimates hydropower generation, the simulated annual vulnerability for the historical period is 17.03 GWh, even though the real system had zero vulnerability during this period (i.e., it generated all recorded hydropower generation).

Hydropower revenue is used as an economic performance metric to stress-test the hydropower system by evaluating the financial implications of meeting the hydropower targets. In this study, the average annual hydropower revenue (AR), expressed in Canadian dollars (CAD), is calculated by accounting for revenue from domestic electricity sales (E^{dom}), revenue from electricity exports (E^{exp}), and the cost of electricity imports (E^{imp}):

$$AR = \frac{1}{Y}\sum_{y=1}^{Y}\left(\left(85.54 \times E_y^{dom}\right) + \left(104 \times E_y^{exp}\right) - \left(111.61 \times E_y^{imp}\right)\right) \tag{4.5}$$

Where y (= 1, …., Y) indexes years, and coefficients represent unit electricity prices (CAD/MWh) in 2023 for domestic sales, exports, and imports, respectively (Manitoba Hydro, 2024). When generation falls short of the hydropower target, the deficit is treated as imported electricity at import cost. Revenue is calculated by separating total generation into domestic and export sales; historically, 12% of annual generation is assumed exported, while future export share declines linearly to about 1.39% (Manitoba Hydro, 2023b), reflecting reduced export opportunities as provincial demand increases. Due to the lack of seasonal export-share information, the economic assessment is conducted only at the annual scale. To simplify the economic stress testing, the effect of inflow conditions on export volumes is not modeled. Moreover, the analysis

focuses on direct hydropower revenue, excluding other operational or administrative expenses. Historical simulations yield an average annual revenue of 2.29 billion CAD, close to Manitoba Hydro (2024) reported annual 2.04 billion CAD (2015-2024). However, the economical stress testing should emphasize relative revenue changes rather than absolute values, because future price structures may change.

Alongside hydropower performance, a key system state in this study is the frequency of days when Lake Winnipeg water levels fall outside the preferred operating band. Lake Winnipeg is the most important control point for regulating water supplied to the Lower Nelson River where most hydropower facilities are installed, making its water level excursions a critical indicator of system stress. The percentage of days (P) outside the licensed operational range, 216.712 m (711 ft) to 217.932 m (715 ft) from Manitoba Hydro (2014), in Lake Winnipeg (LW) is calculated as:

$$P_{LW} = \frac{100}{D}\sum_{d=1}^{D} O_d, \qquad O_d = \begin{cases} 1, WSE_d^{LW} < 216.712 \\ 1, WSE_d^{LW} > 217.932 \\ 0, \quad otherwise \end{cases} \tag{4.6}$$

O is the daily indicator (1 = outside the operating range; 0 = within the range) and WSE is the water surface elevation. P_{LW} is computed at both annual and seasonal scales, analogous to reliability and vulnerability. Based on historical observations, Lake Winnipeg water levels were outside the operating range on 8.43% of days during 1980-2017, all due to an exceedance of the upper limit. MB_HydroSim slightly overestimates this behavior, simulating exceedance of the upper limit on 11.68% of days for the same period.

4.4.5 Annual and Seasonal Heat Maps

Annual and seasonal stress-test heat maps are developed for reliability, vulnerability, and the Lake Winnipeg water level excursion (P_{LW}) for the EH-R and EG-F target cases. Hydropower revenue heat maps are produced for the annual time scale. Since target inflow conditions are defined using 10% increments in monthly magnitude and variability, higher-resolution heat maps (rescaled to 1% increments) are generated by interpolating simulated performance results. Bilinear interpolation is applied, whereby values at intermediate points within each grid cell are estimated using the four surrounding known values. The method performs linear interpolation along both

dimensions, assigning distance-based weights such that closer known points exert greater influence, and computes the result as a weighted average.

Delineation of *success* and *failure* regions on the stress-test heat maps compares the median performance value across 20 realizations relative to the baseline. The resultant reliability, hydropower revenue, and P_{LW} are compared directly to their respective baseline values. Vulnerability, however, is handled differently: vulnerability values for each inflow condition are normalized by subtracting the baseline vulnerability, where negative values indicate improved vulnerability, corresponding to fewer severe failure events. This normalization helps to illustrate the relative reduction in failure severity within a success region.

To estimate the likelihood (%) of success or failure, system performance results from all 20 realizations of each target inflow condition are compared against all 20 realizations of the corresponding baseline condition. Following the Intergovernmental Panel on Climate Change (IPCC) likelihood framework (Mastrandrea et al., 2010), the heat maps include contours representing *likely* (66-100% probability), *very likely* (90-100% probability), and *virtually certain* (99-100% probability) outcomes.

4.5 Results and Discussion

This section presents and discusses results for hydropower and system state performance metrics associated with each target case. It begins with an uncertainty analysis associated with the use of target inflow scenarios, followed by the hydropower system evaluation under stress-testing scenarios in annual and seasonal scale. Subsequently, it demonstrates how stress-testing results are used to hindcast the hydropower system performance during a severe historical drought in Manitoba. Key findings from the application are synthesized in two tables in the Supplementary Material (Table S6 and Table S7) to provide a clearer overall understanding of the results.

4.5.1 Uncertainty Estimation, Case RH-R

Inflow scenarios are stochastically generated, keeping statistical characteristics of their distribution (mean and/or variance) at the target level. According to Figure 4.6, a sample size of 20 realizations for each target inflow scenario is sufficient to capture more than 90% of the variation in annual hydropower and system state performance metrics represented by an ensemble

of 100 target inflow scenarios in RH-R. For all four metrics, the normalized IQR exceeds the 0.90 threshold at this sample size.

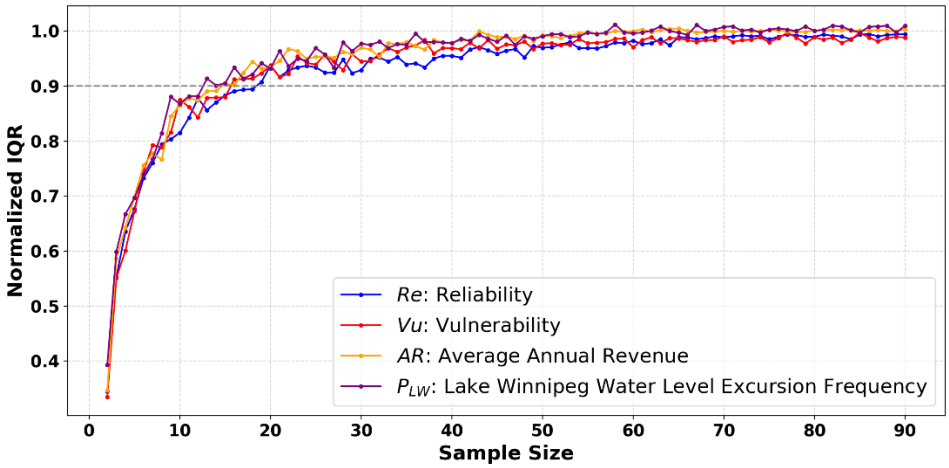


Figure 4.6. Normalized interquartile range (IQR) of hydropower performance and system state metrics as a function of sample size in case RH-R.

Figure 4.6 also highlights that uncertainty levels differ across the four system performance metrics. Reliability exhibits the greatest uncertainty and the slowest convergence (i.e., getting above 0.9 normalized IQR), reflecting its sensitivity to day-to-day inflow variation and its threshold-based definition. Vulnerability converges slightly faster because it depends on the magnitude of deficits on failure events rather than on binary threshold exceedance. In contrast, P_{LW} and hydropower revenue show the smallest uncertainty and the fastest convergence, which is anticipated as P_{LW} is governed by Lake Winnipeg storage dynamics that dampen short-term inflow fluctuations, while revenue is aggregated annually and smooths daily variation, reducing sensitivity to individual inflow realizations.

4.5.2 Annual Evaluation, Case EH-R vs. EG-F

The evaluation of the hydropower system under historical (EH-R) and future (EG-F) suite of scenarios determines how the system responds to target changes in the magnitude, variation, and seasonality of inflow and projected future electricity demand (Figure 4.7). Compared with the historical inflow condition (black squares), the median GCM-driven inflow condition (orange squares) exhibits increasing monthly inflow magnitude from November to April, and increasing variation in inflow across nearly all months in the future. In addition, annual hydropower target increases from historical to future conditions.

Because hindcasted targets do not dynamically adjust to historical inflow, baseline hydropower performance degrades from EH-R to EG-F: reliability declines from 0.88 to 0.55, vulnerability increases from 25.9 to 65.8 GWh, and annual revenue decreases from 2.23 to 2.10 billion CAD. Baseline P_{LW} remains unchanged at 3.6% because lake level excursions depend solely on the baseline inflow condition. This baseline mismatch does not impact system evaluation under EH-R and EG-F, because all metrics are compared against their respective baseline within each target case.

According to nearly vertical contour lines in in Figure 4.7, the system performance is driven primarily by changes in the magnitude of inflow (horizontal axis), while changes in variation of inflow (vertical axis) play a secondary role. This result indicates that reservoir storage and coordinated basin-wide operations effectively buffer short-term inflow variability at the annual time scale. However, sensitivity to inflow variability emerges near critical thresholds. For instance, under a constant monthly inflow magnitude change of 0% in EH-R (Figure 4.7a-h), increasing inflow variation moves the system from success to failure across all evaluated metrics. This implies that when inflow magnitude is near the critical threshold, the system becomes sensitive to temporal fluctuations of water availability, such that increased inflow variability generates system failure even though annual inflow volume and seasonal timing remain unchanged.

Under EH-R (Figure 4.7a-d), the heat map scale bars across all four metrics show that failure regions exhibit substantially larger and more proportional performance degradation than the corresponding improvements observed within success regions. This behavior indicates that the hydropower system responds strongly and consistently to changing inflow magnitude, becoming increasingly stressed as magnitude declines, and yielding proportionally smaller gains as magnitude increases. This behavior highlights two key characteristics of the Manitoba hydropower system:

1. **Asymmetric hydropower system response** (Figure 4.7a-c): The system has historically been well tuned to the observed inflow regime to maximize hydropower production. Consequently, reductions in inflow magnitude result in substantial decline in system reliability, increasing vulnerability, and loss in average annual revenue for the given hydropower targets, while additional inflows yield comparatively modest performance gains. This asymmetry arises because, in Manitoba, hydropower generation depends

primarily on streamflow rather than hydraulic head, given the limited storage capacity of the hydropower stations relative to the volume of water passing through the system (Gozini et al., 2026a). As flows increase, spill also increases, thereby limiting proportional gains in power generation.

2. **Limited water storage capacity** (Figure 4.7d): The system has a limited ability to store water at its primary storage and control point, Lake Winnipeg, and therefore cannot absorb large inflow surpluses without exceeding upper operating thresholds. This reflects constrained long-term storage capacity within the river-reservoir system, which in turn limits the ability to retain surplus water under favorable conditions for hydropower generation.

Under EG-F (Figure 4.7e-h), hydropower reliability and revenue exhibit proportionally larger gains with increasing inflow magnitude; however, the overall response pattern remains consistent with EH-R for vulnerability and the frequency of Lake Winnipeg water level excursions. The implications of such changes are explained in the following for each system performance metric.

4.5.2.1 Hydropower Reliability

Hydropower reliability is governed primarily by changes in inflow magnitude, with success and failure separated by a nearly vertical baseline that ranges from -3% to +3% change in inflow magnitude while inflow variation changes ranges respectively from -20% to +20%, see Figure 4.7a for EH-R. This sharp baseline indicates that reliability responds rapidly to even small shifts in water availability, while reservoir storage and coordinated basin operations effectively dampen the influence of monthly inflow variation except near critical limits.

Under future conditions (Figure 4.7e), overall reliability improves despite higher hydropower targets and increased inflow variability. The success region expands relative to historical conditions (Figure 4.7a), reflecting projected increases in inflow magnitude and, critically, the added generating capacity from the Keeyask station. Improvements in reliability are larger in magnitude than corresponding degradations, demonstrating that capacity expansion enhances system robustness. Therefore, it is concluded that additional infrastructure can materially improve reliability under future climate conditions, provided annual inflow magnitude does not decline beyond the analyzed threshold levels.

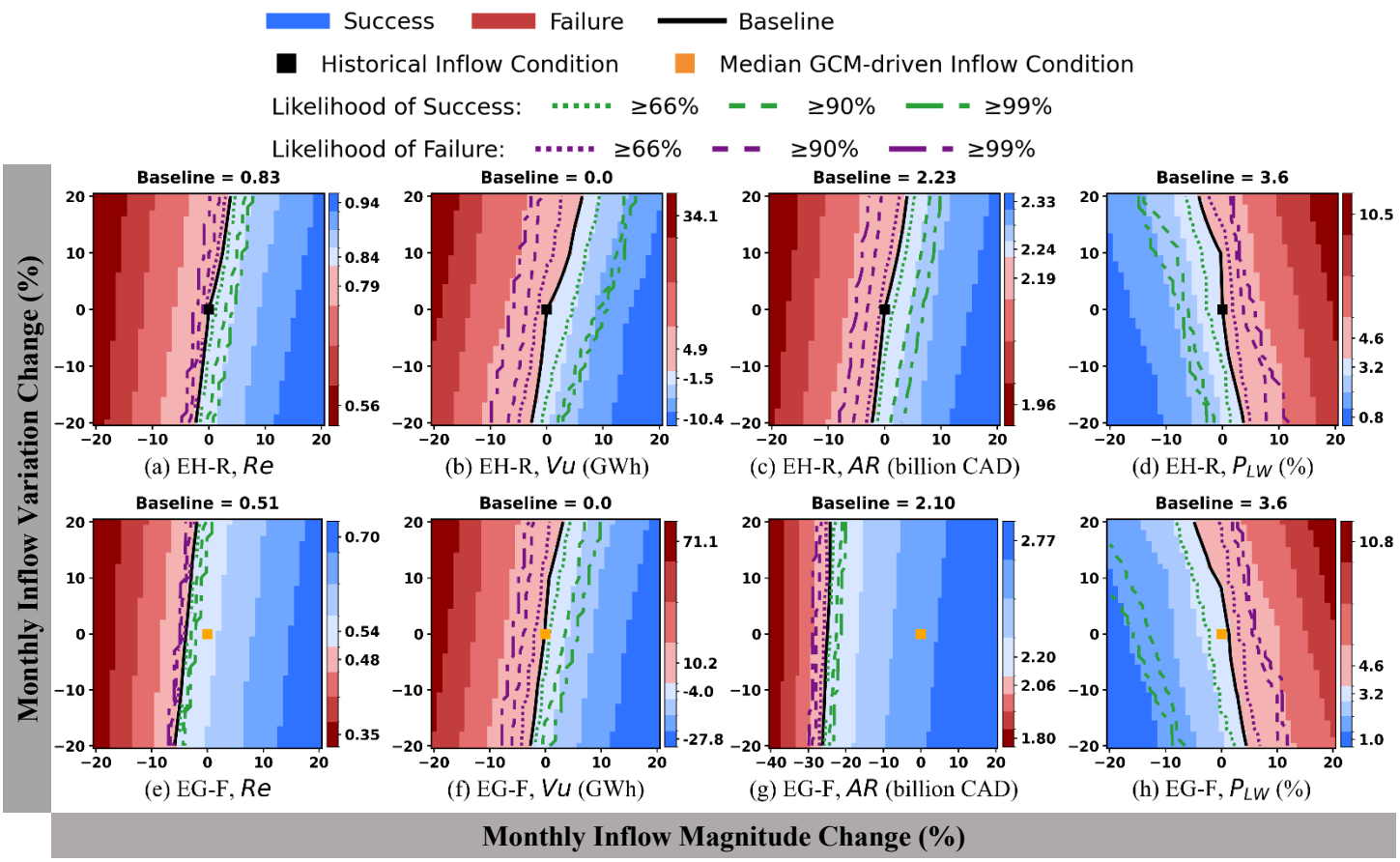


Figure 4.7. Annual-scale stress-testing heat maps for the hydropower (*Re*: Reliability, *Vu*: Vulnerability, *AR*: Average Annual Revenue) and system state (P_{LW}: Lake Winnipeg water level excursion) metrics under target case EH-R (a-d) and EG-F (e-h). Blue regions indicate success (improved performance relative to the baseline), while red regions indicate failure (reduced performance). The solid black contour represents the baseline threshold separating success from failure. For EH-R, the baseline is the center point equivalent to target case RH-R; for EG-F, the baseline is the target case RH-H. Baseline vulnerability is normalized to zero from its original value of 25.9 GWh and 65.75 GWh for EH-R and EG-F, respectively.

4.5.2.2 Hydropower Vulnerability

Hydropower vulnerability exhibits a stronger sensitivity to inflow variation than reliability, revealing a key distinction between the two system performance metrics (compare Figure 4.7a and b). While higher inflow magnitude reduces the severity of hydroelectricity shortfalls, increased variability erodes these gains, particularly in the success region. As a result, vulnerability improves more slowly under surplus conditions than it degrades under deficits, highlighting an inherent asymmetry in system response to hydrologic change.

Under future conditions, the influence of inflow variability within the success region is reduced, and vulnerability thresholds shift toward smaller required increases in inflow magnitude (compare

Figure 4.7e and f). This indicates that the addition of Keeyask improves the ability of the system to translate higher inflows into reduced failure severity. However, overall system stress remains similar under historical and future conditions because increases in inflow magnitude are largely offset by higher variability and higher demand. The system remains more sensitive to inflow shortages than surpluses, underscoring the need for adaptive operational strategies in addition to infrastructure expansion.

4.5.2.3 Hydropower Revenue

Under historical conditions, average annual revenue closely mirrors reliability, confirming that both metrics are primarily controlled by the system's ability to meet hydropower targets through sufficient inflow (compare Figure 4.7c and a). Revenue losses resulting from inflow reductions are substantially larger than gains achieved under inflow increases, reinforcing the asymmetric financial risk associated with hydrologic deficits.

Under future conditions (Figure 4.7g), revenue improves markedly and does not exhibit stress within the tested inflow range. The median future inflow condition *virtually certain* lies within the success region, yielding substantial revenue gains driven by higher targets and increased generation capacity from Keeyask. These results demonstrate strong upside potential under future conditions; however, the assumption of constant imported-energy costs may understate financial risk if import capacity becomes constrained, leading to higher import costs under ongoing energy system transitions.

4.5.2.4 Lake Winnipeg Water Level Excursion

Lake Winnipeg water level excursion responds fundamentally differently from hydropower performance metrics because it is driven by high-inflow extremes rather than deficits. Reduced inflow magnitude consistently lowers excursion risk, while relatively small inflow increases sharply elevate the frequency of excursions, reflecting limited system capacity to absorb surplus water (see Figure 4.7d and h). This creates a broad safety margin on the dry side but a rapid transition to failure under wetter conditions.

Under both historical and future conditions, improvements in hydropower reliability and vulnerability coincides with the onset of increased water level excursion frequency, revealing a benefit-stability trade-off between energy performance and lake-level management under wet

conditions. However, the severity and consequences of these excursions, particularly those related to the potential for flooding, require further investigation to assess the full implications of such changes. Under future conditions (Figure 4.7h), the stress is slightly reduced overall due to offsetting seasonal inflow changes, but annual-scale analysis masks these dynamics. Because the annual-scale patterns for both hydropower and system state metrics obscure important seasonal behaviors, the next section focuses on seasonal stress testing.

4.5.3 Seasonal Evaluation, Case EH-R vs. EG-F

The seasonal distribution of the hydropower system performance is evaluated under historical (EH-R) and future (EG-F) suite of scenarios. The seasons are spring (March-May), summer (June-August), autumn (September-November), and winter (December-February). Historically (black squares in Figure 4.8, Figure 4.9, and Figure 4.10), summer and spring contribute the largest fractions of annual total inflow to the system, whereas autumn and winter receive less. The highest electricity demand historically occurs from November to March, corresponding to late-autumn and winter. Therefore, the water system stores spring and summer inflow for autumn and winter energy supply (see Figure 2b in Gozini et al. (2026a)).

In the future (orange squares in Figure 4.8, Figure 4.9, and Figure 4.10), the median GCM-driven inflow condition exhibits increase in monthly inflow magnitude during winter, spring and autumn, but decrease in summer, while inflow variation increases across all seasons (based on Figure 4.4). At the same time, overall hydropower targets rise in every season, though their proportional share of annual generation changes under Scenario 1 (based on Table 4.3): winter and summer shares decrease, whereas spring and autumn shares increase. These combined changes in seasonal inflow and hydropower target shape the relative stress that could be experienced by each season under future conditions. The following seasonal evaluation of the system for EG-F are based on Scenario 1 of monthly proportional hydropower targets and therefore represent conservative outcomes that may become more pronounced under Scenarios 2 or 3.

Seasonal evaluation of the system performance reemphasizes that monthly inflow magnitude remains the dominant driver of system performance in all seasons, see nearly vertical contour lines in Figure 4.8, Figure 4.9, and Figure 4.10.

4.5.3.1 Hydropower Reliability

Hydropower reliability shows a relatively uniform seasonal stress pattern under historical conditions, with comparable portions of the exposure space falling within the failure region across winter, spring, summer, and autumn (Figure 4.8a-d). Under future conditions, however, seasonal stress becomes more uneven (Figure 4.8e-h). Relative to historical conditions, the system is expected to be more stressed in winter, less stressed in spring, and similarly stressed in summer and autumn.

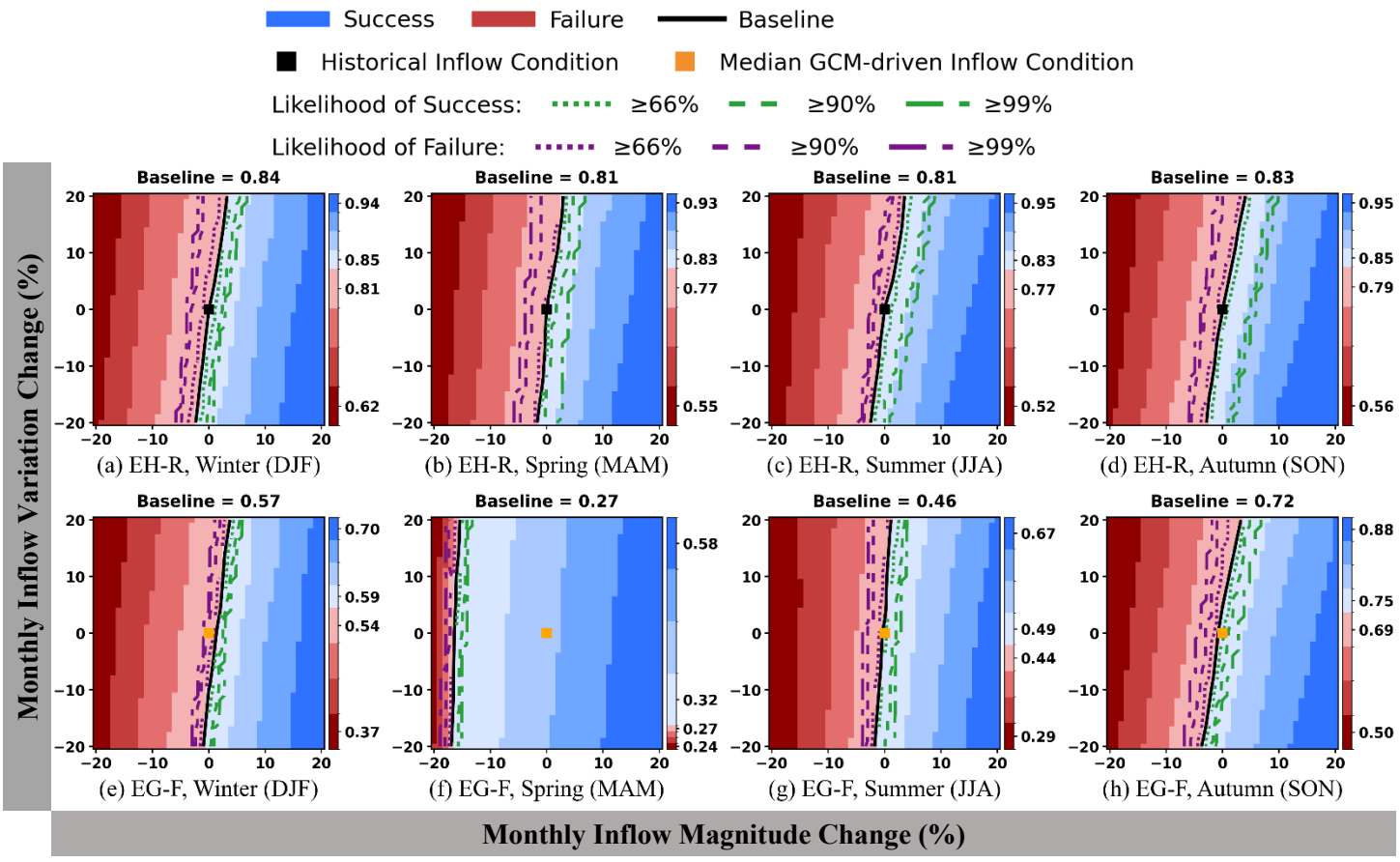


Figure 4.8. Seasonal-scale stress-testing heat maps for the hydropower reliability under target case EH-R (a-d) and EG-F (e-h). Blue regions indicate success (improved performance relative to the baseline), while red regions indicate failure (reduced performance). The solid black contour represents the baseline threshold separating success from failure. The solid black contour marks the baseline threshold separating success from failure. For EH-R (a-c), the baseline is the center point equivalent to target case RH-R; for EG-F (d-f), the baseline is the target case RH-H.

The increase in winter stress occurs because projected winter inflow gains are insufficient to offset higher future winter hydropower targets and the carry-over effects of reduced summer inflows. Although the seasonal redistribution of demand reduces the winter share of the annual

target, the absolute winter target still increases, requiring an additional inflow magnitude increase beyond the median GCM projection to maintain historical stress levels. Spring provides the clearest reliability improvement under future conditions, as the median GCM-driven inflow condition lies within the *virtually certain* success region. This reflects that strong projected increase in spring inflows sufficiently meet higher hydropower targets in future. In contrast, summer and autumn reliability stress is expected to remain broadly similar to historical conditions.

Under future conditions, the addition of Keeyask enhances the system ability to convert high-inflow conditions into reliability gains across all seasons, particularly in spring. However, winter reliability degradation is more severe under low-inflow conditions, indicating that higher hydropower targets increase the system susceptibility to winter inflow shortages.

4.5.3.2 Hydropower Vulnerability

Under historical conditions (Figure 4.9a-d), seasonal hydropower vulnerability shows a broadly similar level of stress across winter, spring, summer, and autumn, but the severity of vulnerability responses to inflow changes varies substantially by season. Summer experiences the largest vulnerability degradation under reduced inflows, reflecting the system reliance on summer storage to meet critical autumn and winter electricity demand. Conversely, increased summer inflows result in the largest vulnerability improvement as surplus water can be directly converted into additional generation in this season. Winter induces the smallest vulnerability degradation despite being the lowest-flow season, because reservoir operations prioritize firm winter supply and are designed to limit deficit severity in this season. Spring and autumn fall between these extremes, with moderate vulnerability degradation under reduced inflow.

Under future conditions (Figure 4.9e-h), seasonal vulnerability stress is expected to become uneven. The system is expected to be less stressed in spring, similarly stressed in winter, and more stressed in summer and autumn relative to historical conditions. Spring provides the strongest future vulnerability improvement, supporting surplus hydropower production and potential export benefits that may help reduce import costs in subsequent seasons. The system is expected to remain at a similar level of stress level during winter, because projected winter inflow increases, together with stored spring and summer water, nearly offset higher winter hydropower targets. However, the severity of winter hydroelectricity shortfalls is expected to increase under low-inflow conditions. The greatest increase in future vulnerability occurs in summer and autumn. Reduced

summer inflows place the median GCM-driven summer condition within the *virtually certain* failure region and limit both immediate generation and water storage for subsequent seasons. These reductions also propagate into autumn, where the median GCM-driven condition is *very likely* to remain within the failure region.

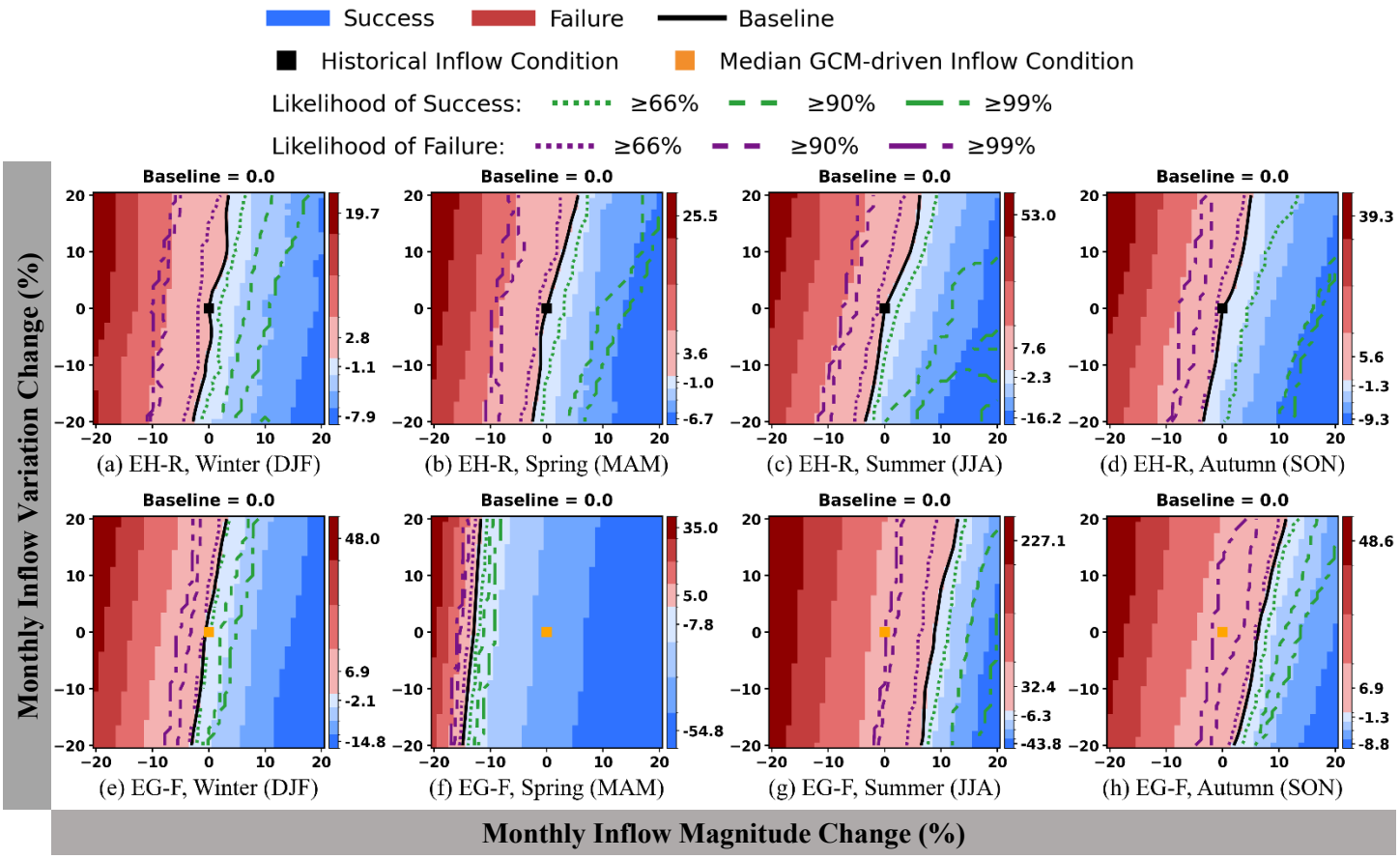


Figure 4.9. Seasonal-scale stress-testing heat maps for hydropower vulnerability (GWh) under target case EH-R (a-d) and EG-F (e-h). Blue regions indicate success (improved performance relative to the baseline), while red regions indicate failure (reduced performance). The solid black contour represents the baseline threshold separating success from failure. The solid black contour marks the baseline threshold separating success from failure. For EH-R (a-c), the baseline is the center point equivalent to target case RH-R; for EG-F (d-f), the baseline is the target case RH-H.

4.5.3.3 Lake Winnipeg Water Level Excursion

Under historical conditions (Figure 4.10a-d), the system is more stressed during summer in terms of water level excursion frequency. This reflects the combined effect of relatively high summer inflows and reservoir operations that prioritize water storage for autumn and winter hydropower demand, which elevates lake levels and increases the frequency of exceeding the upper operating limit. Winter and autumn show lower overall excursion frequencies than summer,

but they are more sensitive to inflow variability: autumn because lake levels remain elevated following summer storage, and winter because ice-management constraints limit operational flexibility. During spring, the system is less stressed than in summer because snowmelt inflows are partly used to refill Lake Winnipeg after winter drawdown.

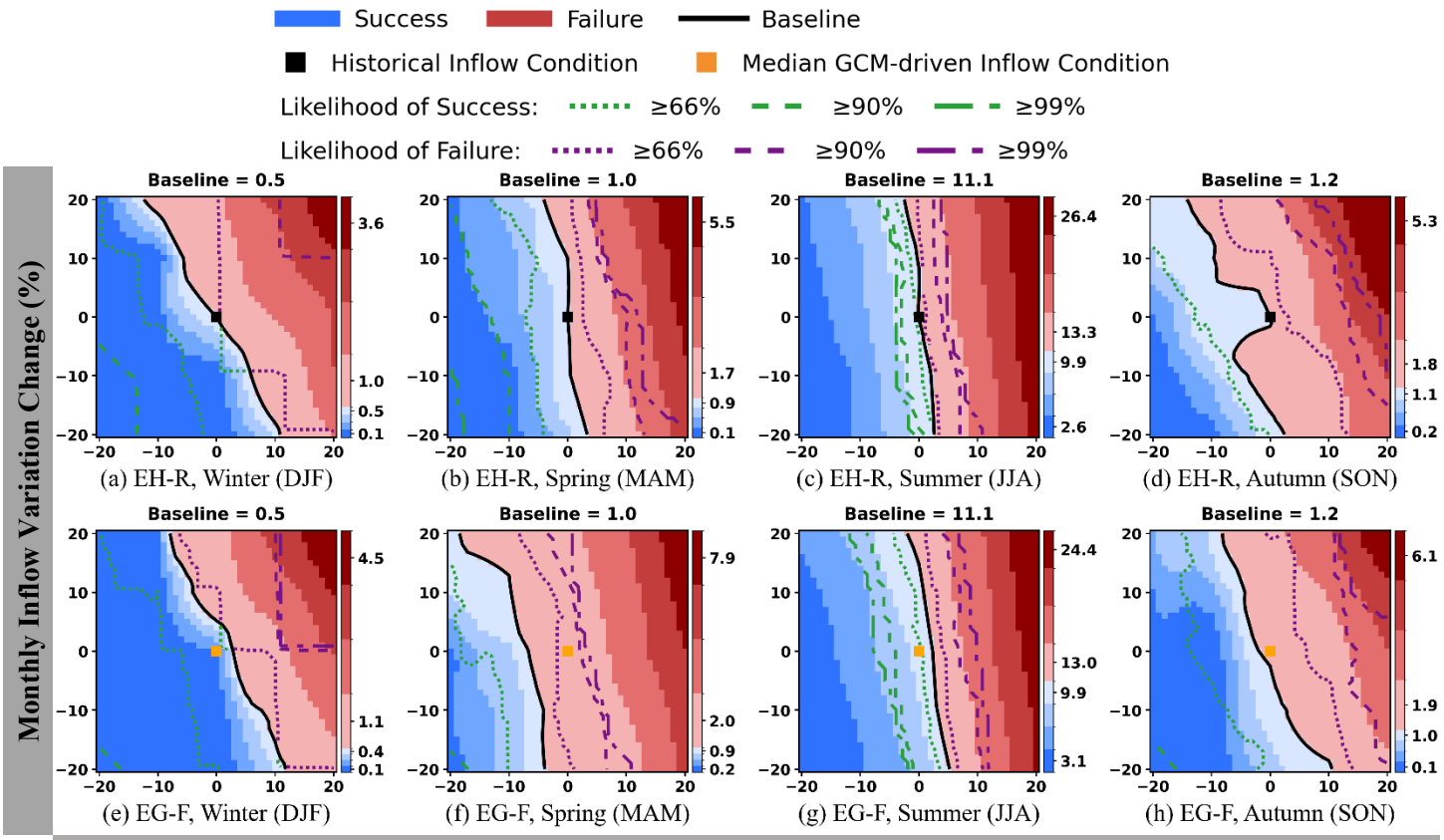


Figure 4.10. Seasonal-scale stress-testing heat maps for Lake Winnipeg water level excursion (P_{LW}, %) under target case EH-R (a-d) and EG-F (e-h). Blue regions indicate success (improved performance relative to the baseline), while red regions indicate failure (reduced performance). The solid black contour represents the baseline threshold separating success from failure. The solid black contour marks the baseline threshold separating success from failure. For EH-R (a-c), the baseline is the center point equivalent to target case RH-R; for EG-F (d-f), the baseline is the target case RH-H.

Under future conditions (Figure 4.10e-h), the seasonal distribution of system stress is expected to shift relative to historical conditions. The system is expected to become less stressed during winter, summer, and autumn, but more stressed during spring. The increase stress in spring occurs because higher projected spring inflows raise lake levels and increase the frequency of upper-level excursions. This suggests that the benefit-stability trade-off identified in the annual analysis is expected to be concentrated during spring. Summer is expected to remain the season with the

highest excursion frequency; however, overall system stress during summer and autumn is expected to decrease relative to historical conditions because projected summer inflows are lower.

4.5.4 Inflow Seasonality Change, Case RG-F vs. EG-F

This section examines how changes in inflow seasonality, beyond changes in annual inflow magnitude, influence hydropower system performance under GCM-projected inflow scenarios in RG-F. It also compares RG-F results with those inferred from the stress-testing space centered on the median GCM seasonality in EG-F, addressing a key question for stress-testing practice: to what extent do conclusions drawn from EG-based annual stress tests remain valid when the system is exposed to the full diversity of GCM-projected seasonal inflow patterns?

Under RG-F, average annual revenue is *virtually certain* to remain within the success region for all GCM projections (Table 4.4), indicating that increased installed capacity largely offsets uncertainty in future inflows. As a result, system sensitivity to inflow seasonality is evaluated primarily through changes in reliability and vulnerability, which provide a clearer signal of hydrologic stress.

4.5.4.1 System response to GCM-projected inflow seasonality

Across the GCM ensemble, RG-F results (Table 4.4) show that annual inflow magnitude change is the dominant driver of annual-scale hydropower performance, while seasonal inflow changes in winter play an important secondary role, and summer and autumn inflow changes exert a tertiary influence that can further amplify or mitigate system stress. When annual inflows increase beyond a modest threshold (+2.74%; as in A10-R41), both reliability and vulnerability remain in the success region across a wide range of seasonal patterns. Even with a slight annual inflow magnitude increase (+0.77%; as in the median), a modest winter inflow increase (+5.6%; as in the median) is sufficient to keep the system within the success region. For larger annual increases (+8.71%; as in GF3-R41) success becomes *virtually certain*. These outcomes occur regardless of the seasonal pattern of inflow variation (see seasonal patterns 1 to 7 in Table S5).

Under RG-F, at least one performance metric shifts into failure when annual inflow magnitude decreases. However, a slight annual inflow magnitude decrease (-0.57%; as in CE2-R41) combined with a relatively large increase in winter inflow magnitude (11.53%; as in CE2-R41) can keep the hydropower system within the annual success region. The poorest outcomes occur

for scenarios combining large annual inflow decreases with substantial seasonal reductions, particularly in winter and, to a lesser extent, summer and autumn (see IAL-R41 and MIE-R81 in Table 4.4). These outcomes occur regardless of the seasonal pattern of inflow variation (see seasonal patterns 9 to 15 in Table S5).

Table 4.4. Annual hydropower performance metrics (median of 20 realizations), along with their likelihood bands and baseline values, for each GCM-driven inflow condition in RG-F compared against extracted values from EG-F. Extracted EG-F values are based on mapping each GCM-driven inflow condition relative to the median projection onto the EG-F annual stress-testing heat maps (in Figure 4.7e-g).

GCM ID	Inflow Magnitude Change (%)					Average Annual Revenue (billion CAD)		Reliability		Vulnerability (GWh)	
	Annual	Seasonal				RG-F	EG-F	RG-F	EG-F	RG-F	EG-F
MR3-R81	23.34	21.75	21.31	27.03	21.75	2.81	2.81	0.67	0.68	45.13	42.47
MR3-R41	13.92	12.98	14.41	14.01	14.22	2.77	2.76	0.65	0.65	46.88	46.67
A13-R81	12.40	14.50	17.35	8.09	9.22	2.77	2.79	0.64	0.67	45.50	41.67
A13-R41	10.88	7.64	12.91	14.43	6.73	2.76	2.70	0.65	0.61	47.49	55.63
MI5-R81	9.67	11.05	8.81	6.73	13.09	2.70	2.70	0.59	0.61	55.32	55.22
A10-R81	9.35	16.59	17.25	3.46	2.01	2.66	2.65	0.55	0.58	58.37	63.18
GF3-R41	8.71	8.82	10.50	12.93	1.27	2.75	2.73	0.64	0.62	47.67	50.17
CMS-R81	6.84	9.07	12.10	4.1	2.09	2.70	2.62	0.60	0.56	54.58	67.91
A10-R41	2.74	5.59	3.79	1.06	1.08	2.65	2.64	0.55	0.56	61.11	61.83
Median	0.77	5.59	0.92	-0.19	0.29	2.61	2.61	0.54	0.54	65.35	65.35
INM-R41	0.77	2.47	0.92	-0.19	0.29	2.59	2.51	0.52	0.50	70.06	83.18
CE2-R41	-0.57	11.53	0.12	-5.83	-4.33	2.64	2.61	0.56	0.55	60.11	64.22
IAL-R81	-1.98	-1.73	-0.60	-3.64	-1.82	2.55	2.58	0.50	0.53	73.49	70.69
CN5-R41	-3.09	-1.26	-4.56	-5.15	-0.07	2.61	2.55	0.54	0.51	64.27	74.42
MIC-R81	-4.99	3.84	0.91	-13.35	-8.53	2.56	2.51	0.50	0.49	68.65	81.08
CMM-R41	-8.71	-5.87	-5.98	-12.55	-9.79	2.56	2.50	0.52	0.47	69.09	80.16
NOE-R41	-11.57	-6.39	-7.25	-15.56	-15.95	2.42	2.35	0.44	0.41	89.45	110.99
MI5-R41	-12.73	-10.91	-8.61	-17.05	-14.15	2.42	2.39	0.43	0.42	93.85	100.58
IAL-R41	-15.77	-14.29	-13.95	-17.71	-16.85	2.36	2.35	0.40	0.39	103.23	106.78
MIE-R81	-17.22	-3.25	-13.98	-26.29	-20.33	2.35	2.24	0.41	0.35	101.91	133.68
Baseline	0	0	0	0	0	2.10		0.51		65.75	

Success				Failure			
>=99%	>=90%	>=66%	<66%	>=99%	>=90%	>=66%	<66%

4.5.4.2 Consistency and divergence between EG-F and RG-F

In terms of metric values reported in Table 4.4, extracted EG-F consistently indicate lower revenue and reliability and higher vulnerability than those obtained under RG-F, reflecting a conservative bias in the EG-based estimates.

At the level of success/failure classification and associated likelihoods, EG-F and RG-F produce consistent conclusions when annual inflow magnitude changes are large. Under strongly wetter (> +12.4%; as in A13-R81) or drier (< -11.57%; as in NOE-R41) conditions, EG-based

stress-test results remain feasible even when inflow seasonality varies substantially across GCMs. In contrast, discrepancies between EG-F and RG-F arise primarily for moderate annual inflow changes (+6.84% in CMS-R81 to -8.71% in CMM-R41), where system performance lies near the success-failure boundary. In this regime, differences in seasonal inflow structure can shift system behavior in ways that are not explicitly represented in EG-F.

4.5.5 The Dirty Thirties Stress Test

Manitoba experienced a prolonged multi-year drought during the 1930s (1929- 1942), with the most severe year occurring in 1940 (Government of Manitoba, 2025c), which is considered the "drought of record" for stress testing water allocation in Manitoba. Due to its widespread dust storms, this period is referred to as the "The Dirty Thirties" across the Canadian prairie region. Over this 14-year period of drought, the annual inflow magnitude was approximately 20.48% lower than the 1980-2017 (estimated from Figure A1.11 in Appendix 1 of Manitoba Hydro (2023a)). A -20.48% reduction in annual inflow magnitude represents a large and clearly defined shift in system inflow, and therefore can be mapped onto the annual stress-test heat map under EH-R, Figure 4.7. Based on this mapping, the Dirty Thirties drought corresponds to an average annual revenue of 1.96 billion CAD, representing a roughly 12% decrease relative to the 1980-2017 baseline, with *virtually certain* likelihood. This inflow deficit places the system into the *virtually certain* failure region of system reliability and vulnerability; however, the degree of degradation in these metrics cannot be quantified because they are calculated over a 38-year synthetic realization, whereas this drought spans only 14 years. If these metrics are instead expressed as average annual values, like revenue, events of any duration can be consistently mapped onto the stress-testing heat maps.

4.6 Conclusions, Limitations, and Future Work

This study presents a stress-testing framework to evaluate hydropower system performance under deep uncertainty in monthly inflow magnitude and variability, together with changes in inflow seasonality and electricity demand. The framework systematically links hydrologic uncertainty to the decision-relevant outcomes by identifying the dominant system performance drivers, critical thresholds at which undesired system performance emerges, the likelihood of desired and undesired performance outcomes across the stress-testing space, and the severity of

associated performance changes and their operational implications. In addition, the framework enables comparison of projected future system stress with historical conditions, identifying seasons where the system becomes more or less stressed, and evaluation of how alternative inflow seasonality patterns alter system response.

Application to the Manitoba hydropower system demonstrates the framework ability to diagnose the system behavior across both annual and seasonal scales using hydropower reliability, vulnerability, revenue, and Lake Winnipeg water level excursions. The framework successfully captures system response under the historically extreme drought, demonstrating how stress-testing results can be used to assess system performance under untested extreme inflow conditions. Although demonstrated for hydropower system in Manitoba, the framework is readily transferable to other hydropower systems, as well as other water resource systems through redefinition of performance objectives and thresholds, enabling assessment of outcomes such as flood risk, irrigation reliability, or water-supply security.

Beyond the annual and seasonal scales assessed in this study, the framework can be readily applied at the monthly scale in future work. Because hydropower targets, inflow timing, and operational constraints vary month-to-month, a monthly implementation would enable precise identification of the periods in which the system becomes most vulnerable and support monthly operational adjustments. The method can also be spatially refined to focus on individual stations or sub-systems. For example, in Manitoba, hydropower stations within Sub-system 2 may experience localized stress under a particular inflow condition, while regulation of Lake Winnipeg may buffer these impacts and prevent stress from propagating to Sub-system 3, where most provincial hydropower capacity resides. Such a combined temporal-spatial extension would enable a more nuanced diagnosis of localized and system level stress dynamics.

The framework provides the flexible analytical basis for developing adaptive reservoir operation and hydropower target. By identifying the inflow conditions under which system performance deteriorates, coupling stress testing with optimization in future work would allow operators to evaluate adaptive strategies such as modified drawdown schedules, seasonal or monthly target adjustments, and coordinated reservoir releases. Because the framework quantifies both failure likelihood and failure severity, adaptation policies can be developed within a risk-

informed decision-making context, linking specific operational actions to different regions of the failure space.

One limitation of the present study lies in the simplified treatment of lake level excursions. While excursions beyond preferred operational ranges are identified, the full severity and downstream consequences, particularly those associated with flooding impacts, are not explicitly quantified. Future work should integrate explicit lake-level impact functions and flood-damage relationships within the stress-testing framework. Such integration would allow formal evaluation of interacting risks and enable decision-makers to assess whether temporary reductions in hydropower production could mitigate elevated flood risk under extreme inflow conditions.

Ice conditions impose strong constraints on channel conveyance during winter (e.g., East, West, and South Bay Channels), yet future ice dynamics are not explicitly simulated in this study. Under the same ensemble of GCMs used in this study, Gozini et al. (2023) and Lees (2022) project shorter and warmer ice seasons that increase cumulative winter outflows and create opportunities for additional winter hydropower generation. Accordingly, the winter hydropower performance reported in this study is conservative. Future work can further strengthen the framework by incorporating ice-impact simulations, enabling explicit assessment of how climate-driven changes in ice formation and breakup influence winter hydropower generation and seasonal stress-testing outcomes. Tools developed by Gozini et al. (2023) and Lees et al. (2023) already allow simulation of ice impacts on channel conveyance using GCM-based temperature projections.

Finally, the economic analysis relies on fixed 2024 electricity prices and costs, representing a structural simplification of electricity market dynamics for the Manitoba hydropower system. Because hydropower performance interacts closely with electricity market, future integration of the stress-testing framework with energy system models would enable dynamic estimation of hydropower targets, the system reliance on complementary generation sources, and real-time import-export pricing and decisions, all shaped by inflow conditions. Such coupling would allow explicit assessment of how inflow conditions propagate through electricity markets, thereby strengthening analysis of the water-energy nexus under inflow uncertainty. It would also improve the realism of economic impact assessments and enable seasonal revenue analysis once seasonal export data become available. Furthermore, integration with energy models would facilitate stress testing under elevated hydropower target scenarios (e.g., exceeding 37,000 GWh per year),

allowing identification of the maximum hydropower contribution that can be delivered before inducing unacceptable stress on the water system.

4.7 Availability of Data and Materials

The daily flow data for the hydrometric stations are publicly available from the Environment and Natural Resources website (https://wateroffice.ec.gc.ca/index_e.html). GCM-driven streamflow scenarios are generated by Stadnyk et al. (2021), with details on data access and availability provided therein. Daily recorded hydropower generation data are provided by Manitoba Hydro and are subject to access restrictions; requests for these data must be made directly to Manitoba Hydro. Information on electricity demand projections is available in Manitoba Hydro (2023a), and the methodology used to generate forecasted and hindcasted hydropower targets is fully described in this manuscript. Target inflow scenarios are generated using the framework developed by Gozini et al. (2026b), for which the Python implementation is publicly available on Zenodo (Gozini et al., 2025). The hydropower simulation model MB_HydroSim is developed and described by Gozini et al. (2026a); however, full access to the model is restricted due to data and licensing agreements with Manitoba Hydro. The python code for automating parallel execution of MODSIM-DSS models is preserved in Zenodo by Gozini (2026).

CHAPTER 5. RESEARCH SUMMARY, CONTRIBUTION, SIGNIFICANCE, LIMITATIONS, AND RECOMMENDATIONS FOR FUTURE WORK

5.1 Research Summary and Findings

In support of Objective 1 (*Developing a Hydropower System Simulation Tool*), this research developed MB_HydroSim, an integrated, large-scale, and operation-based hydropower simulation model in Manitoba. The model represents the full transboundary river-reservoir system, explicitly incorporates all hydropower stations and key upstream inflow control points, and simulates coordinated system operations using operational rules derived from formal guidelines and observed system behavior. Model evaluation results show that MB_HydroSim successfully reproduces historical system dynamics at a daily time step, with strong agreement between simulated and observed water levels, outflows, and hydropower generation over the 1980-2017 period. The results also confirm that MB_HydroSim effectively captures the operational complexity of Manitoba hydropower system and provides a reliable, system-wide representation suitable for subsequent climate change impact assessment and planning analyses.

In support of Objective 2 (*Developing a Streamflow Scenario Generator*), this research developed a target-based synthetic streamflow generation framework that enables direct control of streamflow properties in real space. Evaluation results demonstrate that the framework successfully generates multisite synthetic inflow scenarios that precisely match target monthly streamflow magnitude, variability, and seasonality, while maintaining physical and mathematical feasibility. The results further show that this approach enables uniform and interpretable sampling of the exposure space for stress-testing applications. Statistical testing results confirm that the framework preserves distributional, temporal, and spatial dependence structures under stationary conditions, and appropriately modifies these structures under non-stationary conditions, demonstrating their ability to generate statistically credible inflow scenarios suitable for large-scale bottom-up system analyses in a computationally efficient manner.

In support of Objective 3 (*Developing a Stress-testing Framework for Climate Change Impact Assessment*), this research applied a bottom-up, stress-testing climate change impact assessment

framework to evaluate hydropower system behavior in Manitoba under inflow-condition uncertainty and increasing electricity demand. The framework yields a more comprehensive and decision-relevant characterization of climate change impacts compared to conventional top-down, GCM-driven approaches.

The key high-level findings for the Manitoba hydropower system are summarized as follows:

- **Inflow magnitude is the dominant driver of hydropower system performance**, governing reliability, vulnerability, and revenue at both annual and seasonal scales.
- **System response to inflow changes is strongly asymmetric**, with inflow reductions producing severe hydropower performance degradation, while equivalent inflow increases yield comparatively limited benefits.
- **Hydropower performance improvements under high inflows are accompanied by increased lake level excursions**, revealing a fundamental trade-off between energy production benefits and system state stability.
- **Future infrastructure expansion (higher hydropower generation capacity) improves reliability and revenue but does not eliminate vulnerability**, as the severity of deficits under dry conditions remains high and benefit-stability trade-offs persist under wet conditions, underscoring the need for adaptive operational strategies to mitigate failure severity under future climates.
- **Climate change redistributes hydropower stress seasonally rather than uniformly intensifying it**, with spring emerging as a surplus-generating season and vulnerability increasingly concentrated in summer and autumn.
- **Seasonal system stress analysis is critical for understanding hydropower performance,** as annual results indicate lower overall system stress, while seasonal results reveal increased stress during summer and autumn, demonstrating that annual assessments can mask important seasonal system behavior.
- **Winter hydropower performance remains relatively robust**, although future conditions increase sensitivity to winter electricity shortages due to higher hydropower targets and reliance on seasonal storage.
- **Annual hydropower performance depends on both annual inflow magnitude and its seasonal distribution, with winter inflow gains providing a critical compensating**

mechanism: system-wide performance improvement is maintained under small annual inflow increases or decreases (as low as +0.77% and -0.57%) only when accompanied by sufficiently large winter inflow gains (> +5.6% and > +11.53%), while reductions in summer and autumn inflows consistently amplify performance degradation by weakening seasonal storage.

- **Accounting for electricity demand reveals vulnerabilities and trade-offs that are not apparent in generation-only assessments**, underscoring the importance of explicitly including electricity demand in climate change impact analyses.
- **The framework successfully captures system behavior under historically extreme drought conditions**, demonstrating applicability beyond the historical record and GCM-projected futures.

Rather than simply determining whether future system performance is favorable or unfavorable, the findings identify potential directions for preparing for future climate conditions, such as reassessing summer and autumn storage levels and exploring a wider operating range for Lake Winnipeg. However, further risk assessment is required to evaluate the potential benefits, feasibility, and associated trade-offs of these options before their effectiveness can be established.

5.2 Research Contribution and Significance

This research addresses the absence of a comprehensive, operation-based hydropower simulation model for Manitoba. Methodologically, MB_HydroSim advances existing hydropower-simulation modeling by moving beyond localized or median-based representations and establishing a unified, province-scale model that explicitly represents coordinated, real-world system operations across a transboundary watershed. From a practical perspective, MB_HydroSim serves as a foundational decision-support tool for evaluating climate change impacts, testing operational adaptations, and assessing trade-offs related to both flood management and hydropower generation in Manitoba. In addition, MB_HydroSim offers a platform for advancing Water-Energy Nexus analysis in Manitoba through dynamic coupling with energy system models, enabling two-way feedback in which hydropower generation respond to evolving energy system conditions. More broadly, the rule-based implementation within the MODSIM-DSS environment provides a transferable example for developing and customizing operation-focused models for other complex, large-scale river-reservoir systems.

A second major contribution of this research is addressing a fundamental limitation in bottom-up water-system assessments: the lack of computationally efficient, target-based inflow scenario generator for multisite studies operating in real space. Methodologically, the proposed inflow scenario generator advances existing scenario-generation approaches by enabling explicit control over key streamflow properties while implicitly preserving or appropriately modifying stationary and non-stationary statistical structures of streamflow. This capability enables transparent and uniform exploration of deep inflow-condition uncertainty and facilitates reliable and interpretable identification of critical system thresholds that may not be revealed by historical records or GCM-driven projections alone. From a practical perspective, the proposed scenario generator tool complements top-down climate scenarios by using them to provide a baseline-consistent and broader characterization of inflow uncertainty, thereby supporting stress testing for multisite water systems under climate change across objectives extending beyond hydropower generation, including flood and drought analysis.

The final contribution of this research is the application of a bottom-up climate change impact assessment approach that addresses key limitations of both top-down and existing bottom-up methods in characterizing decision-relevant impacts on hydropower systems. Specifically, the research demonstrates how systematic exploration of a wide range of plausible inflow conditions, in combination with increasing electricity demand, can be used to evaluate hydropower system behavior.

Methodologically, the significance of advancing bottom-up climate change impact assessment lies in explicitly linking hydrologic uncertainty and electricity demand to system performance within a stress-testing context. This linkage enables identification of dominant system performance drivers, critical thresholds at which undesired system behavior emerges, the likelihood of desired and undesired outcomes across the stress-testing space, and the severity of associated performance changes and their operational implications. The analytical approach further enables direct comparison of projected future system stress with historical conditions and systematic evaluation of how alternative inflow seasonality patterns alter system response, capabilities that are not readily available within existing analytical approaches. These analyses are scalable across spatial and temporal dimensions, including annual, seasonal, monthly, station-level, and sub-system scales.

From a practical perspective, the significance of this bottom-up analysis lies in its support for risk-informed operational planning. The analysis enables evaluation of adaptive strategies such as modified drawdown rules, seasonal target adjustments, and coordinated reservoir operations under a wide range of plausible inflow conditions. More broadly, the research establishes a transferable bottom-up approach for climate-adaptation planning in regulated water-resource systems, with clear pathways for incorporating additional system drivers, including flood-management objectives, ice-affected conveyance, dynamic electricity-market interactions, and broader Water-Energy Nexus considerations. While demonstrated for hydropower systems, the approach is applicable to other regulated water-resource systems through redefinition of performance objectives and thresholds, providing a robust foundation for system-wide risk assessment under deep inflow-condition uncertainty.

5.3 Limitations and Recommendations for Future Work

One limitation of simulating future hydropower generation in this research is the reliance of MB_HydroSim on the median recorded Ice Factor, which may not adequately represent evolving winter ice-on conditions under a changing climate. Recent studies by Gozini et al. (2023) and Lees et al. (2023) project shorter and warmer ice seasons, leading to increased cumulative winter outflows and potential gains in winter hydropower generation. Consequently, the winter hydropower performance reported in this study is likely conservative, as future ice dynamics were not explicitly represented. Future work will focus on incorporating the ice-affected hydraulics under climate-driven scenarios, building on the tools developed by Gozini et al. (2023) and Lees et al. (2023). In particular, the temperature-based Ice Factor simulations conducted by Gozini et al. (2023) for each individual GCM scenario can be directly imported into MB_HydroSim when simulating future hydropower generation. This extension would enable a more realistic representation of future ice impacts on channel conveyance and hydropower generation relative to historical conditions.

Another limitation in simulating future hydropower generation in this study is the treatment of "local flow". Because MODSIM-DSS is an integrated water-resources management model, unrecorded tributary inflows as well as lake-surface precipitation and evaporation cannot be represented explicitly. In this research, these contributions are calculated based on historical data and held constant across all hydropower simulations for both historical and future periods. Under

high-inflow conditions, local flow contributions would increase system inflows and enhance hydropower generation, whereas under low-flow conditions they would contribute to greater net water losses from lakes and reduced hydropower generation. As a result, the magnitude of hydropower performance improvements under wet conditions and performance degradation under dry conditions is likely underestimated in the current framework. In future work, local flow could be simulated explicitly using hydrological modeling and applied consistently across historical and future periods for each GCM ensemble member. Subsequently incorporating these process-based local flow simulations into the system model would provide a more accurate calculation of future hydropower generation. It should be noted that, despite this limitation, the results presented in this research remain valid, as the analysis focuses on directional system responses and relative performance comparisons between historical and future conditions rather than precise estimates of absolute changes in hydropower generation.

The synthetic streamflow generator underestimates temporal (autocorrelation) and spatial (cross-correlation) dependence, which in turn leads to underestimation of system performance metrics. Importantly, this limitation does not affect the directional interpretation of system response in the stress-testing analysis, because both the historical baseline and all future synthetic scenarios share the same bias in dependence structure and are therefore evaluated consistently relative to one another. Future work could reduce this underestimation by explicitly incorporating autocorrelation and cross-correlation targets into the optimization process, thereby improving representation of dependence structures at the expense of increased computational effort. In addition, persistence characteristics, such as multi-year drought duration, could be explicitly targeted alongside magnitude, variability, and seasonality, further enhancing the realism and applicability of the framework for long-term planning.

In this research, future hydropower generation is analyzed under the assumption that current reservoirs and control points operation remain unchanged. As a result, hydropower generation under varying inflow conditions does not reflect optimized operational responses aimed at maximizing benefits or minimizing losses for specific inflow conditions. Future work can build on this foundation by incorporating adaptive operational policies, thereby further enhancing the decision relevance of the analysis. The tools and analytical structure developed in this research already provide a basis for such extensions. MB_HydroSim employs custom-coded operational

rules that can be optimized using external optimization algorithms. The stress-testing framework can be extended to support adaptation-policy development within a risk-informed decision-making context, allowing specific operational actions to be associated with different regions of system failure or stress and their associated likelihoods. This capability is particularly valuable for examining interacting risks related to hydropower performance and flooding, as inflow conditions that are highly favorable for hydropower generation may simultaneously elevate flood risk.

Another limitation of this study is that electricity market dynamics are not represented explicitly, and hydropower targets and economic evaluations are therefore treated as static. In practice, hydropower system performance is closely coupled with electricity markets, where generation targets, import-export decisions, and electricity prices evolve in response to hydrologic conditions and broader energy system constraints. Future work can address this limitation by coupling the hydropower stress-testing analysis with energy system models that explicitly represent electricity demand, generation portfolios, and market behavior, thereby enabling evaluation of dynamic hydropower targets, real-time pricing and export decisions, and seasonal revenue outcomes. Such Water-Energy Nexus analysis would also support development of adaptive operational policies, allowing reservoir and generation strategies to adjust in response to evolving energy-system conditions while managing trade-offs between hydropower performance, flood risk, and system reliability. Because MB_HydroSim supports dynamic interaction with external models, it can be integrated with energy system models to enable two-way feedback between hydropower operations and electricity-market conditions, providing a more comprehensive and decision-relevant assessment of climate change impacts.

Another direction for future work is to apply stress-testing analyses at alternative spatial and temporal scales, depending on the specific decision context. Because hydropower targets, inflow timing, and operational constraints vary throughout the year, the analysis can be conducted at the monthly scale to more precisely identify periods of heightened stress and to support seasonally targeted operational adjustments. Similarly, the analysis can be spatially focused on individual hydropower stations or sub-systems to diagnose localized stress responses that may not be apparent at the system-wide scale. For example, hydropower stations along the Winnipeg River may experience localized stress under certain inflow conditions, while regulation of Lake Winnipeg may buffer these impacts and limit stress propagation to hydropower stations along the Nelson

River. Applying the framework across multiple spatial and temporal scales would therefore enable a more nuanced assessment of both localized and system-level stresses, supporting more targeted and context-specific adaptation planning.

REFERENCES

A. Thomas, J., B Fiering, M., 1962. Mathematical synthesis of streamflow sequences for the analysis of river basins by simulation, in: Design of Water-Resource Systems: New Techniques for Relating Economic Objectives, Engineering Analysis, and Governmental Planning. Harvard University Press, pp. 459–493. https://doi.org/10.4159/harvard.9780674421042.c15

Ahmed, M.I., Stadnyk, T., Pietroniro, A., Mai, J., Tolson, B.A., Shen, H., Craig, J.R., Taheri, M., 2024. Navigating Hydrological Model Intercomparison Projects in Cold Regions: Unveiling Challenges, Insights, and Future Paths–a Case from Nelson-Mip Il. Federated Research Data Repository. https://doi.org/10.20383/103.0913

Ali Shah, S.M., 2019. Integrated water resources management in a transboundary river basin: model development and sensitivity analysis (Master of Science Thesis). University of Saskatchewan. https://harvest.usask.ca/items/825f98bf-695d-465b-a3b5-06d7db3c1549.

Alipour, M.H., 2015. Risk-Informed Decision Making Framework for Operating a Multi-Purpose Hydropower Reservoir During Flooding and High Inflow Events, Case Study: Cheakamus River System. Water Resources Management 29, 801–815. https://doi.org/10.1007/s11269-014-0844-3

Alodah, A., Seidou, O., 2019. Assessment of climate change impacts on extreme high and low flows: An improved bottom-up approach. Water (Basel). 11. https://doi.org/10.3390/w11061236

Arnal, L., Pietroniro, A.C., Pomeroy, J.W., Fortin, V., Casson, D.R., Stadnyk, T.A., Rokaya, P., Durnford, D., Friesenhan, E., Clark, M.P., 2023. Towards a coherent flood forecasting framework for Canada: Local to global implications. J. Flood Risk Manag. 12, e12895. https://doi.org/10.1111/jfr3.12895

Arsenault, R., Brissette, F., Malo, J.S., Minville, M., Leconte, R., 2013. Structural and Non-Structural Climate Change Adaptation Strategies for the Péribonka Water Resource System. Water Resources Management 27, 2075–2087. https://doi.org/10.1007/s11269-013-0275-6

Bajracharya, A.R., Ahmed, M.I., Stadnyk, T., Asadzadeh, M., 2023. Process based calibration of a continental-scale hydrological model using soil moisture and streamflow data. J. Hydrol. Reg. Stud. 47, 101391. https://doi.org/10.1016/j.ejrh.2023.101391

Beh, E.H.Y., Maier, H.R., Dandy, G.C., 2015. Adaptive, multiobjective optimal sequencing approach for urban water supply augmentation under deep uncertainty. Water Resour. Res. 51, 1529–1551. https://doi.org/10.1002/2014WR016254

Beiraghdar, P., 2019. Developing an Integrated Water Management Model for Simulating the River-Reservoir System Operated by Manitoba Hydro (Master of Science Thesis). University of Manitoba. https://mspace.lib.umanitoba.ca/items/70e315f2-c279-4ebb-8191-02bd5df4bad6.

Berardi, U., Jafarpur, P., 2020. Assessing the impact of climate change on building heating and cooling energy demand in Canada. Renewable and Sustainable Energy Reviews 121, 109681. https://doi.org/10.1016/j.rser.2019.109681

Bhattarai, U., Maraseni, T., Devkota, L.P., Apan, A., 2024. Hydropower and Climate Resilience of Nepal Himalaya: A bottom-up Hydrological Approach. Earth Systems and Environment. https://doi.org/10.1007/s41748-024-00529-3

Borgomeo, E., Farmer, C.L., Hall, J.W., 2015. Numerical rivers: A synthetic streamflow generator for water resources vulnerability assessments. Water Resour. Res. 51. https://doi.org/10.1002/2014WR016827

Braun, M., Thiombiano, A.N., Vieira, M.J.F., Stadnyk, T.A., 2021. Representing climate evolution in ensembles of GCM simulations for the Hudson Bay System. Elem Sci Anth 9, 00011. https://doi.org/10.1525/elementa.2021.00011

Brown, C., Werick, W., Leger, W., Fay, D., 2011. A decision-analytic approach to managing climate risks: Application to the upper great lakes. J. Am. Water Resour. Assoc. 47, 524–534. https://doi.org/10.1111/j.1752-1688.2011.00552.x

Bush, E., Lemmen, D.S., 2019. Canada's Changing Climate. Government of Canada. Ottawa. https://changingclimate.ca/CCCR2019/.

Caceres, A.L., Jaramillo, P., Matthews, H.S., Samaras, C., Nijssen, B., 2021. Hydropower under climate uncertainty: Characterizing the usable capacity of Brazilian, Colombian and Peruvian power plants under climate scenarios. Energy for Sustainable Development 61, 217–229. https://doi.org/10.1016/j.esd.2021.02.006

Canada Energy Regulator, 2024. Canada's Energy Future 2023: Energy Supply and Demand Projections to 2050 [WWW Document]. URL https://www.cer-rec.gc.ca/en/data-analysis/canada-energy-future/2023/index.html

Candido, L.A., Coêlho, G.A.G., de Moraes, M.M.G.A., Florêncio, L., 2022. Review of Decision Support Systems and Allocation Models for Integrated Water Resources Management Focusing on Joint Water Quantity-Quality. J. Water Resour. Plan. Manag. 148, 03121001. https://doi.org/10.1061/(asce)wr.1943-5452.0001496

Chernet, H.H., Alfredsen, K., Killingtveit, Å., 2013. The impacts of climate change on a Norwegian high-head hydropower system. Journal of water and climate change 4, 17–37. https://doi.org/10.2166/wcc.2013.042

Chowdhury, A.F.M.K., Dang, T.D., Nguyen, H.T.T., Koh, R., Galelli, S., 2021. The Greater Mekong's Climate-Water-Energy Nexus: How ENSO-Triggered Regional Droughts Affect Power Supply and CO2 Emissions. Earths Future 9, e2020EF001814. https://doi.org/10.1029/2020EF001814

Côté, P., Haguma, D., Leconte, R., Krau, S., 2011. Stochastic optimisation of Hydro-Quebec hydropower installations: A statistical comparison between SDP and SSDP methods. Canadian Journal of Civil Engineering 38, 1427–1434. https://doi.org/10.1139/L11-101

Culley, S., Bennett, B., Westra, S., Maier, H.R., 2019. Generating realistic perturbed hydrometeorological time series to inform scenario-neutral climate impact assessments. J. Hydrol. (Amst). 576, 111–122. https://doi.org/10.1016/j.jhydrol.2019.06.005

Culley, S., Maier, H.R., Westra, S., Bennett, B., 2021. Identifying critical climate conditions for use in scenario-neutral climate impact assessments. Environmental Modelling and Software 136. https://doi.org/10.1016/j.envsoft.2020.104948

Culley, S., Noble, S., Yates, A., Timbs, M., Westra, S., Maier, H.R., Giuliani, M., Castelletti, A., 2016. A bottom-up approach to identifying the maximum operational adaptive capacity of water resource systems to a changing climate. Water Resour. Res. 52. https://doi.org/10.1002/2015WR018253

Dallison, R.J.H., Patil, S.D., Williams, A.P., 2021. Impacts of climate change on future water availability for hydropower and public water supply in Wales, UK. J. Hydrol. Reg. Stud. 36, 100866. https://doi.org/10.1016/j.ejrh.2021.100866

de Oliveira Serrão, E.A., Silva, M.T., Ferreira, T.R., Freitas Xavier, A.C., dos Santos, C.A., Paiva de Ataide, L.C., Pontes, P.R.M., Rodrigues da Silva, V. de P., 2023. Climate and land use change: future impacts on hydropower and revenue for the amazon. J. Clean. Prod. 385, 135700. https://doi.org/10.1016/j.jclepro.2022.135700

Dias, V. de S., da Luz, M.P., Medero, G.M., Nascimento, D.T.F., 2018. An overview of hydropower reservoirs in Brazil: Current situation, future perspectives and impacts of climate change. Water (Basel). 10, 592. https://doi.org/10.3390/w10050592

Eamen, L., Brouwer, R., Razavi, S., 2022. Comparing the applicability of hydro-economic modelling approaches for large-scale decision-making in multi-sectoral and multi-regional river basins. Environmental Modelling & Software 152, 105385. https://doi.org/10.1016/j.envsoft.2022.105385

Eamen, L., Brouwer, R., Razavi, S., 2021. Integrated modelling to assess the impacts of water stress in a transboundary river basin: Bridging local-scale water resource operations to a river basin economy. Science of The Total Environment 800, 149543. https://doi.org/10.1016/j.scitotenv.2021.149543

Ember, 2025. 2025 Statistical Review of World Energy [WWW Document]. URL https://www.energyinst.org/statistical-review

Fontenelle, A.L., Nilsson, E., Hidalgo, I.G., Uvo, C.B., Peyerl, D., 2022. Temporal Understanding of the Water–Energy Nexus: A Literature Review. Energies (Basel). 15, 2851. https://doi.org/10.3390/en15082851

Fowler, K.J.A., McMahon, T.A., Westra, S., Horne, A., Guillaume, J.H.A., Guo, D., Nathan, R., Maier, H.R., John, A., 2024. Climate stress testing for water systems: Review and guide for applications. Wiley Interdisciplinary Reviews: Water. https://doi.org/10.1002/wat2.1747

François, B., Hingray, B., Borga, M., Zoccatelli, D., Brown, C., Creutin, J.D., 2018. Impact of climate change on combined solar and run-of-river power in Northern Italy. Energies (Basel). 11. https://doi.org/10.3390/en11020290

Gaudard, L., Gilli, M., Romerio, F., 2013. Climate Change Impacts on Hydropower Management. Water Resources Management 27, 5143–5156. https://doi.org/10.1007/s11269-013-0458-1

Giuliani, M., Quinn, J.D., Herman, J.D., Castelletti, A., Reed, P.M., 2018. Scalable Multiobjective Control for Large-Scale Water Resources Systems under Uncertainty. IEEE Transactions on Control Systems Technology 26, 1492–1499. https://doi.org/10.1109/TCST.2017.2705162

Gold, D.F., Reed, P.M., Gorelick, D.E., Characklis, G.W., 2023. Advancing Regional Water Supply Management and Infrastructure Investment Pathways That Are Equitable, Robust, Adaptive, and Cooperatively Stable. Water Resour. Res. 59. https://doi.org/10.1029/2022WR033671

Government of Manitoba, 2025a. Lakes, Beaches and Rivers [WWW Document]. URL https://www.gov.mb.ca/sd/water/lakes-beaches-rivers/index.html

Government of Manitoba, 2025b. 2025/26 Second Quarter Report, Fiscal and Economic Update.

Government of Manitoba, 2025c. Manitoba Drought Management Strategy [WWW Document]. URL https://www.gov.mb.ca/sd/pubs/research-data-and-maps/drought_condition/index.html (accessed 12.9.25).

Gozini, H., 2026. Automated MODSIM-DSS Run (v1.0) [software]. Zenodo. https://doi.org/10.5281/zenodo.21501336

Gozini, H., Asadzadeh, M., Stadnyk, T.A., 2025. Target Synthetic Streamflow Generator (v1.0) [software]. Zenodo. https://doi.org/10.5281/zenodo.17195525

Gozini, H., Asadzadeh, M., Stadnyk, T.A., Riddell, P., Tolossa, H., 2026a. Integrated Water Resources and Hydropower Generation Modelling in a Complex, Cold-Regions River-Reservoir System. Sustain. Water Resour. Manag. 12, 20. https://doi.org/10.1007/s40899-026-01335-7

Gozini, H., Asadzadeh, M., Stadnyk, T.A., Slota, P., 2026b. Inflow Generation for Water System Planning in Multisite Studies Using Target Synthetic Streamflow Generation. Water Resour. Res. 62. https://doi.org/10.1029/2025WR042355

Gozini, H., Wilson, S., Asadzadeh, M., Lees, K., Kim, S.J., 2023. Statistical modeling of ice cover impact on flow conveyance in the Nelson River West Channel. Canadian Water Resources Journal 9, 2–22. https://doi.org/10.1080/07011784.2023.2218328

Gozini, H., Zahraie, B., Ravar, Z., 2021. System Dynamics Modeling of Water-Energy Nexus for Resource-Saving Policy Assessment. Int. J. Environ. Res. 15, 349–367. https://doi.org/10.1007/s41742-021-00321-5

Graabak, I., Jaehnert, S., Korpås, M., Mo, B., 2017. Norway as a battery for the future European power system-impacts on the hydropower system. Energies (Basel). 10, 2054. https://doi.org/10.3390/en10122054

Graham, L.P., Andreáasson, J., Carlsson, B., 2007. Assessing climate change impacts on hydrology from an ensemble of regional climate models, model scales and linking methods - A case study on the Lule River basin. Clim. Change 81, 293–307. https://doi.org/10.1007/s10584-006-9215-2

Guo, D., Westra, S., Maier, H.R., 2017. Use of a scenario-neutral approach to identify the key hydro-meteorological attributes that impact runoff from a natural catchment. J. Hydrol. (Amst). 554, 317–330. https://doi.org/10.1016/j.jhydrol.2017.09.021

Guo, D., Westra, S., Maier, H.R., 2016. An inverse approach to perturb historical rainfall data for scenario-neutral climate impact studies. J. Hydrol. (Amst). 556, 877–890. https://doi.org/10.1016/j.jhydrol.2016.03.025

Gupta, H. V., Kling, H., Yilmaz, K.K., Martinez, G.F., 2009. Decomposition of the mean squared error and NSE performance criteria: Implications for improving hydrological modelling. J. Hydrol. (Amst). 377, 80–91. https://doi.org/10.1016/j.jhydrol.2009.08.003

Hadjimichael, A., Quinn, J., Wilson, E., Reed, P., Basdekas, L., Yates, D., Garrison, M., 2020. Defining Robustness, Vulnerabilities, and Consequential Scenarios for Diverse Stakeholder Interests in Institutionally Complex River Basins. Earths Future 8. https://doi.org/10.1029/2020EF001503

Haguma, D., Leconte, R., 2018. Long-Term Planning of Water Systems in the Context of Climate Non-Stationarity with Deterministic and Stochastic Optimization. Water Resources Management 32, 1725–1739. https://doi.org/10.1007/s11269-017-1900-6

Haguma, D., Leconte, R., Côté, P., 2017a. Evaluating Transition Probabilities for a Stochastic Dynamic Programming Model Used in Water System Optimization. Water Resources Planning and Management 144. https://doi.org/10.1061/(ASCE)WR.1943

Haguma, D., Leconte, R., Côté, P., Krau, S., Brissette, F., 2014. Optimal Hydropower Generation Under Climate Change Conditions for a Northern Water Resources System. Water Resources Management 28, 4631–4644. https://doi.org/10.1007/s11269-014-0763-3

Haguma, D., Leconte, R., Krau, S., 2017b. Hydropower plant adaptation strategies for climate change impacts on hydrological regime. Canadian Journal of Civil Engineering 44, 962–970. https://doi.org/10.1139/cjce-2017-0141

Haguma, D., Leconte, R., Krau, S., Côté, P., Brissette, F., 2015. Water Resources Optimization Method in the Context of Climate Change. Water Resources Planning and Management 141. https://doi.org/10.1061/(asce)wr.1943-5452.0000445

Herman, J.D., Ph, D., Asce, A.M., Zeff, H.B., Ph, D., Lamontagne, J.R., Ph, D., Reed, P.M., Ph, D., Asce, A.M., Characklis, G.W., Ph, D., Asce, M., 2016. Synthetic Drought Scenario Generation to Support Bottom-Up Water Supply Vulnerability Assessments. J. Water Resour. Plan. Manag. 1–13. https://doi.org/10.1061/(ASCE)WR.1943-5452.0000701.

Herman, J.D., Reed, P.M., Zeff, H.B., Characklis, G.W., 2015. How should robustness be defined for water systems planning under change? J. Water Resour. Plan. Manag. 141, 1–14. https://doi.org/10.1061/(ASCE)WR.1943-5452.0000509

Heryani, N., Kartiwa, B., Sosiawan, H., Rejekiningrum, P., Adi, S.H., Apriyana, Y., Pramudia, A., Yufdy, M.P., Tafakresnanto, C., Rivaie, A.A., Suratman, Dariah, A., Malik, A., Yusuf, Setiani, C., 2022. Analysis of Climate Change Impacts on Agricultural Water Availability in Cimanuk Watershed, Indonesia. Sustainability (Switzerland) 14. https://doi.org/10.3390/su142316236

Hipel, K.W., McLeod, A.I., Lennox, W.C., 1977. Advances in box-jenkins modeling: 1. Model construction. Water Resour. Res. 13, 567–575. https://doi.org/10.1029/WR013i003p00567

Hou, R., Li, S., Wu, M., Ren, G., Gao, W., Khayatnezhad, M., gholinia, F., 2021. Assessing of impact climate parameters on the gap between hydropower supply and electricity demand by RCPs scenarios and optimized ANN by the improved Pathfinder (IPF) algorithm. Energy 237, 121621. https://doi.org/10.1016/j.energy.2021.121621

Huaringa Alvarez, U.F., Trudel, M., Leconte, R., 2014. Impacts and adaptation to climate change using a reservoir management tool to a northern watershed: Application to Lièvre river watershed, Quebec, Canada. Water Resources Management 28, 3667–3680. https://doi.org/10.1007/s11269-014-0694-z

Jabbari, A.A., Nazemi, A., 2019. Alterations in canadian hydropower production potential due to continuation of historical trends in climate variables. Resources 8. https://doi.org/10.3390/RESOURCES8040163

Jamali, S., Abrishamchi, A., Madani, K., 2013. Climate Change and Hydropower Planning in the Middle East: Implications for Iran's Karkheh Hydropower Systems. Journal of Energy Engineering 139, 153–160. https://doi.org/10.1061/(ASCE)EY.1943-7897.0000115.

Karan, K., Singh, D., Singh, P.K., Bharati, B., Singh, T.P., Berndtsson, R., 2022. Implications of future climate change on crop and irrigation water requirements in a semi-arid river basin using CMIP6 GCMs. J. Arid Land 14, 1234–1257. https://doi.org/10.1007/s40333-022-0081-1

Kim, S.J., Asadzadeh, M., Stadnyk, T.A., 2022. Climate change impact on water supply and hydropower generation potential in Northern Manitoba. J. Hydrol. Reg. Stud. 41, 101077. https://doi.org/10.1016/j.ejrh.2022.101077

Kirsch, B.R., Characklis, G.W., Zeff, H.B., 2013. Evaluating the Impact of Alternative Hydro-Climate Scenarios on Transfer Agreements: Practical Improvement for Generating Synthetic Streamflows. J. Water Resour. Plan. Manag. 139, 396–406. https://doi.org/10.1061/(asce)wr.1943-5452.0000287

Labadie, J.W., 2006. MODSIM: decision support system for integrated river basin management, in: 3rd International Congress on Environmental Modelling and Software. Burlington, Vermont, USA. https://scholarsarchive.byu.edu/iemssconference/2006/all/242/.

Lall, U., Sharma, A., 1996. A nearest neighbor bootstrap for resampling hydrologic time series. Water Resour. Res. 32, 679–693. https://doi.org/10.1029/95WR02966

Lau, L.B., Reed, P.M., Gold, D.F., 2023. Evaluating Implementation Uncertainties and Defining Safe Operating Spaces for Deeply Uncertain Cooperative Multi-City Water Supply Investment Pathways. Water Resour. Res. 59. https://doi.org/10.1029/2023WR034841

Lees, K., 2022. Investigation and Modelling of Ice Processes in the Nelson River's Outlet Lakes Area (PhD Thesis). University of Manitoba, Winnipeg. https://mspace.lib.umanitoba.ca/items/6f3657ff-57c0-4e78-9256-0ae0bfb13136.

Lees, K., Clark, S.P., Malenchak, J., Chanel, P., 2023. A novel methodology to quantify hydraulic conveyance through an ice-impacted lake-outlet system. Cold Reg. Sci. Technol. 206, 103713. https://doi.org/10.1016/j.coldregions.2022.103713

Li, J., Wang, Z., Wu, X., Ming, B., Chen, L., Chen, X., 2020. Evident response of future hydropower generation to climate change. J. Hydrol. (Amst). 590, 125385. https://doi.org/10.1016/j.jhydrol.2020.125385

Lilhare, R., Déry, S.J., Stadnyk, T.A., Pokorny, S., Koenig, K.A., 2022. Warming soil temperature and increasing baseflow in response to recent and potential future climate change across northern Manitoba, Canada. Hydrol. Process. 36. https://doi.org/10.1002/hyp.14748

Liu, B., Lund, J.R., Liu, L., Liao, S., Li, G., Cheng, C., 2020. Climate change impacts on hydropower in Yunnan, China. Water (Basel). 12, 197. https://doi.org/10.3390/w12010197

Liu, Yuan, Ji, C., Wang, Y., Zhang, Y., Jiang, Z., Ma, Q., Hou, X., 2023. Effect of the quality of streamflow forecasts on the operation of cascade hydropower stations using stochastic optimization models. Energy 273, 127298. https://doi.org/10.1016/j.energy.2023.127298

Liu, Yueyi, Zheng, H., Wan, W., Zhao, J., 2023. Optimal operation toward energy efficiency of the long-distance water transfer project. J. Hydrol. (Amst). 618. https://doi.org/10.1016/j.jhydrol.2023.129152

MacDonald, M.K., Stadnyk, T.A., Déry, S.J., Braun, M., Gustafsson, D., Isberg, K., Arheimer, B., 2018. Impacts of 1.5 and 2.0 °C Warming on Pan-Arctic River Discharge Into the Hudson Bay Complex Through 2070. Geophys. Res. Lett. 45, 7561–7570. https://doi.org/10.1029/2018GL079147

Mandal, S., Arunkumar, R., Breach, P.A., Simonovic, S.P., Asce, F., 2019. Reservoir Operations under Changing Climate Conditions: Hydropower-Production Perspective. J. Water Resour. Plan. Manag. 145, 04019016. https://doi.org/10.1061/(ASCE)WR.1943-5452.0001061.

Manitoba Hydro, 2025. Generating stations [WWW Document]. URL https://www.hydro.mb.ca/corporate/operations/generation/

Manitoba Hydro, 2024. Manitoba Hydro-Electric Board 73rd Annual Report. https://www.hydro.mb.ca/docs/corporate/annual_report_2023_24.pdf.

Manitoba Hydro, 2023a. Integrated Resource Plan. https://www.hydro.mb.ca/docs/corporate/irp/irp-2023-integrated-resource-plan.pdf.

Manitoba Hydro, 2023b. 2023/24 & 2024/25 General Rate Application. https://www.hydro.mb.ca/corporate/regulatory-affairs/electric/gra_2023_2025/.

Manitoba Hydro, 2022. Churchill River Diversion, License Implementation Guide. Winnipeg, Manitoba Hydro. https://www.gov.mb.ca/sd/pubs/water/licensing/crd_lig.pdf.

Manitoba Hydro, 2014. Lake Winnipeg Regulation, Manitoba Hydro, Winnipeg. https://www.hydro.mb.ca/docs/regulatory_affairs/pdf/lake_wpg_regulation/lwr_complete_report.pdf .

Mastrandrea, M.D., Field, C.B., Stocker, T.F., Edenhofer, O., Ebi, K.L., Frame, D.J., Held, H., Kriegler, E., Mach, K.J., Matschoss, P.R., Plattner, G.-K., Yohe, G.W., Zwiers, F.W., 2010. Guidance Note for Lead Authors of the IPCC Fifth Assessment Report on Consistent Treatment of Uncertainties.

Meresa, H., Murphy, C., Fealy, R., Golian, S., 2021. Uncertainties and their interaction in flood hazard assessment with climate change. Hydrol. Earth Syst. Sci. 25, 5237–5257. https://doi.org/10.5194/hess-25-5237-2021

Minville, M., Brissette, F., Krau, S., Leconte, R., 2009. Adaptation to climate change in the management of a Canadian water-resources system exploited for hydropower. Water Resources Management 23, 2965–2986. https://doi.org/10.1007/s11269-009-9418-1

Minville, M., Brissette, F., Leconte, R., 2010a. Impacts and uncertainty of climate change on water resource management of the Peribonka River System (Canada). J. Water Resour. Plan. Manag. 136, 376–385. https://doi.org/10.1061/(ASCE)WR.1943-5452.0000041

Minville, M., Krau, S., Brissette, F., Leconte, R., 2010b. Behaviour and performance of a water resource system in Québec (Canada) under adapted operating policies in a climate change context. Water Resources Management 24, 1333–1352. https://doi.org/10.1007/s11269-009-9500-8

Moges, E., Demissie, Y., Larsen, L., Yassin, F., 2021. Review: Sources of hydrological model uncertainties and advances in their analysis. Water (Basel). 13, 28. https://doi.org/10.3390/w13010028

Mutschler, R., Rüdisüli, M., Heer, P., Eggimann, S., 2021. Benchmarking cooling and heating energy demands considering climate change, population growth and cooling device uptake. Appl. Energy 288, 116636. https://doi.org/10.1016/j.apenergy.2021.116636

Ng, J.Y., Turner, S.W.D., Galelli, S., 2017. Influence of El Niño Southern Oscillation on global hydropower production. Environmental Research Letters 12, 034010. https://doi.org/10.1088/1748-9326/aa5ef8

Nowak, K., Prairie, J., Rajagopalan, B., Lall, U., 2010. A nonparametric stochastic approach for multisite disaggregation of annual to daily streamflow. Water Resour. Res. 46. https://doi.org/10.1029/2009WR008530

Obahoundje, S., Diedhiou, A., Dubus, L., Adéchina Alamou, E., Amoussou, E., Akpoti, K., Antwi Ofosu, E., 2022. Modeling climate change impact on inflow and hydropower generation of Nangbeto dam in West Africa using multi-model CORDEX ensemble and ensemble machine learning. Appl. Energy 325, 119795. https://doi.org/10.1016/j.apenergy.2022.119795

OECD, 2011. Water Governance in OECD Countries: A Multi-level Approach, OECD Studies on Water, OECD Pub. OECD Paris. https://doi.org/http://dx.doi.org/10.1787/9789264119284-en

O'Shea, D., Nathan, R., Wasko, C., Ho, M., Sharma, A., 2024. Evaluation of key flood risk drivers under climate change using a bottom-up approach. J. Hydrol. (Amst). 640. https://doi.org/10.1016/j.jhydrol.2024.131694

Prime Minister of Canada, 2026. Prime Minister Carney launches AI for All: Canada's new national artificial intelligence strategy [WWW Document]. URL https://www.pm.gc.ca/en/news/news-releases/2026/06/04/prime-minister-carney-launches-ai-all-canadas-new-national-artificial (accessed 6.12.26).

Prime Minister of Canada, 2025. Prime Minister Carney announces second tranche of nation-building projects referred to the Major Projects Office [WWW Document]. URL https://www.pm.gc.ca/en/news/news-releases/2025/11/13/prime-minister-carney-announces-second-tranche-nation-building-projects (accessed 6.12.26).

Prudhomme, C., Wilby, R.L., Crooks, S., Kay, A.L., Reynard, N.S., 2010. Scenario-neutral approach to climate change impact studies: Application to flood risk. J. Hydrol. (Amst). 390, 198–209. https://doi.org/10.1016/j.jhydrol.2010.06.043

Qin, P., Xu, H., Liu, M., Du, L., Xiao, C., Liu, L., Tarroja, B., 2020a. Climate change impacts on Three Gorges Reservoir impoundment and hydropower generation. J. Hydrol. (Amst). 580, 123922. https://doi.org/10.1016/j.jhydrol.2019.123922

Qin, P., Xu, H., Liu, M., Xiao, C., Forrest, K.E., Samuelsen, S., Tarroja, B., 2020b. Assessing concurrent effects of climate change on hydropower supply, electricity demand, and greenhouse gas emissions in the Upper Yangtze River Basin of China. Appl. Energy 279, 115694. https://doi.org/10.1016/j.apenergy.2020.115694

Quinn, J.D., Hadjimichael, A., Reed, P.M., Steinschneider, S., 2020. Can Exploratory Modeling of Water Scarcity Vulnerabilities and Robustness Be Scenario Neutral? Earths Future 8. https://doi.org/10.1029/2020EF001650

Quinn, J.D., Reed, P.M., Giuliani, M., Castelletti, A., 2024. Average domination: A new multi-objective value metric applied to assess the benefits of forecasts in reservoir operations under different flood design levels. Adv. Water Resour. 185. https://doi.org/10.1016/j.advwatres.2024.104638

Quinn, J.D., Reed, P.M., Giuliani, M., Castelletti, A., 2017. Rival framings: A framework for discovering how problem formulation uncertainties shape risk management trade-offs in water resources systems. Water Resour. Res. 53, 7208–7233. https://doi.org/10.1002/2017WR020524

Quinn, J.D., Reed, P.M., Giuliani, M., Castelletti, A., Oyler, J.W., Nicholas, R.E., 2018. Exploring How Changing Monsoonal Dynamics and Human Pressures Challenge Multireservoir Management for Flood Protection, Hydropower Production, and Agricultural Water Supply. Water Resour. Res. 54, 4638–4662. https://doi.org/10.1029/2018WR022743

Raman, H., Sunilkumar, N., 1995. Multivariate modelling of water resources time series using artificial neural networks. Hydrological Sciences Journal 40, 145–163. https://doi.org/10.1080/02626669509491401

Rasmussen, P.F., Salas, J.D., Fagherazzi, L., Rassam, J., Bobée, B., 1996. Estimation and validation of contemporaneous PARMA models for streamflow simulation. Water Resour. Res. 32, 3151–3160. https://doi.org/10.1029/96WR01528

Ray, P.A., Bonzanigo, L., Wi, S., Yang, Y.C.E., Karki, P., García, L.E., Rodriguez, D.J., Brown, C.M., 2018. Multidimensional stress test for hydropower investments facing climate, geophysical and financial uncertainty. Global Environmental Change 48, 168–181. https://doi.org/10.1016/j.gloenvcha.2017.11.013

Rezazadeh, H., Bruckmann, L., Fernandes Marques, G., Tilmant, A., 2025. Water Resources Planning Under Deep Uncertainty and Multiple Criteria–An Example in the Senegal River Basin. Water Resour. Res. 61. https://doi.org/10.1029/2025WR041058

Ritchie, H., Roser, M., Rosado, P., 2020. Renewable Energy [WWW Document]. URL https://ourworldindata.org/renewable-energy#hydropower-generation

Sakki, G.K., Tsoukalas, I., Kossieris, P., Makropoulos, C., Efstratiadis, A., 2022. Stochastic simulation-optimization framework for the design and assessment of renewable energy systems under uncertainty. Renewable and Sustainable Energy Reviews 168, 112886. https://doi.org/10.1016/j.rser.2022.112886

Sant'Anna, C., Tilmant, A., 2025. Designing decision-relevant partitions of the exposure space for the adaptation of reservoir operating policies under climate-change uncertainty. Canadian Water Resources Journal 50, 175–190. https://doi.org/10.1080/07011784.2025.2512787

Sant'Anna, C., Tilmant, A., Pulido-Velazquez, M., 2022. A hydrologically-driven approach to climate change adaptation for multipurpose multireservoir systems. Clim. Risk Manag. 36. https://doi.org/10.1016/j.crm.2022.100427

Savelsberg, J., Schillinger, M., Schlecht, I., Weigt, H., 2018. The impact of climate change on Swiss hydropower. Sustainability 10, 2541. https://doi.org/10.3390/su10072541

Sharma, A., Tarboton, D.G., Lall, U., 1997. Streamflow simulation: A nonparametric approach. Water Resour. Res. 33, 291–308. https://doi.org/10.1029/96WR02839

Spanoudaki, K., Dimitriadis, P., Varouchakis, E.A., Corzo Perez, G.A., 2022. Estimation of Hydropower Potential Using Bayesian and Stochastic Approaches for Streamflow Simulation and Accounting for the Intermediate Storage Retention. Energies (Basel). 15, 1413. https://doi.org/10.3390/en15041413

Stadnyk, T.A., Tefs, A., Broesky, M., Déry, S.J., Myers, P.G., Ridenour, N.A., Koenig, K., Vonderbank, L., Gustafsson, D., 2021. Changing freshwater contributions to the Arctic: A 90-year trend analysis (1981- 2070). Elementa 9, 00098. https://doi.org/10.1525/elementa.2020.00098

Steinschneider, S., Asce, M., Mccrary, R., Wi, S., Mulligan, K., Asce, S.M., Mearns, L.O., Brown, C., Asce, M., 2015. Expanded Decision-Scaling Framework to Select Robust Long-Term Water-System Plans under Hydroclimatic Uncertainties. J. Water Resour. Plan. Manag. https://doi.org/10.1061/(ASCE)WR.1943-5452.0000536.

Studnicka, S., Panu, U.S., 2025. Techniques and Developments in Stochastic Streamflow Synthesis—A Comprehensive Review. Encyclopedia 5, 198. https://doi.org/10.3390/encyclopedia5040198

Taner, M.Ü., Ray, P., Brown, C., 2017. Robustness-based evaluation of hydropower infrastructure design under climate change. Clim. Risk Manag. 18, 34–50. https://doi.org/10.1016/j.crm.2017.08.002

Trindade, B.C., Reed, P.M., Herman, J.D., Zeff, H.B., Characklis, G.W., 2017. Reducing regional drought vulnerabilities and multi-city robustness conflicts using many-objective optimization under deep uncertainty. Adv. Water Resour. 104, 195–209. https://doi.org/10.1016/j.advwatres.2017.03.023

Turner, S.W.D., Voisin, N., 2022. Simulation of hydropower at subcontinental to global scales: A state-of-the-art review. Environmental Research Letters. https://doi.org/10.1088/1748-9326/ac4e38

Van Staveren, M., 2018. Uncertainty and ground conditions: A risk management approach. CRC Press. https://doi.org/doi.org/10.1201/b12859

Walker, W.E., Haasnoot, M., Kwakkel, J.H., 2013. Adapt or perish: A review of planning approaches for adaptation under deep uncertainty. Sustainability (Switzerland) 5, 955–979. https://doi.org/10.3390/su5030955

Wasti, A., Ray, P., Wi, S., Folch, C., Ubierna, M., Karki, P., 2022. Climate change and the hydropower sector: A global review. Wiley Interdiscip. Rev. Clim. Change. https://doi.org/10.1002/wcc.757

Whateley, S., Steinschneider, S., Brown, C., 2014. A climate change range-based method for estimating robustness for water resources supply. Water Resour. Res. 50. https://doi.org/10.1002/2014WR015956

Whateley, S., Walker, J.D., Brown, C., 2015. A web-based screening model for climate risk to water supply systems in the northeastern United States. Environmental Modelling and Software 73, 64–75. https://doi.org/10.1016/j.envsoft.2015.08.001

Wheeler, K.G., Simpson, M., Borgomeo, E., Hall, J.W., 2025. Multisite Nonparametric Stochastic Streamflow Generation for the Eastern Nile Basin. J. Hydrol. Eng. 30. https://doi.org/10.1061/jhyeff.heeng-6329

Widén, Å., Renöfält, B.M., Jansson, R., 2024. Environmental flows in a future climate: Balancing hydropower production and ecosystem rehabilitation in the Ume River system, Sweden. Science of the Total Environment 955, 176622. https://doi.org/10.1016/j.scitotenv.2024.176622

Wild, T.B., Reed, P.M., Loucks, D.P., Mallen-Cooper, M., Jensen, E.D., 2019. Balancing Hydropower Development and Ecological Impacts in the Mekong: Tradeoffs for Sambor Mega Dam. J. Water Resour. Plan. Manag. 145, 05018019. https://doi.org/10.1061/(asce)wr.1943-5452.0001036

Wu, W., Eamen, L., Dandy, G., Maier, H.R., Razavi, S., Kwakkel, J., Huang, J., Kuczera, G., 2025. Beyond the traditional paradigm of water resources management: scenario thinking to address deep uncertainty. J. Hydrol. (Amst). 661. https://doi.org/10.1016/j.jhydrol.2025.133547

Yakowitz, S.J., 1979. A nonparametric Markov Model for daily river flow. Water Resour. Res. 15, 1035–1043. https://doi.org/10.1029/WR015i005p01035

Yan, B., Mu, R., Guo, J., Liu, Y., Tang, J., Wang, H., 2022. Flood risk analysis of reservoirs based on full-series ARIMA model under climate change. J. Hydrol. (Amst). 610. https://doi.org/10.1016/j.jhydrol.2022.127979

You, G.J.Y., Thum, B.H., Lin, F.H., 2014. The examination of reproducibility in hydro-ecological characteristics by daily synthetic flow models. J. Hydrol. (Amst). 511, 904–919. https://doi.org/10.1016/j.jhydrol.2014.02.047

Zeff, H.B., Herman, J.D., Reed, P.M., Characklis, G.W., 2016. Cooperative drought adaptation: Integrating infrastructure development, conservation, and water transfers into adaptive policy pathways. Water Resour. Res. 52, 7327–7346. https://doi.org/10.1002/2016WR018771

Zhao, Y., Xu, K., Dong, N., Wang, H., 2022. Projection of climate change impacts on hydropower in the source region of the Yangtze River based on CMIP6. J. Hydrol. (Amst). 606, 127453. https://doi.org/10.1016/j.jhydrol.2022.127453

Zhou, T., Voisin, N., Fu, T., 2018. Non-stationary hydropower generation projections constrained by environmental and electricity grid operations over the western United States. Environmental Research Letters 13, 074035. https://doi.org/10.1088/1748-9326/aad19f

SUPPLEMENTARY MATERIAL

SM.1 Summarized Operational Rules

Table S1. Summary of the methods used in the operational models. All methods are custom coded except red-highlighted ones.

Sub-system	Sub-basin	Location	Location Detail	Node Type	Method
1	Winnipeg River	St. Joseph	This lake has two control structures. Rat Rapids Dam flows to Albany River, and Root River Dam flows downstream towards Winnipeg River	Reservoir	12 linear regression equations (for each month) were developed to calculate the target storage of the lake. DOY, storage, inflow, and outflow in the previous timestep were the independent variables, and the next timestep storage (target storage) was the dependent variable. The total outflow of the lake was defined to go through Root River Dam. However, in case of exceeding a threshold of water level in St. Joseph and Lac Seul Lake, the lake outflow was defined to be released from Rat Rapids Dam.
		Root River Dam	Control Structure. The outlet to Lac Seul towards Manitoba.	Flowthru Demand	
		Rat Rapids Dam	Control Structure. The outlet to Albany River in Ontario.	Flowthru Demand	
		Lac Seul	Controlled Lake. Its outlet name is Ear Falls	Reservoir	Target storage of the lake was calculated the same as St. Joseph (12 linear regression equations for each month).
		Pakwash	Controlled Lake. Its outlet name is Manitou Falls	Reservoir	One linear regression equation to calculate target storage with the same independent variables used for St. Joseph.
		Ball	Uncontrolled Lake	Reservoir	Same as Pakwash (one linear regression equation)
		Separation	Uncontrolled Lake	Reservoir	Same as Pakwash (one linear regression equation)
		Umfreville	Controlled Lake. Its outlet name is Caribou Falls	Reservoir	Same as Pakwash (one linear regression equation)
		Lac La Croix	Uncontrolled Lake	Reservoir	Same as Pakwash (one linear regression equation)
		Namakan	Controlled Lake. Its outlet name is Kettle Falls	Reservoir	Same as St. Joseph (12 linear regression equations for each month)
		Rainy	Controlled Lake. Its outlet name is Fort Frances	Reservoir	Same as St. Joseph (12 linear regression equations for each month)
		Lake of the Woods	Controlled Lake. Outlets' names are Kenora and Norman Dam	Reservoir	Same as St. Joseph (12 linear regression equations for each month)
		Minaki	Hydrometric station. The water level is controlled by Whitedog	Reservoir	Daily median historical recorded storage was used as the target storage when the outflow from Lake of the Woods was below 700 m^3/s. For an outflow of more than 700 m^3/s, Minaki target storage was calculated based on a linear regression using Lake of the Woods outflow as the independent variable.
		Whitedog	Controlled Dam	Non-storage	No available data for water level and storage to simulate the dam
		Pt. Du Bois	Hydropower station	Reservoir	Daily median recorded storage as the target storage
		Slave Falls	Hydropower station	Reservoir	Daily median recorded storage as the target storage
		Seven Sisters	Hydropower station. The outlet of Natalie Lake	Reservoir	Daily median recorded storage as the target storage

		McArthur	Hydropower station. The outlet of Lac Du Bonnet.	Reservoir	Daily median recorded storage as the target storage
		Great Falls	Hydropower station	Reservoir	Daily median recorded storage as the target storage
	Lake Winnipeg	Pine Falls	Hydropower station	Reservoir	Daily median recorded storage as the target storage
2	Assiniboine River	Shellmouth	Controlled Dam	Reservoir	Target storage was calculated based on the suitable outflow which keeps the water level and outflow in the required range. The water level and outflow range vary for different seasons and inflow volumes.
		Russel	Hydrometric station	Non-storage	MODSIM-DSS mass-balance
		Miniota	Hydrometric station	Non-storage	MODSIM-DSS mass-balance
		Brandon	Hydrometric station	Non-storage	MODSIM-DSS mass-balance
		Holland	Hydrometric station	Non-storage	MODSIM-DSS mass-balance
		Portage Diversion	Control Structure. Diversion of Assiniboine River flow towards Lake Manitoba	Flowthru Demand	Streamflow would be diverted if Assiniboine streamflow at Southport or the water level in James Avenue exceeds their maximum thresholds. To meet these criteria, the suitable amount of diversion at Portage and Floodway was calculated simultaneously.
		Southport	Hydrometric station	Non-storage	MODSIM-DSS mass-balance
		Headingly	Hydrometric station	Non-storage	Routed from Southport using lag time in MODSIM-DSS
	Red River	Floodway	Control Structure. Diversion of Red River streamflow from its mainstream.	Flowthru Demand	Streamflow would be diverted if the water level in James Avenue exceeds its maximum threshold. To meet this criterion, the suitable amount of diversion at Portage and Floodway was calculated simultaneously.
		James Avenue	Hydrometric station	Non-storage	The water level was calculated based on the discharge-level tables
	Lake Winnipeg	Winnipegosis	Uncontrolled lake. The outlet is Waterhen River	Reservoir	Two stage-discharge curves for summer and winter seasons
		Manitoba	Controlled lake. The outlet is Fairford River	Reservoir	Stage-discharge rule curves for different operation conditions depending on the water level of the lake. The lake also has an outlet channel which is not being operated now; however, its rule curve is also included in the model using a "flowthru" demand node.
		St. Martin	Uncontrolled lake. The outlet is the Dauphin River	Reservoir	Two stage-discharge curves for summer and winter seasons. The lake also has an outlet channel which is not being operated now; however, its rule curve is also included in the model using a "flowthru" demand node.
3	Saskatchewan River	Grand Rapids	Hydropower station on the outlet of Cedar Lake	Reservoir	Target storage was calculated based on the sum of powerhouse and spill discharge from the lake. A linear regression equation was used to calculate powerhouse discharge based on the hydropower target and spillway discharge based on the storage.
	Churchill River	Southern Indian Lake	This lake has two control structures. Missi falls and	Reservoir	Target storage was calculated based on linear and non-linear monthly regression equations with the inflow as the sole independent variable. The

			Notigi. Notigi is connected to the lake through the South Bay Channel.		calculated target storage was bounded to minimum and maximum amounts determined by inflow and median historical target storage.
		Missi	The control structure on Southern Indian Lake that regulates flow towards Hudson Bay	Flowthru Demand	Outflow from Missi was determined by the sum of outflow resulting from the minimum flow curve, which depends on the current month, and regression equations. The equations calculate additional discharge based on inflow to Southern Indian Lake. Two regression equations were used based on the thresholds of current Southern Indian Lake inflow and storage.
	Nelson River	Notigi	The control structure is connected to Southern Indian Lake via the South Bay Channel and regulates flow towards the Nelson River.	Reservoir	The target storage at Notigi is calculated using regression equations based on Southern Indian Lake target storage. Maximum and minimum thresholds of outflow were determined by regression equations with Notigi water level as the independent variable. Linear equation for maximum and third-order polynomial for minimum.
		Wapisu	Uncontrolled Lake	Reservoir	Daily median recorded storage as the target storage
		Footprint	Uncontrolled Lake. Its outlet name is Gods Rapids.	Reservoir	Target storage was calculated using the stage-discharge curve
		Wuskwatim	Hydropower station on the outlet of Wuskwatim Lake	Reservoir	Daily median recorded storage as the target storage
		Opegano	Uncontrolled Lake. Its outlet name is Jack Pine Falls.	Reservoir	Daily median recorded storage as the target storage
		Birchtree	Uncontrolled Lake. Its outlet name is Manasan Groin.	Reservoir	Daily median recorded storage as the target storage
	Lake Winnipeg	Lake Winnipeg	The outlets of the lake are the West and East channels.	Reservoir	The target storage is defined using 3D curves of the channels. The curves determine the outflow. Then target storage is calculated based on the outflow and inflow of the lake.
	Nelson River	Jenpeg	Hydropower station which is connected to Lake Winnipeg by the West Channel	Reservoir	Target storage was defined using daily median historical recorded storage, minimum storage, and linear and non-linear regression equations. The current date and Lake Winnipeg storage determine the appropriate method to use.
		Cross	Uncontrolled Lake	Reservoir	Target storage was calculated using the stage-discharge curve
		Sipiwesk	Uncontrolled Lake	Reservoir	Target storage was calculated using the stage-discharge curve
		Kelsey	Hydropower station	Reservoir	Daily median recorded storage as the target storage
		Split	Uncontrolled Lake	Reservoir	Target storage was calculated using the stage-discharge curve
		Kettle	Hydropower station. Located at the outlet of Stephens Lake	Reservoir	Daily median recorded storage as the target storage
		Long Spruce	Hydropower station	Reservoir	Daily median recorded storage as the target storage
		Limestone	Hydropower station	Reservoir	Daily median recorded storage as the target storage

SM.2 Detailed Performance Results for Each Sub-system

The detailed model performance is presented for both mass-balance and operational models using **monthly** KGE of water level and outflow, and hydropower generation. The term "level" refers to the forebay water surface elevation in lakes and reservoirs. The weighted average of monthly KGE is calculated for level and outflow, based on mean recorded storage and mean recorded outflow, respectively. To present the model performance, KGE greater than 0.8 is categorized as "high performance", between 0.4 and 0.8 as "acceptable performance", and less than 0.4 as "low performance".

S2.1. Sub-System 1: Winnipeg River Basins

All variables are simulated with high performance by the mass-balance model, which was expected because recorded daily storages were used as target storages (Table S2). KGE exceeds 0.93 for all evaluations of the mass-balance model, with 24 out of 41 evaluations achieving the ideal value of 1. The weighted average of KGE is 1 and 0.96 for level and outflow, respectively. A KGE of 0.96 is achieved for the total hydropower generation in the sub-system.

The operational model has relatively lower performance mainly because the operational rules do not perfectly match daily recorded storage values. However, results demonstrate high and acceptable performance of the operational model in this sub-system. KGE is more than 0.8 (high performance) in 29 out of 41 evaluations. The weighted average of KGE for the entire sub-system is 0.83 for level and 0.88 for outflow. A KGE of 0.92 is achieved for total hydropower generation in sub-system 1, with the lowest KGE of 0.88 at McArthur and Pine Falls stations. Figure S1-a represents that simulated hydropower follows a similar pattern and magnitude to the historical hydropower generation. Such high performance implies the efficiency of the model in simulating the main control points of streamflow in upstream, as well as turbine outflows. KGE of total outflow at hydropower stations ranges from 0.87 to 0.92, with turbine outflow between 0.86 to 0.93, and side channels between 0.57 to 0.87. Level and outflow in Lac Seul, Rainy Lake, and Lake of the Woods, as the main streamflow controllers of the sub-system, are simulated with high KGE: 0.88, 0.89, and 0.91 for level, and 0.8, 0.96, and 0.91 for outflow, respectively. Figure S1-b and c illustrate how Lac Seul and Lake of the Woods responded to the variations in the sub-system based on the defined operations, mirroring the pattern of recorded levels.

Five out of 41 evaluations demonstrate acceptable performance in the operational model, with KGE ranging from 0.47 to 0.75. Among these, the relatively lower KGE in outflow simulation at Rat Rapid (0.67) and Root River (0.47) is attributed to the defined operational threshold. As presented in Figure S1-d and e, the defined operational threshold does not model Rat Rapid and Root River outflow precisely from 1980 to 2004. Consequently, the defined operation better complies with the current one, which is also preferred in this study.

Seven out of 41 evaluations exhibit low performance with a negative KGE. However, it does not affect the overall performance of the model. This includes the negative KGE for level simulation of Umfreville and all 6 hydropower stations from Pointe du Bois to Pine Falls. Level variations at these locations have a minimal impact on outflow due to having low storage compared to the amount of water passing through. This means outflow roughly equals inflow at these locations at the daily timescale, with the outflow simulation performance mainly affected by the estimated inflow. Therefore, despite their high performance in outflow simulation, they have inconsistencies in correlation and variability of level simulation. For instance, Pine Falls has KGE of 0.93, 0.85, and 0.92 for turbine, side channel, and total outflow, respectively, while its level simulation KGE is -0.22 (see Figure S1-f, -g, and -h). It is expected that the level simulation performance would not significantly impact hydropower output at daily time resolution, since the plants are typically operated with daily cycling patterns that are dependent on the inflow. Notably, a slight negative bias is observed for hydropower generation at all stations, for both mass-balance and operational model. It is mainly due to the inability to accurately capture the precise level and consequently head and efficiency for hydropower generation.

Table S2. Performance results for sub-system 1. The red color shows deviations from 1 for r, α, and β and KGE less than zero. The green color represents a monthly KGE of more than 0. The size of the bars in each metric and for each variable is determined by comparing locations in both operational and mass-balance models. The weighted average metric for level is based on mean recorded storage and for outflow is based on mean recorded outflow for each location.

Variable	Location	Mass-Balance				Operational			
		(r-1)	(β-1)	(α-1)	KGE	(r-1)	(β-1)	(α-1)	KGE
Level	*St Joseph*	0.00	0.00	0.00	1.00	-0.19	0.00	0.09	0.79
	Lac Seul	0.00	0.00	0.00	1.00	-0.11	0.00	-0.06	0.88
	Pakwask	0.00	0.00	0.00	1.00	-0.29	0.00	-0.38	0.53
	Ball	0.00	0.00	0.00	1.00	-0.10	0.00	-0.16	0.81
	Separation	0.00	0.00	0.00	1.00	-0.09	0.00	-0.24	0.74
	Umfreville	0.00	0.00	0.00	1.00	-0.87	0.00	-0.63	-0.07
	Lac La Croix	0.00	0.00	0.00	1.00	-0.02	0.00	-0.04	0.96
	Namakan	0.00	0.00	0.00	1.00	-0.10	0.00	-0.14	0.83
	Rainy	0.00	0.00	0.00	1.00	-0.11	0.00	0.01	0.89
	Lake of the Woods	0.00	0.00	0.00	1.00	-0.09	0.00	-0.01	0.91
	Minaki	0.00	0.00	0.00	1.00	-0.10	0.00	-0.23	0.75
	Pointe du Bois	0.00	0.00	0.00	1.00	-0.95	0.00	-0.90	-0.31
	Slave Falls	0.00	0.00	0.00	1.00	-0.75	0.00	-0.93	-0.19
	Seven Sisters	0.00	0.00	0.00	1.00	-0.90	0.00	-0.97	-0.33
	Mc Arthur	0.00	0.00	0.00	1.00	-0.79	0.00	-0.69	-0.05
	Great Falls	0.00	0.00	0.02	0.98	-0.87	0.00	-0.99	-0.32
	Pine Falls	0.00	0.00	0.01	0.99	-0.88	0.00	-0.84	-0.22
	Weighted Average	0.00	0.00	0.00	1.00	-0.14	0.00	-0.07	0.83
Outflow	*Rat Rapid*	0.00	0.00	0.00	1.00	-0.31	-0.10	0.02	0.67
	Root River	0.00	0.00	0.00	1.00	-0.51	0.02	0.13	0.47
	Lac Seul	0.00	0.00	0.00	1.00	-0.10	-0.05	-0.16	0.80
	Pakwash	-0.01	-0.01	-0.01	0.98	-0.10	-0.07	-0.16	0.80
	Ball	-0.01	-0.01	-0.01	0.99	-0.07	-0.04	-0.19	0.79
	Separation	-0.01	0.00	0.00	0.99	-0.06	-0.04	-0.19	0.80
	Umfreville	-0.02	0.01	-0.01	0.97	-0.07	-0.04	-0.11	0.87
	LacLaCroix	0.00	0.00	0.00	1.00	0.00	0.00	0.00	1.00
	Namakan	0.00	0.00	0.00	1.00	-0.02	0.00	0.03	0.96
	Rainy	0.00	0.00	0.00	1.00	-0.04	0.00	0.00	0.96
	Lake of The Woods	0.00	0.00	0.00	1.00	-0.09	0.00	0.02	0.91
	Whitedog	0.00	0.00	0.00	1.00	-0.09	0.00	0.03	0.90
	Pointe du Bois	-0.01	-0.03	-0.04	0.93	-0.06	-0.05	-0.11	0.87
	Slave Falls	-0.01	-0.01	-0.05	0.93	-0.06	-0.05	-0.11	0.87
	Seven Sisters	-0.01	-0.02	-0.06	0.95	-0.05	-0.03	-0.07	0.90
	Mc Arthur	-0.01	-0.09	-0.13	0.94	-0.05	-0.03	-0.08	0.90
	Great Falls	-0.01	0.17	0.01	0.93	-0.05	-0.03	-0.09	0.89
	Pine Falls	-0.01	-0.02	-0.06	0.96	-0.05	-0.01	-0.06	0.92
	Weighted Average	-0.01	0.00	-0.04	0.96	-0.06	-0.03	-0.08	0.88
Hydropower	*Pt Du Bois*	0.00	0.00	0.00	0.99	-0.02	-0.02	0.01	0.97
	SlaveFalls	0.00	-0.01	0.01	0.98	-0.02	-0.02	0.03	0.96
	Seven Sisters	0.00	-0.01	0.03	0.97	-0.01	-0.02	0.04	0.95
	McArthur	-0.01	-0.03	0.07	0.93	-0.04	-0.05	0.10	0.88
	Great Falls	0.00	-0.01	0.03	0.97	-0.02	-0.02	0.05	0.94
	Pine Falls	-0.01	-0.02	0.06	0.94	-0.04	-0.04	0.11	0.88
	Total	0.00	-0.01	0.04	0.96	-0.01	-0.01	0.07	0.93

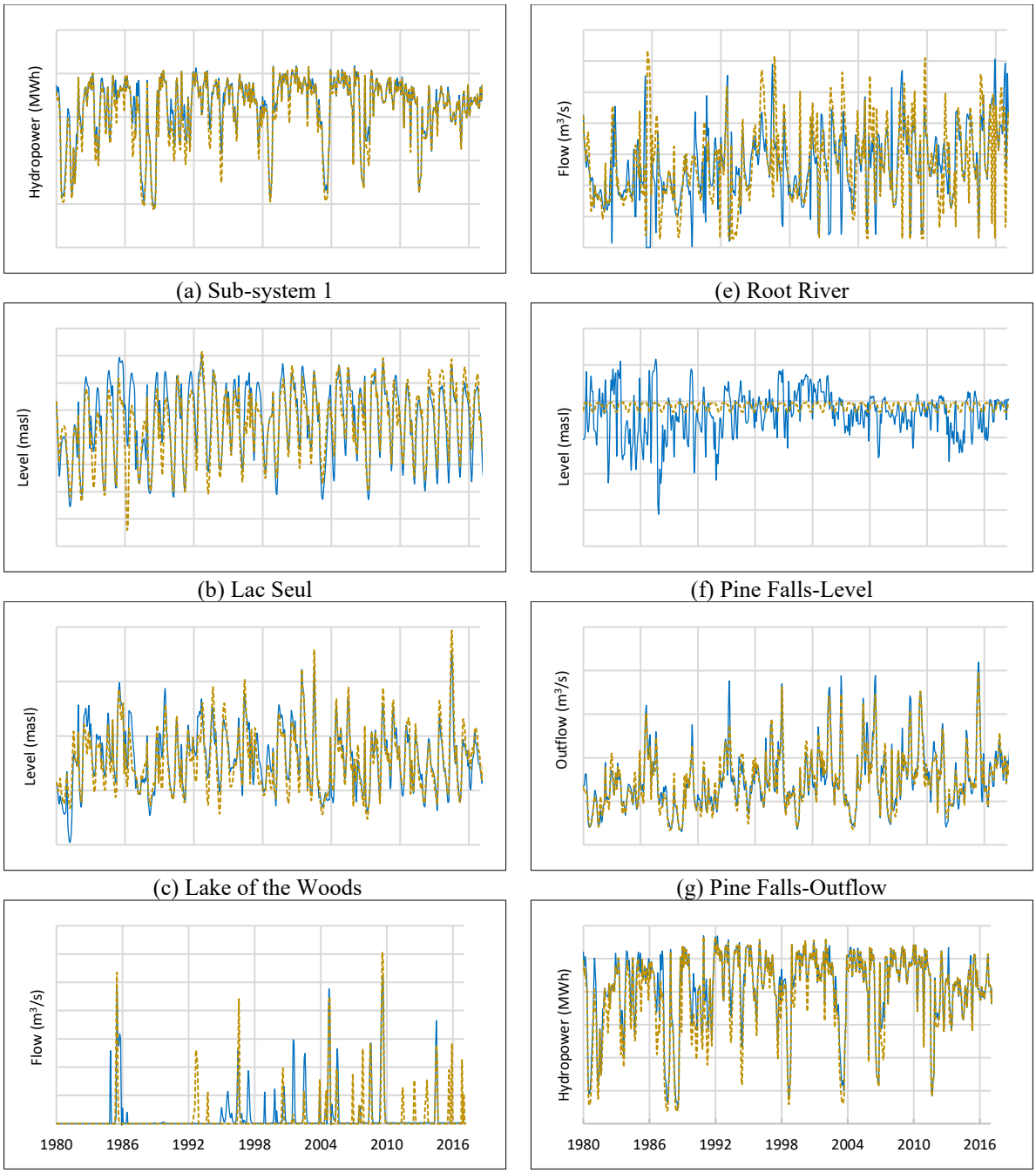


Figure S1. Monthly timeseries of recorded (blue) vs. simulated (gold) in sub-system 1 operational model from 1980 to 2017.

S2.2. Sub-System 2: Lake Winnipeg and Assiniboine and Red River Basins

The mass-balance model demonstrates high and acceptable performance in this sub-system. KGE exceeds 0.93 in 12 out of 16 evaluations, with 7 achieving the ideal value of 1 (Table S3). The weighted average of KGE in the sub-system is as high as 1 and 0.90 for level and outflow,

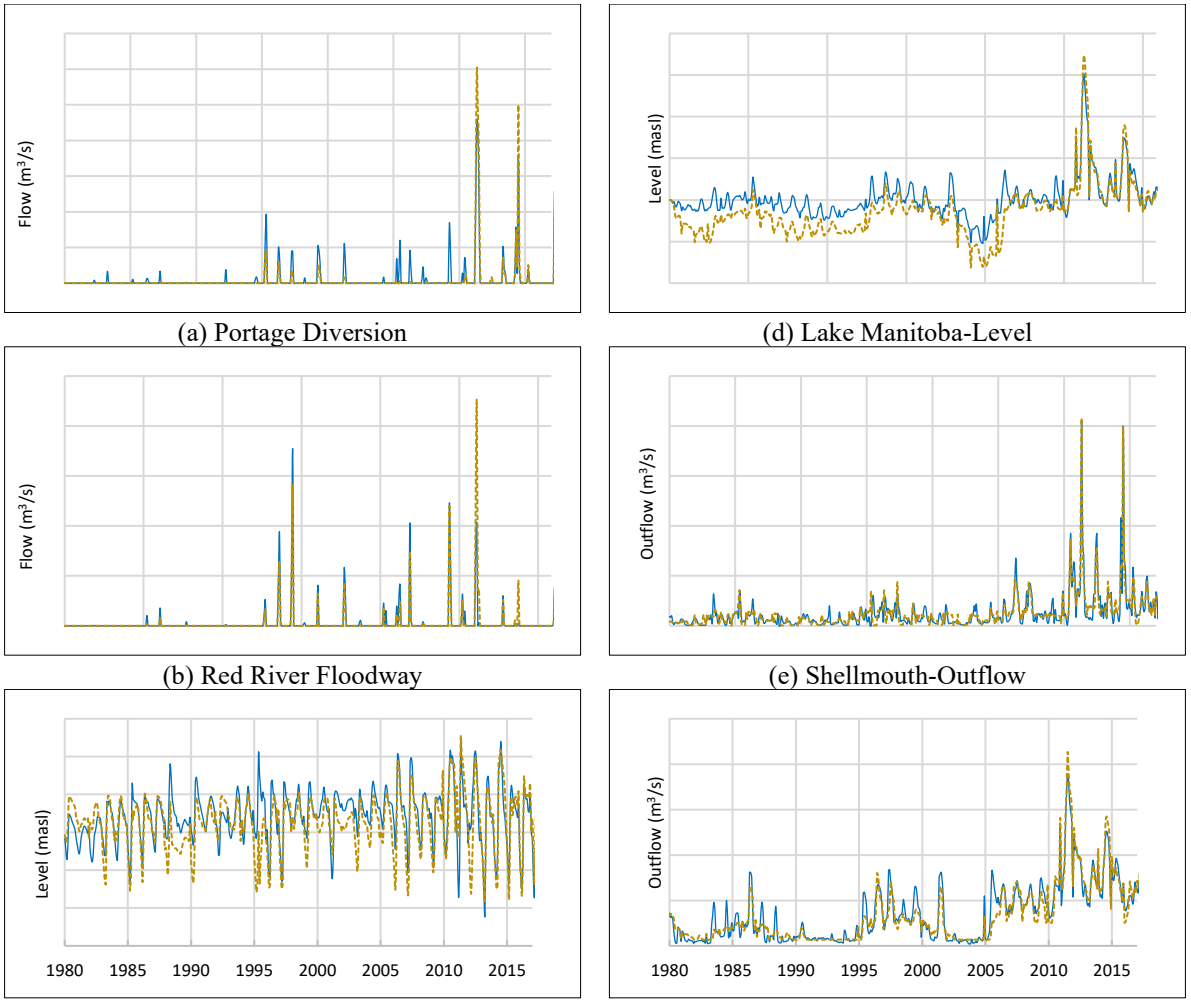
respectively. The other 4 evaluation criteria, including streamflow at Russel, Brandon, Portage Diversion, and Southport, demonstrate relatively lower KGE ranging from 0.68 to 0.88. This indicates that the recorded inflows are insufficient to accurately simulate mass-balance at these stations. This issue similarly affects the operational model. Routing would improve the flow simulation at these stations. Although the simple routing method included in MODSIM-DSS was attempted, it proved insufficient for this reach.

Table S3. Performance results for sub-system 2. The red color shows deviations from 1 for r, α, and β and KGE less than zero. The green color represents a monthly KGE of more than 0. The size of the bars in each metric and for each variable is determined by comparing locations in both operational and mass-balance models. The weighted average metric for level is based on mean recorded storage and for outflow is based on mean recorded outflow for each location.

Variable	Location	Mass-Balance				Operational			
		(r-1)	(β-1)	(α-1)	KGE	(r-1)	(β-1)	(α-1)	KGE
Level	*Shellmouth*	0.00	0.00	0.00	1.00	-0.23	0.00	0.07	0.76
	Winnipegosis	0.00	0.00	0.00	1.00	0.00	0.00	0.00	0.99
	Manitoba	0.00	0.00	0.00	1.00	-0.08	0.00	0.34	0.65
	St. Martin	0.00	0.00	0.00	1.00	-0.07	0.00	0.00	0.93
	Weighted Average	0.00	0.00	0.00	1.00	-0.05	0.00	0.18	0.81
Outflow	*Shellmouth*	0.00	0.00	0.00	1.00	-0.08	0.00	-0.07	0.90
	Russel	-0.11	0.00	-0.04	0.88	-0.12	0.00	-0.10	0.84
	Miniota	-0.04	0.00	-0.05	0.93	-0.04	0.00	-0.07	0.92
	Brandon	-0.08	-0.05	-0.30	0.68	-0.12	-0.05	-0.36	0.62
	Holland	-0.02	-0.01	-0.04	0.95	-0.02	-0.01	-0.05	0.95
	Portage Diversion	-0.01	0.30	0.05	0.70	-0.09	-0.26	0.12	0.70
	Southport	-0.08	-0.16	-0.16	0.76	-0.12	-0.01	-0.11	0.84
	Headingly	-0.06	-0.02	-0.03	0.93	-0.08	0.05	-0.07	0.88
	Floodway	0.00	0.00	0.00	1.00	-0.12	-0.04	0.10	0.84
	Winnipegosis	0.00	0.00	0.00	1.00	-0.05	0.00	0.01	0.95
	Manitoba	-0.01	0.04	0.03	0.95	-0.05	-0.04	0.00	0.94
	St. Martin	-0.01	0.05	0.04	0.94	-0.06	-0.04	-0.02	0.93
	Weighted Average	-0.03	0.00	-0.05	0.90	-0.07	-0.02	-0.07	0.87

The results demonstrate the high and acceptable performance of the operational model in this sub-system. KGE is more than 0.8 (high performance) in 12 out of 16 evaluations. The lowest KGE of 0.62 is calculated for the flow at Brandon hydrometric station. The weighted average of KGE for the entire sub-system is 0.81 for level and 0.87 for outflow. The outflow is simulated with KGE values of 0.7 and 0.86 at Portage Diversion (see Figure S2-a) and Floodway (see Figure S2-b), the two main diversion structures for flood control and management. Shellmouth and Lake Manitoba, the other two main control points in the sub-system record a KGE of 0.76 and 0.65 for level simulation, respectively. For Shellmouth, results indicate that the current guidelines have been applicable for simulating the level since 2006 (see Figure S2-c). Additionally, Shellmouth

relatively small reservoir storage contributes to the complexity of its operation. Similarly, Lake Manitoba operations are applicable for simulating its level since 2006 (see Figure S2-d). Outflows of Shellmouth and Lake Manitoba are simulated with high KGE values of 0.83 and 0.94, respectively (see Figure S2-e and f).



(a) Portage Diversion

(d) Lake Manitoba-Level

(b) Red River Floodway

(e) Shellmouth-Outflow

(c) Shellmouth-Level

(f) Lake Manitoba-Outflow

Figure S2. Monthly timeseries of recorded (blue) vs. simulated (gold) in the sub-system 2 operational model from 1980 to 2017.

S2.3. Sub-System 3: Lake Winnipeg and Saskatchewan, Churchill, and Nelson Rivers Basins

Mass-balance model has high performance in this sub-system. KGE exceeds 0.83 in all evaluations, with 13 out of 45 achieving the ideal value of 1 (Table S4). Weighted average of KGE is 0.98 for both level and outflow. A KGE of 0.92 is achieved for the total hydropower generation in the sub-system.

Results demonstrate high and acceptable performance in the operational model. KGE is more than 0.8 (high performance) in 26 out of 45 evaluations. The weighted average of KGE for the entire sub-system is 0.89 for level and 0.84 for outflow. A KGE of 0.95 is achieved for total hydropower generation in the sub-system, with the lowest KGE of 0.81 at Kelsey station. Figure S3-a represents that simulated hydropower follows a similar pattern and magnitude to the historical hydropower generation. Such high performance implies the efficiency of the model in simulating the main control points of streamflow in upstream, as well as turbine outflows. KGE of total outflow at hydropower stations ranges from 0.48 to 0.95, with turbines outflow between 0.75 to 0.99. Southern Indian Lake level and outflow are simulated with a high KGE of 0.82 and 0.92, respectively. This is an example of the improvement in simulating sub-system 1, where Beiraghdar (2019) simulated the level with KGE of 0.63 at Southern Indian Lake. Lake Winnipeg as the other major control point in the sub-system produces a high KGE value of 0.96 for level (Figure S3-b) and 0.92 for outflow. This is a significant improvement in simulating Lake Winnipeg, comparing the results with Beiraghdar (2019) model with a KGE of 0.23 in level simulation. Such high performance is attributed to the strong performance at Jenpeg, the West Channel, and the East Channel (see Figure S3-c, d, and e), with an outflow KGE of 0.9. This indicates that the combination of the 3D curve, median Ice Factor, and the specified operations and thresholds simulate this major control point with high accuracy. Operations were defined at Grand Rapids and Jenpeg, instead of using median recorded storage. These operations exhibit high KGE in level (0.89 and 0.96), outflow (0.95 and 0.9), and hydropower simulation (0.97 and 0.91). This is another example of improvement in sub-system 1 simulation. In Beiraghdar (2019) model, level simulation at Jenpeg had a KGE of 0.63 where median recorded storage was used as its operations.

KGE ranges from 0.43 to 0.75 (acceptable performance) for 13 out of 45 evaluations. Due to its complexities, the simulation of Notigi was the most challenging and required the most effort among all the control points. However, it successfully achieved a KGE of 0.66 for level and 0.51 for outflow. Due to time constraints, Beiraghdar (2019) used historical recorded storage for this control dam to avoid removing it from the model. Notigi small storage relative to its inflow makes it difficult to accurately simulate its water level variability (see Figure S3-f). This directly impacts the South Bay Channel flow simulation (Figure S3-g) with a relatively high deviation from one in its variability. The reason is the backwater-affected relationship between Southern Indian Lake and Notigi through the South Bay Channel. Notigi outflow performance is affected by the

inconsistencies in its inflow through the South Bay Channel and it causes further deterioration in the performance of level simulation at Notigi. The simulation of outflow through Missi Falls, the other control structure of Southern Indian Lake, produces a KGE of 0.7.

Six out of 45 evaluations show low performance in the operational model of this sub-system. Figure S4 illustrates that the water release at Notigi approximately equals the water release at Birchtree in downstream, and the relatively small storages in between do not significantly alter the streamflow pattern. Consequently, Wapisu, Footprint, Wuskwatim, Opegano, and Birchtree have the same simulation performance as Notigi. However, level and outflow performance at Split Lake (see outflow time series on Figure S3-h), where diverted Churchill water joins Nelson River, is simulated with a KGE of 0.91. The reason is that, on average, 75% of the inflow to Split Lake sources from Nelson River, while the remaining 25% is diverted from Churchill River. Similar to sub-system 1, the level is not simulated with pinpoint accuracy at hydropower stations where median recorded storage was used as the operational rule. KGE of -0.88 and -0.28 is calculated for level simulation at Kettle and Limestone. A slight negative bias is calculated for hydropower generation due to the discrepancies in head calculation.

Table S4. Performance results for sub-system 3. The red color shows deviations from 1 for r, α, and β and KGE less than zero. The green color represents a monthly KGE of more than 0. The size of the bars in each metric and for each variable is determined by comparing locations in both operational and mass-balance models. The weighted average metric for level is based on mean recorded storage and for outflow is based on mean recorded outflow for each location.

Variable	Location	Mass-Balance				Operational			
		(r-1)	(β-1)	(α-1)	KGE	(r-1)	(β-1)	(α-1)	KGE
Level	*Southern Indian Lake*	-0.01	0.00	0.09	0.91	-0.14	0.00	-0.10	0.83
	Notigi	0.00	0.00	0.00	1.00	-0.23	0.00	-0.25	0.66
	Wapisu	0.00	0.00	0.01	0.99	-0.56	0.00	-0.12	0.43
	Footprint	0.00	0.00	0.00	1.00	-0.37	0.00	-0.35	0.49
	Wuskwatim	0.00	0.00	0.00	1.00	-0.46	0.00	-0.40	0.39
	Opegano	0.00	0.00	0.00	1.00	-0.58	0.00	-0.37	0.32
	Birchtree	0.00	0.00	0.00	1.00	-0.75	0.00	-0.46	0.12
	Grand Rapids	0.00	0.00	0.00	1.00	-0.04	0.00	0.00	0.96
	Lake Winnipeg	-0.02	0.00	-0.01	0.97	-0.03	0.00	-0.03	0.96
	Jenpeg	0.00	0.00	0.00	1.00	-0.10	0.00	-0.06	0.89
	Cross Lake	0.00	0.00	0.00	1.00	-0.09	0.00	-0.23	0.75
	Sipiwesk	0.00	0.00	0.00	1.00	-0.09	0.00	0.15	0.83
	Kelsey	0.00	0.00	0.00	1.00	-0.60	0.00	-0.42	0.27
	Split Lake	0.00	0.00	0.00	1.00	-0.09	0.00	-0.02	0.91
	Kettle	0.00	0.00	0.00	1.00	-0.90	0.00	-0.59	-0.08
	Long Spruce	0.00	0.00	0.00	1.00	-0.22	0.00	-0.26	0.66
	Limestone	0.00	0.00	-0.02	0.98	-0.89	0.00	-0.92	-0.28
	Weighted Average	-0.02	0.00	0.00	0.98	-0.08	0.00	-0.05	0.89
Outflow	*Southern Indian Lake*	-0.01	0.00	0.02	0.98	-0.05	0.00	-0.05	0.93
	Missi Falls	0.00	0.08	0.02	0.92	-0.09	0.26	-0.13	0.70
	Southbay Channel	-0.03	0.00	-0.08	0.92	-0.37	-0.03	-0.41	0.45
	Notigi	-0.03	0.00	-0.04	0.95	-0.33	-0.03	-0.35	0.51
	Wapisu	-0.03	0.00	-0.04	0.95	-0.36	-0.03	-0.34	0.50
	Footprint	-0.03	0.00	-0.02	0.96	-0.35	-0.03	-0.29	0.54
	Wuskwatim	-0.06	-0.02	-0.01	0.94	-0.47	0.01	-0.22	0.48
	Opegano	-0.03	-0.01	-0.02	0.96	-0.33	-0.04	-0.29	0.56
	Birchtree	-0.03	-0.01	-0.02	0.96	-0.33	-0.04	-0.28	0.57
	Grand Rapids	0.00	0.01	-0.01	0.98	-0.01	0.01	-0.04	0.95
	Lake Winnipeg	-0.03	0.01	0.08	0.91	-0.05	0.00	0.07	0.92
	West Channel	-0.02	0.00	0.12	0.88	-0.06	0.01	0.08	0.90
	East Channel	-0.04	0.02	0.00	0.96	-0.05	-0.04	-0.07	0.91
	Jenpeg	-0.02	0.00	0.12	0.88	-0.06	0.01	0.08	0.90
	Cross Lake	-0.02	0.02	0.11	0.88	-0.05	0.02	0.09	0.90
	Sipiwesk	-0.03	0.02	0.11	0.88	-0.05	0.02	0.08	0.91
	Kelsey	-0.03	0.03	0.10	0.89	-0.05	0.03	0.07	0.91
	Split Lake	-0.03	-0.01	0.07	0.92	-0.05	-0.01	0.09	0.90
	Kettle	-0.02	-0.01	0.08	0.92	-0.04	-0.01	0.09	0.90
	Long Spruce	-0.02	-0.01	0.08	0.91	-0.04	-0.01	0.11	0.88
	Limestone	-0.02	0.00	0.05	0.94	-0.04	-0.01	0.06	0.92
	Weighted Average	-0.02	0.00	0.00	0.98	-0.10	0.00	0.01	0.84
Hydropower	*Wuskwatim*	0.00	-0.03	-0.03	0.95	0.00	-0.05	-0.06	0.92
	Grand Rapids	0.00	-0.08	-0.01	0.92	0.00	-0.02	-0.01	0.97
	Jenpeg	-0.05	-0.06	0.06	0.90	-0.06	-0.05	0.05	0.91
	Kelsey	-0.06	-0.03	0.15	0.83	-0.06	-0.02	0.18	0.81
	Kettle	-0.01	-0.01	0.06	0.94	-0.01	-0.02	0.09	0.91
	Long Spruce	-0.01	-0.01	0.06	0.94	-0.02	-0.02	0.10	0.90
	Limestone	0.00	-0.01	-0.01	0.99	0.00	-0.02	-0.01	0.97
	Total	-0.01	-0.07	0.02	0.92	-0.01	-0.02	0.05	0.95

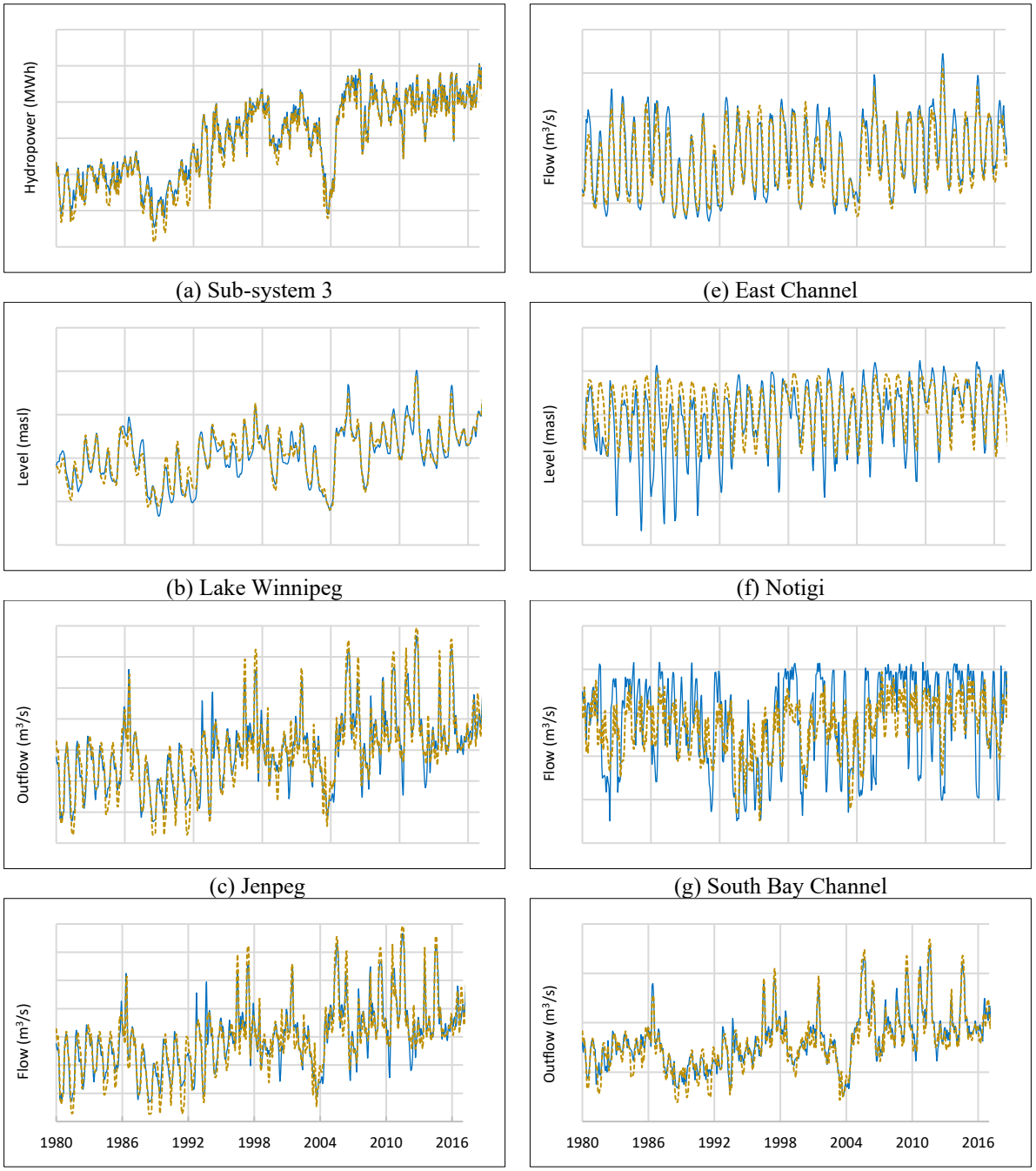


Figure S3. Monthly timeseries of recorded (blue) vs. simulated (gold) in the sub-system 3 operational model from 1980 to 2017.

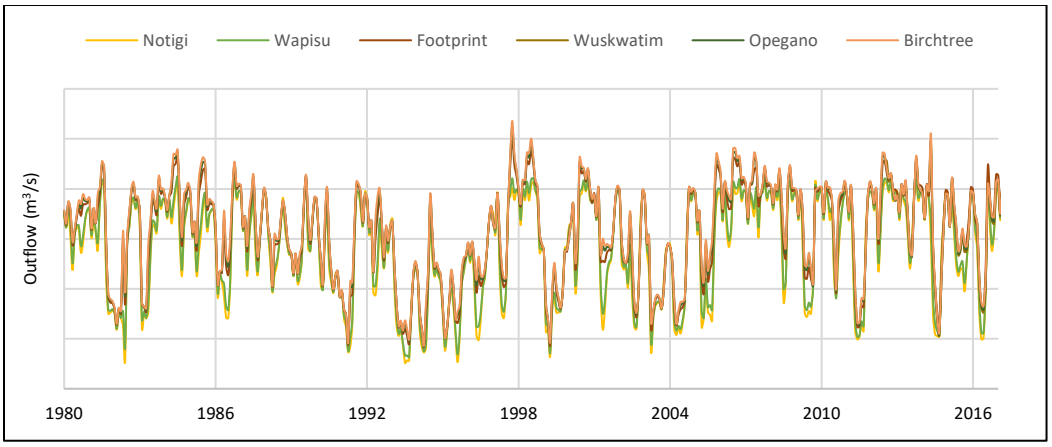


Figure S4. Recorded monthly outflow timeseries in sub-system 3: from Notigi to Birchtree

SM.3 MB_HydroSim

MB_HydroSim is an integrated water resources management tool developed for the Province of Manitoba, Canada. The model represents approximately 30% of the vast Nelson-Churchill River Basin, which drains the Canadian Rockies, portions of the north-central United States, and north-western Ontario into Manitoba and ultimately into Hudson Bay. Developed using MODSIM-DSS, MB_HydroSim simulates daily water levels, outflows, and hydropower generation while explicitly representing key system characteristics and operational rule sets. The model has been successfully evaluated against observed water levels, outflows, and hydropower generation for the period 1980-2017. Further details on model development, calibration, and performance are provided in Gozini et al. (2026a).

MB_HydroSim is composed of three interconnected sub-systems. The first sub-system represents the Winnipeg River sub-basin, where water operations are primarily focused on hydropower generation. The second sub-system represents the Assiniboine and Red River sub-basins, together with the western portion of the Lake Winnipeg sub-basin and is operated primarily for flood management. The third sub-system represents the Saskatchewan, Churchill, and Nelson River sub-basins, along with the remaining portion of the Lake Winnipeg sub-basin, with water operations again focused predominantly on hydropower generation.

SM.4 Stress-Testing Application: Hydropower Generation

Sub-system 1 is used as the illustrative example case (Figure 4 in the main manuscript) demonstrating how target synthetic streamflow scenarios in a multisite water-resources system can

be used for stress-testing of hydropower systems. This sub-system includes 14 inflow locations and a cascade of six hydropower stations along the Winnipeg River, with a combined installed capacity of 580 MW.

The stress-testing application is conducted by generating 25 daily synthetic streamflow scenarios, each spanning a 38-year period, for 14 inflow locations. Target deviations in monthly inflow mean and standard deviation (SD) range from -20% to +20% in increments of 10%, while imposing no change (0%) in monthly mean and SD seasonality. This design preserves the historical seasonal inflow pattern observed during the 1980-2017 reference period. For each target synthetic inflow scenario, daily hydropower generation is simulated at the six Winnipeg River hydropower stations. System performance is evaluated using hydropower reliability, computed by comparing simulated generation against observed generation over the 1980-2017 period, which is treated as the effective hydropower demand. Reliability (*Re*) is unitless, ranges from 0 to 1, and represents the fraction of days on which the system generates at least 95% of the daily hydropower demand:

$$Re = \frac{1}{D}\sum_{d=1}^{D} I_d, \qquad I_d = \begin{cases} 1, E_d^{gen} \geq 0.95E_d^{dem} \\ 0, E_d^{gen} < 0.95E_d^{dem} \end{cases} \tag{S.1}$$

Where d (= 1, …., D) indexes days, I is the daily reliability indicator, E^{gen} is the total daily hydropower generation, and E^{dem} is the total daily hydropower demand. Reliability is computed at both annual and seasonal scales. For annual reliability, D represents the total number of days in the full simulation period; for seasonal reliability, D represents the total number of days within a given season aggregated across all years.

SM.5 Stress-Testing Application: Flood and Water Demand Management

From sub-system 2 in MB_HydroSim, Shellmouth Dam (location F in Figure 1 of Gozini et al. (2026a)) is used as the example application of stress testing related to flood and water-demand management. Shellmouth Dam is the primary flood-control structure within sub-system 2, complementing other regional flood-mitigation infrastructure such as the Portage Diversion, Red River Floodway, and Fairford control structure. Operationally, Shellmouth Dam is managed to draw down reservoir water levels during winter (November-March) to create storage capacity for spring runoff (April-June). The reservoir receives inflows from three upstream tributaries, and

flood conditions are considered to occur during the spring season when reservoir water levels exceed the spillway elevation of 1408.5 ft.

During summer and autumn (July-October), Shellmouth levels are maintained within an operating range of 1400-1404 ft to meet downstream water-demand requirements along the Assiniboine River, including licensed municipal and private withdrawals, irrigation needs, and minimum ecological flow requirements. The lower operating bound of 1400 ft represents a critical guideline level for maintaining minimum downstream flows of 100 cfs at Brandon and 200 cfs at Headingley hydrometric stations. Although six downstream inflow locations also contribute to meeting these flow requirements, reservoir levels below 1400 ft substantially increase the risk of failing to satisfy downstream demands. In MB_HydroSim, when minimum flow requirements at Brandon or Headingley are not met, Shellmouth outflows are increased to compensate, which can further depress reservoir levels below the lower operating threshold and exacerbate water-supply risk.

The stress-testing analysis is conducted using 25 daily synthetic streamflow scenarios (38 years) generated for nine inflow locations, including three upstream inflows to the Shellmouth Dam and six downstream inflow locations along the Assiniboine River. Target deviations in monthly inflow mean and SD range from -20% to +20% in increments of 10%, while preserving historical inflow seasonality. For each synthetic scenario, daily reservoir water levels are simulated and evaluated against flood- and demand-management thresholds. The frequency of flood occurrence and water-demand shortage is quantified as the percentage of days on which Shellmouth water levels violate either water-level threshold, calculated as:

$$P = \frac{100}{D}\sum_{d=1}^{D} O_d, \qquad O_d = \begin{cases} 1, WSE_d < 1400\ ft \\ 1, WSE_d > 1408.5\ ft \\ 0, \quad otherwise \end{cases} \tag{S.2}$$

O is the daily exceedance indicator (1 = exceeding the operating water level; 0 = otherwise) and *WSE* is the water surface elevation at Shellmouth Dam. For flood management, exceedance of the spillway elevation (1408.5 ft) during the spring season (April-June) is considered indicative of flood risk, with *D* representing the number of days in this period. For water-demand management, reservoir levels falling below the lower operating guideline (1400 ft) during summer and autumn (July-October) are considered indicative of elevated water-supply risk, with *D* representing the total number of days in these seasons.

SM.6 Summary of seasonal inflow patterns

Table S5. Summary of seasonal total inflow response patterns across the GCM ensemble in the period 2018-2055 relative to 1981-2017. For each pattern, the signs denote the direction of change (+ increase, − decrease) in different seasons (winter, spring, summer, autumn).

Pattern	Mean (Winter, Spring, Summer, Autumn)	SD (Winter, Spring, Summer, Autumn)	Members
1	+,+,+,+	+,+,+,+	A10-R81, A13-R41, CMS-R81, MR3-R81
2	+,+,+,+	+,+,+,−	MR3-R41
3	+,+,+,+	−,+,+,+	MI5-R81
4	+,+,+,+	−,−,+,−	GF3-R41
5	+,+,+,+	−,−,−,+	A13-R81
6	+,+,+,+	−,−,−,−	A10-R41
7	+,+,−,+	−,−,+,+	Median*
8	+,+,−,+	+,+,+,+	INM-R41
9	+,+,−,−	+,+,+,−	MIC-R81
10	+,+,−,−	+,−,−,−	CE2-R41
11	−,−,−,−	+,−,+,+	MIE-R81
12	−,−,−,−	−,−,+,+	NOE-R41
13	−,−,−,−	−,+,−,−	IAL-R81
14	−,−,−,−	−,−,−,+	CN5-R41
15	−,−,−,−	−,−,−,−	CMM-R41, IAL-R41, MI5-R41

* Seasonal mean change (%; winter-autumn): 5.59, 0.92, -0.19, 0.29; SD change (%): -0.22, -2.56, 5.74, 4.43

SM.7 Summary of Stress-Testing Findings for the Hydropower System in Manitoba

Table S6. Summary of annual stress-testing findings.

Aspect	Historical (EH-R)	Future (EG-F & RG-F)	Key Insight
Primary control	Inflow magnitude dominates system performance; variability impacts only near critical thresholds	For relatively small annual inflow changes, seasonality plays an important role in system performance	System performance is primarily controlled by inflow magnitude, with seasonality providing a secondary control on outcomes
System performance under wet and dry condition	Highly asymmetric: large degradation under dry conditions and limited gains under wet conditions	Asymmetry persists for vulnerability and Lake Winnipeg water level excursions	The system cannot fully capitalize on wet conditions due to limited storage in stations and upstream lakes
Reliability	Declines sharply under dry conditions	System is expected to be less stressed and sensitive to dry conditions	Future hydropower reliability is expected to improve due to added capacity (Keeyask)
Vulnerability	Most sensitive metric to dry conditions; degradation exceeds improvement by >3×	Sensitivity persists; added capacity (Keeyask) provides limited improvement	Storage limitations continue to drive high vulnerability under dry conditions
Average annual revenue	Declines sharply under low inflow; limited gains under high inflow	System is expected to be substantially less stressed	Financial performance improves under future conditions due to added capacity (Keeyask)
Frequency of Lake Winnipeg water level excursion	Sensitive to high inflow; excursions increase under wet conditions	Sensitivity to high inflow persists	Wet conditions destabilize system state with increased excursion frequency
Benefit-stability trade-off	Hydropower performance gains under high inflow coincide with higher frequency of water level excursions	Trade-off persists under future conditions	Improved performance under wet conditions can destabilize system state; adaptive operational strategies are required
Heat map-based performance extraction	–	Reliable for large inflow magnitude changes; provides a conservative performance estimate	A single future heat map helps locate system outcomes, but accuracy is limited to large annual inflow changes

Table S7. Summary of seasonal stress-testing findings.

Aspect	Historical (EH-R)	Future (EG-F & RG-F)	Key Insight
Seasonal distribution of stress	System stress in vulnerability and lake level excursions is strongly seasonal	Stress is expected to redistribute non-uniformly across seasons	Seasonal system stress analysis is critical for understanding system performance
Summer (critical season)	Highest degradation of vulnerability and Lake Winnipeg level excursions under dry conditions	Remains critical; system stress is expected to intensify in vulnerability, with greater degradation under dry conditions	Summer controls system resilience through storage; expected lower inflows strongly amplify system stress in this season
Winter (highest electricity demand)	Lowest vulnerability degradation under dry condition due to operational prioritization of firm supply	Slightly higher system stress in reliability; vulnerability more sensitive under dry conditions	System remains tuned for winter demand, but becomes more sensitive to water supply shortages
Spring (surplus generation)	Moderate sensitivity to dry conditions	Substantially less stressed; becomes potential surplus-generating season	Increased spring inflows reduce system stress and support system recovery
Autumn (higher system stress)	Moderate sensitivity to dry conditions	System stress in vulnerability is expected to increase	More stress is projected in autumn due to projected decline in summer inflow
Frequency of Lake Winnipeg water level excursion	Majority of excursions occur in summer	Summer remains the dominant season for excursions, but overall stress shifts toward spring and autumn	Critical benefit-stability trade-off is expected in spring
Future seasonal operational focus	-	Seasonal target redistribution has minimal influence on long-term performance; system stress is primarily driven by inflow changes, higher hydropower targets, and operational constraints	Operations remain optimized for winter demand, but greater focus is required in other seasons, particularly summer during which system stress intensifies

SM.8 Stress Testing Graphical Abstract

